



Delft University of Technology

Intrinsic Scintillators

The Scintillating Search for and Exploration of Small Bandgap Scintillators

van Blaaderen, J.J.

DOI

[10.4233/uuid:85b77254-03f5-43c3-aa0b-6217ed92198f](https://doi.org/10.4233/uuid:85b77254-03f5-43c3-aa0b-6217ed92198f)

Publication date

2025

Document Version

Final published version

Citation (APA)

van Blaaderen, J. J. (2025). *Intrinsic Scintillators: The Scintillating Search for and Exploration of Small Bandgap Scintillators*. [Dissertation (TU Delft), Delft University of Technology].
<https://doi.org/10.4233/uuid:85b77254-03f5-43c3-aa0b-6217ed92198f>

Important note

To cite this publication, please use the final published version (if applicable).
Please check the document version above.

Copyright

Other than for strictly personal use, it is not permitted to download, forward or distribute the text or part of it, without the consent of the author(s) and/or copyright holder(s), unless the work is under an open content license such as Creative Commons.

Takedown policy

Please contact us and provide details if you believe this document breaches copyrights.
We will remove access to the work immediately and investigate your claim.

Intrinsic Scintillators

**The Scintillating Search for and Exploration
of Small Bandgap Scintillators**



J. Jasper van Blaaderen

Intrinsic Scintillators

The Scintillating Search for and Exploration
of Small Bandgap Scintillators

Jacob Jasper VAN BLAADEREN

Intrinsic Scintillators

The Scintillating Search for and Exploration of Small Bandgap Scintillators

Dissertation

for the purpose of obtaining the degree of doctor
at Delft University of Technology
by the authority of the Rector Magnificus Prof. dr. ir. T. H. J. J. van der Hagen
chair of the Board of Doctorates

to be defended publicly on
Thursday 13 March 2025 at 15:00 o'clock

Jacob Jasper VAN BLAADEREN

Master of Science in Chemical Engineering
Delft University of Technology, the Netherlands
born in Amsterdam, the Netherlands

This dissertation has been approved by the promotor.

Composition of the doctoral committee:

Rector Magnificus,	chairperson
Prof. dr. P. Dorenbos	Delft University of Technology, promotor
Dr. E. van der Kolk	Delft University of Technology, promotor

Independent members:

Prof. dr. A. J. Houtepen	Delft University of Technology
Prof. dr. K. W. Krämer	University of Bern, Switzerland
Prof. dr. A. Meijerink	Utrecht University
Dr. V. O. Ouspenski	Saint-Gobain Research, France
Dr. ir. T. J. Savenije	Delft University of Technology
Prof. dr. E. H. Brück	Delft University of Technology, reserve member



Key words: scintillator, small bandgap scintillators, intrinsic scintillators, halides, single crystals, photon counting detectors

Printed by: Ipskamp

Cover: Artistic interpretation of a pulse of scintillation photons leaving a crystal visualised by a climbing wall symbolising both the mental and physical challenges of a PhD, and the need to balance them.

Copyright © 2024 Jacob Jasper van Blaaderen

ISBN: 978-94-6518-004-5

An electronic version of this thesis is freely available at:
<https://repository.tudelft.nl>

Scintillatoren moeten loodzwaar zijn

- *P. Dorenbos*
April 2021



Table of Content

Chapter 1: Introduction	2
Chapter 2: The Temperature Dependent Optical and Scintillation Characterisation of Bridgman Grown CsPbX_3 (X = Br, Cl) Single Crystals	18
Chapter 3: Photoluminescence and Scintillation Mechanism of Cs_4PbBr_6	38
Chapter 4: Temperature Dependent Scintillation Properties and Mechanisms of $(\text{PEA})_2\text{PbBr}_4$ Single Crystals	68
Chapter 5: $(\text{BZA})_2\text{PbBr}_4$: A Potential Scintillator for Photon-Counting Computed Tomography Detectors	90
Chapter 6: Scintillation and Optical Characterisation of CsCu_2I_3 Single Crystals from 10 to 400 K	104
Chapter 7: The search for and Selection of Scintillators for Photon Counting Detectors	122
Summary	184
Samenvatting	190
Acknowledgements	196
Supervised Thesis Projects	202
List of Publications	203
Curriculum Vitae	204

1

— 1 —

Introduction

On a daily basis you, the reader, is bombarded by ionising radiation. This cataclysmic fact might sound scary to the average reader. Let me reassure you, it is not. Ionising radiation and its detection is used in many modern day applications. This does raise the question: "How to visualise the invisible?"

As suggested by the title, this thesis deals with the scintillating search for and exploration of small bandgap scintillators. A scintillator is a material which can absorb ionising radiation and convert it into a flash of light, in other words visualising the invisible. In this chapter we will first explore the broader context of radiation detection and some of the theory behind the scintillation process. The main goal will be to answer the question: "Why did you work on small bandgap scintillators?"

1. Visualising the Invisible

Three of the most commonly used types of ionising radiation detectors are: gaseous ionisation detectors, semiconductor detectors, and scintillation detectors. Gaseous ionisation detectors utilise the ionisation of gas molecules or atoms to create an ion-electron pair. There are three general categories of gas filled detectors. In ionisation chamber based detectors, the created charges are collected due to the application of an electric field resulting in either a continuous current or current pulses, the latter is referred to as operating in pulse mode [1]. This type of detector is commonly used as a hand held radiation detector. Proportional counter based detectors always operate in pulse mode and utilise the phenomenon of gas multiplication to amplify the signal of the freed electrons [2]. This requires proportional counters to operate at a higher voltage compared to ionisation chambers. The gas multiplication effect increases the amplitude of the created current pulses enabling these detectors to determine the energy of the incident radiation making them suitable for spectroscopy of low energy X-rays and charged particles. A Geiger-Müller counter based detector also utilises gas multiplication. However, Geiger-Müller counters operate at a higher voltage, compared to a proportional counter, creating a chain reaction of multiplication events [3]. The chain reaction always stops after approximately the same number of events resulting in current pulses with a similar amplitude. All information regarding the energy of the incident radiation is thus lost. Geiger-Müller counter based detectors are often used for the detection of γ - and X-ray photons.

Semiconductor detectors are a form of solid state detectors. Upon absorption of ionising radiation electron-hole pairs are created in the depletion layer of the semiconductor which, due to an electric field, creates a current pulse proportional to the deposited energy [4]. This has some analogy to the ion-electron pair created in gaseous ionisation detectors. Examples of commonly used semiconductor materials in these detectors are: Silicon (Si), high purity germanium (HPGe), cadmium telluride (CdTe), cadmium zinc telluride (CZT), mercury iodide (HgI), thallium bromide (TlBr) and more recently metal-halide perovskites [5–10]. HPGe based detectors are commonly used for gamma spectroscopy due to their low energy resolution, reaching values of 0.3% at 662 keV [11]. One of the down

sides of HPGe however, is the need to actively cool the detectors in order to reduce electronic noise. This problem is mitigated in CdTe and CZT based detectors, which can operate at room temperature, reaching energy resolutions of 0.6% at 662 keV [12]. One of the main challenges of these materials however, is the production of low defect density crystals of sufficient size [13,14].

Scintillation detectors are another commonly used type of solid state detectors. It should be noted however, that scintillation detectors can also be based on a low pressure gas [15] or liquid [16]. A scintillator is a material which produces a flash of light, or scintillation flash, upon absorbing ionising radiation. In a detector, this material is mounted on a photo sensor which converts the flash of light into a current pulse. Before the invention of the photomultiplier tube however, scintillation flashes were observed using the naked eye or a microscope. The number of scintillation photons in the scintillation flash scales with the energy of the incident radiation and so will the amplitude of the current pulse produced by the photo sensor. Examples of commonly used scintillators are: NaI:TI⁺, LaBr₃:Ce³⁺, and (Lu,Y)₂SiO₅:Ce³⁺. One of the first scintillators, NaI:TI⁺, was discovered by Hofstadter in 1948 and is still one of the most famous scintillators up to this day [17–19]. Scintillation detectors are used in many different applications, for example medical imaging [20], high-energy physics [21–23], space exploration [24], and nuclear security.

2. The Interaction of Radiation with Matter

In order to better understand the interaction of radiation with a scintillator, a distinction should be made between different types of ionising radiation. Heavy charged particles, like α -particles and protons, interact with electrons in the scintillator crystal via Coulomb forces. Direct interaction with the nucleus, Rutherford scattering, can often be ignored [25]. Upon entering the scintillation crystal, these particles will start to slow down by transferring their energy to electrons. This creates an ionisation track consisting of hot free charge carriers. Both protons (p^+) and α -particles (${}^4_2\text{He}^{2+}$) are significantly more heavy compared to electrons and will create very linear ionisation tracks [25].

Another type of charged particles that needs to be considered are β^- -particles or electrons. Upon entering the scintillator β^- -particles will lose their energy via electron-electron interactions, producing an ionisation track consisting of hot free charge carriers. Compared to the heavy charged particles, β^- -particles will create longer and less linear ionisation tracks because electron-electron interaction involve two particles of the same mass.

The interaction of γ - and X-ray photons with matter is significantly different from the interactions described above. Photons, or electromagnetic radiation, do not have a charge nor mass. The three most important interaction mechanisms of γ - and X-ray photons with matter are: photo-electric absorption, Compton scattering, and pair production. The dominant interaction process depends on the energy of the gamma photons and the effective atomic number of the scintillator.

In photo-electric absorption, a γ -photon interacts with an atom, transferring all its energy to an electron from one of the inner shells. This results in the production of a photo-electron which, similar to a β^- -particle, will create an ionisation track consisting of hot free charge carriers. The vacancy created in the K shell of the, now ionised, absorber atom can be filled by an electron from a higher shell, emitting a characteristic X-ray photon in the process.

When a γ -photon undergoes Compton scattering, it interacts with an electron, transferring only a portion of its energy, thus producing a recoil electron and a lower energy scattered γ -photon. The energy distribution between the recoil electron and scattered γ -photon is determined by the scattering angle.

When the energy of the γ -photon exceeds twice the rest-mass energy of an electron (1.02 MeV), it is also possible for pair production to take place. In pair production the γ -photon disappears and an electron-positron pair is created. The excess energy of the γ -photon above 1.02 MeV is distributed among the positron and electron in the form of kinetic energy. The created positron will, after slowing down, annihilate and produce two 511 keV annihilation photons which will lose their energy due to one of the other interaction mechanisms. It should be noted that the probability of pair production is zero until the incident γ -photons reach energies of 1.02 MeV. All interaction mechanisms described above result in the production of highly energetic electrons that will produce hot electrons and holes along their ionisation track.

3. Scintillator Properties

The influence of the different interaction mechanisms of γ -photons with a scintillator can be observed in a pulse height spectra. Commonly, pulse height spectra are recorded using the 662 keV γ -photons from ^{137}Cs , making photo-electric absorption and Compton scattering the dominant interaction mechanisms. An example of a pulse height spectrum, recorded using a commercial $\text{LaBr}_3:\text{Ce}^{3+}$ is shown in Figure 1. A pulse height spectrum can be seen as a histogram of the number of scintillation photons produced in a scintillation flash, *i.e.*, a histogram of the size of the scintillation flash. The peak on the right side of the spectrum, labelled 1 in Figure 1, is referred to as the full absorption, or photopeak, and corresponds to the complete absorption of the energy of the incident γ -photon.

The second feature that can be observed is the Compton continuum, labelled 2 in Figure 1. This is the direct result of a Compton scattering event where the incident γ -photon has created a recoil electron and where the scattered γ -photon has escaped the scintillator crystal. This means that only a part of the energy of the incident γ -photon is deposited. The Compton edge, labelled 3 in Figure 1, represents the maximum amount of energy which can be transferred in a Compton scattering event. For 662 keV γ -photons the separation between the Compton edge and photopeak is 184 keV. In the limit that the incident γ -photon is very large, $h\nu \gg m_0c^2$ the separation becomes 256 keV [16].

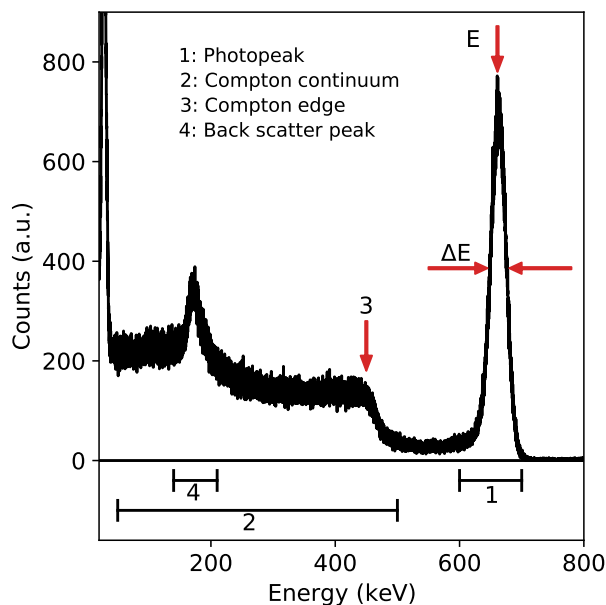


Figure 1: Example of a pulse height spectrum of a commercial $\text{LaBr}_3:\text{Ce}^{3+},\text{Sr}^{2+}$ crystal mounted on a photomultiplier tube (scintiblock 25 S 25 Bril 380 coupled to a AS 20 Saint-Gobain Crystals & Detectors) recorded using the 662 keV γ -photons of ^{137}Cs .

The third feature that can be observed is the backscatter peak, labelled 4 in Figure 1. This peak results from the detection of scattered γ -photons from a Compton scattering event in the material surrounding the scintillator. For excitation with 662 keV γ -photons, the back scatter peak is located at 184 keV. This is equal to the spacing between the photopeak and the Compton edge. It is the smallest amount of energy the scattered γ -photons can retain when the maximum amount of energy is transferred to the primary electron. In fact, the backscatter peak is actually a Compton spectrum extending to higher energies, overlapping with the Compton edge present due to γ -photons scattering in the scintillator.

Two of the most important properties that can be obtained from a pulse height spectrum are the light yield of the scintillator and its energy resolution. The light yield of a scintillator corresponds to the number of scintillation photons produced per unit of deposited energy, *i.e.* photons/MeV or photons/keV. It can be calculated based on the position of the photopeak [26]. The energy resolution of a scintillator can be calculated according to Equation 1.

$$R = \frac{\Delta E}{E} \cdot 100\% \quad (1)$$

Here ΔE represents the full width at half maximum of the photopeak and E its position.

Next to the light yield and energy resolution there are many more material properties that are important for the performance of a scintillator:

- Proportionality of the light yield
- Emission wavelength
- Decay time
- Afterglow
- Density
- Effective atomic number
- Intrinsic activity
- Radiation hardness
- Crystal structure
- Material cost

The importance of these properties will change depending on the application of the scintillation detector. Hence, it is more effective to design a scintillator for a specific application instead of developing a perfect scintillator. The trivial exercise of imagining the impact of the "perfect" scintillator on the world is left to the reader.

4. A Theoretical Approach

The energy resolution of a scintillation detector can be broken down into three contributions, as shown in Equation 2 [27–30] .

$$R^2 = R_{\text{stat}}^2 + R_{\text{np}}^2 + R_{\text{in}}^2 \quad (2)$$

Here R_{stat} represents the standard deviation in the number of detected scintillation photons (N_{dp}) and R_{np} the contribution of the non-proportionality of the scintillator. All other contributions like non-uniform dopant distributions and light collection efficiency are summarised in R_{in} . The dependence of R_{stat} on N_{dp} is given in Equation 3 and is a characteristic of the detection system, the combination of both scintillator and photodetector.

$$R_{\text{stat}} \propto 2.35 \cdot \sqrt{\frac{1}{N_{\text{dp}}}} \quad (3)$$

The statistical limit of the energy resolution can only be reached when the other contributions, R_{np} and R_{in} , are negligible. The current record energy resolution of 2%, measured by Alekhin *et al.* in 2013, was measured using $\text{LaBr}_3:\text{Ce}^{3+}, \text{Sr}^{2+}$ [32].

This value approaches the statistical energy resolution of 1.5%, calculated based on the detection of 24.000 photons from a scintillation pulse originating from the photopeak. This means that the contributions of R_{np} and R_{in} are very small and that the energy resolution is mainly determined by the number of detected photons.

The 2% energy resolution of $\text{LaBr}_3:\text{Ce}^{3+},\text{Sr}^{2+}$ can only be surpassed when the number of detected scintillation photons is increased. This can be done in one of two ways. Either by increasing the detection efficiency of the photodetector or by developing scintillators with higher light yields. Scintillation photons are usually detected with a photomultiplier tube which has a typical detection efficiency lower than 40%. Higher detection efficiencies can be reached when switching to an avalanche photodiode or silicon photomultipliers which compared to a photomultiplier tube will have their own challenges and problems that need to be dealt with.

The theoretical maximum number of scintillation photons created upon absorption of γ -photons with energy E_γ can be estimated according to Equation 4.

$$N_{dp} = \frac{1,000,000}{\beta E_g} \quad (\text{photons / MeV}) \quad (4)$$

Here, E_g represents the band gap of the scintillator. The factor β takes into account the momentum conservation of electron-electron interactions and can be taken to be approximately 2.5 [31].

Equation 4 can be used to plot the theoretical limit of the light yield as function of the bandgap. This curve is shown in Figure 2, indicated by the dashed black line, with β taken to be 2.5. Additionally, data points are plotted of the experimentally determined light yield of several scintillators. The experimentally determined light yield of some scintillators fall in close proximity to the dashed line, reaching their maximum attainable light yield. Three examples of such compounds are $\text{LaBr}_3:\text{Ce}^{3+},\text{Sr}^{2+}$ [32], $\text{SrI}_2:\text{Eu}^{2+}$, and $\text{CsBa}_2\text{I}_5:\text{Eu}^{2+}$ [33] for which light yields of 70.000, 90.000, and 80.000 photons/MeV have been reported. The light yield of these compounds could in theory be surpassed by developing new scintillators with bandgaps smaller than 5 eV

At this point you, the reader, will probably think something along the lines of: "That sounds very simple, you just have to find a new small bandgap material and dope it with either Ce^{3+} or Eu^{2+} ". If the reader is familiar with the art of science this will probably change to something along the lines of: "It cannot be this simple — their must be something else".

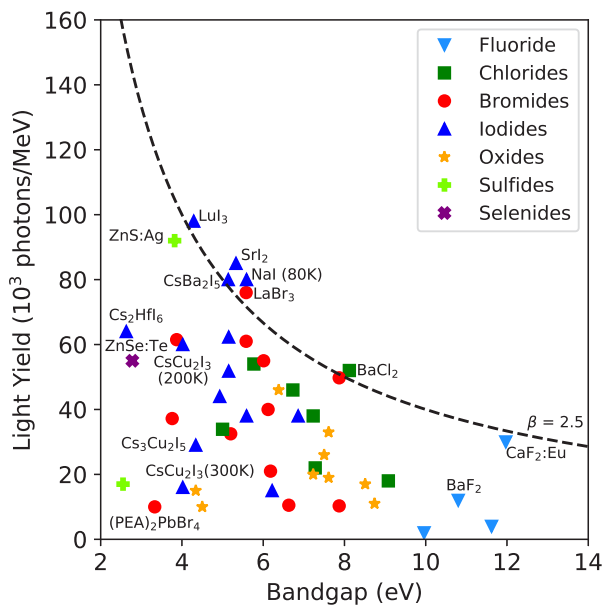


Figure 2: The theoretical limit of the light yield as function of the bandgap compared to the measured light yield of different scintillators.

5. The Nuances of Small Bandgap Scintillators

Since 1970 many scintillators have been developed based on the 5d- 4f emission of Ce^{3+} or Eu^{2+} , and in a lesser degree based on the 5d- 4f emission of Pr^{3+} , in halide based scintillators [27,35]. The degree to which the bandgap of a Ce^{3+} , Eu^{2+} , or Pr^{3+} doped scintillator can be reduced depends on the occurrence of the 5d- 4f emission. When the bandgap becomes too small, this type of emission will no longer be observed. There are two criteria, formulated by Dorenbos [28], that need to be satisfied in order to have efficient room temperature 5d- 4f emission. 1) the lowest energy 5d state needs to have sufficient spacing from the bottom of the conduction band. For Ce^{3+} and Eu^{2+} , the distance needs to be at least 410 and 490 meV, respectively [36]. 2) a Stokes' shift of at least 0.5 eV for the highest energy emission band in order to prevent self absorption. Based on these criteria Dorenbos predicted that the smallest bandgaps in which 5d- 4f emission is present at room temperature are approximately 3.5, 3.3, and 5.5 eV for Ce^{3+} , Eu^{2+} , and Pr^{3+} [28].

For halide based scintillators the size of the bandgap is constrained by the need to have sufficient spacing between the conduction band minimum compared to the lowest energy 5d state and the position of the valance band maximum. The positions of the valance band maxima (VBM) and conduction band minima (CBM) for several selected Cl^- , Br^- , and I^- compounds are shown in the stacked vacuum referred binding energy (VRBE) diagrams in Figure 3.

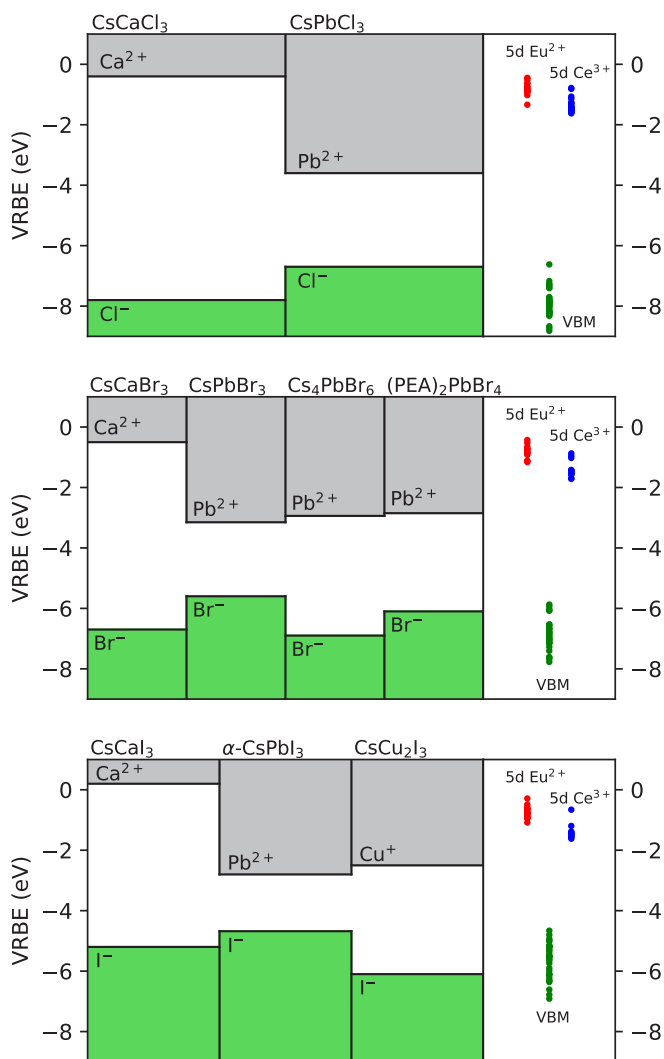


Figure 3: Stacked vacuum referred binding energy (VRBE) diagram of, from top to bottom, a selection of Cl^- , Br^- , and I^- based compounds, respectively. Next to each stacked VRBE a set of the lowest 5d level positions of Eu^{2+} and Ce^{3+} in materials with the same halogen composition is shown.

Next to each diagram three sets of data are shown. The green points indicate the spread of the position of the VBM among Cl^- , Br^- , and I^- compounds. The red and blue points represent the position of the lowest energy 5d level of Ce^{3+} , Eu^{2+} . The spread among these points is a direct result of the influence of crystal field splitting. The lowest energy 5d levels lay at approximately the same energy for Cl^- , Br^- , and I^- compounds [37].

From Figure 3 it can be observed that there is only a little spread in the position of the VBM among different Cl^- , Br^- , and I^- compounds. Upon comparing CsCaCl_3 , CsCaBr_3 , and CsCaI_3 it can be observed that the band gap tends to become smaller upon going from Cl^- to Br^- to I^- . The change in the bandgap in this case is mainly due to the upward shift of the VBM. Moreover, 5d- 4f emission of both Ce^{3+} and Eu^{2+} can be observed in these compounds because the emitting 5d level falls below the CBM. Upon comparing CsCaCl_3 and CsPbCl_3 the bandgap also changes significantly. However, the majority of the decrease in this case is due to the lowering of the conduction band minimum. This means that the required distance between the conduction band minimum and the lowest 5d level is no longer adequate; the 5d levels even lay within the conduction band and no emission is observed. Taking into account the minimal spacing needed between the conduction band minimum and the lowest 5d level, the smallest bandgap which still shows 5d- 4f emission is approximately 4 eV in iodide based compounds [38]. Further decreasing the bandgap, as explored by van Aarle [38], could potentially be achieved by shifting from halide based compounds to chalcogenide based compounds, like sulphites. Another approach is to develop small bandgap scintillators that no longer rely on 5d- 4f emission. In other words intrinsic, or self activated scintillators. Opening the marvellous world of small bandgap halide materials.

6. Research Objective and Dissertation Outline

The development of intrinsic small bandgap halide scintillators is a largely unexplored field. Small steps have been made by studying the scintillation properties of the lead halide perovskites *i.e.* CsPbX_3 and MAPbX_3 (MA = methylammonium and X = Cl, Br, I) [27]. The perovskite crystal structure, with stoichiometry ABX_3 , consists of a three dimensional network of corner sharing BX_6 octahedra. These compounds mainly gained popularity for their use in optoelectronic applications [39–41]. One of the main problems of these materials however is their small Stokes shift [42].

The scintillation properties and problems of CsPbBr_3 and CsPbCl_3 are explored in Chapter 2. Several potential solutions have been suggested to solve the small Stokes shift problem, for example shifting to lower dimension crystal structures or doping. The dimensionality of the crystal structure, in this case, refers to connectivity of the corner sharing BX_6 octahedra network. In Chapter 3, the scintillation properties of Cs_4PbBr_6 are explored. Compared to the perovskite crystal structure (ABX_3) Cs_4PbBr_6 has a zero dimensional crystal structure where the BX_6 octahedra are isolated and separated by the A cations. A comparison between the perovskite crystal structure and the crystal structure of Cs_4PbBr_6 is shown in Figure 4. This separation makes the optical behaviour of Cs_4PbBr_6 similar to the optical behaviour of isolated Pb^{2+} ions. In Chapter 4, the scintillation properties of $(\text{PEA})_2\text{PbBr}_4$ ((phenethylammonium) $_2\text{PbBr}_4$) are explored. In this hybrid organic-inorganic compound, the A cation of the perovskite crystal structure is replaced with a large organic molecule, a comparison of the molecular structure of

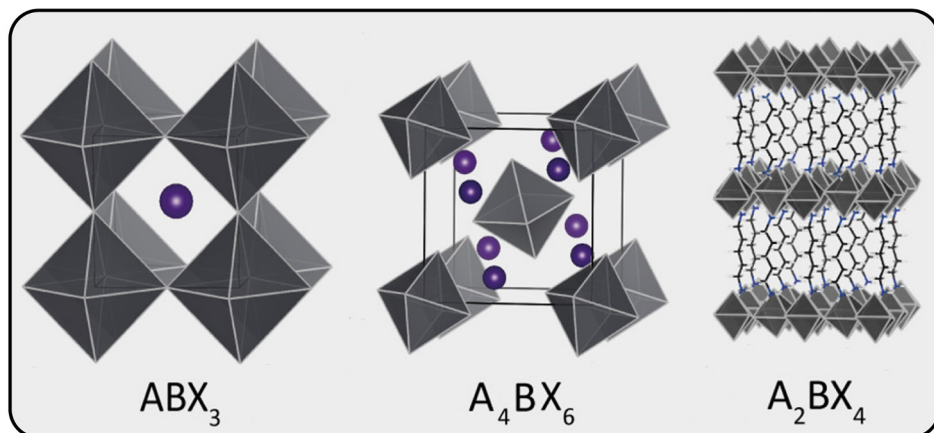


Figure 4: Comparison of, from left to right, the three dimensional perovskite crystal lattice, an example of the zero dimensional crystal lattice, and an example of a two dimensional crystal lattice of an organic inorganic hybrid compound. Adapted from Akkerman *et al.* [43].

PEA and MA is shown in Figure 5. This creates alternating layers of organic molecules and sheets of corner connected PbBr_6 octahedra, giving this material a two dimensional crystal structure, as shown in Figure 4. These materials often show fast room temperature near bandgap excitonic emission. In Chapter 5, the fast emission of the two dimensional organic-inorganic hybrid compound $(\text{BZA})_2\text{PbBr}_4$ ((benzylammonium) $_2\text{PbBr}_4$) is explored for its use in a scintillator- Silicon photon multiplier (SiPM) based photon counting detector (PCD). A comparison of the molecular structure of BZA and PEA is shown in Figure 5. Lead halide based compounds are not the only interesting intrinsic small bandgap compounds. In Chapter 6, the copper based compound CsCu_2I_3 is studied. It has a one dimensional crystal structure consisting of ribbons of copper iodide tetrahedra which are separated by caesium ions. This leads to the formation of self trapped excitons and emission with a large Stokes shift. In Chapter 7, the focus is shifted to the application of different scintillators in scintillator-SiPM based PCDs. In this chapter an overview of different classes of scintillators is presented in order to make a first assessment for their suitability to be used in a scintillator-SiPM based PCD.

Methylammonium (MA) Benzylammonium (BZA) Phenethylammonium (PEA)

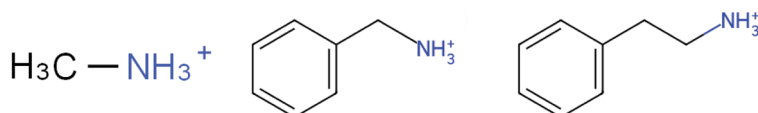


Figure 5: Comparison of the molecular structure of, from left to right, methylammonium, benzylammonium, and phenethylammonium.

References

- [1] G. F. Knoll, Radiation Detection and Measurement, Chapter 5 Ionisation Chambers, third edition (2000), ISBN 0-471-07338-5
- [2] G. F. Knoll, Radiation Detection and Measurement, Chapter 6 Proportional Counters, third edition (2000), ISBN 0-471-07338-5
- [3] G. F. Knoll, Radiation Detection and Measurement, Chapter 7 Geiger-Müller Counters, third edition (2000), ISBN 0-471-07338-5
- [4] G. F. Knoll, Radiation Detection and Measurement, Chapter 11 Semiconductor Diode Detectors, third edition (2000), ISBN 0-471-07338-5
- [5] A. Owens, A. Peacock, Nuclear Instruments and Methods in Physics Research Section A: Accelerators, Spectrometers, Detectors and Associated Equipment 531 (2004) 1-2, <https://doi.org/10.1016/j.nima.2004.05.071>
- [6] S. Kasap, J. B. Frey, G. Belev, O. Tousignant, H. Mani, J. Greenspan, L. Laperriere, O. Bubon, A. Reznik, G. DeCrescenzo, K. S. Karim, J. A. Rowlands, Sensors 11 (2021) 5112-5157, <https://doi.org/10.3390/s110505112>
- [7] M. Guerra, M. Manso, S. Longelin, S. Pessanha, M. L. Carvalho, Journal of Instrumentation 7 (2012) C10004, <https://doi.org/10.1088/1748-0221/7/10/C10004>
- [8] T. Yang, F. Li, R. Zheng, Materials Advances 6 (2021) 6744-6767, <https://doi.org/10.1039/D1MA00569C>
- [9] K. R. Dudipala, T.-H. Le, W. Nie, R. L. Z. Hoyer, Advanced Materials 36 (2024) 8, <https://doi.org/10.1002/adma.202304523>
- [10] L. Basirico, A. Ciavatti, B. Fraboni, Advanced Materials Technologies 6 (2021) 1, <https://doi.org/10.1002/admt.202000475>
- [11] A. Drescher, M. Yoho, S. Landsberger, M. Durbin, S. Biegalski, D. Meier, J. Schwantes, Applied Radiation and Isotopes 122 (2017) 116-120, <https://doi.org/10.1016/j.apradiso.2017.01.012>
- [12] F. Zhang, C. Herman, Z. He, G. De Geronimo, E. Vernon, J. Fried, IEEE Transactions on Nuclear Science 59 (2012) 1, <https://doi.org/10.1109/TNS.2011.2175948>
- [13] T. Flohr, M. Petersilka, A. Henning, S. Ulzheimer, J. Freda, B. Schmidt, Physica Medica 79 (2020) 126-136, <https://doi.org/10.1016/j.ejmp.2020.10.030>
- [14] U. N. Roy, G. S. Camarda, Y. Cui, R. Gul, A. Hossain, G. Yang, J. Zazvorka, V. Dedic, J. Franc, R. B. James, Scientific Reports 9 (2019) 1620, <https://doi.org/10.1038/s41598-018-38188-w>
- [15] M. Mutterer, Nuclear Instruments and Methods in Physics Research 196 (1982) 1, [https://doi.org/10.1016/0029-554X\(82\)90619-X](https://doi.org/10.1016/0029-554X(82)90619-X)

- [16] G. F. Knoll, Radiation Detection and Measurement, Chapter 10 Radiation Spectroscopy with Scintillators, third edition (2000), ISBN 0-471-07338-5
- [17] R. Hofstadter, Physical Review Journals Archive 74 (1948) 1, <https://doi.org/10.1103/PhysRev.74.100>
- [18] R. Hofstadter, Physical Review Journals Archive 75 (1949) 5, <https://doi.org/10.1103/PhysRev.75.796>
- [19] R. Hofstadter, J. A. McIntyre, Physical Review Journals Archive 80 (1950) 4, <https://doi.org/10.1103/PhysRev.80.631>
- [20] P. Lecoq, Nuclear Instruments and Methods in Physics Research Section A: Accelerators, Spectrometers, Detectors and Associated Equipment 809 (2016) 130-139, <https://doi.org/10.1016/j.nima.2015.08.041>
- [21] P. Lecoq, I. Dafinei, E. Auffray, M. Schneegans, M. V. Korlzhik, O. V. Missevitch, V. B. Pavlenko, A. A. Fedorov, A. N. Annenkov, V. L. Kostylev, V. D. Ligon, Nuclear Instruments and Methods in Physics Research Section A: Accelerators, Spectrometers, Detectors and Associated Equipment 365 (1995) 2-3, [https://doi.org/10.1016/0168-9002\(95\)00589-7](https://doi.org/10.1016/0168-9002(95)00589-7)
- [22] W. W. Moses, Nuclear Instruments and Methods in physics Research Section A: Accelerators, Spectrometers, Detectors and Associated Equipment 487 (2002) 1-2, [https://doi.org/10.1016/S0168-9002\(02\)009555](https://doi.org/10.1016/S0168-9002(02)009555)
- [23] C. L. Melcher, Nuclear Instruments and Methods in Physics Research Section A: Accelerators, Spectrometers, Detectors and Associated Equipment 537 (2005) 1-2, <https://doi.org/10.1016/j.nima.2004.07.222>
- [24] F. G. A. Quarati, LaBr₃ gamma-ray spectrometers for space Application, ISBN 9789088915642, <https://doi.org/10.4233/uuid:7d1f7672-5d97-4b32-9c44-ad0bcc259b82>
- [25] G. F. Knoll, Radiation Detection and Measurement, Chapter 2 Radiation interactions, third edition (2000), ISBN 0-471-07338-5
- [26] J. T. M. De Haas, P. Dorenbos, IEEE Transactions on Nuclear Science 53 (2008) 3, <https://doi.org/10.1109/TNS.2008.922819>
- [27] P. Dorenbos, Optical Materials: X 1 (2019) 100021, <https://doi.org/10.1016/j.omx.2019.100021>
- [28] P. Dorenbos, IEEE Transactions on Nuclear Science 57 (2010) 3, <https://doi.org/10.1109/TNS.2009.2031140>
- [29] P. Dorenbos, J. T. M. de Haas, C. W. E. van Eijk, IEEE Transactions on Nuclear Science 42 (1995) 6, <https://doi.org/10.1109/23.489415>
- [30] M. Moszynski, Nuclear Instruments and Methods in Physics Research Section A: Accelerators, Spectrometers, Detectors, and Associated Equipment, 505 (2003) 101-110, [https://doi.org/10.1016/S01689002\(03\)01030-1](https://doi.org/10.1016/S01689002(03)01030-1)

- [31] P. A. Rodnyi, P. Dorenbos, C. W. E. van Eijk, *basic solid state physics* 187 (1995) 15, <https://doi.org/10.1002/pssb.2221870102>
- [32] M. S. Alekhin, J. T. M. de Haas, I. V. Khodyuk, K. W. Krämer, P. R. Menge, V. Ouspenski, P. Dorenbos, *Applied physics letters* 102 (2013) 161915, <https://doi.org/10.1063/1.4803440>
- [33] M. S. Alekhin, D. A. Biner, K. W. Krämer, P. Dorenbos, *Journal of Luminescence* 145 (2014) 723-728, <http://dx.doi.org/10.1016/j.jlumin.2013.08.058>
- [34] Y. Wu, Q. Li, D. J. Rutstrom, I. Greeley, L. Stand, M. Loyd, M. Koschan, C. L. Melcher, *Nuclear Inst. and Methods in Physics Research, A*, 954 (2020) 161242, <https://doi.org/10.1016/j.nima.2018.09.077>
- [35] M. J. Weber, *Journal of Luminescence* 100 (2002) 1-4, [https://doi.org/10.1016/S0022-2313\(02\)00423-4](https://doi.org/10.1016/S0022-2313(02)00423-4)
- [36] P. Dorenbos, *Journal of Materials Chemistry C* 11 (2023) 8129, <https://doi.org/10.1039/D2TC04439K>
- [37] P. Dorenbos, A. Josef, J. T. M. de Haas, K. W. Krämer, *Journal of Luminescence* 208 (2019) 463-467, <https://doi.org/10.1016/j.jlumin.2019.01.009>
- [38] C. van Aarle, Chapter 7, *Black scintillators*, thesis Delft University of Technology (2024), ISBN: 978-94-6366-873-6, <http://resolver.tudelft.nl/uuid:37091b0a-1a34-4213-a2f1-4a883d4da721>
- [39] M. A. Green, A. Ho-Naillie, H. J. Snaith, *Nature Photonics* 8 (2014) 506, <https://doi.org/10.1038/nphoton.2014.134>
- [40] X. Y. Chin, D. Cortecchia, J. Yin, A. Bruno, C. Soci, *Nature Communications* 6 (2015) 7383, <https://doi.org/10.1038/ncomms8383>
- [41] L. Dou, Y. M. Yang, J. You, Z. Hong, W.-H. Chang, G. Li, Y. Yang, *Nature Communications* 5 (2014) 5404, <https://doi.org/10.1038/ncomms6404>
- [42] R. T. Williams, W. W. Wolszczak, X. Yan, D. L. Carrol, *ACS Nano* 14 (2020) 5161-5169, <https://doi.org/10.1021/acsnano.0c02529>
- [43] Q. A. Akkerman, L. Manna, *ACS Energy Letters* 5 (2020) 2, <https://doi.org/10.1021/acsenergylett.0c00039>

2

— 2 —

The Temperature Dependent Optical and Scintillation Characterisation of Bridgman Grown CsPbX_3 ($\text{X} = \text{Br}, \text{Cl}$) Single Crystals

Abstract

Lead halide perovskites are reportedly a very promising group of materials for scintillation due to their fast sub-nanosecond exciton luminescence, small bandgaps, and high theoretical light yield. Unfortunately, they only show emission at cryogenic temperatures. In this work single crystals of CsPbBr_3 and CsPbCl_3 are studied at cryogenic temperatures. Upon comparing the 10 K emission spectra measured under X-ray and UV-vis excitation, a new near-infrared emission was found for both CsPbBr_3 and CsPbCl_3 only present under X-ray excitation. The integral light yields of CsPbBr_3 and CsPbCl_3 at 10 K are estimated to be 34,000 and 2,200 photons/MeV under 40 keV X-ray excitation, respectively. The main components of the light yield of CsPbBr_3 at 10 K are the near bandgap free exciton emission that suffers from self-absorption and the broad near-infrared emission that falls outside the typical detection range of a photomultiplier tube. Due to the combination of the two aforementioned effects it was not possible to measure a γ -ray pulse height spectrum for CsPbBr_3 at 10 K. Despite all the suitable properties, like the fast decay, a small bandgap, and the positive prospects of 3D perovskite based scintillators, we conclude that these materials perform poorly as scintillation crystals

The content of this chapter is based on: J. Jasper van Blaaderen, Daniel Biner, Karl W. Krämer, Pieter Dorenbos, Nuclear Instruments and Methods in Physical Research Section A: Accelerators, Spectrometers, Detectors and Associated Equipment 1064 (2024) 169322

1. Introduction

Lead based halide perovskites are studied and used in many different optoelectronic applications [1–3]. Due to their fast excitonic emission, perovskites [4,5] and perovskite related compounds [6–10] gained interest in the field of scintillation. A clear distinction should be made between true perovskites and perovskite related compounds, as elaborately discussed by Akkerman and Manna [11]. The small bandgap of these materials, around 3 eV, significantly increases their theoretical maximum light yield compared to traditional scintillators [4,12,13]. Based on Equation (1), the maximum possible light yield is estimated around 130,000 photons/MeV.

$$N_{eh} = \frac{1,000,000}{\beta E_g} \quad (\text{e}^- \text{ - h}^+ \text{ pairs / MeV}) \quad (1)$$

Here N_{eh} represents the number of electron-hole pairs created in the scintillator, β is taken to be ≈ 2.5 , and E_g represents the bandgap. Lead halide perovskites differ from traditional impurity activated scintillators [12,14–17], by being intrinsic scintillators. Perovskites are defined by an ABX_3 stoichiometry, consisting of a three dimensional corner sharing network of BX_6 octahedra. Often they have been studied in the form of thin films and nanocrystals [18–20].

Lead halide perovskites, both organic-inorganic and completely inorganic compounds, have also been explored for their use in direct radiation detection [21–26]. In this application, the energy deposited by X-rays and γ -photons is converted into a charge pulse. For indirect detection, or scintillation, the energy deposited by X-rays and γ -photons is first converted into a pulse of light. This requires the use of single crystalline materials.

Unfortunately, perovskites show no room temperature emission, which is ascribed to thermal quenching of the exciton luminescence and a small Stokes shift [27–29]. Williams *et al.* [27] and Wolszczak *et al.* [28] have proposed several strategies to overcome these problems at room temperature. Examples are using nano materials, doping bulk crystals with activator ions, or utilising the formation of self trapped excitons in lower dimensional compounds. The difference between lower dimensional and nano-structured perovskites is discussed elaborately by Zhou *et al.* [30].

Another approach to utilise the small bandgap and fast exciton luminescence of perovskites for scintillation is to operate the detector system at cryogenic temperatures. This approach has been explored by Mykhaylyk *et al.* using CsPbBr_3 and CsPbCl_3 [5,31]. These inorganic compounds have a higher X-ray absorption and better chemical stability compared to their organic-inorganic counterparts used for direct detection. Mykhaylyk *et al.* performed low temperature X-ray excited emission and decay measurements, focusing on the fast excitonic emission [5,31].

In this work, single crystals of the inorganic perovskites CsPbBr_3 (4.57 g/cm^3) and CsPbCl_3 (4.21 g/cm^3) are characterised as function of temperature using a combination of X-ray excitation and UV-vis excitation techniques. Both exhibit an orthorhombic GdFeO_3 -type perovskite structure with corner-sharing $\text{PbX}_{6/2}$ octahedra at room temperature and down to 4 K [32,33]. In contrast, CsPbI_3 adopts an orthorhombic $(\text{NH}_4)\text{CdCl}_3$ -type structure with edge-sharing octahedra at room temperature [34]. Hence only the bromide and chloride based caesium lead perovskites are studied. The goal of this work is to develop a better understanding of the low temperature scintillation and optical properties of CsPbBr_3 and CsPbCl_3 single crystals grown from the melt.

2. Results

Figure 1a shows the photoluminescence and X-ray excited emission spectra of CsPbBr_3 measured at 10 K. The photoluminescence spectrum contains three bands at 535, 544, and 568 nm. These bands were also observed by Nitsch *et al.* and Dendebera *et al.* for melt grown CsPbBr_3 single crystals [35,36]. The 535 nm peak can be assigned to free exciton emission [36–40]. The origin of the 544 nm shoulder peak and 568 nm peak is still under debate. Explanations range from bound exciton emission, indirect radiative transitions from a Rashba minimum, donor-acceptor emission, to self trapped exciton emission [35,41–45].

The 10 K X-ray excited emission spectrum of CsPbBr_3 contains four peaks at 538, 555, 580, and 925 nm. The 538 nm peak is assigned to free exciton emission [5,37–40]. The origin of the 555 and 580 nm emissions, similar to the 544 and 568 nm emissions in the photoluminescence spectrum, is still under debate [35,43–45].

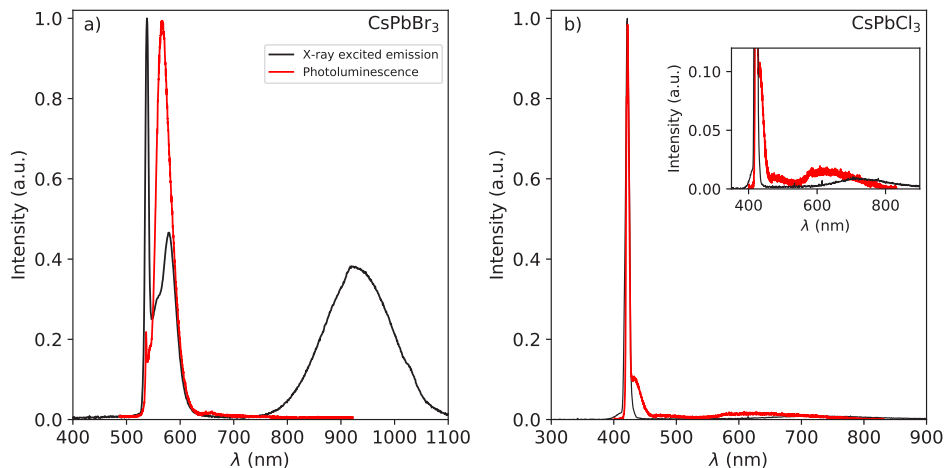


Figure 1: (a) X-ray excited emission (black line) and photoluminescence emission (red line, $\lambda_{\text{ex}} = 310 \text{ nm}$ (4 eV)) of CsPbBr_3 at 10 K. (b) X-ray excited emission (black line) and photoluminescence emission (red line, $\lambda_{\text{ex}} = 354 \text{ nm}$ (3.5 eV)) of CsPbCl_3 at 10 K. The inset shows a zoom in of both spectra.

The presence and intensity of these emission peaks strongly depend on the used synthesis method, like whether it is grown from solution or from the melt [46,47]. The broad band 925 nm emission is only observed under X-ray excitation and has never been reported before.

Figure 1b shows the photoluminescence and X-ray excited emission spectra of CsPbCl_3 measured at 10 K. The photoluminescence spectrum contains a sharp peak at 420 nm and a broad band around 625 nm. Peters *et al.*, Sebastian *et al.*, and Nikl *et al.* have suggested that the 420 nm peak is related to bound exciton emission [40,48,49]. On the long wavelength side of the 420 nm peak, a shoulder centred around 435 nm is observed. It is ascribed to trapped exciton emission [31,48]. The 625 nm emission peak is ascribed to defect related emission [50,51]. Kobayashi *et al.* observed that the yellow colour of the crystals correlates with the intensity of the 625 nm band [50].

The 10 K X-ray excited emission spectrum of CsPbCl_3 contains a single sharp peak at 422 nm and a broad band at 710 nm. Similarly to the 420 nm emission observed in the photoluminescence spectrum, the 422 nm emission is attributed to bound exciton emission [40,48]. The shift of the 625 nm emission observed under UV-vis excitation to 710 nm under X-ray excitation has not been observed before.

To further study the new near infrared emissions observed under X-ray excitation, a series of photoluminescence emission spectra were recorded using excitation energies ranging from 3 to 10 eV at 10 K. The respective spectra for CsPbBr_3 and CsPbCl_3 are shown in Figure 2a and 2b. The reported bandgaps of CsPbBr_3 and CsPbCl_3 are 2.4 and 3 eV, respectively [57–59]. Hence the lowest excitation energy excites electrons just above the conduction band edge, while the highest excitation energy excites electrons far into the conduction band. The broad near infrared emission bands observed under X-ray excitation are absent within this excitation energy range.

The temperature dependent X-ray excited emission spectra and the respective quenching curves of the integrated peak intensities of CsPbBr_3 are shown in Figure 3a and 3b. The 538, 555, and 580 nm emissions undergo strong thermal quenching below 100 K. The intensity of the 925 nm emission increases upon heating from 10 K, reaching its maximum at 60 K. Above 60 K the emission starts to quench. Based on the quenching curves, shown in Figure 3b, the temperatures (T_{50}) at which the intensity drops below 50 % of the maximum intensity are determined. T_{50} values of 35, 25, 25, and 135 K were determined for the 538, 555, 580, and 925 nm emissions, respectively. The relative contributions of the different emissions to the total intensity at 10 K under X-ray excitation are determined to be 1, 0.7, 1.7, and 7.6 for the 538, 555, 580, and 925 nm emissions, respectively.

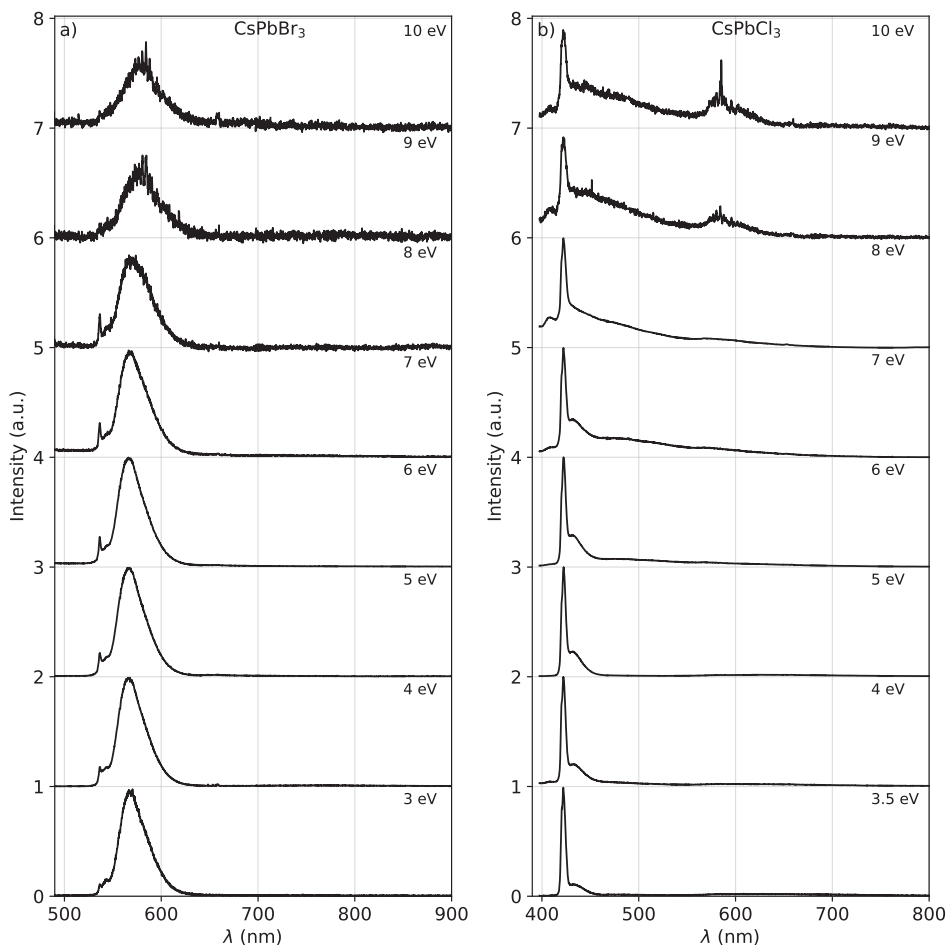


Figure 2: (a) Photoluminescence emission spectra of CsPbBr_3 at 10 K recorded using excitation energies from 3 to 10 eV. (b) Photoluminescence emission spectra of CsPbCl_3 at 10 K recorded using excitation energies from 3.5 to 10 eV.

The temperature dependent X-ray excited emission spectra and quenching curves of the integrated peak intensities of CsPbCl_3 are shown in Figure 3c and 3d. The 422 nm emission shows strong thermal quenching below 100K. The intensity of the 710 nm emission shows similar behaviour as the 925 nm emission observed in CsPbBr_3 . Its intensity increases upon heating from 10 K, reaching its maximum at 75 K. Above this temperature the emission starts to quench. Based on the quenching curves, shown in Figure 3d, T50 values of 45 and 105 K were determined for the 422 and 710 nm emissions, respectively. The relative contributions of the 422 and 710 nm emissions to the total intensity at 10 K under X-ray excitation were determined to be 1 and 0.28, respectively.

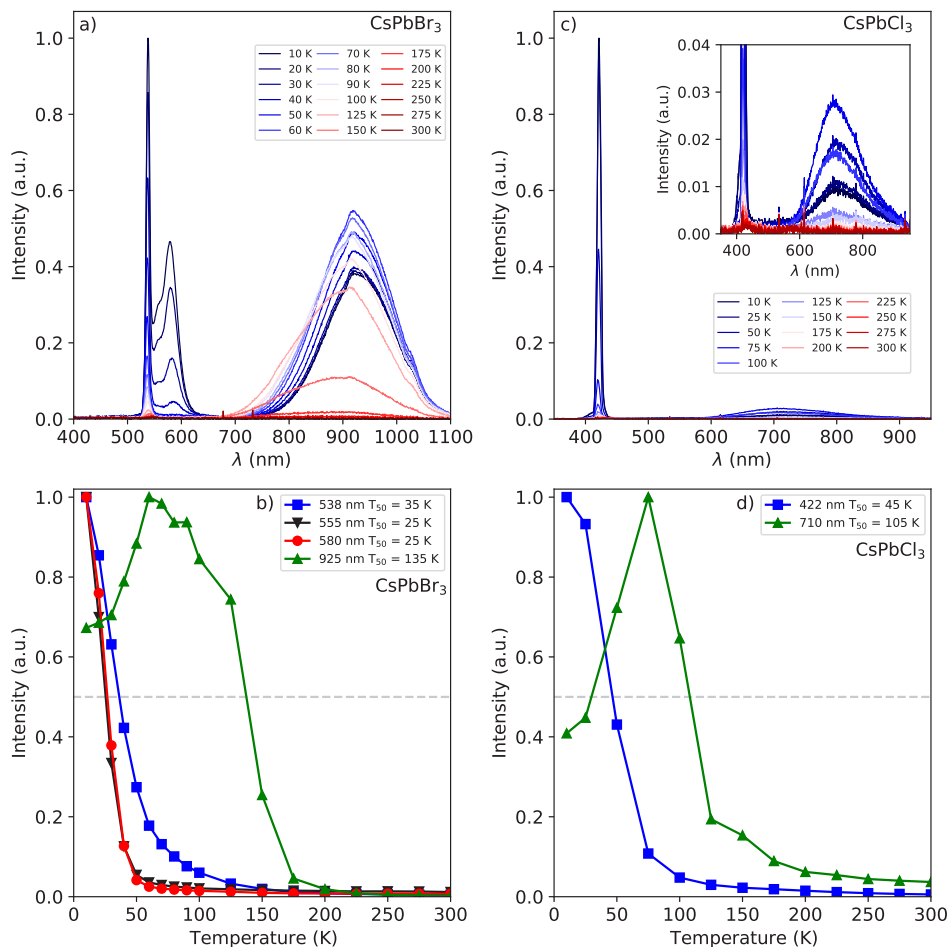


Figure 3: (a) Temperature dependent X-ray excited emission spectra of CsPbBr₃ measured from 10 to 300 K. (b) Temperature dependent integrated emission intensities of the 538 nm, 555 nm, 580 nm, and 925 nm emissions of CsPbBr₃. (c) Temperature dependent X-ray excited emission spectra of CsPbCl₃ measured from 10 to 300 K. (d) Temperature dependent integrated emission intensities of the 422 nm and 710 nm emissions of CsPbCl₃.

The temperature dependent pulsed X-ray excited decay curves of the 538 nm emission of CsPbBr₃ are shown in Figure 4a. Upon heating from 10 to 75 K, the decay time decreases from 440 to 330 ps. This matches with the measurements presented by Mykhaylyk *et al.* [5]. The decay curves shown in Figure 4b were recorded by placing a 550 nm long pass filter in front of the detector. Now the decay curve shows two components. The fast component is an artefact from part of the 538 nm emission leaking through the long pass filter. The slow component, with a life time of 36 ns, results from both the 555 and 580 nm emissions. The life time of these emissions decreases to 22.5 ns at 25 K.

The temperature dependent pulsed X-ray excited decay curves of the 422 nm emission of CsPbCl_3 are shown in Figure 4c. From 10 to 25 K the decay time increases slightly from 440 to 460 ps. Upon heating from 25 to 75 K the decay time decreases to 260 ps. A similar trend is observed in the quenching curves shown in Figure 3d. This behaviour matches the measurements presented by Mykhaylyk *et al.* [31].

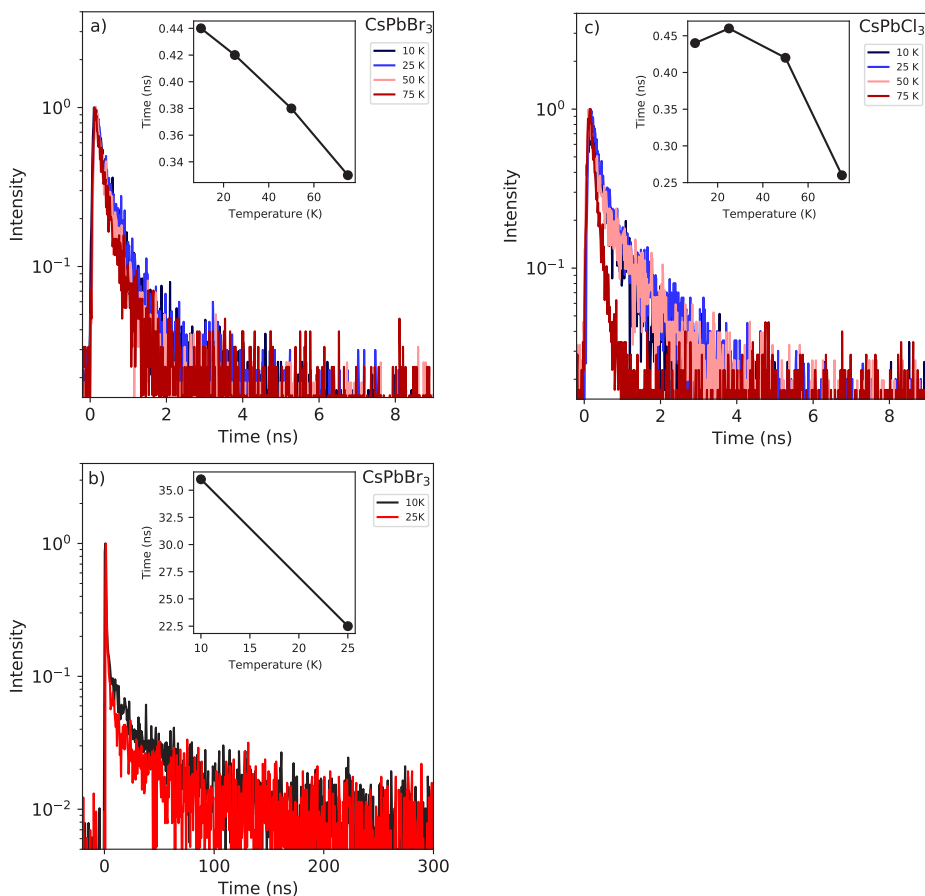


Figure 4: (a) Temperature dependent pulsed X-ray excited decay curves of the 538 nm emission of CsPbBr_3 between 10 and 75 K. The inset shows the temperature dependent change of the life time. (b) Temperature dependent pulsed X-ray excited decay curves of CsPbBr_3 in which the 538 nm emission is filtered out by placing a 550 nm long pass filter in front of the detector. The inset shows the temperature dependent change of the life time. (c) Temperature dependent pulsed X-ray excited decay curves of the 422 nm emission of CsPbCl_3 between 10 and 75 K. The inset shows the temperature dependent change of the life time.

3. Discussion

Upon exciting CsPbBr_3 and CsPbCl_3 with X-rays, as shown in Figure 1a and 1b, near infrared emissions are observed at 925 nm and 710 nm, respectively. These emissions are not present under UV-vis excitation, even upon using excitation energies of 3 to 4 times the bandgap energy. Upon excitation with an X-ray photon all energy is transferred to an electron. This so called primary electron subsequently excites secondary electrons, via electron-electron interactions. This creates spatially separated electrons and holes, originating from states deep in the conduction and valence band, that need to meet each other to form electron-hole pairs. The free electrons, created under X-ray excitation, have a larger mobility compared to holes and diffuse further away from the initial ionisation track [52–55]. Moreover, X-rays create excitations in the bulk of the crystal. Upon excitation with UV-vis photons however, electron-hole pairs, or excitons, are formed directly. The resulting exciton formation happens on a shorter time scale compared to the recombination of spatially separated electrons and holes. The excitons, upon excitation with UV-vis photons, are created close to the surface of the crystal.

Based on the different excitation mechanisms described above two potential explanations can be formulated for the origin of the near infrared emissions based on the transport of the spatially separated electrons and holes. The free holes have sufficient lifetime to be trapped on a F centre or to self-trap. F centres are colour centres where an electron is trapped on a halide vacancy. After capturing a hole a F^+ centre is created. Sequentially the F^+ centre can trap a conduction band electron to form an excited F centre that emits a photon.

The other potential origin of the near-infrared emissions is self-trapping. This is an intrinsic effect where a free hole first forms a V_k centre. A conduction band electron can then recombine with the V_k centre to form a self-trapped exciton (STE) [56]. The 710 and 925 nm emissions observed under X-ray excitation of CsPbCl_3 and CsPbBr_3 have a full width at half maximum of 0.42 and 0.21 eV, respectively. Based on the respective bandgaps, 2.4 and 3 eV, the Stokes shifts are determined to be 1.25 and 1.06 eV [57–59]. These are typical values for both F-centre emission and STE emission [60,61].

We estimated the scintillation light yields of CsPbBr_3 and CsPbCl_3 at 10 K by comparing the intensity of their X-ray excited emission spectra, measured using an average X-ray energy of 40 keV, to that of CsCu_2I_3 [10]. The estimated integral scintillation light yields were determined to be 34,000 and 2,200 photons/MeV for CsPbBr_3 and CsPbCl_3 , respectively. These numbers are much lower than the theoretical maxima of 166,000 and 133,000 photons/MeV estimated based on the bandgaps of CsPbBr_3 and CsPbCl_3 with Equation 1, respectively. The contributions from the different emission to the total estimated light yields are calculated based on the relative intensities in Figure 1, as summarised in Table I. The estimated light yield of CsPbCl_3 at 10 K is approximately 1.3% of its calculated maximum theoretical value. The main contribution is from its 422 nm

Table I: Summary and comparison of the relative intensity of the emissions observed under X-ray excitation and their respective contributions to the total light yield at 10 K for CsPbBr₃ and CsPbCl₃.

		Relative intensity	Light yield Photons/MeV	
CsPbBr ₃	538 nm	1	3,100	Self-Absorption
	555 nm	0.7	2,200	Useful yield
	580 nm	1.7	5,200	Useful yield
	925 nm	7.6	23,500	Outside PDE PMT
	All		34,000	
	Theoretical		166,000	
CsPbCl ₃	422 nm	1	1,700	Self-Absorption
	710 nm	0.28	500	Outside PDE PMT
	All		2,200	
	Theoretical		133,000	

emission. For CsPbBr₃ the estimated light yield at 10 K is approximately 25.5% of its calculated maximum theoretical value. The main contribution is from its 925 nm emission. Both compounds have also been used to measure 662 keV γ -photon excited pulse height spectra at 10 K; a 662 keV photopeak could not be distinguished from the background.

The estimated light yields summarised in Table I were determined based on the X-ray excited emission spectra using an average X-ray energy of 40 keV. The calculated attenuation length for 40 keV photons in CsPbCl₃ and CsPbBr₃ are approximately 250 μ m. The 662 keV γ -photon used in the pulse height measurement on the other hand excite the bulk of the crystal.

Mykhaylyk *et al.* reported light yields of 109.000 and 47.000 photons/MeV for CsPbBr₃ and CsPbCl₃ at 7 K, respectively [5,31]. These numbers were estimated by comparing a pulse height spectrum, recorded under alpha excitation of ²⁴¹Am at 7K, of CsPbBr₃ and CsPbCl₃ to that of LYSO. The later has a light yield of 34.000 photons/MeV under γ -ray excitation. However, under α excitation LYSO is much less efficient. With an α/β ratio of 0.14, from Wolszczak *et al.* [62], an α -particle light yield of 4,760 photons/MeV occurs. This aspect was not taken into account by Mykhaylyk *et al.* [5,31]. The α/β ratio and proportionality of CsPbBr₃ and CsPbCl₃ is also not known. Mykhaylyk *et al.*, in their publication on CsPbBr₃, also estimated the light yield in a similar way as presented in this work, reporting 50.000 photons/MeV [5].

The 10 K X-ray excited emission spectra of both compounds, combined with the typical photo-detection efficiency curve of a photo-multiplier tube (PMT), are shown in Figure 5. The detection efficiency of the PMT drops below 2% at wavelengths longer than 620 nm. This means that the 925 nm emission of CsPbBr₃ falls completely outside the detection range, drastically decreasing the number of photons available for detection. The 710 nm emission of CsPbCl₃ only partial-

ly falls within the low side of detection efficiency. The other emissions, for both compounds, fall within the detection range of the PMT. However, as discussed by Williams *et al.* [27] and Wolszczak *et al.* [28], the exciton emissions close to the bandgap suffer from self-absorption. The bandgaps of both materials with respect to their emissions are represented in Figure 5 by the vertical dashed lines. Only the 555 and 580 nm emissions from CsPbBr_3 have a potentially useful contribution to the light yield. However, as shown in Figure 5, they emit in the spectral region where the PDE drops below 10%. In total these emissions contribute approximately 7.000 photons/MeV, corresponding with less than 350 detected photons/MeV. This number is further reduced by the presence of tail states, as shown in the room temperature absorbance spectra in Figure S1, and large penetration depth of 662 keV γ -photons increasing the chance of re-absorption. Due to the geometric restrictions needed to perform the measurement at 10 K, the sample could not be mounted directly on the entrance window of the PMT, reducing the light collection efficiency. The absence of a pulse height spectrum at 10 K is thus ascribed to a combination of self-absorption related problems, emission falling outside the PMT detection range, and sub-optimal experimental conditions.

It has been suggested by Stoumpos *et al.* that the defect related emissions on the long wavelength side of the free exciton emission could be suppressed by growing these materials from solution instead of the melt [46,47]. However, this will not solve any self-absorption related problems of the free exciton emissions [63]. The near infrared emissions, if originating from F-centres might also be

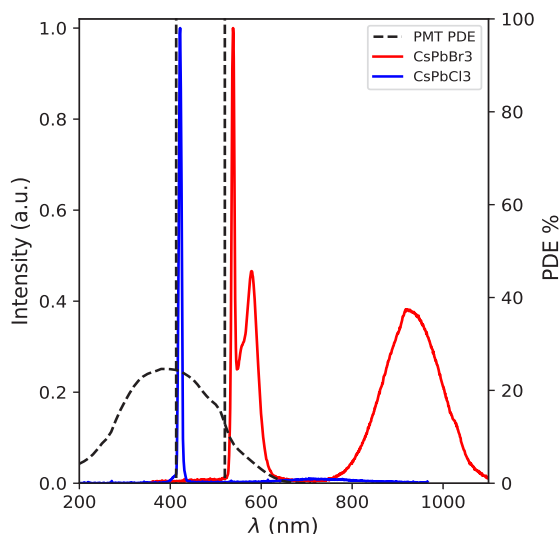


Figure 5: X-ray excited emission spectra of CsPbCl_3 (blue) and CsPbBr_3 (red) measured at 10 K compared to the detection efficiency of a Hamamatsu Super Bialkali R6231-100 (SN ZE4500) (black dashed line). The vertical black dashed lines at 413 nm (3 eV) and 520 nm (2.4 eV) represent the bandgaps of CsPbCl_3 and CsPbBr_3 , respectively.

suppressed when crystals are produced from solution. Self-trapping however, is an intrinsic effect and will thus not be influenced. Similar problems should be expected for the organic-inorganic methylammonium based perovskites, $\text{CH}_3\text{NH}_3\text{PbX}_3$ ($\text{X} = \text{Cl}, \text{Br}, \text{I}$) which show similar near band-edge emission as the completely inorganic perovskites. Scintillation characterisations have been performed on $\text{CH}_3\text{NH}_3\text{PbBr}_3$ [64,65]. Li *et al.* demonstrated that $\text{CH}_3\text{NH}_3\text{PbBr}_3$ also shows self-absorption related problems, thus performing poorly as a scintillator crystal [65].

4. Conclusion

In this work, the inorganic perovskites CsPbBr_3 and CsPbCl_3 have been studied under X-ray and UV-vis excitation at cryogenic temperatures. Upon comparing the emission spectra measured at 10K using the different excitation methods, new broad near-infrared emissions were discovered in both compounds. Based on the peak width, large Stokes shift, and red shift of the emission when going from CsPbCl_3 to CsPbBr_3 it is suggested that it originates from F-centres or self trapping. Both compounds show fast exciton related emissions of approximately 450 ps at 10 K. For CsPbBr_3 an additional 36 ns component was measured related to the 555 nm and 580 nm emissions. The light yields of CsPbBr_3 and CsPbCl_3 were estimated to be 34,000 and 2,200 photons/MeV. In CsPbBr_3 , the major part of the light yield is emitted in the 925 nm emission band, which falls outside the detection range of a typical photo-multiplier tube. The other emissions suffer from self-absorption. Hence no pulse height spectrum was observed under 662 keV γ -photon excitation at 10 K.

5. Experimental

CsPbCl_3 and CsPbBr_3 crystals were grown from stoichiometric amounts of the binary halides in sealed silica ampoules by the vertical Bridgman technique. CsCl (Alfa, 5N) and CsBr (Fluka, >99.5%) were dried in high vacuum at 200°C. PbCl_2 and PbBr_2 (both Alfa, 5N) were sublimed in a silica apparatus under high vacuum for purification at 480°C and 375°C, respectively. Typical batch size was 5 g. The powder was molten up at 30 K above the congruent melting point of CsPbCl_3 at 615°C and CsPbBr_3 at 570°C, respectively. The temperature was kept for one day and then the crystal growth was started. The furnace was moved upwards by ca. 15 mm/day; samples reached room temperature in about 10 days. Transparent crystal pieces were cleaved from the boule and sealed in silica ampoules under He gas for the spectroscopic characterisations. All handling of starting materials and products were done under dry conditions in glove boxes or sealed sample containers. Powder X-ray diffraction patterns were measured with $\text{Cu K}\alpha 1$ radiation in reflection geometry at room temperature, see Figure S2 and S3 of supporting information. CsPbCl_3 and CsPbBr_3 adopt the GdFeO_3 -type perovskite structure at room temperature [32].

The X-ray excited emission spectra were measured using a tungsten anode X-ray tube at an operation voltage of 79 kV. The average X-ray energy from this tube is 40 keV. The low energy X-rays from the spectrum produced by the tube are removed by placing a 3 mm aluminium filter in front of the tube in order to prevent radiation damage to the sample. The crystals were mounted on the cold finger of a closed cycle helium cryostat operating below 10^{-4} bar. The crystal is excited and the emitted light is detected from the same surface; the measurement is performed in reflectivity mode.

The estimated light yields were calculated by comparing the total spectral intensity of the 10 K X-ray excited emission spectra of CsPbBr_3 and CsPbCl_3 to that of a CsCu_2I_3 crystal. The experimental conditions, sample alignment, X-ray fluence, and size of the samples were similar for all three measurements. The scintillation yield of CsCu_2I_3 has been determined in a separate experiment under 662 keV γ -photon excitation on an APD as described in Ref [10]. In Ref [10] the non-proportionality of CsCu_2I_3 was also measured, showing only a 4% difference upon comparing the light yield determined at 60 and 662 keV. The spectral intensity is corrected for the detection efficiency.

The photoluminescence emission spectra were measured by exciting the samples either with the light of a 450 W xenon lamp passing through a Horiba Gemini 180 monochromator or by exciting with a Hamamatsu L1835 deuterium lamp passing through an Action Research Corporation VM 502 monochromator. The emission light passed through a Princeton Instruments SpectraPro-SP2358 monochromator and was detected using a Hamamatsu C9100-13 EM CCD. The crystals were mounted on the cold finger of a closed cycle helium cryostat operating below 10^{-4} bar.

The pulsed X-ray decay cures were measured by the time-correlated single photon counting method. A PicoQuant LDH-P-C440M pulsed laser, generating the start signal, directly excites a Hamamatsu N5084 light excited X-ray tube, creating a pulse of X-rays with an average energy of 18.2 keV and temporal resolution of 200 ps. The scintillation photons are detected by an ID Quantique id100-50 single-photon counter, which is used as the stop signal. An Ortec 567 time-to-amplitude converter was used to process the start and stop signals. An Ortec AD 144 16K ADC was used to digitise the signal. The crystals were mounted on the cold finger of a closed cycle helium cryostat operating below 10^{-4} bar. The crystal is excited and the emitted light is detected from the same surface; the measurement is performed in reflectivity mode.

In order to record pulse height spectra at 10 K the samples were mounted on a parabolic stainless steel reflector covered with aluminium foil to improve the light collection efficiency. The reflector was mounted on the cold finger of a closed cycle helium cryostat operating below 10^{-4} bar. A Hamamatsu Super Bialkali R6231-100 (SN ZE4500) PMT was used to detect the scintillation photons. It was placed close to the window on the outside of the sample chamber. The distance between the sample and PMT was approximately 5 cm.

6. Conflicts of Interest

There are no conflicts to declare.

7. Acknowledgements

The authors acknowledge financial support from the TTW-OTP grant no. 18040 of the Dutch Research Council.

References

- [1] M. A. Green, A. Ho-Naillie, H. J. Snaith, *Nature Photonics* 8 (2014) 506, <https://doi.org/10.1038/nphoton.2014.134>
- [2] X. Y. Chin, D. Cortecchia, J. Yin, A. Bruno, C. Soci, *Nature Communications* 6 (2015) 7383, <https://doi.org/10.1038/ncomms8383>
- [3] L. Dou, Y. M. Yang, J. You, Z. Hong, W.-H. Chang, G. Li, Y. Yang, *Nature Communications* 5 (2014) 5404, <https://doi.org/10.1038/ncomms6404>
- [4] M. D. Bitowosuto, D. Cortecchia, W. Drozdowski, K. Brylew, W. Lachmanski, A. Bruno, C. Soci, *Scientific Reports* 6 (2016) 37254, <https://doi.org/10.1038/srep37254>
- [5] V. B. Mykhaylyk, H. Kraus, V. Kapustianyk, H. J. Kim, P. Mercere, M. Rudko, P. Da Silva, O. Antonyak, M. Dendebera, *Scientific Reports* 10 (2020) 8601, <https://doi.org/10.1038/s41598-020-65672-z>
- [6] F. Maddalena, L. Tjahjana, A. Xie, Arramel, S. Zeng, H. Wong, P. Coquet, W. Drozdowski, C. Dujardin, C. Dang, M. D. Birowosuto, *Crystals* 9 (2019) 88, <https://doi.org/10.3390/cryst9020088>
- [7] A. Xie, F. Maddalena, M. E. Witkowski, M. Makowski, B. Mahler, W. Drozdowski, S. V. Springham, P. Coquet, C. Dujardin, M. D. Birowosuto, C. Dang, *Chemistry of materials*, 32 (2020) 19, <https://doi.org/10.1021/acs.chemmater.0c02789>
- [8] J. J. van Blaaderen, F. Maddalena, C. Dong, M. D. Birowosuto, P. Dorenbos, *Journal of Materials Chemistry C* 10 (2022) 11598-11606, <https://doi.org/10.1039/D2TC01483A>
- [9] J. J. van Blaaderen, S. van der Sar, D. Onggo, Md Abdul K. Sheikh, D. R. Schaart, M. D. Birowosuto, P. Dorenbos, *Journal of Luminescence* 263 (2023) 120012, <https://doi.org/10.1016/j.jlumin.2023.120012>
- [10] J. J. van Blaaderen, L. A. van den Brekel, K. W. Krämer, P. Dorenbos, *Chemistry of Materials* 35 (2023) 9623-9631, <https://doi.org/10.1021/acs.chemmater.3c01810>

- [11] A. Akkerman, L. Manna, *ACS Energy Letters*, 5 (2020) 604-610, <https://doi.org/10.1021/acsenenergylett.0c00039>
- [12] P. Dorenbos, *Optical Materials: X* 1 (2019) 100021, <https://doi.org/10.1016/j.omx.2019.100021>
- [13] P. Dorenbos, Fundamental Limitations in the Performance of Ce³⁺-, Pr³⁺-, and Eu²⁺- Activated Scintillators, *IEEE transactions on nuclear science* 57 (2010) 3, <https://doi.org/10.1109/TNS.2009.2031140>
- [14] C. van Aarle, K. W. Krämer, P. Dorenbos, *Journal of Materials Chemistry C* 11 (2023) 2336-2344, <https://doi.org/10.1039/D2TC05311J>
- [15] C. van Aarle, K. W. Krämer, P. Dorenbos, *Journal of Luminescence* 251 (2022) 119209, <https://doi.org/10.1016/j.jlumin.2022.119209>
- [16] C. van Aarle, K. W. Krämer, P. Dorenbos, *Journal of Luminescence* 238 (2021) 118257, <https://doi.org/10.1016/j.jlumin.2021.118257>
- [17] E. V. D. van Loef, P. Dorenbos, C. W. E. van Eijk, *Applied Physics Letters*, 79 (2001) 1573, <https://doi.org/10.1063/1.1385342>
- [18] Z. Shaki, M. M. Byranvand, N. Taghavinia, M. Kedia, M. Saliba, *Energy and Environmental Science* 14 (2021) 5690-5722, <https://doi.org/10.1039/D1EE02018H>
- [19] W. A. Dunlap-Shohl, Y. Zhou, N. P. Padture, D. B. Mitzi, *Chemical Reviews* 119 (2019) 3193-3295, <https://doi.org/10.1021/acs.chemrev.8b00318>
- [20] Q. A. Akkerman, G. Raino, M. V. Kovalenko, L. Manna, *Nature Materials* 17 (2018) 394-405, <https://doi.org/10.1038/s41563-018-0018-4>
- [21] J. Peng, C. Q. Xia, Y. Xu, R. Li, L. Cui, J. K. Clegg, L. M. Harz, M. B. Johnston, Q. Lin, *Nature Communucations* 12 (2020) 153, <https://doi.org/10.1038/s41467-021-21805-0>
- [22] Y. He, Z. Liu, K. M. McCall, W. Lin, D. Y. Chung, B. W. Wessells, M. G. Kanatzidis, *Nuclear Instruments and Methods in Physics Research Section A: Accelerators, Spectrometers, Detectors and Associated equipment* 992 (2019) 217-221, <https://doi.org/10.1016/j.nima.2019.01.008>
- [23] L. Pan, Y. Feng, P. Kandlakunta, J. Huang, L. R. Cao, *IEEE Transactions on Nuclear Science* 67 (2020) 443-449, <https://doi.org/10.1109/TNS.2020.2964306>
- [24] Y. He, L. Matei, H. J. Jung, K. M. McCall, M. Chen, C. C. Staumpos, Z. Liu, J. A. Peters, D. Y. Chung, B. W. Wessels, M. R. Wasielewski, V. P. Dravid, A. Burger, M. G. Kanatzidis, *Nature Communications* 9 (2018) 1609, <https://doi.org/10.1038/s41467-018-04073-3>
- [25] S. Yakunin, D. N. Dirin, Y. Shynkarenko, V. Morad, I. Cherniukh, O. Nazarenko, D. Kreil, T. Nauser, M. V. Kovalenko, *Nature Photonics* 10 (2016) 585-589, <https://doi.org/10.1038/nphoton.2016.139>

- [26] H. Wei, Y. Fang, P. Mulligan, W. Chuirazzi, H.-H. Fang, C. Wang, B. R. Ecker, Y. Gao, M. A. Loi, L. Cao, J. Huang, *Nature Photonics* 10 (2016) 333-339, <https://doi.org/10.1038/nphoton.2016.41>
- [27] R. T. Williams, W. W. Wolszczak, X. Yan, D. L. Carrol, *ACS Nano* 14 (2020) 5161-5169, <https://doi.org/10.1021/acsnano.0c02529>
- [28] W. W. Wolszczak, D. L. Carroll, R. T. Williams, *Advanced X-ray Detector Technologies*, Chapter 1 (2022), https://doi.org/10.1007/978-3-030-64279-2_1
- [29] F. Staub, I. Anusca, D. C. Lupascu, U. Rau, T. Kirchartz, *Journal of Physics: Materials* 3 (2020) 2, <https://doi.org/10.1088/2515-7639/ab6fd0>
- [30] C. Zhou, H. Lin, Q. He, L. Xu, M. Worku, M. Chaaban, S. Lee, X. Shi, M.-H. Du, B. Ma, *Materials Science and Engineering: R: Reports* 137 (2019) 38-65, <https://doi.org/10.1016/j.mser.2018.12.001>
- [31] V. B. Mykhaylyk, M. Rudko, H. Kraus, V. Kapustianyk, V. Kolomiets, N. Vitoratou, Y. Chornodolsky, A. S. Voloshinovskii, L. Vasylechko, *Journal of Materials Chemistry C* 11 (2023) 656-665, <https://doi.org/10.1039/D2TC04631H>
- [32] M. R. Linaburg, E. T. McClure, J. D. Majher, P. M. Woodward, *ACS Chemistry of Materials*, 23 (2017) 3507-3514, <https://doi.org/10.1021/acs.chemmater.6b05372>
- [33] C. A. Lopez, G. Abia, M. C. Alvarez-Galvan, B.-K. Hong, M. V. Martinez-Huerta, F. Serrano-Sanchez, F. Carrascoso, A. Castellanos-Gomez, M. T. Fernandez-Diaz, J. A. Alonso, *ACS Omega*, 5 (2020) 5931-5938, <https://doi.org/10.1021/acsomega.9b04248>
- [34] Z. Yao, W. Zhao, S. Liu, *Journal of materials chemistry A* 9 (2021) 11124-11144, <https://doi.org/10.1039/D1TA01252E>
- [35] K. Nitsch, V. Hamplova, M. Nikl, K. Polak, M. Rodava, *Chemical Physics Letters* 258 (1996) 518-522, [https://doi.org/10.1016/0009-2614\(96\)00665-3](https://doi.org/10.1016/0009-2614(96)00665-3)
- [36] M. Dendebera, Y. Chornodolskyy, R. Gamernyk, O. Antonyak, I. Pashuk, S. Myagkota, I. Gnilitzkyi, V. Pankratov, V. Vistovskyy, V. Mykhaylyk, M. Grinberg, *Journal of Luminescence* 225 (2020) 117346, <https://doi.org/10.1016/j.jlumin.2020.117346>
- [37] J. A. Steele, P. Puech, B. Monserrat, B. Wu, R. X. Yang, T. Kirchartz, H. Yuan, G. Fleury, D. Giovanni, E. Fron, M. Keshavarz, E. Debroye, G. Zhou, T. C. Sum, A. Walsh, J. Hofkent, M. B. J. Roelfaers, *ACS Energy Letters* 4 (2019) 2205-2212, <https://doi.org/10.1021/acsenenergylett.9b01427>
- [38] W. Du, S. Zhang, Z. Wu, Q. Shang, Y. Mi, J. Chen, C. Qin, X. Qiu, Q. Zhang, X. Liu, *Nanoscale* 11 (2019) 3145-3153, <https://doi.org/10.1039/C8NR09634A>
- [39] C. Wolf, T.-W. Lee, *Materialstoday Energy* 7 (2018) 199-207, <https://doi.org/10.1016/j.mtener.2017.09.010>

- [40] M. Sebastian, J. A. Peters, C. C. Stoumpos, J. Im, S. S. Kostina, Z. Liu, M. G. Kanatzidis, A. J. Freeman, B. W. Wessels, *Physical Review B* 92 (2015) 235210, <https://doi.org/10.1103/PhysRevB.92.235210>
- [41] X. Fang, K. Zhang, Y. Li, L. Yao, Y. Zhang, Y. Wang, W. Zhai, L. Tao, H. Du, G. Ran, *Applied Physics Letters* 108 (2016) 071109, <https://doi.org/10.1063/1.4942410>
- [42] E. M. Hutter, M. C. Gelvez-Rueda, A. Osherov, V. Bulovic, F. C. Grozema, S. D. Stranks, T. J. Savenije, *Nature Materials* 16 (2017) 115-120, <https://doi.org/10.1038/nmat4765>
- [43] X. Lao, Z. Yang, Z. Su, Z. Wang, H. Ye, M. Wang, X. Yao, S. Xu, *Nanoscale* 10 (2018) 9949-9956, <https://doi.org/10.1039/C8NR01109E>
- [44] H. Linnenbank, M. Saliba, L. Gui, B. Metzger, S. G. Tikhodeev, J. Kadro, G. Nasti, A. Abate, A. Hagfeldt, M. Graetzel, G. Giessen
- [45] T. M. Demkiv, S. V. Myagkota, T. Malyi, A. S. Pushak, V. V. Vistovskyy, P. M. Yakibchuk, O. V. Shapoval, N. E. Mitina, A. S. Zaichenko, A. S. voloshinovskii, *Journal of Luminescence* 198 (2018) 103-107, <https://doi.org/10.1016/j.jlumin.2018.02.021>
- [46] C. C. Stoumpos, M. G. Kanatzidis, *Accounts of Chemical Research* 48 (2015) 2791-2802, <https://doi.org/10.1021/acs.accounts.5b00229>
- [47] C. C. Stoumpos, C. D. Malliakas, J. A. Peters, Z. Liu, M. Sebastian, J. Im, T. C. Chasapis, A. C. Wibowo, D. Y. Chung, A. J. Freeman, B. W. Wessels, M. G. Kanatzidis, *Crystal Growth and Design* 13 (2013) 2722-2727, <https://doi.org/10.1021/cg400645t>
- [48] J. A. Peters, Z. Liu, M. C. De Siena, M. G. Kanagzidis, B. W. Wessels, *Journal of Luminescence* 243 (2022) 118661, <https://doi.org/10.1016/j.jlumin.2021.118661>
- [49] M. Nikl, E. Mihokoba, K. Nitsch, K. Polak, M. Rodova, M. Dusek, G. P. Pazzi, P. Fabeni, L. Salvini, M. Gurioli, *Chemical Physics Letters* 220 (1994) 1-2, [https://doi.org/10.1016/0009-2614\(94\)00127-8](https://doi.org/10.1016/0009-2614(94)00127-8)
- [50] M. Kobayashi, K. Omata, S. Sigimoto, Y. Tamagawa, T. Kuroiwa, H. Asada, H. Takeuchi, S. Kondo, *Nuclear Instruments and Methods in Physics Research A* 592 (2008) 369-373, <https://doi.org/10.1016/j.nima.2008.04.079>
- [51] K. Watanabe, M. Koshimizu, T. Yanagida, Y. Fujimoto, K. Asai, *Japanese Journal of Applied Physics* 55 (2016) 0BC20, <http://doi.org/10.7567/JJAP.55.02BC20>
- [52] R. T. Williams, J. Q. Grim, Q. Li, K. B. Ucer, W. W. Moses, *Basic Solid State Physics* 248 (2011) 426-438, <https://doi.org/10.1002/pssb.201000610>
- [53] W. W. Moses, G. Bizarri, R. T. Williams, S. A. Payne, A. N. Vasilev, J. Singh, Q. Li, J. Q. Grim, W.-S. Choong, *IEEE Transactions on Nuclear science* 59 (2012) 2038-2044, <https://doi.org/10.1109/TNS.2012.2186463>

- [54] A. N. Vasilev, IEEE Transactions on Nuclear Science 55 (2008) 3, <https://doi.org/10.1109/TNS.2007.914367>
- [55] I. V. Khodyuk, Nonproportionality of inorganic scintillators, ISBN:9789088915536, <https://doi.org/10.4233/uuid:cb4008a8-981a-4283-b213-199d41756269>
- [56] K. S. Song, R. T. Williams, Self trapped Excitons (Springer Series in Solid-State Sciences 105), 1993, ISBN: 3-540-55906-X
- [57] T. Ma, S. Wang, Y. Zhang, K. Zhang, L. Yi, Journal of Materials Science 55 (2020) 464-479, <https://doi.org/10.1007/s10853-019-03974-y>
- [58] L. Y. Bai, S. W. Wang, Y. W. Zhang, K. X. Zhang, L. X. Yi, Journal of luminescence 227 (2020) 117592, <https://doi.org/10.1016/j.jlumin.2020.117592>
- [59] K. Heidrich, H. Kunzel, J. Treusch, Solid State Communications 25 (1978) 887-889, [https://doi.org/10.1016/0038-1098\(78\)90294-6](https://doi.org/10.1016/0038-1098(78)90294-6)
- [60] F. Agullo-Lopez, C. R. A. Catlow, D. P. townsend, Point Defects in Materials, Chapter 5, 1998, ISBN 0-12-044510-7
- [61] S. Li, J. Luo, J. Liu, J. Tang, The Journal of Physical Chemistry Letters 10 (2019) 1999-2007, <https://doi.org/10.1021/acs.jpcclett.8b03604>
- [62] W. Wolszczak, P. Dorenbos, IEEE Transactions on Nuclear Science 64 (2017) 6, <https://doi.org/10.1109/TNS.2017.2699327>
- [63] S. Gull, M. H. Jamil, X. Zhang, H.-S. Kwok, G. Li, Chemistry Open 11 (2022) 3, <https://doi.org/10.1002/open.202100285>
- [64] V. B. Mykhaylyk, H. Kraus, M. Saliba, Materials Horizons 6 (2019) 1740-1747, <https://doi.org/10.1039/C9MH00281B>
- [65] Y. Li, W. Shao, X. Ouyang, Z. Zhu, H. Zhang, X. Ouyang, B. Liu, Q. Xu, The Journal of Physical Chemistry C 123 (2019) 28, <https://doi.org/10.1021/acs.jpcc.9b05269>

Supplementary Information

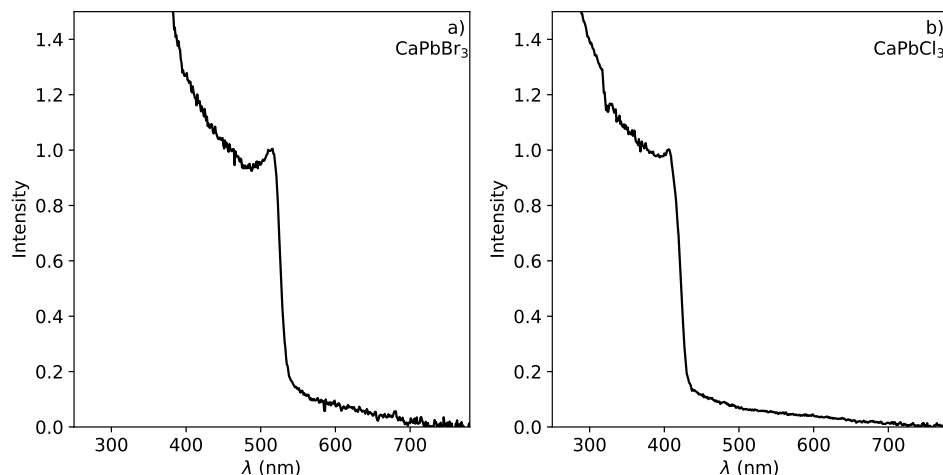


Figure S1: Room temperature absorbance spectra of (a) CsPbBr₃ single crystal and (b) CsPbCl₃ single crystal.

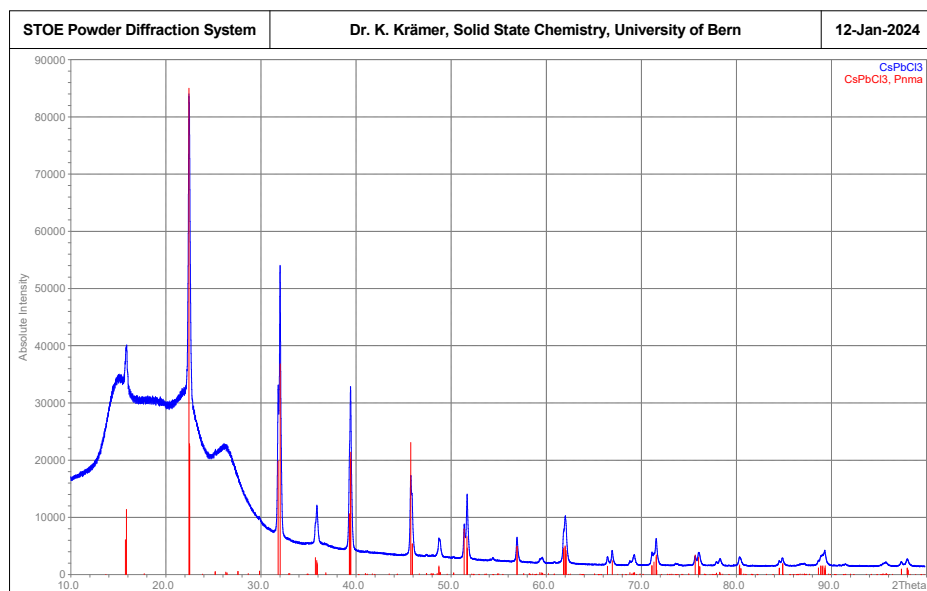


Figure S2: Powder diffraction pattern of CsPbCl₃ measured with Cu K_{α1} radiation at room temperature. CsPbCl₃ adopts the GdFeO₃-type perovskite structure in very good agreement with the calculated pattern according to Linburg *et al.* [1]. The three broad peaks below 30° 2-Theta originate from the Mylar window of the sample holder.

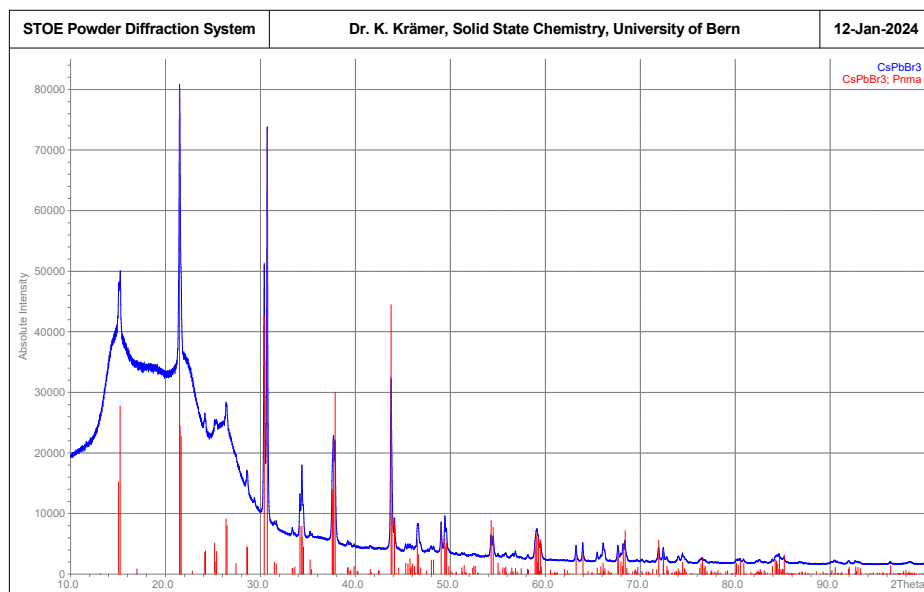


Figure S3: Powder diffraction pattern of CsPbBr_3 measured with $\text{Cu K}_{\alpha 1}$ radiation at room temperature. CsPbBr_3 adopts the GdFeO_3 -type perovskite structure in very good agreement with the calculated pattern according to Linaburg *et al.* [1]. The three broad peaks below 30° 2-Theta originate from the Mylar window of the sample holder.

3

Photoluminescence and Scintillation Mechanism of Cs_4PbBr_6

Abstract

Small bandgap scintillators have gained significant attention in recent years. Especially Cs_4PbBr_6 is an interesting material, mitigating the Stokes shift problem of perovskites like CsPbBr_3 . In this work optical and scintillation properties of Cs_4PbBr_6 single crystals are investigated as function of temperature, with a detailed focus at 10 K. The Cs_4PbBr_6 single crystals were grown using the vertical Bridgman method. Due to incongruent melting, CsPbBr_3 inclusions are formed generating a 540 nm emission band. Preparing Cs_4PbBr_6 via solid state synthesis yields CsPbBr_3 inclusion free material, showing no green 540 nm emission band. In Cs_4PbBr_6 samples with and without CsPbBr_3 inclusions, a new emission band at 610 nm, ascribed to an unknown defect, was found. Based on the presented experiments, an emission mechanism is proposed for Cs_4PbBr_6 . This shows that both defects and CsPbBr_3 inclusions play a role in the emission behaviour of Cs_4PbBr_6 but only the CsPbBr_3 inclusions are responsible for the 540 nm emission.

The content of this chapter is based on: J. Jasper van Blaaderen, Andries van Hattem, Jence T. Mulder, Daniel Biner, Karl W. Krämer, Pieter Dorenbos, Photoluminescence and Scintillation Mechanism of Cs_4PbBr_6 , ACS The Journal of Physical Chemistry C 128 (2024) 46, 19921-19932

1. Introduction

In the last 10 years, lead halide perovskites [1–3] and lead halide perovskite-related compounds [4, 5] have gained interest in the field of X-ray and gamma photon scintillation detection. A clear distinction should be made, as discussed by Akkerman and Manna, between true perovskites and perovskite-related compounds [7]. The perovskite crystal structure, with stoichiometry ABX_3 , consists of a three dimensional network of corner sharing BX_6 octahedra. The small bandgap of lead halide perovskites, approximately 3 eV, increases their theoretical maximum light yield compared to larger bandgap traditional scintillators [1, 8, 9]. Using Equation 1 and a bandgap of 3 eV, it can be estimated that perovskites could surpass 100,000 photons/MeV scintillation photon yield.

$$N_{eh} = \frac{1,000,000}{\beta E_g} \quad (\text{e}^- \text{ - h pairs / MeV}) \quad (1)$$

Here N_{eh} represents the number of created electron-hole pairs, β is taken to be ≈ 2.5 , and E_g represents the bandgap of the scintillator. Perovskite-based scintillators differ from traditional scintillators, often doped or co-doped, by being intrinsic scintillators [10–14].

One of the shortcomings of lead halide perovskite-based scintillators, however, is their small Stokes shift, which results in losses due to self-absorption [3, 15, 16]. This problem has been addressed in detail by Wolszczak *et al.* [15] and Williams *et al.* [16]. For other applications, like light emitting diodes, this is a significantly smaller problem; these applications often use either thin films or nanocrystals [17–19]. Potential solutions to deal with the small Stokes shift of perovskites are lower dimensional lead halide compounds or the introduction of a dopant to down shift the emission wavelength. Dimension, in this case, refers to the connectivity of the PbX_6 octahedral network. In the genuine perovskite structure, ABX_3 , the PbX_6 network is connected in three-dimensions. The dimensionality decreases to two-dimensional in compounds like $(PEA)_2PbBr_4$ or zero-dimensional in compounds like Cs_4PbBr_6 . Lower-dimensional compounds often show self-trapped exciton emission which, compared to the near bandgap free exciton emission of perovskites, has a significantly larger Stokes shift [20–23].

Examples of lower-dimensional lead-based compounds that have been studied for their scintillation properties are the two-dimensional hybrid organic-inorganic perovskites phenethylammonium lead bromide ($(PEA)_2PbBr_4$), butylammonium lead bromide ($(BA)_2PbBr_4$), and 2,2-(ethylenedioxy)bis(ethylammonium) lead chloride ($(EDBE)PbCl_4$) [1, 4, 24, 25]. In these compounds, the cation located on the A site is replaced with a relatively large ammonium ion, creating an alternating layered structure of PbX_6 octahedra and organic layers.

In this work, the low temperature optical and scintillation properties of the zero dimensional lead halide compound Cs_4PbBr_6 are studied. Cs_4PbBr_6 crystallises in the K_4CdCl_6 structure with space group $\text{R}\bar{3}\text{c}$ [26, 27], has a density of 4.19 g/cm^3 , and a 3.9 eV bandgap [28–30]. Compared to the corner-sharing network of BX_6 octahedra in the perovskite crystal structure, the A_4BX_6 structure consists of isolated BX_6 octahedra [31, 32]. This results in the formation of localised states, comprised of the $6s^2$ and $6s6p$ states of Pb^{2+} , on the BX_6 octahedra. This closely resembles low doping concentrations of Pb^{2+} in face-centred cubic (fcc) alkali halide crystals, also resulting in the formation of isolated $[\text{PbX}_6]^{4-}$ octahedra [29, 33].

A general schematic of the energy levels of ions with a ns^2 electronic configuration, e.g., Tl^+ , Pb^{2+} , and Bi^{3+} , is shown in Figure 1. The energy levels of a free ns^2 ion shift and split due to a combination of electrostatic, exchange, and spin-orbit interactions [34, 35]. In a crystal field, the levels will split further forming three distinct absorption bands, labelled the A ($^1\text{S}_0 \rightarrow ^3\text{P}_1$), B ($^1\text{S}_0 \rightarrow ^3\text{P}_2$), and C ($^1\text{S}_0 \rightarrow ^1\text{P}_1$) band, which correspond with transitions between the ns^2 ground state and $nsnp$ excited states [34, 35]. The $^1\text{S}_0 \rightarrow ^1\text{P}_1$ transition, or C-band, is allowed. The $^1\text{S}_0 \rightarrow ^3\text{P}_0$, $^1\text{S}_0 \rightarrow ^3\text{P}_1$ (A-band), and $^1\text{S}_0 \rightarrow ^3\text{P}_2$ (B-band) transitions are spin forbidden. The $^1\text{S}_0 \rightarrow ^3\text{P}_1$ transition, or A-band, becomes partially allowed due to the spin-orbit coupling mixing the $^3\text{P}_1$ and $^1\text{P}_1$ states [34]. The $^1\text{S}_0 \rightarrow ^3\text{P}_2$ transition, or B-band, can be induced due to vibrational coupling with the crystal lattice but it remains weak and often escapes observation [35, 36]. Additionally, a fourth band, labelled the D-band, corresponding to a metal to metal charge transfer state between the ground state of Pb^{2+} and the conduction band is often observed [37, 38]. Emission typically takes place due to transitions from the $^3\text{P}_1$ (excited) state to the $^1\text{S}_0$ (ground) state and is commonly referred to as A-band emission [34, 35].

Cs_4PbBr_6 has been studied in different morphologies: nanocrystals [28, 39–41], thin films [29, 30, 42], single crystals [27, 43, 44], and powders [45, 46]. Next to the potential interest of Cs_4PbBr_6 as a scintillator, it has also gained interest to be used in light emitting diodes (LEDs) [47, 48], luminescent solar concentrates [49], and UV detectors [50]. Additionally, Cs_4PbBr_6 has been explored as host matrix for the production of CsPbBr_3 nanocrystals, an overview of which is presented by Akkerman *et al.* [50]. Cs_4PbBr_6 especially gained a lot of interest due to its intense green 540 nm emission in addition to its UV 380 nm emission. The origin of the 540 nm emission is sometimes still under debate. It was suggested to either originate from bromine vacancies [27, 41, 51–53] or CsPbBr_3 nanocrystal inclusions [29, 30, 44, 54–58]. The latter is seen as the more favourable explanation. This debate has recently been summarised in the review articles of Wang *et al.* [59], Biswas [60], and Akkerman *et al.* [50]. In general two different types of Cs_4PbBr_6 can be classified in literature: Cs_4PbBr_6 with CsPbBr_3 inclusions, showing UV 380 nm and green 540 nm emission, and phase pure Cs_4PbBr_6 , showing only UV 380 nm emission. The goal of this work is to propose a general emission mechanism for Cs_4PbBr_6 , done by studying the low temperature optical and scintillation properties of Cs_4PbBr_6 . The experiments are performed on a Cs_4PbBr_6 single crystal, grown using the vertical Bridgman method. One of the problems of producing single crystals from the melt, however, is the incongruent

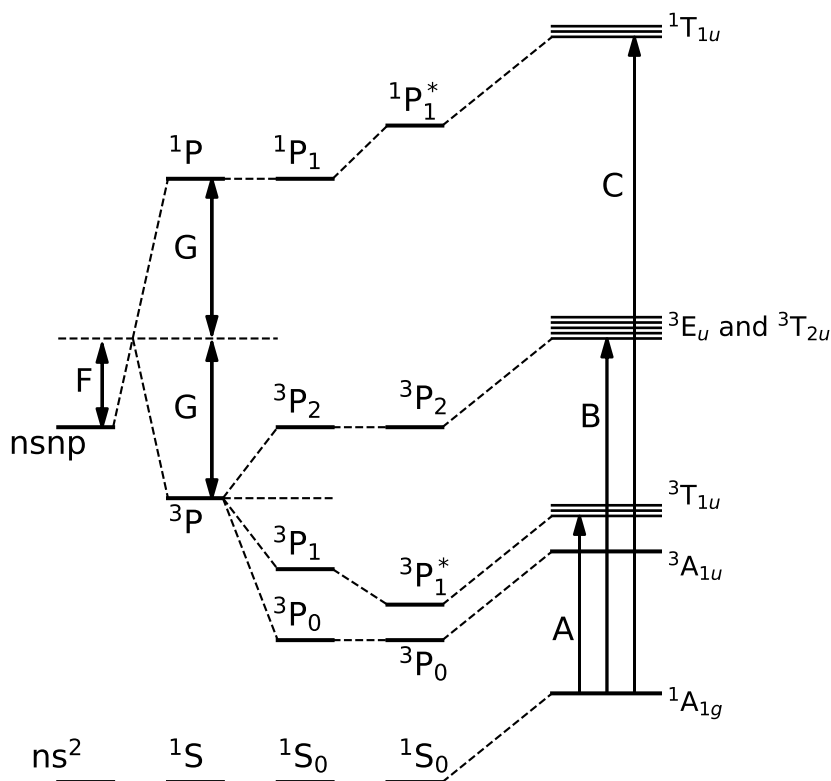


Figure 1: Schematic energy level diagram of ions with an ns^2 electronic ground state. Here F represents the shift of the energy levels due to electrostatic interactions, G represents the shift due to exchange interactions. The final formation of the A-, B-, and C-band and the corresponding symmetries are shown for an octahedrally surrounded ns^2 ion. The * indicates the mixing of the 3P_1 and 1P_1 levels due to spin-orbit interaction.

melting of Cs_4PbBr_6 [61]. This results in the formation of $CsPbBr_3$ inclusions [29, 30]. Such inclusions have also been observed in $CsBr$ crystals doped with Pb^{2+} [62–64]. Zhang *et al.* demonstrated that Cs_4PbBr_6 single crystals can be grown from solution without $CsPbBr_3$ inclusions in the presence of an excess of Cs^+ and Br^- ions, which stabilise the formation of Cs_4PbBr_6 [55]. Akkermann *et al.* have demonstrated a similar approach for the production of Cs_4PbBr_6 nanocrystals [28]. We have chosen to use a solid state synthesis, next to the Bridgman grown single crystal, to produce a Cs_4PbBr_6 powder without $CsPbBr_3$ inclusions. The solid state reaction between $CsBr$ and $PbBr_2$ takes place below the incongruent melting point of Cs_4PbBr_6 [61]. A slight excess of $CsBr$ was chosen to prevent formation of $CsPbBr_3$ inclusions. This approach has also been used for the synthesis of Cs_4PbI_6 [65].

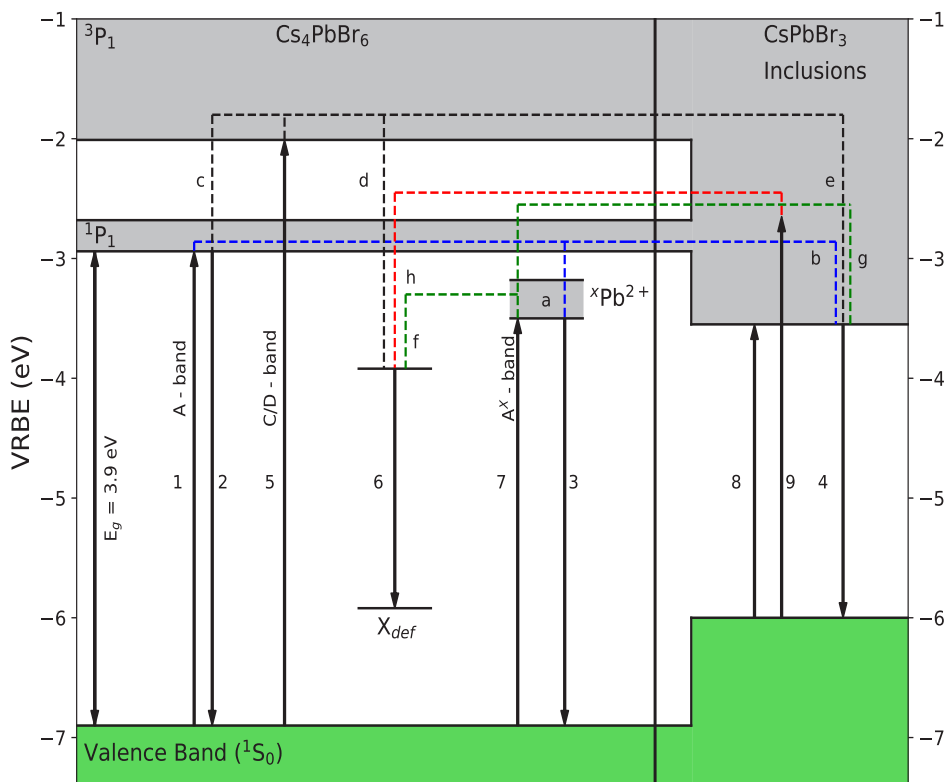


Figure 2: Vacuum referred binding energy (VRBE) diagram and the processes taking place in Cs_4PbBr_6 on the left and the VRBE plus additional processes taking place in Cs_4PbBr_6 with CsPbBr_3 inclusions on the right. Excitation and emission processes are represented by arrows and labelled using numbers. Energy transfer processes are indicated by dashed lines and labelled using letters. The label X_{def} represents the defect related emission, the label $x\text{Pb}^{2+}$ represents Pb^{2+} ions with a perturbed coordination shell.

In order to aid the presentation of the results and discussion presented in this work, Figure 2 shows the vacuum referred binding energy (VRBE) diagram applicable to Cs_4PbBr_6 on the left side and to CsPbBr_3 on the right side. The valence band of Cs_4PbBr_6 consists of bromine 4p orbitals and lead 6s orbitals while the conduction band consists of bromine 5p orbitals and lead 6s6p orbitals [41, 55, 66]. Vertical arrows represent excitation and emission transitions identified in the results section of this work. The horizontal dashed lines illustrate the energy and/or charge carrier transfer routes proposed in the discussion section.

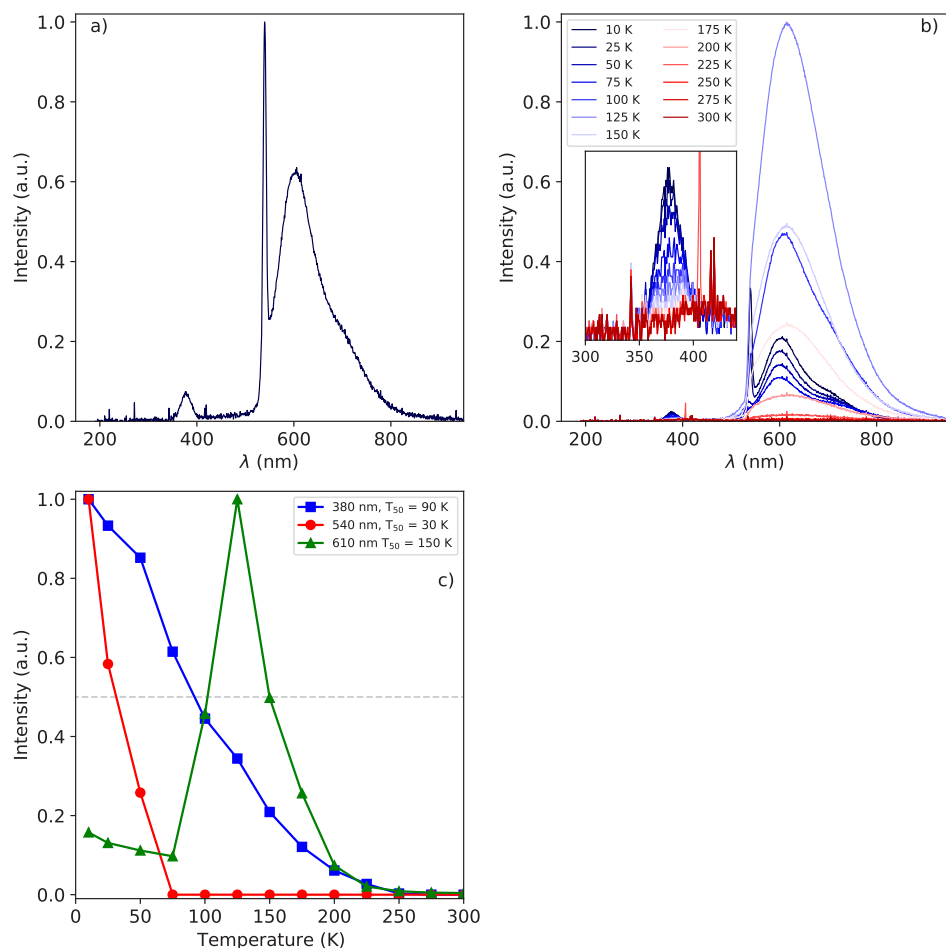


Figure 3: (a) X-ray excited emission spectrum of a Cs_4PbBr_6 single crystal with CsPbBr_3 inclusions recorded at 10 K. (b) Temperature dependent X-ray excited emission spectra of a Cs_4PbBr_6 single crystal measured from 10 to 300 K. The inset shows a zoom in of the 380 nm emission peak. (c) Temperature dependent integrated emission intensities of the 380, 540, and 630 nm emission bands.

2. Results

Cs_4PbBr_6 with CsPbBr_3 Inclusions

Figure 3a shows the 10 K X-ray excited emission spectrum of the Cs_4PbBr_6 single crystal. The spectrum contains three emission bands at 380, 540, and 610 nm. These emission bands have also been observed by Kubota *et al.* [67] and Ding *et al.* [68]. Wu *et al.* only studied the emission at wavelengths longer than 400 nm

under X-ray excitation, hence only observing the 540 and 610 nm emissions [69, 70]. The relative integral spectral intensity of the three emission bands are 1, 4.8, and 40.6, respectively. This means that the majority of the produced scintillation photons is present in the 610 nm emission band. The 380 nm UV band can be assigned to the intrinsic emission of Cs_4PbBr_6 (arrow 2 in Figure 2) [28, 30, 55, 67]. The powder X-ray diffraction pattern of the Cs_4PbBr_6 sample in Figure S1 shows that the single crystal contains CsPbBr_3 related impurities to which the 540 nm emission can be ascribed (arrow 4 in Figure 2). It has been suggested by Kubota *et al.* that the 610 nm emission could be related to bromine vacancies (arrow 6 in Figure 2) [67–69].

The X-ray excited emission spectra, measured as function of temperature, are shown in Figure 3b. The integrated intensities of the 380, 540, and 610 nm bands are shown in Figure 3c. The 540 nm emission band is fully quenched above 100 K. The intensity of the 610 nm emission shows a mild decrease until 75 K. Above 75 K its intensity increases, reaching a maximum at 125 K and then starts to quench. Based on the integrated peak intensities, the temperature (T_{50}) at which the intensity drops below 50% of its maximum intensity for the 380, 540, and 610 nm emissions are 90, 30, and 150 K, respectively.

The 10K pulsed X-ray excited decay curve of the total emission spectrum of the Cs_4PbBr_6 single crystal is shown in Figure 4a. The inset shows the first 150 ns of the decay curve where two decay components of 0.66 and 16.5 ns can be observed. On longer time scales a significantly slower component of 770 ns can also be observed. The measurement was repeated by placing a 630 nm long pass filter in front of the photo-detector, removing the contribution of both the 380 and 540 nm emissions. The resulting decay curve is shown in Figure 4b, with the inset showing the first 150 ns of the decay. The decay curve no longer contains the sub nanosecond decay component observed in Figure 4a. The decay contains three decay components of 10, 140, and 790 ns. Nikl *et al.* have studied the decay behaviour of Cs_4PbBr_6 with CsPbBr_3 inclusions under photo-excitation finding a sub nanosecond decay component for the 540 nm emission [30]. Additionally the sub nanosecond decay component is similar to the decay curves measured on CsPbBr_3 single crystals under pulsed X-ray excitation [3]. This suggests that the sub nanosecond decay component observed in Figure 3a can be assigned to the 540 nm emission.

Figure 5 shows the room temperature absorbance spectrum of the Cs_4PbBr_6 single crystal revealing two peaks at 260 nm (4.77 eV) and 315 nm (3.94 eV). An additional absorption edge is observed around 520 nm (2.38 eV). The 315 nm absorption band can be ascribed to the A-band transitions of Pb^{2+} (arrow 1 in Figure 2). Kondo *et al.* ascribed the 260 nm band to a combination of the C- and D-band transitions [29]. The overlap of these two transitions has also been observed in alkali halides doped with low concentrations of Pb^{2+} for example KBr which behaves similar to Cs_4PbBr_6 [71, 72]. Hence, the 260 nm absorption band will be labelled as C/D-band transition (arrow 5 in Figure 2). The observed absorption edge, in Figure 5, around 520 nm (arrow 8 in Figure 2) can be ascribed

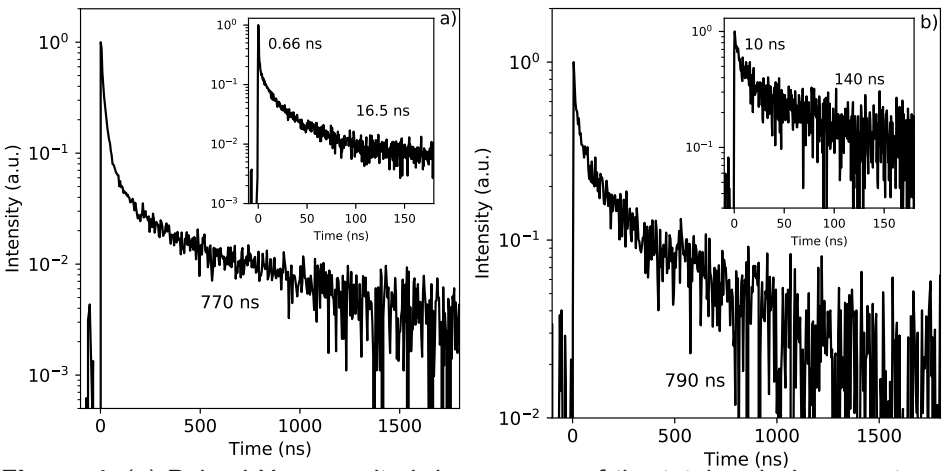


Figure 4: (a) Pulsed X-ray excited decay curve of the total emission spectrum of a Cs_4PbBr_6 single crystal with CsPbBr_3 inclusions at 10 K. (b) Pulsed X-ray excited decay curve, recorded by placing a 630 nm long pass filter in front of the detector, of a Cs_4PbBr_6 single crystal with CsPbBr_3 inclusions at 10 K.

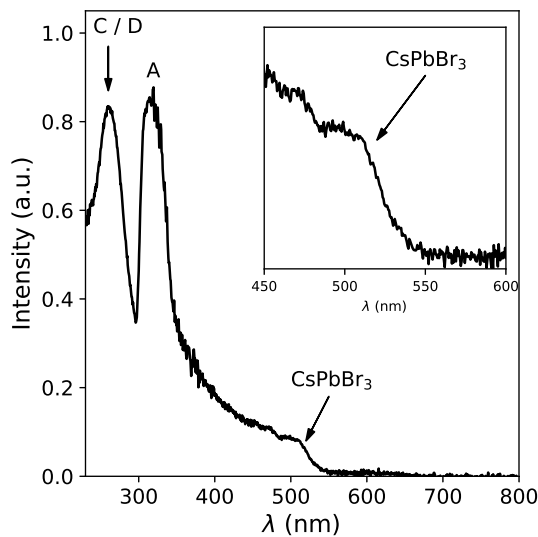


Figure 5: Room temperature absorbance spectrum of a Cs_4PbBr_6 single crystal with CsPbBr_3 inclusions, the inset shows a zoom-in of the feature observed between 500 and 550 nm.

to the presence of CsPbBr_3 inclusions [29, 30]. For comparison the absorption spectrum of a CsPbBr_3 single crystal is shown in Figure S2, revealing a similar absorption edge around 520 nm. Based on these similarities and the powder diffraction pattern of the Cs_4PbBr_6 single crystals, the 540 nm emission is ascribed to CsPbBr_3 inclusions (arrow 4 in Figure 2).

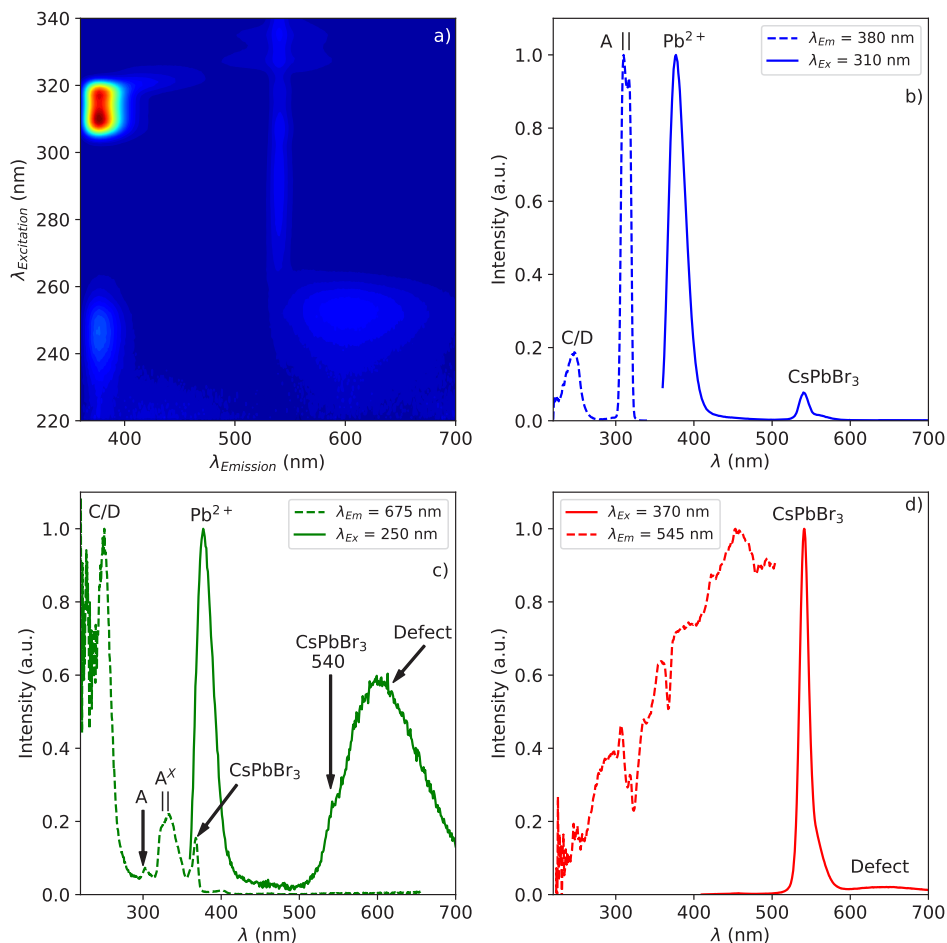


Figure 6: (a) Photoluminescence emission intensity of a Cs_4PbBr_6 single crystal with CsPbBr_3 inclusions as function of excitation wavelength at 10 K. Photoluminescence excitation and emission spectra at 10 K measured at emission and excitation wavelengths of (b) 380 and 310 nm, (c) 675 and 250 nm, and (d) 545 and 370 nm.

To further investigate the nature of the different absorption and emission bands, the photoluminescence emission of Cs_4PbBr_6 was measured as function of the excitation wavelength at 10 K. The resulting image plot is shown in Figure 6a. From this image plot, two emission spectra are extracted at excitation wavelengths of 310 and 250 nm, shown in Figure 6b and c, respectively. Upon exciting the A-band (arrow 1 in Figure 2) at 310 nm, as shown in Figure 6b, two emission bands are observed at 378 and 540 nm. The 378 nm emission can be assigned to the intrinsic A-band emission of Cs_4PbBr_6 (arrow 2 in Figure 2) [30], and the 540 nm emission to the presence of CsPbBr_3 inclusions (arrow 4 in Figure 2) [19, 29, 30]. Analogous behaviour is observed in Cs_4PbCl_6 due to the presence

CsPbCl₃ inclusions [73]. The excitation spectrum of the 378 nm A-band emission in Figure 6b shows two excitation bands at 250 and 310 nm. Similar to the absorbance spectrum shown in Figure 5, these are assigned to the C/D- and A-band transitions (arrows 1 and 5 in Figure 2), respectively. Note that the 310 nm excitation band actually consists of two bands, at 310 and 317 nm, which is typical of the A-band and caused by a Jahn-Teller splitting [34, 35]. From the image plot in Figure 6a, it can be observed that the 378 nm emission band excited via the A band-transition is the most intense emission band observed.

Upon exciting in the C/D-band (arrow 5 in Figure 2) at 250 nm, as shown in Figure 6c, two main emission bands at 378 and 610 nm are observed (arrows 2 and 6 in Figure 2). The 540 nm band is also present in the form of a shoulder on the shorter wavelength side of the 610 nm band. The 610 nm emission band has not been observed before under photo-excitation but is the dominant emission band under X-ray excitation, as shown in Figure 3a. The excitation spectrum, recorded at 675 nm, in Figure 6c shows an intense 250 nm C/D- and a weak 310 nm A-band, which are also observed in Figure 6b but with a much different intensity ratio. Additionally, a second Jahn-Teller split A-band, (arrow 7 in Figure 2) is observed at 325 and 332 nm which is labelled as A^x and there is also an excitation band at 370 nm, attributed to the CsPbBr₃ inclusions [34, 35]. Upon exciting at 370 nm (arrow 9 in Figure 2), two emission bands are observed at 540 and 610 nm as shown in Figure 6d. The excitation spectrum recorded at 545 nm is also shown in Figure 6d.

The quenching behaviour under optical excitation is similar to the quenching behaviour under X-ray excitation. The T_{50} values for the 378, 540, 600 nm emissions are approximately 110, 60, and 160 K. The temperature dependence of the different emission bands upon exciting at the 250 nm C/D-band, 310 nm A-band, and 370 nm CsPbBr₃ inclusions is shown in Figure S3.

Cs₄PbBr₆ without CsPbBr₃ Inclusions

Cs₄PbBr₆ without CsPbBr₃ inclusions was synthesised using a solid state synthesis. After the heat treatment of the CsBr:PbBr₂ (4:1) mixture, a light grey powder was obtained. The X-ray diffraction pattern of the synthesised material only exhibits diffraction peaks of Cs₄PbBr₆ and CsBr. The diffraction pattern is shown in Figure S4 and S5 together with a two-phase Rietveld profile refinement. The refinement yielded expected mass fractions of > 99% for Cs₄PbBr₆ and < 1% for CsBr. In contrast to the diffraction pattern of the Cs₄PbBr₆ single crystal, no peaks related to CsPbBr₃ were observed.

To investigate the nature of the different absorption and emission bands of Cs₄PbBr₆ without CsPbBr₃ inclusions, the photoluminescence emission was measured as function of the excitation wavelength at 10 K. The resulting image plot, plotted on a log scale, is shown in Figure 7a. From the image plot, two emission spectra are extracted at excitation wavelengths of the 310 nm A-band and 250 nm C/D-band, shown in Figure 7b and c, respectively. Upon exciting the A-band (arrow 1 in Figure 2), two emission bands at 378 and 455 nm (arrows 2 and 3 in Figure 2)

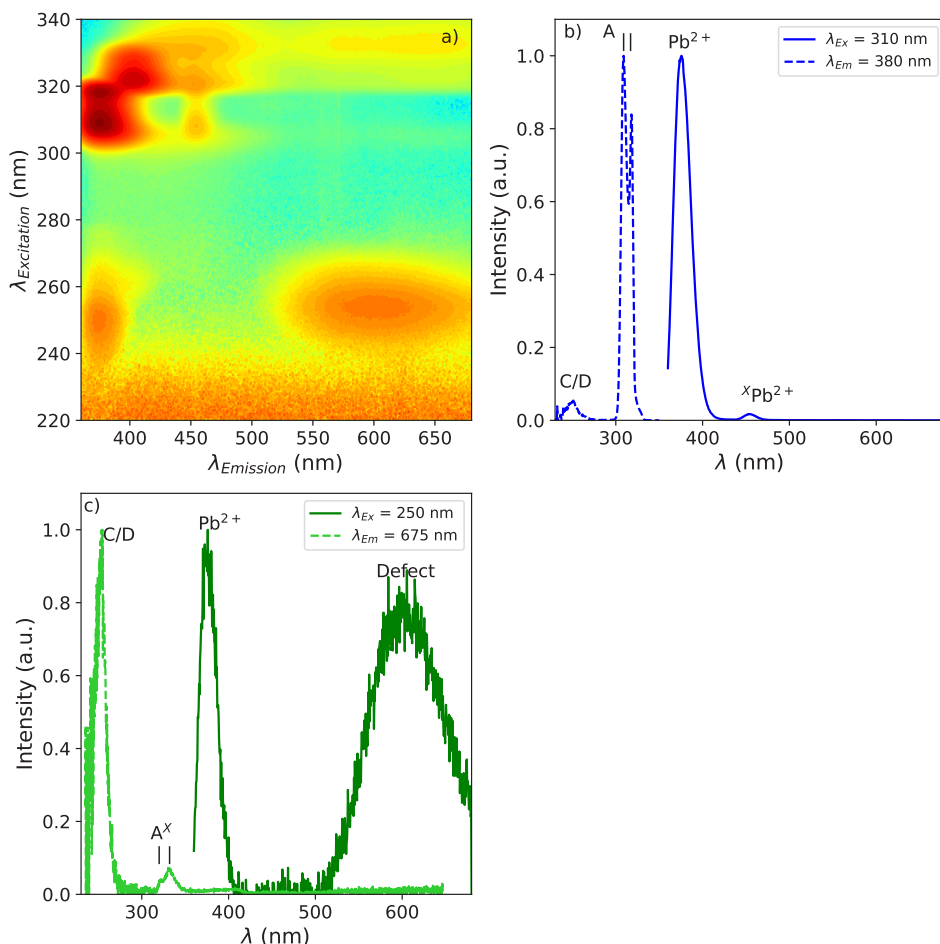


Figure 7: (a) Photoluminescence emission intensity of Cs_4PbBr_6 without CsPbBr_3 inclusions as function of excitation wavelength at 10K, on a log scale. Photoluminescence excitation and emission spectra at 10K measured at emission and excitation wavelengths of (b) 380 and 310 nm and (c) 675 and 250 nm, respectively.

are observed. The 540 nm emission (arrow 4 in Figure 2), observed in Figure 6b and related to the CsPbBr_3 inclusions, is no longer present. The excitation spectrum of the 378 nm A-band Pb^{2+} emission, in Figure 7b, shows the C/D band at 250 nm and the strong Jahn-Teller split A-band at 310 and 317 nm [34, 35]. Upon exciting the C/D band (arrow 5 in Figure 2) both the 378 nm A-band emission and 610 nm emission (arrows 2 and 6 in Figure 2) are observed. The excitation spectrum recorded at 675 nm, in Figure 7c, contains the C/D band at 250 nm and the Jahn-Teller split A^x -band at 320 and 332 nm.

Figure 8 shows the 10 K X-ray excited emission spectrum of Cs_4PbBr_6 without CsPbBr_3 inclusions. Two emission bands are observed at 380 and 610 nm with relative intensity of 1 and 25, respectively. The T_{50} temperature for both emission bands is 150 K as was obtained from temperature dependent behaviour of both bands, as shown in Figure S6a and S6b.

3. Discussion

Perturbed Pb^{2+} Coordination Sphere

Depending on the emission wavelength at which the excitation spectra are recorded, two different A-excitation bands are observed. A comparison of the two excitation bands for Cs_4PbBr_6 with and without CsPbBr_3 inclusions is shown in Figure 9a and b, respectively. Figure 9c shows three emission spectra excited at 310 nm (only A-band transition, arrow 2 in Figure 2), 320 nm (mixed A- and A^\times -band transitions) and 332 nm (only A^\times -band transition, arrow 7 in Figure 2) of the Cs_4PbBr_6 sample without CsPbBr_3 inclusions. Exciting only in the A-band yields two emission bands at 378 (strong) and 455 nm (weak). Exciting in the A^\times -band yields three emission bands at 405, 455, and 610 nm. It is known that the presence of defects close to Pb^{2+} ions influences both the excitation and emission properties of Pb^{2+} ions [74]. This has been studied extensively in the alkali halides [75–82]. Based on these observations the A-band excitation and A-band emission (arrows 1 and 2 in Figure 2, respectively) are attributed to originate from a Pb^{2+} ion on an unperturbed site. The A^\times -band (arrow 7 in Figure 2) and the 405 and 455 nm emission bands (arrow 3 in Figure 2) originate from a Pb^{2+} ion with a different or perturbed coordination shell.

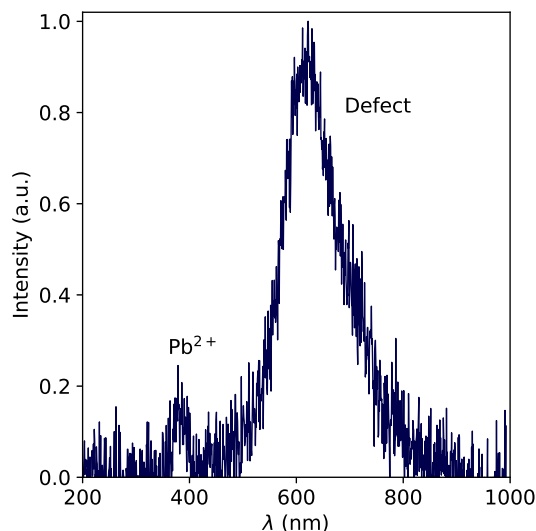


Figure 8: X-ray excited emission spectrum of Cs_4PbBr_6 without CsPbBr_3 inclusions recorded at 10 K.

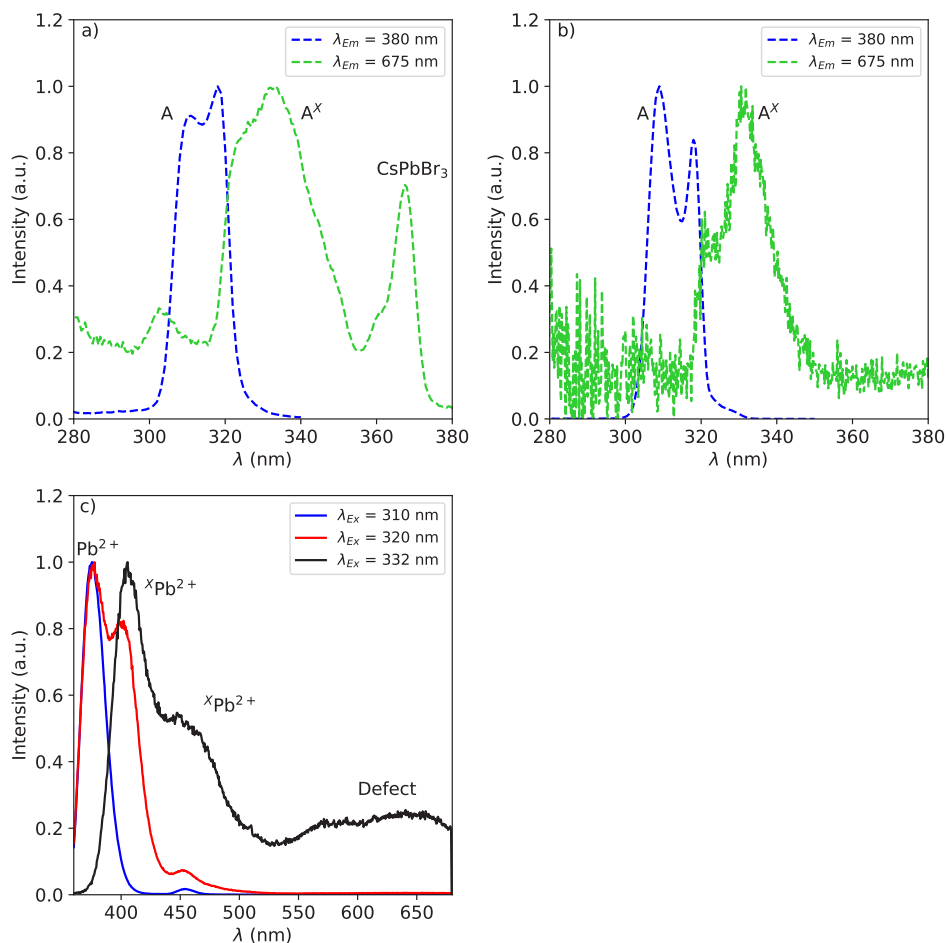


Figure 9: Comparison of the A-band transitions of (a) Cs₄PbBr₆ with CsPbBr₃ inclusions and (b) Cs₄PbBr₆ without CsPbBr₃ inclusions. The two excitation spectra shown for both forms of Cs₄PbBr₆ are recorded at 380 and 675 nm. The A-band transition of Pb²⁺ ions with an unperturbed coordination sphere are labelled A and those of Pb²⁺ ions with a perturbed coordination sphere are labelled A^x. (c) Emission spectra of Cs₄PbBr₆ without CsPbBr₃ inclusions excited in the A- and A^x-bands.

The presence of two additional emission bands points to at least two different perturbed coordination spheres of Pb²⁺. These could for example be a Pb²⁺ interstitial, a bromine vacancy next to Pb²⁺, or Pb²⁺ on a Cs⁺ site.

After exciting the A-band transition, next to A-band emission, energy transfer to a Pb²⁺ ion with perturbed coordination sphere can take place, as evident from the 455 nm emission band in Figure 7b. Energy transfer can also take place to the CsPbBr₃ inclusions, if present, as evident from the 540 nm emission band in

Figure 6b. After exciting the A^X -band, next to the 405 and 455 nm emissions, the 610 nm emission band can also be observed, as seen in Figure 9c.

Defect Related Emission

The 610 nm emission band is mainly observed upon exiting the C/D-band at 250 nm, as evident from the intensities of the excitation bands shown in Figure 6c and 7c. It is also possible to observe the 610 nm emission upon exciting the A^X -band, excluding D-band emission [83–85] as potential explanation. The 610 nm emission excitation via the A-band is weak, excitation via the A^X -band is significantly stronger as shown in Figure 6c. This all suggests that the 610 nm emission originates from a defect in the vicinity of a Pb^{2+} ion, resulting in a perturbation of the coordination sphere of Pb^{2+} and the observation of the A^X -band. The 610 nm emission band cannot be excited directly. The defect seems to first need to trap a mobile charge carrier before it can become emissive. This can happen by exciting the C/D-band, upon which mobile charge carriers are created, or via excitation of a $CsPbBr_3$ inclusion well above the band gap, at 370 nm (arrow 9 in Figure 2), or a Pb^{2+} ion with a perturbed coordination sphere, illustrated by energy transfer pathway d, h, and f in Figure 2, respectively. The excitation spectra of the 610 nm emission, Figure 6c and 7c, show that exciting the C/D band is the dominant pathway to excite the defects.

Inclusion Related Emission

The emission peak, linked to the $CsPbBr_3$ inclusions, was located at 540 nm in the Cs_4PbBr_6 single crystals used in this work. The green $CsPbBr_3$ inclusion emission in nanocrystals however is typically reported to be located from 515 to 524 nm [50]. It has been demonstrated by Chen *et al.* and Almeida *et al.*, in Cs_4PbBr_6 nanocrystals with $CsPbBr_3$ inclusions, that the emission wavelength of the $CsPbBr_3$ emission can be tuned by altering the synthesis and effectively changing the size of the $CsPbBr_3$ inclusions [44, 86]. The 540 nm emission wavelength observed in this work matches with the emission wavelength observed for bulk $CsPbBr_3$ [3]. This suggests that during the synthesis process from the melt, $CsPbBr_3$ domains are formed large enough to not be influenced by confinement effects and show bulk properties. When Cs_4PbBr_6 with $CsPbBr_3$ inclusions is excited at wavelengths longer than 350 nm it is possible to directly excite the $CsPbBr_3$ inclusions, as demonstrated in Figure 6d. The inclusions can also be excited by an energy transfer process from either the A-band, C/D-band, or a Pb^{2+} ion with a perturbed coordination sphere, illustrated by energy transfer pathway b, e, and g in Figure 2, respectively.

Excitation and Emission Mechanism

Based on the results and discussion, a vacuum referred binding energy diagram can be constructed to explain the observed emission processes. The resulting diagram is shown in Figure 2. Based on computational methods presented by Kang *et al.* [87] and information from He *et al.* [88] we tentatively placed the valence band (VB) top of Cs_4PbBr_6 at - 7 eV and that of $CsPbBr_3$ 1 eV higher. The optical bandgap of Cs_4PbBr_6 , which equals the A-band transition energy, is 3.9

eV. This value has been determined experimentally [29, 89]. The bottom of the conduction band (CB) of Cs_4PbBr_6 is determined by adding the optical bandgap to the VRBE of the top of the VB. The CB-bottom of CsPbBr_3 is determined by adding the emission energy to the VRBE of its VB-top; due to the small Stokes shift of CsPbBr_3 it can be assumed that the emission energy is approximately equal to the optical bandgap. It is estimated that the error margins in placing the top of the VB are approximately ± 0.3 eV; essential is that the VB-top and CB-bottom of CsPbBr_3 both fall well inside the bandgap of Cs_4PbBr_6 . The C/D-band transition energy is defined as the mobility bandgap, where mobile charge carriers are created upon excitation. The position of the A- and C/D-band transitions is determined based on the excitation spectra shown in Figure 6b and 7b.

The diagram consists of two sections, on the left the processes taking place in Cs_4PbBr_6 . On the right the additional processes taking place due to the presence of CsPbBr_3 inclusions. The position of the A^\times -band transitions, labelled $^\times\text{Pb}^{2+}$ are determined using Figure 6c and 7c. The exact position of the defect-related energy levels, labelled X_{def} in the diagram, is uncertain. The spacing between the levels is based on the emission wavelength of the defect related emission.

After exciting the A-band (arrow 1) three processes can take place: A-band emission (arrow 2), or energy transfer (pathways a and b) resulting in emission from a $^\times\text{Pb}^{2+}$ ion (arrow 3) or CsPbBr_3 inclusions (arrow 4). After exciting the C/D-band (arrow 5) three different processes can take place: A-band emission (arrow 2), or energy and/or charge carrier transfer (pathways d and e) resulting in emission from a defect (arrow 6) or CsPbBr_3 inclusions (arrow 4). It is also possible to excite a $^\times\text{Pb}^{2+}$ ion (arrow 7) after which three processes can take place: A^\times -band emission (arrow 3) or energy transfer (pathways f and g) resulting in emission from a defect (arrow 6) or CsPbBr_3 inclusions (arrow 4). The CsPbBr_3 inclusions can also be excited directly (arrows 8 and 9) after which two processes can take place: emission from the inclusion (arrow 4) or energy transfer (pathway h), if excited well above the band gap (arrow 9), resulting in emission from a defect (arrow 6).

X-ray Versus Optical Excitation

Under X-ray excitation, as shown in Figure 3a, the 610 nm emission band is 40.6 times more intense compared to the A-band emission. Upon exciting the C/D-band the intensity of the 610 nm emission is only 2.5 times stronger compared to the A-band emission. Moreover, it is completely absent upon exciting the A-band. The observed intensity difference can be explained based on the difference between X-ray excitation and optical excitation. Upon X-ray excitation all energy of the incident X-ray is transferred to a primary electron. This hot electron creates secondary excitations via electron-electron interactions along its ionisation track. This results in the formation of spatially separated electrons and holes. The electrons, due to their larger mobility, will diffuse further away from the initial ionisation track compared to the holes [90–93]. The separated electrons and holes first need to approach each other before emission can take place. Upon optically exciting the C/D-band transition, the formed electrons and holes stay in

closer proximity; emission can take place immediately. This happens on a shorter time scale compared to the recombination of the spatially separated electrons and holes formed upon X-ray excitation. The latter thus have more time to move through the crystal lattice and find a defect thus leading to a more intense 610 nm emission band upon X-ray excitation.

4. Conclusion

In this work the zero-dimensional caesium lead halide compound Cs_4PbBr_6 has been studied as function of temperature under both X-ray and UV-vis excitation. Cs_4PbBr_6 is studied with and without CsPbBr_3 inclusions. Upon X-ray excitation most of the scintillation light is present in the 610 nm emission band for both forms of Cs_4PbBr_6 . This is ascribed to the formation of spatially separated charge carriers reaching lattice defects. The pulsed X-ray excited decay curves show multiple decay components, the longest being approximately 800 ns. Upon exciting the C/D-band at 250 nm, the 610 nm emission band was also found which has not been reported before. The excitation spectrum of the 610 nm emission band contains an excitation band, labelled A^X , which is ascribed to Pb^{2+} ions with a perturbed coordination sphere. It is suggested that the 610 nm emission originates from defects in the vicinity of Pb^{2+} ions, leading to the perturbation of the coordination sphere. The 540 nm emission, based on the X-ray diffraction patterns and absorption spectra, is assigned to the presence of CsPbBr_3 inclusions. It is thus shown experimentally that both CsPbBr_3 inclusions and defects play a role in the photoluminescence behaviour of Cs_4PbBr_6 . All experimental results could be combined to formulate a general mechanism for the emission behaviour of Cs_4PbBr_6 .

5. Experimental

Crystals of Cs_4PbBr_6 were grown by the vertical Bridgman technique in sealed silica ampoules. Since Cs_4PbBr_6 melts incongruently at 500 °C [61], a non-stoichiometric mixture of 75% CsBr and 25% PbBr_2 was used. CsBr (Fluka, >99.5%) and PbBr_2 (Alpha, 5N) were dried at 200 °C in vacuum. In a dry box the starting materials were filled into a silica ampoule and sealed off under vacuum. The mixture was molten at 550 °C and slowly cooled by moving up the furnace within 10 days. The product contained a white tip of CsBr and Cs_4PbBr_6 , a yellow-orange middle part of Cs_4PbBr_6 , and an orange top part of Cs_4PbBr_6 and CsPbBr_3 eutecticum. Cs_4PbBr_6 crystals from the middle part were used for spectroscopic characterisations. Powder X-ray diffraction, see Figure S1, and spectroscopic data revealed that the sample (middle part) contained about 90% Cs_4PbBr_6 and 10% CsPbBr_3 . The phase separation in the CsBr - PbBr_2 melt did not work well, as also can be seen from the formation of a white tip containing CsBr .

CsBr (99.999 %, Sigma Aldrich) and PbBr_2 (>98 %, Alfa Aesar) were mixed in a 4.024 to 1.000 ratio and ground for 15 minutes. The mixture was loaded in a closed crucible and heated for 48 h at 600 K, after which it was let to cool down to room temperature. The as-obtained powder was loaded in a X-ray diffraction sample holder closed with Kapton foil to prevent powder spreading and reaction with moisture. The sample was measured on a PANalytical X'Pert PRO using Cu K_α -radiation (45 kV, 40 mA) in the range $10^\circ < 2\theta < 120^\circ$ with an increment of 0.008° for a total measurement time of 9h. The pattern was recorded using an X'Celerator detector. The obtained diffraction pattern was analysed using Rietveld profile refinement [94, 95] in the FullProf suite [96, 97]. The analysed powder diffraction pattern contained only the peaks of Cs_4PbBr_6 (>99 %) and CsBr (<1 %) as determined using Rietveld refinement.

X-ray excited emission spectra were recorded using a tungsten anode X-ray tube, operated at 79 kV. This produces X-rays with an average energy of 40 keV. The low energy part of the produced X-ray spectrum was removed by placing a 3 mm aluminium filter in front of the X-ray tube. This prevents radiation damage. The samples were mounted on the cold finger of a closed cycle helium cryostat operated below 10^{-4} bar.

Pulsed X-ray excited emission spectra were recorded using the time-correlated single photon counting method. The start signal of the measurements was generated by a PicoQuant LDH-P-C440 M pulsed laser, which directly excites a Hamamatsu N5084 light-excited X-ray tube. This results in the production of X-ray pulses with an average energy of 18.2 keV. The stop signal of the measurements was generated by the detection of a single photon by an ID Quantique id100-50 single-photon counter. Both start and stop signals were processed by an Ortec 567 time-to-amplitude converter whose output signal was digitised by an Ortec AD 144 16K ADC. The samples were mounted on the cold finger of a closed cycle helium cryostat operated below 10^{-4} bar.

Photoluminescence excitation and emission spectra were recorded using light from a 450 W xenon lamp passing through a Horiba Gemini 180 monochromator to excite the sample. The emitted light was collected at a 90° angle with respect to the excitation source. The emitted light passed through a Princeton Instruments SpectraPro-SP2358 monochromator before being detected by a Hamamatsu R7600u-20. Any reflected excitation light was removed using a long pass filter in front of the Princeton monochromator. All spectra were corrected for the lamp intensity. The samples were mounted on the cold finger of a closed cycle helium cryostat operated below 10^{-4} bar.

The presented absorbance spectra were recorded using a PerkinElmer Lambda 1050 equipped with an integrating sphere.

6. Conflicts of Interest

There are no conflicts to declare.

7. Acknowledgements

The authors would like to thank John Vlieland for his help in the solid state synthesis process. The authors acknowledge financial supports from the TTW/OTP grant no. 18040 of the Dutch Research Council.

References

- [1] M. D. Birowosuto, D. Cortecchia, W. Drozdowski, K. Brylew, W. Lachmanski, A. Bruno, C. Soci, *Scientific Reports* 6 (2016) 37254, <https://doi.org/10.1038/srep37254>
- [2] Y. Li, W. Shao, X. Ouyang, Z. Zhu, H. Zhang, X. Ouyang, B. Liu, Q. Xu, *The Journal of Physical Chemistry C* 123 (2019) 28, <https://doi.org/10.1021/acs.jpcc.9b05269>
- [3] J. J. van Blaaderen, D. Biner, K. W. Krämer, P. Dorenbos, *Nuclear Instruments and Methods in Physics Research Section A: Accelerators, Spectrometers, Detectors and Associated Equipment* 1064 (2024) 169322, <https://doi.org/10.1016/j.nima.2024.169322>
- [4] J. J. van Blaaderen, F. Maddalena, C. Dong, M. D. Birowosuto, P. Dorenbos, *Journal of Materials Chemistry C* 10 (2022) 11598-11606, <https://doi.org/10.1039/D2TC01483A>
- [5] J. J. van Blaaderen, S. van der Sar, D. Onggo, Md Abdul K. Sheikh, D. R. Schaart, M. D. Birowosuto, P. Dorenbos, *Journal of Luminescence* 263 (2023) 120012, <https://doi.org/10.1016/j.jlumin.2023.120012>
- [6] J. J. van Blaaderen, L. A. van den Brekel, K. W. Krämer, P. Dorenbos, *Chemistry of Materials* 35 (2023) 9623-9631, <https://doi.org/10.1021/acs.chemmater.3c01810>
- [7] Q. A. Akkerman, L. Manna, *ACS Energy Letters*, 5 (2020) 604-610, <https://doi.org/10.1021/acsenergylett.0c00039>
- [8] P. Dorenbos, *Optical Materials: X* 1 (2019) 100021, <https://doi.org/10.1016/j.omx.2019.100021>
- [9] P. Dorenbos, *Fundamental Limitations in the Performance of Ce³⁺-, Pr³⁺-, and Eu²⁺- Activated Scintillators*, *IEEE transactions on nuclear science* 57 (2010) 3, <https://doi.org/10.1109/TNS.2009.2031140>
- [10] E. V. D. van Loef, P. Dorenbos, C. W. E. van Eijk, *Applied Physics Letters*, 79 (2001) 1573, <https://doi.org/10.1063/1.1385342>

- [11] M. S. Alekhin, D. A. Biner, K. W. Krämer, P. Dorenbos, *Journal of Luminescence* 145 (2014) 723-728, <http://dx.doi.org/10.1016/j.jlumin.2013.08.058>
- [12] E. D. Bourret-Courchesne, G. Bizarri, R. Borade, Z. Yan, S. M. Hanrahan, G. Gundiah, A. Choudhry, A. Canning, S. E. Derenzo, *Nuclear Instruments and Methods in Physics Research A* 612 (2009) 138-142, <https://doi.org/10.1016/j.nima.2009.10.146>
- [13] C. van Aarle, K. W. Krämer, P. Dorenbos, *Journal of Materials Chemistry C* 11 (2023) 2336-2344, <https://doi.org/10.1039/D2TC05311J>
- [14] C. van Aarle, K. W. Krämer, P. Dorenbos, *Journal of Luminescence* 251 (2022) 119209, <https://doi.org/10.1016/j.jlumin.2022.119209>
- [15] W. W. Wolszczak, D. L. Carroll, R. T. Williams, *Advanced X-ray Detector Technologies*, Chapter 1 (2022), https://doi.org/10.1007/978-3-030-64279-2_1
- [16] R. T. Williams, W. W. Wolszczak, X. Yan, D. L. Carroll, *ACS Nano* 14 (2020) 5161-5169, <https://doi.org/10.1021/acsnano.0c02529>
- [17] Z. Shaki, M. M. Byrannvand, N. Taghavinia, M. Kedia, M. Saliba, *Energy and Environmental Science* 14 (2021) 5690-5722, <https://doi.org/10.1039/D1EE02018H>
- [18] W. A. Dunlap-Shohl, Y. Zhou, N. P. Padture, D. B. Mitzi, *Chemical Reviews* 119 (2019) 3193-3295, <https://doi.org/10.1021/acs.chemrev.8b00318>
- [19] Q. A. Akkerman, G. Raino, M. V. Kovalenko, L. Manna, *Nature Materials* 17 (2018) 394-405, <https://doi.org/10.1038/s41563-018-0018-4>
- [20] K. S. Song, R. T. Williams, *Springers Series in Solid State Sciences*, Self trapped Excitons, 2nd ed, SpringerVerlag: Berlin, 1996, 105
- [21] Z. Yuan, C. Zhou, Y. Tian, Y. Shu, J. Messier, J. C. Wang, L. J. van de Burght, Y. Kountouriotis, E. Xin, E. Holt, K. Schanze, R. Clark, T. Siegrist, B. Ma, *Nature Communications* 8 (2017) 14051, <https://doi.org/10.1038/ncomms14051>
- [22] E. R. Dohner, A. Jaffe, L. R. Bradshaw, H. I. Karunadasa, *Journal of the American Chemical Society* 136 (2014) 38, <https://doi.org/10.1021/ja507086b>
- [23] L. Mao, Y. Wy, C. C. Stoumpos, M. R. Wasielewski, M. G. Kanatzidis, *Journal of the American Chemical Society*, 139 (2017) 14, <https://doi.org/10.1021/jacs.7b01312>
- [24] F. Maddalena, A. Xie, Arramel, M. E. Witkowski, M. Makowski, B. Mahler, W. Drozdowski, T. Mariyappan, S. V. Springham, P. Coquet, C. Dujardin, M. D. Birowosuto, C. Dang, *Journal of Materials Chemistry C* 9 (2021) 2504, <https://doi.org/10.1039/D0TC05647B>
- [25] A. Xie, F. Maddalena, M. E. Witkowski, M. Makowski, B. Mahler, W. Drozdowski, S. V. Springham, P. Coquet, C. Dujardin, M. D. Birowosuto, C. Dong, *Chemistry of Materials* 32 (2020) 8530- 8539, <https://doi.org/10.1021/acs.chemmater.0c02789>

- [26] C. K. Moller, On the structure of cesium hexahalogeno-plumbates, *Kongelige Danske Videnskabernes Selskab, Matematisk-Fysike Meddeleser*, 32, 1-13, 1960
- [27] M. De Bastiani, I. Dursun, Y. Zhang, B. A. Alshankiti, X.-H. Miao, J. Yin, E. Yengel, E. Alarousu, B. Turedi, J. M. Almutlaq, M. I. Saidaminov, S. Mitra, I. Ger-eige, A. Al Saggaf, Y. Zhu, Y. Han, I. S. Roquan, J.-L. Bredas, O. F. Mohammed, O. M. Bakr, *Chemistry of Materials* 29 (2017) 7108-7113, <https://doi.org/10.1021/acs.chemmater.7b02415>
- [28] Q. A. Akkerman, S. Park, E. Radicchi, F. Nunzi, E. Mosconi, F. De Angelis, R. Brescia, P. Rastogi, M. Prato, L. Manna, *Nano Letters* 17 (2017) 1924- 1930, <http://dx.doi.org/10.1021/acs.nanolett.6b05262>
- [29] S. Kondo, K. Amaya, T. Saito, *Journal of physics: Condensed Matter* 14 (2002) 2093-2099, <http://dx.doi.org/10.1088/0953-8984/14/8/334>
- [30] M. Nikl, E. Mihokova, K. Nitsch, F. Somma, C. Giampaolo, G. P. Pazzi, P. Fabeni, S. Zazubovich, *Chemical Physical Letters* 306 (1999) 5-6, [https://doi.org/10.1016/S00092614\(99\)00477-7](https://doi.org/10.1016/S00092614(99)00477-7)
- [31] H. Lin, C. Zhou, Y. Tian, T. Siegrist, B. Ma, *ACS Energy Letters* 3 (2018) 1, <https://doi.org/10.1021/acsenergylett.7b00926>
- [32] M. I. Saidaminov, A. F. Mohammed, A. M. Bakr, *ACS Energy Letters* 2 (2017) 4, <https://doi.org/10.1021/acsenergylett.6b00705>
- [33] A. Bohun, J. Dolejsi, C. Barta, *chechoslovak Journal of Physics B* 20 (1970) 803-807, <https://doi.org/10.1007/BF01726608>
- [34] P. W. M. Jacobs, *Journal of Physics and Chemistry of Solids* 52 (1991) 1, [https://doi.org/10.1016/0022-3697\(91\)90059-9](https://doi.org/10.1016/0022-3697(91)90059-9)
- [35] A. Ranfagni, D. Mugnai, M. Bacci, *Advances in Physics* 32 (1983) 6, <https://doi.org/10.1080/00018738300101621>
- [36] M. Forro, *Z. Physik* 56 (1929) 534-543, <https://doi.org/10.1007/BF01338864>
- [37] G. Blasse, *Optical Electron transfer between metal ions and its consequences, complex chemistry structure and bonding*, vol 76, ISBN: 978-3-540-53499-0, <https://doi.org/10.1007/3-54053499-7>
- [38] H. F. Folkerts, M. A. Hamstra, G. Blasse, *Chemical Physics Letters* 246 (1995) 1-2, [https://doi.org/10.1016/0009-2614\(95\)01067-J](https://doi.org/10.1016/0009-2614(95)01067-J)
- [39] Y. Zhang, M. I. Saidaminov, I. Dursun, H. Yang, B. Murali, E. Alarousu, E. Yengel, B. A. Alshankiti, A. M. Bakr, A. F. Mohammed, *The Journal of Physical Chemistry Letters* 8 (2017) 5, <https://doi.org/10.1021/acs.jpcclett.7b00105>
- [40] Z. Liu, Y. Bekenstein, X. Ye, S. N. Nguyen, J. Swabeck, D. Zhang, S. T. Lee, P. Yang, W. Ma, A. P. Alivisatos, *Journal of the American Chemical Society* 139 (2017) 15, <https://doi.org/10.1021/jacs.7b01409>

- [41] J. Yin, Y. Zhang, A. Bruno, C. Soci, A. M. Bakr, J. L. Bredas, A. F. Mohammad, *ACS Energy Letters* 2 (2017) 12, <https://doi.org/10.1021/acsenenergylett.7b01026>
- [42] H. Cai, M. Lao, J. Xu, Y. Chen, C. Zhong, S. Lu, A. Hao, R. Chen, *Ceramic International* 45 (2019) 5, <https://doi.org/10.1016/j.ceramint.2018.12.038>
- [43] J. H. Cha, J. H. Han, W. Yin, C. Park, Y. Park, T. K. Ahn, J. H. Cho, D. Y. Jung, *The Journal of Physical Chemistry Letters* 8 (2017) 3, <https://doi.org/10.1021/acscjpclett.6b02763>
- [44] X. Chen, F. Zhang, Y. Ge, L. Shi, S. Huang, J. Tang, Z. Lv, L. Zhang, B. Zou, H. Zhong, *Advanced Functional Materials* 28 (2018) 16, <https://doi.org/10.1002/adfm.201706567>
- [45] M. I. Saidaminov, J. Almutlaq, S. Sarmah, I. Dursun, A. A. Zhumekenov, R. Begum, J. Pan, N. Cho, A. F. Mohammed, A. M. Bakr, *ACS Energy Letters* 1 (2016) 4, <https://doi.org/10.1021/acsenenergylett.6b00396>
- [46] Y. Zhou, J. Ding, Z. Wang, Y. Tong, X. Liang, J. Du, W. Xia, Z. Liu, W. Xiang, *Chemical Engineering Journal*, 426 (2021) 130786, <https://doi.org/10.1016/j.cej.2021.130786>
- [47] Z. Bao, H.-C. Wang, Z.-F. Jiang, R. J. Chung, R.-S. Liu, *Inorganic Chemistry* 57 (2018) 21, <https://doi.org/10.1021/acs.inorgchem.8b01985>
- [48] Y.-M. Chen, Y. Zhou, Q. Zhao, J.-Y. Zhang, J.-P. Ma, T.-T. Xuan, S.-Q. Guo, Z.-J. Yong, J. Wang, Y. Kuroiwa, C. Moriyoshi, H.-T. Sun, *ACS Applied Materials and Interfaces* 10 (2018) 18, <https://doi.org/10.1021/acsaami.8b04556>
- [49] H. Zhao, R. Sun, Z. Wang, K. Fu, X. U, Y. Zhang, *Advanced Functional Materials* 29 (2019) 30, <https://doi.org/10.1002/adfm.201902262>
- [50] Q. A. Akkerman, A. L. Abdelhady, L. Manna, *The Journal of Physical Chemistry Letters* 9 (2018) 9, <https://doi.org/10.1021/acscjpclett.8b00572>
- [51] J. H. Cha, H. J. Lee, S. H. Kim, K. C. Ko, B. J. Suh, O. H. Han, D. Y. Jung, *ACS Energy Letters* 5 (2020) 7, <https://doi.org/10.1021/acsenenergylett.0c00964>
- [52] K. Wang, Y. Yuan, S. Du, Q. Yao, J. Chang, C. Shang, C. Li, H. Sun, W. Zhang, J. Ding, T. Zhou, *The Journal of Physical Chemistry C* 125 (2021) 28, <https://doi.org/10.1021/acs.jpcc.1c04696>
- [53] S. Seth, A. Samanta, *The Journal of Physical Chemistry Letters* 8 (2017) 18, <https://doi.org/10.1021/acscjpclett.7b02100>
- [54] Z. Qin, S. Dai, V. G. Hadjiev, C. Wang, L. Xie, Y. Ni, C. Wu, G. Yang, S. Chen, L. Deng, Q. Yu, G. Feng, Z. M. Wang, J. Bao, *Chemistry of Materials* 31 (2019) 21, <https://doi.org/10.1021/acs.chemmater.9b03426>
- [55] Z. Zhang, Y. Zhu, W. Wang, W. Zheng, R. Lin, X. Li, H. Zhang, D. Zhong, F. Huang, *Crystal Growth and Design* 18 (2018) 11, <https://doi.org/10.1021/acs.cgd.8b00817>

- [56] L. N. Quan, R. Quintero-Bermudez, O. Voznyyy, G. Walters, A. Jain, J. Z. Fan, X. Zheng, Z. Yang, E. H. Sargent, *Advanced Materials* 29 (2017) 21, <https://doi.org/10.1002/adma.201605945>
- [57] A. Ray, D. Maggioni, D. Baranov, Z. Dang, M. Prato, Q. A. Akkerman, L. Golidoni, E. Caneva, L. Manna, A. L. Abdelhady, *Chemistry of Materials* 31 (2019) 18, <https://doi.org/10.1021/acs.chemmater.9b02944>
- [58] N. Riesen, M. Lockrey, K. Badek, H. Riesen, *Nanoscale* 11 (2019) 3925, <https://doi.org/10.1039/C8NR09255A>
- [59] L. Wang, H. Liu, Y. Zhang, A. F. Mohammed, *ACS Energy Letters* 5 (2020) 1, <https://doi.org/10.1021/acsenergylett.9b02275>
- [60] K. Biswas, *Materials Advances* 3 (2022) 6791, <https://doi.org/10.1039/D2MA00544A>
- [61] M. Cola, V. Massarotti, R. Riccardi, C. Sinistri, *Zeitschrift fur Naturforschung A* 26.8 (1971) 1328-1332, <https://doi.org/10.1515/zna-1971-0812>
- [62] M. Nikl, K. Nitsch, E. Mikokova, K. Polak, P. Fabeni, G. P. Pazzi, M. Gurioli, S. Santucci, R. Phani A. Scacco, F. Somma, *Physica E Low-dimensional systems and nanostructures* 4 (1999) 4, [https://doi.org/10.1016/S1386-9477\(99\)00016-8](https://doi.org/10.1016/S1386-9477(99)00016-8)
- [63] R. Aceves, V. Babin, M. Barboza Flores, P. Fabeni, A. Maaros, M. Nikl, K. Nitsch, G. P. Pazzi, R. Perez Salas, I. Sildos, N. Zazubovich, S. Zazubovich, *Journal of Luminescence* 93 (2001) 1, [https://doi.org/10.1016/S0022-2313\(01\)00175-2](https://doi.org/10.1016/S0022-2313(01)00175-2)
- [64] M. Nikl, K. Nitsch, K. Polak, E. Mihokova, S. Zazubovich, G. P. Pazzi, P. Fabeni, L. Salvini, R. Aceves, M. Barbose-Flores, R. Perez Salas, M. Gurioli, A. Scacco, *Journal of Luminescence* 72-74 (1997) 377-379, [https://doi.org/10.1016/S0022-2313\(96\)00341-9](https://doi.org/10.1016/S0022-2313(96)00341-9)
- [65] A. van Hattem, D. Alders, R. J. M. konings, A. L. Smith, *The Journal of Physical Chemistry C* 127 (2023) 35, <https://doi.org/10.1021/acs.jpcc.3c02696>
- [66] B. Kang, K. Biswas, *The Journal of Physical Chemistry Letters* 9 (2018) 4, <https://doi.org/10.1021/acs.jpcclett.7b03333>
- [67] T. Kubota, S. Yanagimoto, H. Saito, K. Akiba, A. Ishii, T. Sannomiya, *Applied Physics Express* 17 (2024) 015005, <https://doi.org/10.35848/1882-0786/ad1bc4>
- [68] Y. Ding, R. Lin, Y. Lioang, W. Zheng, L. Chen, X. Ouyang, F. Huang, *The Journal of Physical Chemistry Letters* 12 (2021) 30, <https://doi.org/10.1021/acs.jpcclett.1c01615>
- [69] Y. Li, L. Chen, B. Liu, J. Ruan, J. Liu, X. Ouyang, Q. Xu, *Ceramics International* 48 (2022) 12, <https://doi.org/10.1016/j.ceramint.2022.02.222>
- [70] X. Wu, Q. Zhou, H. Wu, X. Du, G. Niu, G. Liang, Q. Hy, J. Xiao, *The Journal of Physical Chemistry C* 125 (2021) 26619-26626, <https://doi.org/10.1021/acs.jpcc.1c08178>

- [71] P. R. Collins, W. J. Fredericks, *Journal of Physics and Chemistry of Solids*, 47 (1986) 5, [https://doi.org/10.1016/0022-3697\(86\)90053-3](https://doi.org/10.1016/0022-3697(86)90053-3)
- [72] S. B. S. Sastry, V. Viswanathan, C. Ramasastry, *Journal of the Physical Society of Japan* 33 (1973) 508-513, <https://doi.org/10.1143/JPSJ.35.508>
- [73] M. Nikl, E. Mihokova, K. Nitsch, *Solid State Communications* 4 (1992) 12, [https://doi.org/10.1016/0038-1098\(92\)90691-2](https://doi.org/10.1016/0038-1098(92)90691-2)
- [74] S. Zazubovich, *International Journal of Modern Physics B* 8 (1993) 8, <https://doi.org/10.1142/S0217979294000506>
- [75] A. A. Bol, A. Meijerink, *Physica Chemistry Chemical Physics* 3 (2001) 2105-2112, <https://doi.org/10.1039/B100968K>
- [76] E. Goovaerts, S. V. Nistor, D. Schoemaker, *Physical Review B* 28 (1983) 3712, <https://doi.org/10.1103/PhysRevB.28.3712>
- [77] J. Kerssen, W. G. De Gruijter, J. Volger, *Physica* 70 (1973) 2, [https://doi.org/10.1016/00318914\(73\)90255-3](https://doi.org/10.1016/00318914(73)90255-3)
- [78] P. Fabeni, A. Krasnikov, M. Nikl, G. P. Pazzi, S. Zazubovich, *Solid State Communications* 126 (2003) 12, [https://doi.org/10.1016/S0038-1098\(03\)00333-8](https://doi.org/10.1016/S0038-1098(03)00333-8)
- [79] Zh. Egemberdiev, V. Nagirnyi, T. Soovik, S. Zazubovich, *Basic Solid State Physics* 126 (1984) 1, <https://doi.org/10.1002/pssb.2221260147>
- [80] Zh. Egemberdiev, A. Usarov, S. Zazubovich, *Basic Solid State Physics* 164 (1991) 1, <https://doi.org/10.1002/pssb.2221640120>
- [81] Zh. Egemberdiev, K. Ismailov, A. Usarov, S. Zazubovich, N. Jaanson, *Basic Solid State Physics* 163 (1991) 1, <https://doi.org/10.1002/pssb.2221630118>
- [82] L. E. Nagli, S. V. Dyachenko, *Basic Solid State Physics*, 146 (1988) 1, <https://doi.org/10.1002/pssb.2221460131>
- [83] A. van Dijken, H. F. Folkerts, G. Blasse, *Journal of luminescence* 72-74 (1997) 660-661, [https://doi.org/10.1016/S0022-2313\(96\)00431-0](https://doi.org/10.1016/S0022-2313(96)00431-0)
- [84] H. F. Folkerts, F. Ghianni, G. Blasse, *Journal of Physics and Chemistry of Solids* 57 (1996) 11, [https://doi.org/10.1016/0022-3697\(96\)00041-8](https://doi.org/10.1016/0022-3697(96)00041-8)
- [85] H. F. Folkerts, A. van Dijken, G. Blasse, *Journal of Physics Condensed Matter* 7 (1995) 50, <https://doi.org/10.1088/0953-8984/7/50/034>
- [86] G. Almeida, L. Goldoni, Q. Akkerman, Z. Dang, A. H. Khan, S. Marras, I. Moreels, L. Manna, *ACS Nano* 12 (2018) 2, <https://doi.org/10.1021/acsnano.7b08357>
- [87] Byungkyun Kang, Koushik Biswas, *Journal of Physical Chemistry Letters* 9 (2018) 830, <https://doi.org/10.1021/acs.jpcllett.7b03333>

[88] Yihui He, Liviu Matei, Hee Joon Jung, Kyle M. McCall, Michelle Chen, Constantinos C. Stoumpos, Zhifu Liu, John A. Peters, Duck Young Chung, Bruce W. Wessels, Michael R. Wasielewski, Vinayak P. Dravid, Arnold Burger, Mercouri G. Kanatzidis, *Nature Communications* 9 (2018) 1609, <https://doi.org/10.1038/s41467-018-04073-3>

[89] M. shin, S. W. Nam, A. Sadhanala, R. Shivanna, M. Anaya, A. Jimenez-Solano, H. Yoon, S. Jeon, S. D. Stranks, R. L. Z. Hoyer, B. Shin, *ACS Applied Energy Materials* 3 (2019) 1, <https://doi.org/10.1021/acsaem.9b02214>

[90] R. T. Williams, J. Q. Grim, Q. Li, K. B. Ucer, W. W. Moses, *Basic Solid State Physics* 248 (2011) 426-438, <https://doi.org/10.1002/pssb.201000610>

[91] W. W. Moses, G. Bizarri, R. T. Williams, S. A. Payne, A. N. Vasilev, J. Singh, Q. Li, J. Q. Grim, W.-S. Choong, *IEEE Transactions on Nuclear science* 59 (2012) 2038-2044, <https://doi.org/10.1109/TNS.2012.2186463>

[92] A. N. Vasilev, *IEEE Transactions on Nuclear Science* 55 (2008) 3, <https://doi.org/10.1109/TNS.2007.914367>

[93] I. V. Khodyuk, *Nonproportionality of inorganic scintillators*, ISBN:9789088915536, <https://doi.org/10.4233/uuid:cb4008a8-981a-4283-b213-199d41756269>

[94] H.M. Rietveld, *Applied Crystallography* 2 (1969) 64-71, <http://dx.doi.org/10.1107/S0021889869006558>

[95] B. van Laar, H. Schenk, *Acta Crystallographica Section A: Foundations and Advances* 74.2 (2018) 88-92, <https://doi.org/10.1107/S2053273317018435>

[96] J. Rodríguez-Carvajal, LLB Sacley and LCSIM Rennes, 2003

[97] T. Roisnel, J. Rodríguez-Carvajal, J. Gonzalez-Platas, *Mater. Sci. Forum* 378 (2001) 118-123

Supplementary Information

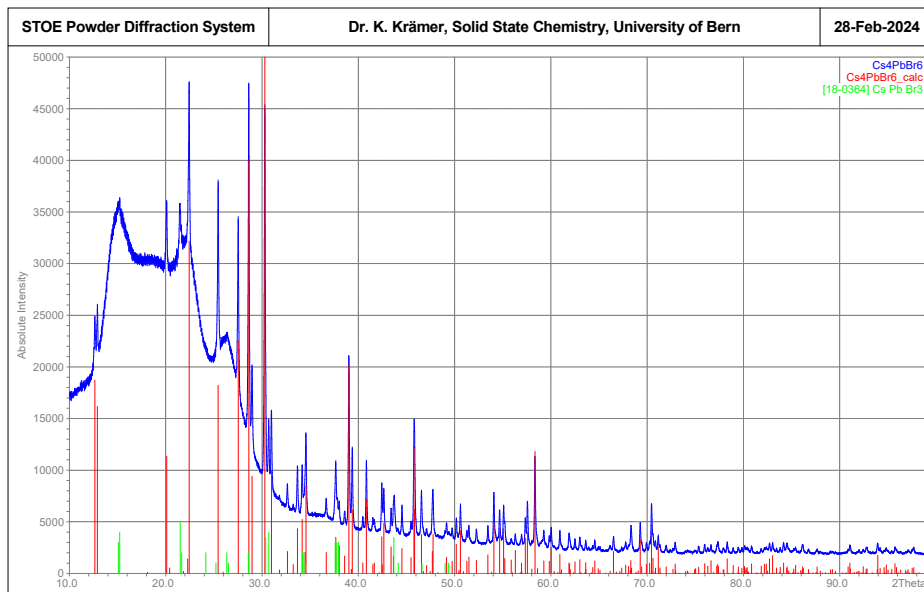


Figure S1: Powder diffraction pattern of Cs₄PbBr₆ with about 10% CsPbBr₃ inclusions measured with Cu K_{α1} radiation at room temperature. The three broad peaks below 30° 2-Theta originate from the Mylar window of the sample holder.

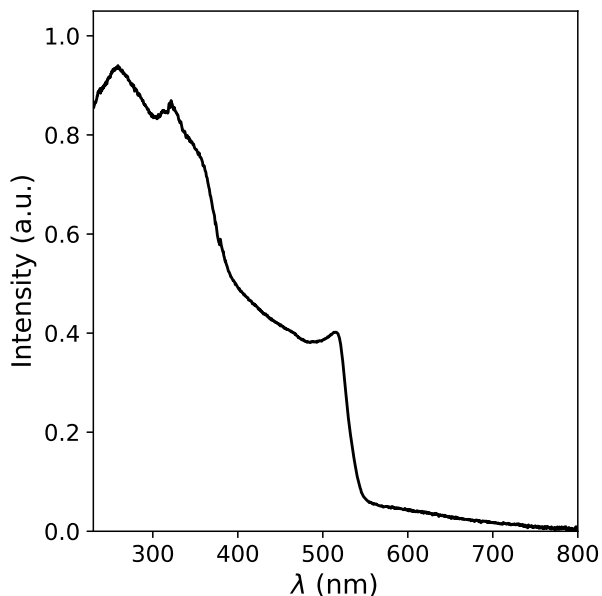


Figure S2: Room temperature absorbance spectrum of the CsPbBr₃ single crystal.

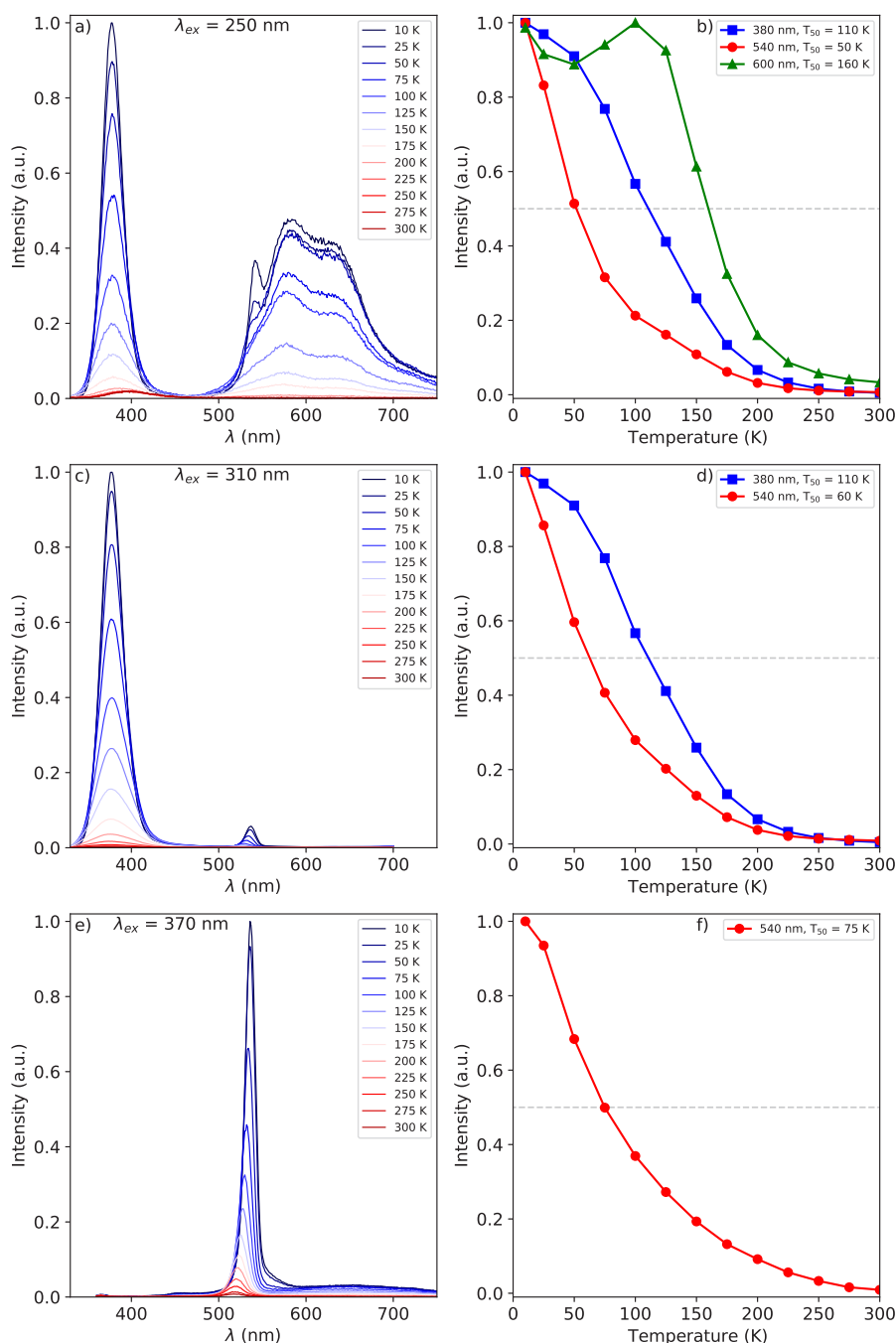


Figure S3: Temperature dependent photoluminescence emission spectra of Cs_4PbBr_6 single crystal with CsPbBr_3 inclusions from 10 to 300 K recorded by exciting at (a) 250 nm, (c) 310 nm, and (e) 350nm.

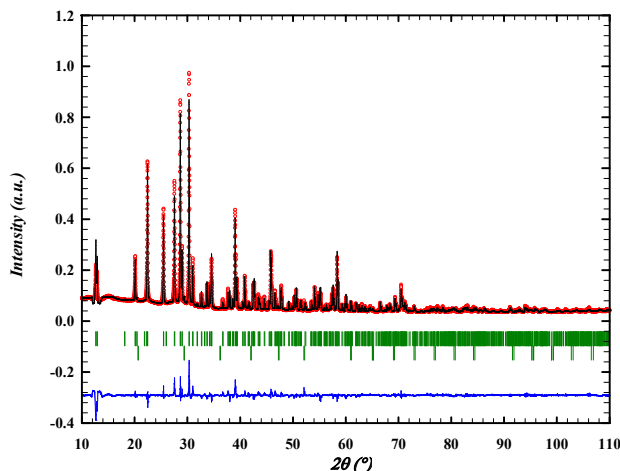


Figure S4: Experimental (Y_{observed} , in red circles) and calculated ($Y_{\text{calculated}}$, in black) powder XRD patterns of synthesised Cs_4PbBr_6 . The difference between calculated and experimental intensities, $Y_{\text{observed}} - Y_{\text{calculated}}$, is shown in blue. The angular positions of Bragg reflections for Cs_4PbBr_6 and CsBr are shown in green. Measurement at $\lambda = \text{Cu K}\alpha$. Rietveld refinement of Cs_4PbBr_6 in space group $R3c$ (167) and CsBr in $\text{Pm}3m$ (221).

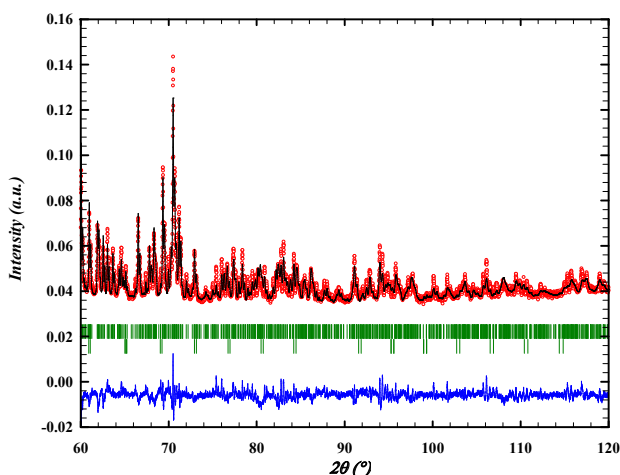


Figure S5: Zoom in of the experimental (Y_{observed} , in red circles) and calculated ($Y_{\text{calculated}}$, in black) powder XRD patterns of synthesised Cs_4PbBr_6 . The difference between calculated and experimental intensities, $Y_{\text{observed}} - Y_{\text{calculated}}$, is shown in blue. The angular positions of Bragg reflections for Cs_4PbBr_6 and CsBr are shown in green. Measurement at $\lambda = \text{Cu K}\alpha$. Rietveld refinement of Cs_4PbBr_6 in space group $R3c$ (167) and CsBr in $\text{Pm}3m$ (221).

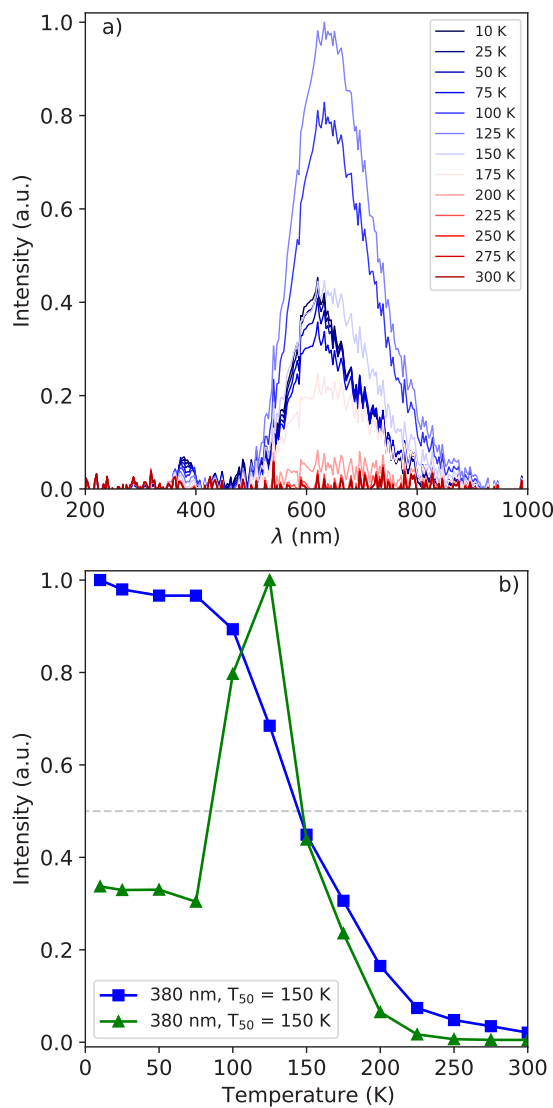


Figure S6: (a) Temperature dependent X-ray excited emission spectra of Cs_4PbBr_6 without CsPbBr_3 inclusions. (b) Integrated spectral intensity.

4

Temperature Dependent Scintillation Properties and Mechanisms of $(\text{PEA})_2\text{PbBr}_4$ Single Crystals

Abstract

In this work the scintillation properties of $(\text{PEA})_2\text{PbBr}_4$ are studied as function of temperature, accessing the potential use of this materials for low temperature applications. The scintillation properties and mechanism have been studied using a combination of temperature dependent photoluminescence emission and excitation, X-ray excited emission and decay measurements. At room temperature the X-ray excited emission is dominated by the 442 nm emission with a lifetime of 35.2 ns. Under UV-Vis photon excitation an additional emission peak is observed at 412 nm. At 10K, both X-ray and UV-Vis photon excited emission spectra show a narrow emission peak at 412 nm and a broad emission band centred around 525 nm with a lifetime of 1.53 ns (24%) and 154 ns (76%), respectively. The exact nature of the observed emission peaks is not known. For this reason two potential mechanisms explaining the difference between UV-Vis photon and X-ray excitation and their temperature dependent emissions are explored. The total spectral intensity decreases to 72% of the intensity at room temperature at 10 K. It is suggested that the observed negative thermal quenching behaviour results from a combination of more self absorption and a higher degree of self trapped exciton formation under X-ray excitation. The observed fast decay component at 10K and light yield of 9400 photons / MeV at room temperature, showing only a 28% decrease at 10K, could make this material potentially interesting for low temperature and fast timing applications.

The content of this chapter is based on: J. Jasper van Blaaderen, Francesco Maddalena, Cuong Dang, Muhammad Danang Birowosuto, Pieter Dorenbos, Journal of Materials Chemistry C 10 (2022) 11598-11606

1. Introduction

In the past two decades, scintillation research has mainly focused on lanthanide activated materials, for example by utilising co-doping strategies [1–3]. Another less studied class of materials, potentially interesting for scintillation, is wide-bandgap semiconductors. Examples of which are HgI₂, PbI₂, and methylammonium lead halides (MAPbX₃, MA = CH₃NH₃, and X = I, Br, or Cl) [4–6]. The latter, belonging to the perovskite family, gained a lot of attention in the early 2010's due to its high efficiency solar cells and optoelectronic applications [7–9] sparking further interest in the lead-halide perovskite family.

Perovskites can be described by the formula ABX₃ in which A and B are different size cations, and X an anion [7]. Crystals can be grown from solution, when A is an organic cation, at relatively low processing temperatures [10, 11]. The presence of heavy Pb atoms in APbX₃ perovskites makes them very suitable for radiation detection [12, 13]. Typical bandgaps of these materials lay in the range of 1 to 3 eV, significantly increasing their theoretical light yields compared to traditional scintillators [14].

Experimental evidence of these potential high light yields has been provided by Birowosuto *et al.* and Mykhaylyk *et al.* when studying the cryogenic (7K) scintillation properties of APbX₃ perovskites [15, 16]. At room temperature however, a strong decrease in the light yield is observed. This is ascribed to quenching of the exciton luminescence and strong self absorption due to a small Stokes shift [17, 18].

Stabilisation of the exciton luminescence could be achieved by introducing quantum confinement in the system, either by using nano-technology or by changing the 3D perovskite crystals structure. For example, CsPbBr₃ nano-particles show luminescence at room temperature while bulk crystals do not [19, 20]. An example of such an approach is the implementation of CsPbBr₃ nano particles in a Cs₄PbBr₆ host matrix (CsPbBr₃@Cs₄PbBr₆) [21]. The potential use of CsPbBr₃@Cs₄PbBr₆ for scintillation has been discussed elaborately in the recent work of Williams *et al.* [22], identifying two main factors prohibiting the use of this material as scintillator: The nano-particle to host energy transfer is not efficient, and the Stokes shift of the exciton luminescence is too small.

There are several ways, as suggested by Wolszczak *et al.* and Williams *et al.* [17, 22], in which "The Stokes Shift Problem" could be solved. Both authors identified roughly the same solutions: surrounding the nano particles with wavelength shifting dyes, doping with activator ions, and utilising the formation of self trapped excitons in lower molecular dimension compounds.

One group of lower dimensional materials, from which some show the formation of self-trapped excitons [23–25], are organic-inorganic lead halide 2D perovskites. They are formed by replacing the A site cation with a large organic molecule, creating a layered structure in which PbX₆ octahedra are corner connected and separated by a layer of organic molecules.

The 2D perovskite phenethylammonium lead bromide ((PEA)₂PbBr₄), is one of the compounds which recently gaining interest due to its scintillation properties [26, 29, 30]. It has a density of 2.36 g/cm³ and effective atomic number of 32.31 [11]. The light yield was estimated to be approximately 11.000 photons/MeV (ph/MeV) at room temperature [27]. Xie *et al.* demonstrated a life time of 11 ns at room temperature, making this material very interesting for fast timing application like in time-of-flight based positron emission tomography (TOF-PET) [31–33].

In this work the scintillation properties of (PEA)₂PbBr₄ are studied as function of temperature. The goal is to assess whether this material is a potentially interesting candidate for low temperature applications, for example TOF-PET. For this (PEA)₂PbBr₄ samples have been studied from 300 down to 10 K. The samples are studied using both visible photons and X-rays. The emission spectra recorded using the different means of excitation are compared in order to obtain a better spectroscopic understanding of the processes at hand. A life time study is performed by measuring pulsed X-ray excited decay spectra. The energy resolution and light yield of these samples have been estimated from pulse height spectra, using a ¹³⁷Cs source.

2. Results

Photoluminescence Excitation and Emission

Figure 1a shows the photoluminescence emission (PL) and excitation (PLE) spectra of (PEA)₂PbBr₄ at 300, 150, and 10 K. An overview of the spectral change upon cooling from 300 down to 10 K is shown in Figure 1b and c. The emission spectrum recorded at 300 K shows two peaks, centred around 412 nm and 442 nm. On the longer wavelength side of the latter, a long tail is observed. Upon cooling a blue shift is observed for the 442 nm emission, eventually merging with the 412 nm emission. This shift is clearly visible in the PL spectrum recorded at 150 K, shown in Figure 1a. Additionally, a broad emission band centred around 525 nm appears at low temperature. The 412 nm emission peak is observed both by Kawano *et al.* in (PEA)₂PbBr₄ single crystals and Guo *et al.* in (PEA)₂PbBr₄ nanoplatelets [26, 34]. Both ascribe it to free exciton emission from the inorganic Pb-Br layer. Kawano *et al.* ascribe the 442 nm emission peak to lattice defects creating donor and acceptor states close to the band edges [26]. The broad 525 nm emission band, observed at low temperatures, is ascribed to the formation of self trapped excitons [35]. The same assignments will be used in this work.

The excitation spectrum recorded at 300 K, shown in Figure 1b, contains three distinct bands centred around 423, 370 with a shoulder on the shorter wavelength side, and 280 nm. The spectra are recorded in the shoulder of the 442 nm emission to reveal the spectral overlap between the PL and PLE spectra. No significant changes were observed when recording the PLE spectra at the emission maxima. The first two bands, 423 and 370 nm, are ascribed to the formation of excitons and across band gap transitions, respectively [37,38]. Additionally, as can be seen in Figure 2a, a second peak is observed in the 423 nm band,

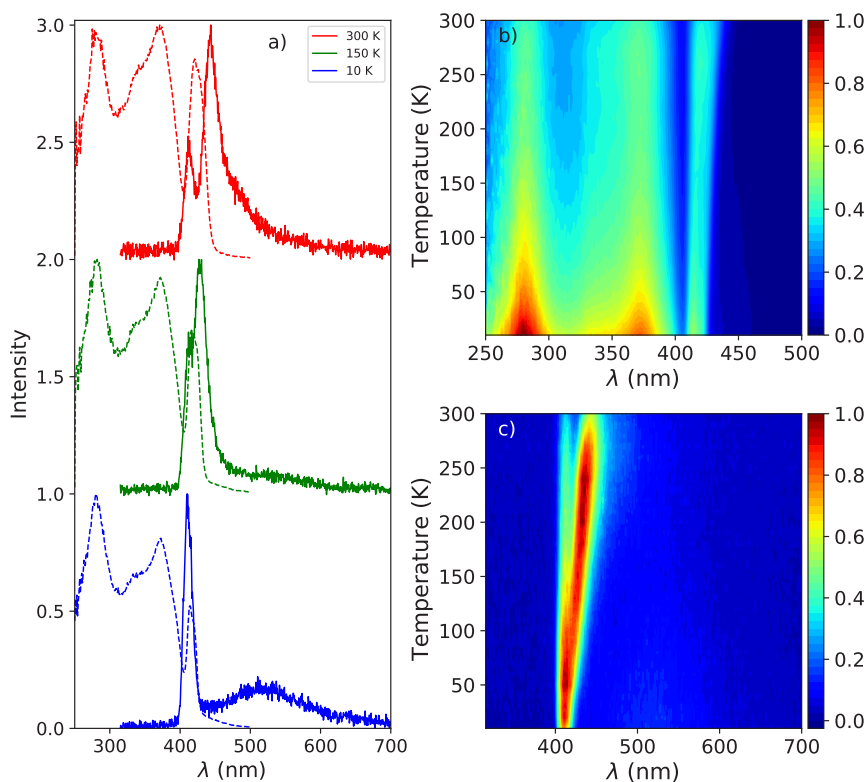


Figure 1: (a) Temperature dependent photoluminescence emission ($\lambda_{\text{ex}} = 260$ nm) and excitation ($\lambda_{\text{em}} = 530$ nm) spectra of $(\text{PEA})_2\text{PbBr}_4$, from top to bottom: 300, 150, and 10 K. (b) Temperature dependent photoluminescence excitation spectra ($\lambda_{\text{em}} = 530$ nm), from 300 down to 10 K. (c) Temperature dependent photoluminescence emission spectra ($\lambda_{\text{ex}} = 260$ nm), from 300 down to 10 K.

suggesting that the observed band could be a combination of the often observed exciton peak and absorption of lattice defects. Upon cooling, the latter shows a blue shift to 413 nm at 10 K, the other bands do not show a wavelength shift, as can be observed in Figure 1b. The blue shift of the 423 nm excitation band can also be observed in Figure 1a. As a result it shows more overlap with the 410 nm emission at 10 K compared to 300 K.

The absorbance spectra of the PEA-Br precursor, dissolved in ethanol, and PbBr_2 precursor in powder form are shown in Figure 2c. The peak observed in the absorbance spectrum of the dissolved PEA-Br precursor salt shows a clear fine structure at the same positions as the different transitions observed for liquid benzene [39]. This same structure is observed, although in a lesser degree, in the band centred around 280 nm in the 10K excitation spectrum shown in Figure 2d. The latter shows the absorbance spectrum of a film of PEA-Br precursors and the 280 nm band from the 10 K PLE spectrum.

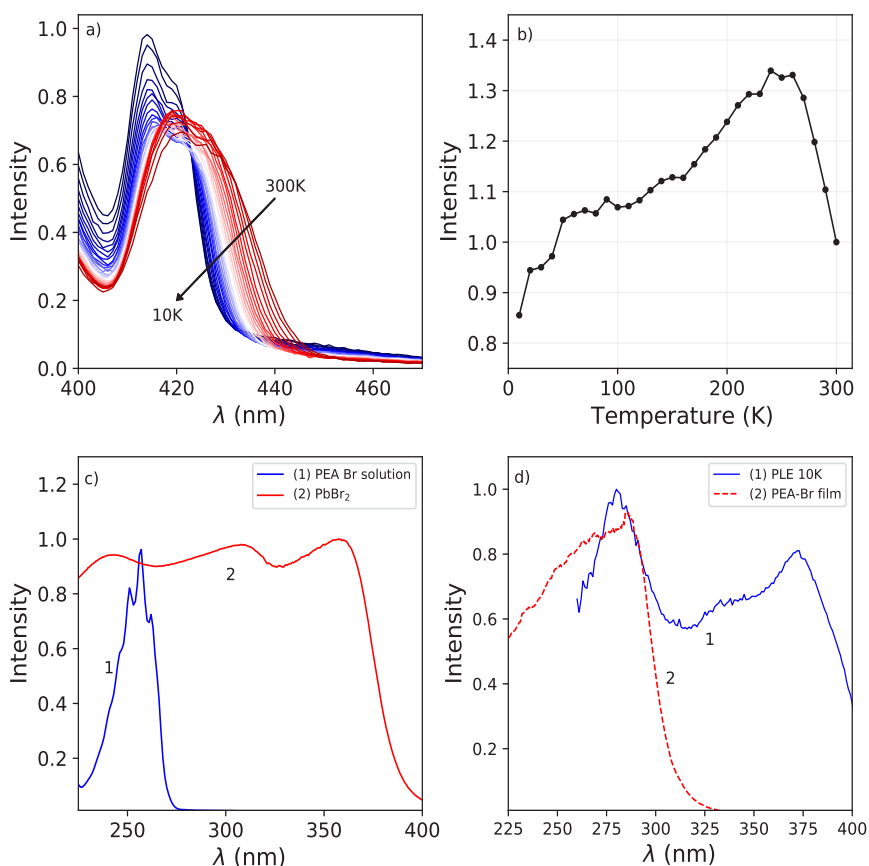


Figure 2: (a) Temperature dependent photoluminescence excitation spectra, showing only the 423 nm excitation band. Temperature decreases in the direction of the arrow. (b) Change of the total spectral photoluminescence emission intensity as function of temperature. (c) Comparison between (1) the absorbance spectrum of PEA-Br salt dissolved in ethanol, and (2) the absorbance spectrum of PbBr₂ powder. (d) Comparison between (1) the 280 nm band from the 10 K PLE spectrum, and (2) the absorbance spectrum of a film of PEA-Br.

Both show significant overlap, suggesting that the absorption wavelength of the PEA-precursor shifts by changing its local surroundings. Based on these spectra, Figures 2c and 2d, the 280 nm band is ascribed to absorption from the organic layer.

The total integrated spectral photoluminescence emission intensity is shown in Figure 2b. Upon cooling the total intensity starts to increase, reaching its maximum around 250 K. Below this temperature the intensity decreases, reaching 82% of the intensity at 300 K. Based on the temperature dependent PL spectra, shown in Figure 1c, it can be concluded that the initial intensity increase originates from the 442 nm emission.

The decrease of the intensity below 250 K looks similar to the behaviour observed by Xie *et al.* and Maddalena *et al.* upon integration of their X-ray excited emission spectra of $(\text{PEA})_2\text{PbBr}_4$ [27, 33]. Such behaviour has also been observed for n-type GaAs and n-type ZnS and is referred to as negative thermal quenching [36]. However, under X-ray excitation Xie *et al.* observed a minimum in the integrated intensity at 190 K, after which the intensity increases again, reaching a plateau value of approximately 25% of the intensity measured at 350 K. This behaviour is not observed under photon excitation, for which only a decrease with intensity is observed, see Figure 2b.

X-ray Excited Luminescence

The X-ray excited emission spectra of $(\text{PEA})_2\text{PbBr}_4$ at 300, 150, and 10 K are shown in Figure 3a. Only one emission peak, centred around 440 nm, is observed at 300 K. Similar results were obtained by van Eijk *et al.* and Maddalena *et al.* [27, 29]. Based on the PL spectrum recorded at 300 K, shown in Figure 1a, this peak is ascribed to lattice defects creating donor and acceptor states close to the band edges. At 10 K, a narrow peak centred around 414 nm and a broad emission band centred around 550 nm are observed. Similar behaviour was observed by Xie *et al.* and Maddalena *et al.* [27, 33]. The 414 and 550 nm peaks are ascribed to free exciton and self trapped exciton emission. This is based on the 10 K PL spectrum shown in Figure 1a. An overview of the spectral change upon cooling from 300 to 10 K is shown in Figure 3b, clearly demonstrating the blue shift of the 440 nm peak and development of the broad 550 nm emission band at low temperature which can also be observed in Figure 3a.

The change in the total spectral intensity of the X-ray excited emission spectra as function of temperature is shown in Figure 4a. At 10 K the intensity has decreased to 72% of the total integrated intensity at 300 K.

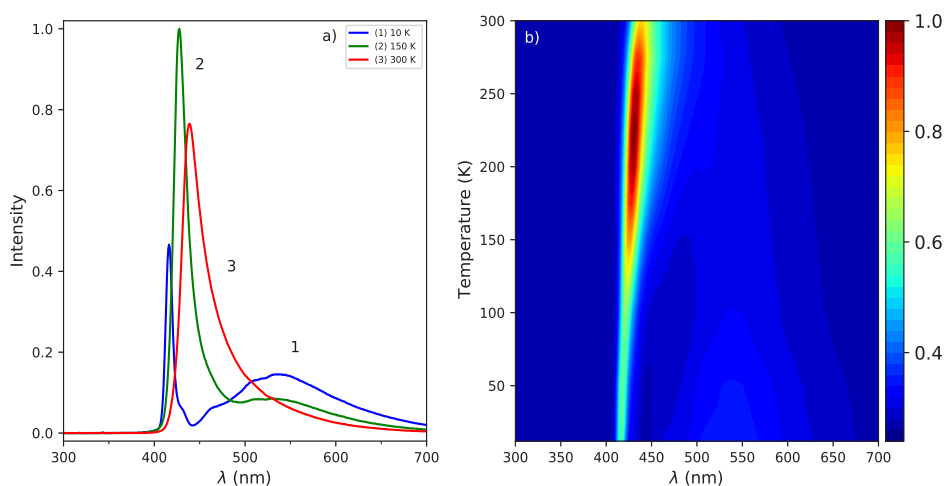


Figure 3: (a) X-ray excited emission spectra at 300, 150, and 10 K. (b) Temperature dependent X-ray excited emission spectra from 300 down to 10 K.

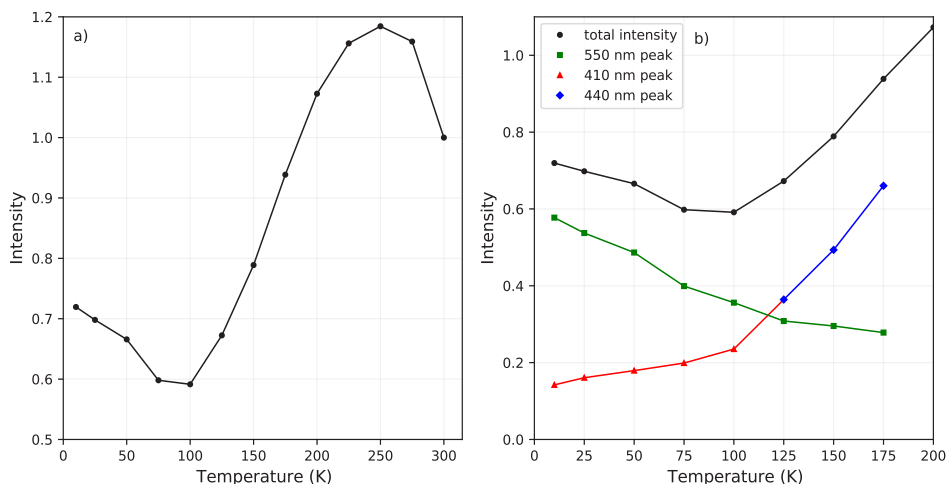


Figure 4: (a) Change of the total spectral intensity as function of temperature upon X-ray excitation. (b) Change of the total spectral intensity and contributions from the 410, 440, and 550 nm peaks between 200 and 10 K.

Similarly to the total spectral photoluminescence intensity, shown in Figure 2a, an initial increase of the intensity is observed upon cooling which was ascribed to the temperature behaviour of the 442 nm band. The decrease after 250 K, with a minimum at 100 K, looks similar to the total integrated spectral intensity already observed for X-ray excited emission spectra of $(\text{PEA})_2\text{PbBr}_4$ [27, 33].

The contribution of the different emission bands to the total spectral intensity under X-ray excitation is shown in Figure 4b, focusing on the range between 10 and 200 K. Below 125 K, the blue shift of the 442 nm emission stops to become completely merged with the 412 nm emission. Both show a decrease in intensity upon cooling. The broad 550 nm emission, ascribed to self trapped exciton formation, shows an increase in its spectral intensity upon cooling resulting in the typical negative thermal quenching behaviour of $(\text{PEA})_2\text{PbBr}_4$.

X-ray Excited Decay

Figure 5a shows the X-ray excited decay curves of $(\text{PEA})_2\text{PbBr}_4$ at 10, 150, and 300 K. The fits to these curves are shown in Figure S2. At 300 K only one decay component is observed with a lifetime of 35.2 ns. This is significantly slower compared to the 11 ns decay time measured under 662 keV gamma excitation as reported by Xie *et al.* [33]. At 150 K the lifetime has increased to 90 ns. Based on the X-ray excited emission spectra shown in Figure 3a it is suggested that the decay between 300 and 125 K originates from the emission band centred around 440 nm. At 10 K the decay curve changes significantly, showing two decay components. A fast component with a life time of 1.53 ns, and a slow component with a life time of 154 ns. Similar behaviour was observed by van Eijk *et al.* at 100 K [29]. The fitted curves and obtained fitting parameters are shown in Figure S2 and Table S I respectively.

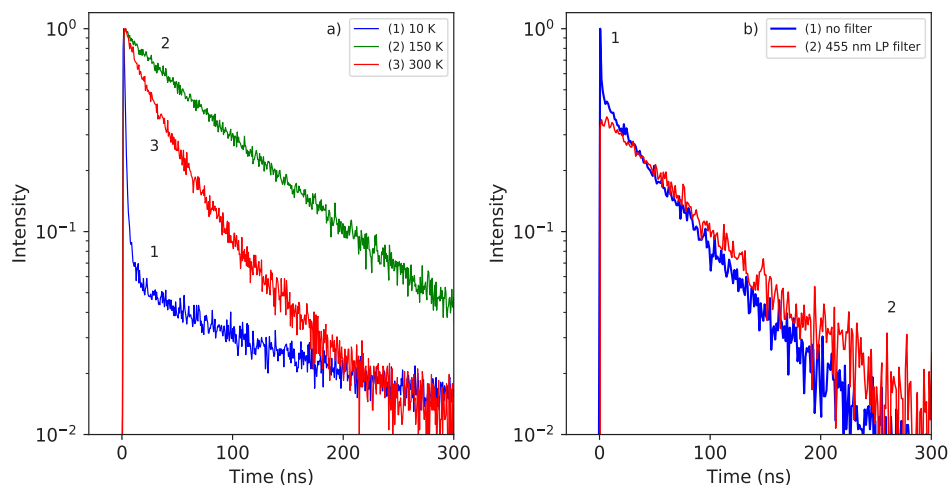


Figure 5: (a) Temperature dependent X-ray excited decay curves of $(\text{PEA})_2\text{PbBr}_4$ recorded at 10, 75, and 300 K. (b) X-ray excited decay curves of $(\text{PEA})_2\text{PbBr}_4$ recorded at 10 K with and without 455 nm long pas filter.

From the latter it is estimated that the intensity of the 1.54 ns component is 6 times smaller compared to the 154 ns component.

In order to distinguish the origin of the two components, the decay curves are recorded using a 455 nm long pass filter, separating the narrow and broad emission bands observed in the 10 K X-ray excited emission spectrum, see Figure 3a. The resulting decay curves are shown in Figure 5b. At 10 K the fast component is no longer present when the long pass filter is placed in front of the detector. This suggests that the fast decay component at 10 K originates from the 414 nm emission, and the slow decay component from the 550 nm emission.

The X-ray excited decay curves measured as function of temperature are shown in Figure 6a and 6b. Upon cooling two different regimes can be identified. An increase of the life time is observed when cooling from 300 to 125 K, as can be observed in Figure 7. The direct comparison of the latter in Figure 6a clearly demonstrates the non-exponential form of the decay curve at 300 K. At lower temperatures the decay spectrum looks more like a single exponential. The temperature range from 125 down to 10 K is shown in Figure 6b, revealing the development of the fast decay component below 125 K. This temperature corresponds to the moment the blue shift of the 442 nm emission band stops, as can clearly be seen in Figure 1c, leaving only the 412 nm and 550 nm emissions. The life time of the 550 nm emission follows a trend similar to the life time of the 440 nm emission, see Figure 7. The lifetime of the 412 nm emission becomes faster upon cooling, interestingly showing an increase at 10 K, see Figure 7.

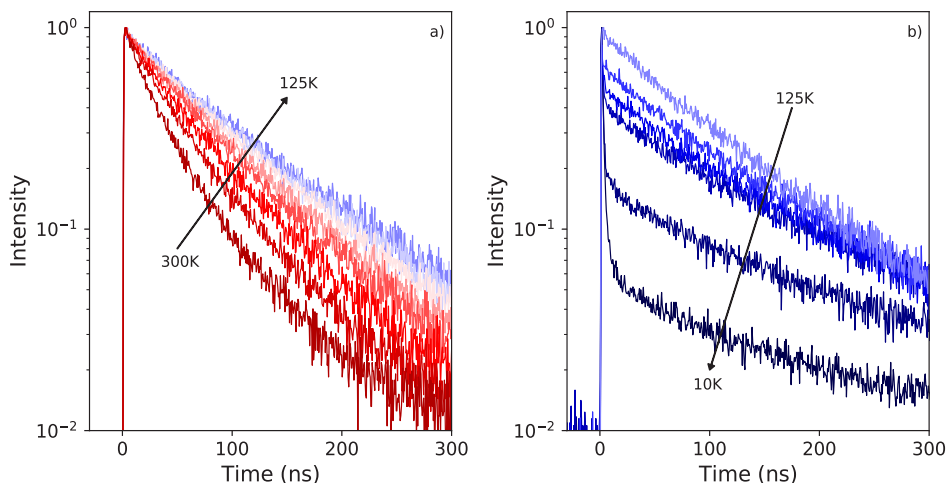


Figure 6: (a) Temperature dependent X-ray excited decay curves of $(\text{PEA})_2\text{PbBr}_4$ recorded from 125 to 300 K, with a 25 K interval. The temperature decreases in the direction of the arrow. (b) Temperature dependent X-ray excited decay curves of $(\text{PEA})_2\text{PbBr}_4$ recorded from 125 to 25 K, with a 25 K interval, and at 10 K. The temperature decreases in the direction of the arrow.

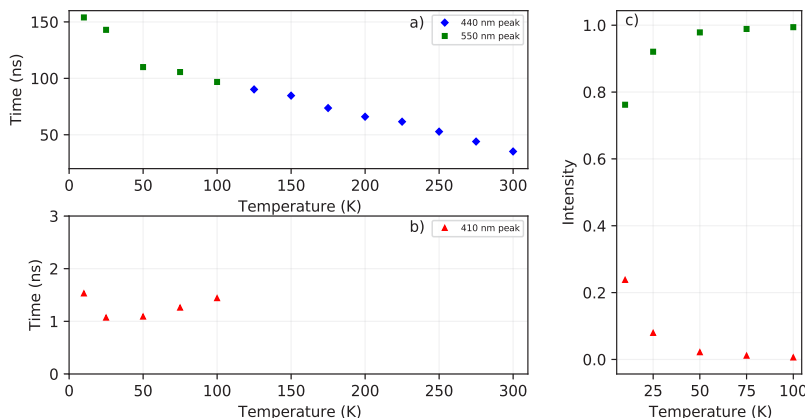


Figure 7: Temperature dependent decay times, obtained from X-ray excited decay curves (a) for the 440 nm and 550 nm decay components (b) for the 410 nm decay component. (c) Intensity of the 410 nm and 550 nm decay components between 10 and 100 K.

Pulse Height Spectroscopy

Figure 8a shows the ^{137}Cs pulse height spectrum of a small $(\text{PEA})_2\text{PbBr}_4$ crystal (2mm x 1mm x 0.3mm). The spectrum is recorded using a PMT and shaping time of 0.5 μs . From this pulse height spectrum, a light yield of 8600 ph/MeV and energy resolution of 29% are estimated. Similar values were reported by van Eijk *et al.* [29]. The light yields were estimated based on the method described by

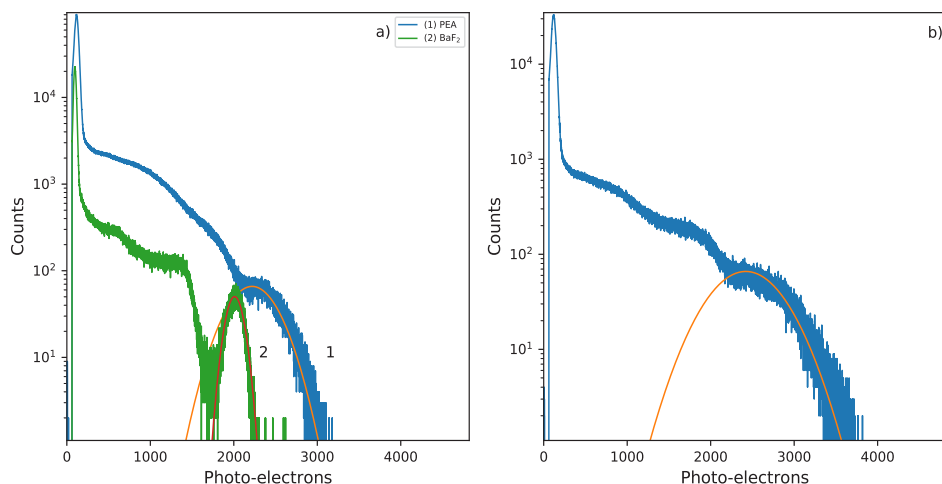


Figure 8: Pulse height spectra recorded using a ^{137}Cs γ -source and a PMT as detector (a) Small, similar sized, $(\text{PEA})_2\text{PbBr}_4$ and BaF_2 . (2mm x 1mm x 0.3mm) (b) Large $(\text{PEA})_2\text{PbBr}_4$ crystal (8mm x 5 mm x 1mm) .

de Haas and Dorenbos [40]. The observed photopeak is significantly broadened due to escape of the 75 keV characteristic K X-rays of lead. The pulse height spectrum of BaF_2 is added as a reference crystal, of similar size, for which a light yield of 7800 ph/MeV and energy resolution of 11% are estimated. The characteristic X-rays of barium are of significantly lower energy 32.2 keV K X-rays, compared to those of lead decreasing the broadening effect, hence improving the energy resolution.

Figure 8b shows the pulse height spectrum of the large crystal (8mm x 5 mm x 1mm), the same sample is used in the decay measurements and X-ray excited emission measurements. The spectrum is recorded using a PMT and shaping time of 0.5 μs . For this sample a light yield of 9400 ph/MeV and energy resolution of 39% are estimated based on the pulse height spectrum. The total spectral intensity of this sample decreases to 72% of the room temperature intensity upon cooling down to 10K, as can be observed in Figure 4a.

3. Discussion

Wavelength shifts, emission, and excitation spectra

Figure 1b and 1c show the photoluminescence emission and excitation spectra as function of temperature. The 442 nm emission peak and 423 nm excitation band both show a blue shift upon cooling. The 410 nm emission peak and the excitation bands centred around 370 and 280 nm, however, do not. For this reason it is suggested that the observed blue shift of the aforementioned peaks does not result from changes in the band gap as function of temperature. If this would be the case one would expect all emissions to show a wavelength shift.

The assignment of the 442 nm emission to bound exciton emission is based on the work of Kawano *et al.* [26]. However, based on the observed behaviour of the 442 nm emission as function of temperature this might not be correct. Based on the spectra shown in Figure 1a it could also suggest that the peak observed at 412 nm is artificial, resulting from self-absorption. A better understanding of the nature of the observed emissions is needed in order to understand the observed temperature dependent behaviour.

X-ray versus UV-Vis photon excited emission

Figure 1a and 3a show the photoluminescence emission spectrum and X-ray excited emission spectrum of $(\text{PEA})_2\text{PbBr}_4$ recorded at 300 K. The main difference is the absence of the 412 nm emission peak, ascribed to free exciton emission, in the X-ray excited spectrum. The X-ray attenuation length is estimated to be 560 μm , based on the linear attenuation coefficient shown in Figure S3 and the average X-ray energy of 40 keV. The samples, as mentioned in the experimental section, have a thickness of 1 mm. Most of the X-ray energy will thus be deposited in the bulk of the crystal, the rest will escape at the back.

From Figure 1a it can be observed that the 412 nm emission peak completely overlaps with the 423 nm excitation peak at 300 K. The overlap does not change upon cooling. This suggests that the 412 nm emission could potentially not be visible under X-ray excitation due to self absorption, but would still be present under UV-Vis excitation due to the difference in penetration depth. This would allow the 412 nm emission to escape at the surface of the crystal before being reabsorbed. The influence of self absorption can be studied by measuring the room temperature PL spectrum in reflectivity and transmission mode. When measuring in reflectivity mode the excitation source and detector are placed at a 90 degree angle. When measuring in transmission mode the excitation source and detector are facing each other, forcing the emission light to pass through the sample before it is detected. The resulting spectra are shown in Figure S4. The 412 nm emission is no longer present when measuring in transmission mode, confirming the presence of self absorption.

Alternatively, one might suggest that the difference is caused from the formation of spatially separated charge carriers created upon X-ray excitation. Before emission, the spatially separated electrons and holes need to approach each other first, before forming excitons. This could allow them to relax to either lattice defects forming the 442 nm emission instead of free exciton emission or for one of the spatially separated charge carriers to self trap contributing to the higher self trapped exciton emission under X-ray excitation. The data presented in this paper does not provide a conclusive argument to distinguish between the mechanisms discussed above.

Negative Thermal Quenching

Figure 2a and 4a show the total integrated intensity upon photon excitation and X-ray excitation respectively. Both show an initial intensity increase upon cooling, ascribed to the 442 nm emission peak, which is rather similar to normal

thermal quenching behaviour reaching its maximum at 250 K. Below this temperature both show an intensity decrease, referred to as negative thermal quenching. Under X-ray excitation an intensity minimum is reached at 100 K, after which the intensity increases again reaching a plateau value of 72% compared to the intensity at 300 K. This behaviour is not observed under photon excitation.

Figure 4b shows the contribution of the different emissions to the total spectral intensity upon X-ray excitation. This Figure nicely demonstrates that the negative thermal quenching behaviour is the result of the self trapped exciton emission increasing in intensity upon cooling, while the other emissions decrease in intensity. Upon comparing the PL spectra at 10 K and X-ray excited emission spectrum at 10 K, a direct comparison is shown in Figure S5, it can be observed that the self trapped exciton emission increases under X-ray excitation. The total spectral intensity under UV-Vis excitation, shown in 2a, does not show an increase below 100 K. The observed difference in the negative thermal quenching behaviour under X-ray and UV-Vis photon excitation is ascribed to the different intensities of the self trapped exciton emission.

4. Conclusion

The potential of $(\text{PEA})_2\text{PbBr}_4$ for low temperature scintillation applications has been accessed. The room temperature emission, under photo excitation, consists of two emissions ascribed to free excitons and excitons bound to lattice defects. Only the latter is observed under X-ray excitation. The precise nature of the emissions, however, is not known thus making it difficult properly explain the temperature dependent photoluminescence behaviour. At 10 K only free exciton emission and self trapped exciton emission are observed, for both photo and X-ray excitation. The intensity of the self trapped exciton emission is larger under X-ray excitation. The observed negative thermal quenching behaviour observed for $(\text{PEA})_2\text{PbBr}_4$, is ascribed to a combination of self absorption and self trapped exciton emission competing with the other emissions.

X-ray excited decay curves have demonstrated that, below 125 K, the decay consists of two components. A fast component ascribed to the free exciton emission and a slow component ascribed to self trapped exciton emission, having a life time of 1.53 ns (24%) and 154 ns (76%) at 10 K. The total spectral intensity, under X-ray excitation, only decreases to 72% at 10 K. The combination of the fast decay component and decent light yield make this material interesting for low temperature and fast timing applications.

5. Experimental

$(\text{PEA})_2\text{PbBr}_4$ crystals were synthesised using dimethyl sulfoxide (DMSO, anhydrous), phenylethylammonium bromide ($(\text{PEA})\text{Br}$, 98 %), and lead bromide (PbBr_2 , 98 %) all were purchased from Sigma-Aldrich and used without further purification. The $(\text{PEA})_2\text{PbBr}_4$ single crystals were synthesised from solution

based on the method described and used by Maddalena *et al.* [27]. A 3 M precursor solution of (PEA)Br and PbBr_2 , in stoichiometric amounts, was dissolved in DMSO and mixed at 100 °C for 2 h under a N_2 -atmosphere. Afterwards, the solution was left to evaporate at room temperature in open air for at least 1 week up to one month until large crystals formed in the liquid. The crystal precipitate was filtered from the solution, washed with hexane and dried under vacuum for future characterisation. This resulted in flat transparent crystals of approximately the following dimensions: 8 mm x 5 mm x 1 mm. Unless mentioned otherwise a crystal of this size was used.

All X-ray diffraction patterns are recorded on a Bruker D8 Discover (Cu K_α ($\lambda = 1.54 \text{ \AA}$)). A step size and integration time of 0.02 and 1 second respectively. The XRD spectrum is shown in Figure S1.

All photoluminescence emission and excitation spectra are recorded using light from a 450 W Xenon lamp passing through a Horiba Gemini 180 monochromator. The emission light passes through a long pass filter and Princeton Instruments SpectraPro-SP2358 monochromator, and is detected by a Hamamatsu R7600U-20 PMT. All recorded spectra are corrected for the lamp intensity. A single crystal was used for all photoluminescence measurements. The crystals were mounted on the cold finger of a closed cycle helium cryostat operating below 10^{-4} mbar. Unless mentioned otherwise all photoluminescence emission spectra are recorded in reflectivity mode.

All absorption spectra are recorded using a Perkin Elmer Lambda 1050. The precursor salt was dissolved in ethanol; the measurement was performed using a quartz cuvette.

X-ray excited luminescence spectra were recorded by exciting the samples with X-rays from a tungsten anode X-ray tube operating at 79 kV resulting in an average x-ray energy of 40 keV. A filter was used to remove the lower energy side of the produced X-ray spectrum in order to prevent radiation damage of the sample. A single crystal was mounted on the cold finger of a closed cycle helium cryostat operating below 10^{-4} mbar. The emission light was collected by a parabolic mirror and coupled into an optical fibre. The spectrum was recorded by an Ocean Insights QE Pro Spectrometer. The parabolic mirror is positioned under a 90 degree angle compared to the X-ray tube.

X-ray excited decay curves were recorded using the time-correlated single photon counting method. A PicoQuant LDH-P-C-440M pulsed diode laser is used to excite a Hamamatsu N5084 light excited X-ray tube producing x-ray with an average energy of 18.5 keV. The laser head is triggered by a Picoquant laser driver. The reference output of the driver is used as start input and is connected to an Ortec 567 time-to-amplitude converter (TAC). The bin width of the latter was calibrated using an Ortec 462 time calibrator. The emitted photons are recorded using an ID Quantique id100-50 single-photon counter whose output signal was used as the stop input of the TAC. The signal first goes through a LeCroy 623B Octal Discriminator and analogue delay. The start and stop time differences are

collected and digitised using an Ortec AD114 amplitude-to-digital converter. All temperature dependent measurements were performed using a closed cycle helium cryostat operating below 10^{-4} mbar.

Pulse height spectra were recorded by mounting the samples on a Hamamatsu R1791 PMT covered with PTFE tape operating at -700 V. The signal passes through an integrated pre-amplifier and Ortec 672 spectroscopic amplifier before it is processed by an Ortec AD114 26K ADC. All measurements were performed without optical coupling, the samples were directly mounted on the entrance window.

6. Author contributions

J. J. B. was responsible for performing all experiment and writing part of the manuscript. F. M. and C. D. were responsible for the synthesised perovskite crystals, reviewing and editing the manuscript. M. D. B. was responsible for the supervision of the project, writing part of the manuscript, and reviewing and editing the manuscript. P. D. was responsible for the supervision of the project, and reviewing and editing the manuscript. All authors have given approval to the final version of the manuscript.

7. Conflicts of interest

There are no conflicts to declare.

8. Acknowledgements

The authors acknowledge financial supports from the TTW/OTP grant no. 18040 of the Dutch Research Council and the Singapore Ministry of Education (T2EP50121-0025) and Thales-CINTRA Funding. The authors would like to thank J. T. Mulder for the measured absorbance spectra.

References

- [1] E. V. D. van Loef, P. Dorenbos, C. W. E. van Eijk, *Applied Physics Letters*, 79 (2001) 1573, <https://doi.org/10.1063/1.1385342>
- [2] P. Dorenbos, *Optical Materials: X 1* (2019) 100021, <https://doi.org/10.1016/j.omx.2019.100021>
- [3] C. van Aarle, K. W. Krämer, P. Dorenbos, *Journal of luminescence* 238 (2021) 11857, <https://doi.org/10.1016/j.jlumin.2021.118257>
- [4] M. K. Klintenberg, M. J. Weber, D. E. Derenzo, *Journal of Luminescence* 102 (2003) 287, [https://doi.org/10.1016/S0022-2313\(02\)00511-2](https://doi.org/10.1016/S0022-2313(02)00511-2)

- [5] S. E. Derenzo, M. J. Weber, M. K. Klintenberg, *Nuclear Instruments and Methods in Physics Research Section A: Accelerators, Spectrometers, Detectors and Associated Equipment* 486 (2002) 214, [https://doi.org/10.1016/S0168-9002\(02\)00705-2](https://doi.org/10.1016/S0168-9002(02)00705-2)
- [6] K. Shibuya, M. Koshimizu, K. Asai, *Applied Physics Letters* 84 (2004) 4370, <https://doi.org/10.1063/1.1756203>
- [7] M. A. Green, A. Ho-Naillie, H. J. Snaith, *Nature Photonics* 8 (2014) 506, <https://doi.org/10.1038/nphoton.2014.134>
- [8] X. Y. Chin, D. Cortecchia, J. Yin, A. Bruno, C. Soci, *Nature Communications* 6 (2015) 7383, <https://doi.org/10.1038/ncomms8383>
- [9] L. Dou, Y. M. Yang, J. You, Z. Hong, W.-H. Chang, G. Li, Y. Yang, *Nature Communications* 5 (2014) 5404, <https://doi.org/10.1038/ncomms6404>
- [10] F. Maddalena, L. Tjahjana, A. Xie, Arramel, S. Zeng, H. Wong, P. Coquet, W. Drozdowski, C. Dujardin, C. Dang, M. D. Birowosuto, *Crystals* 9 (2019) 88, <https://doi.org/10.3390/cryst9020088>
- [11] A. Xie, F. Maddalena, M. E. Witkowski, M. Makowski, B. Mahler, W. Drozdowski, S. V. Springham, P. Coquet, C. Dujardin, M. D. Birowosuto, C. Dang, *Chemistry of materials*, 32 (2020) 19, <https://doi.org/10.1021/acs.chemmater.0c02789>
- [12] S. Yakunin, M. Sytnyk, D. Kriegner, S. Shrestha, M. Richter, G. J. Matt, H. Azimi, C. J. Brabec, J. Stangl, M. V. Kovalenko, W. Heiss, *Nature Photonics* 9 (2015) 444
- [13] H. Wei, Y. Fang, P. Mulligan, W. Chuirazzi, H.-H. Fang, C. Wang, B. R. Ecker, Y. Gao, M. A. Loi, L. Cao, J. Huang, *Nature Photonics* 10 (2016) 333
- [14] P. Dorenbos, *IEEE transactions on nuclear science* 57 (2010) 3, <https://doi.org/10.1109/TNS.2009.2031140>
- [15] M. D. Bitowosuto, D. Cortecchia, W. Drozdowski, K. Brylew, W. Lachmanski, A. Bruno, C. Soci, *Scientific Reports* 6 (2016) 37254, <https://doi.org/10.1038/srep37254>
- [16] V. B. Mykhaylyk, H. Kraus, V. Kapustianyk, H. J. Kim, P. Mercere, M. Rudko, P. Da Silva, O. Antonyak, M. Dendebera, *Scientific Reports* 10 (2020) 8601, <https://doi.org/10.1038/s41598-020-65672-z>
- [17] W. W. Wolszczak, D. L. Carroll, R. T. Williams, *Advanced X-ray Detector Technologies*, Chapter 1 (2022), https://doi.org/10.1007/978-3-030-64279-2_1
- [18] Y. He, L. Matei, H. J. Jung, K. M. McCall, M. Chen, C. S. Stoumpos, Z. Liu, J. A. Peters, D. Y. Chumg, B. W. Wessels, M. R. Wasielewski, V. P. Dravid, A. Burger, M. G. Kanatzidis, *Nature Communications* 9 (2018) 1609, <https://doi.org/10.1038/s41467-018-04073-3>

- [19] Q. Chen, J. Wu, X. Ou, B. Huang, J. Almutlaq, A. A. Zhumeckenov, X. Guan, S. Han, L. Liang, Z. Yi, J. Li, X. Xie, Y. Wang, Y. Li, D. Fan, D. B. L. Teh, A. H. All, O. F. Mohammed, O. M. Bakr, T. Wu, M. Bettinelli, H. Yang, W. Huang, X. Liu, *Nature* 561 (2018) 88-93, <https://doi.org/10.1038/s41586-018-0451-1>
- [20] X. Chen, F. Zhang, Y. Ge, L. Shi, S. Huang, J. Tang, Z. Lu, L. Zhang, B. Zou, H. Zhong, *Advanced Functional Materials* 18 (2018) 16, <https://doi.org/10.1002/adfm.201706567>
- [21] F. Cao, D. Yun, W. Ma, X. Xu, B. Cai, Y. M. Yang, S. Liu, L. He, Y. Ke, S. Lan, K.-L. Cho, H. Zeng, *ACS Nano* 14 (2020) 5183-5193, <https://doi.org/10.1021/acsnano.9b06114>
- [22] R. T. Williams, W. W. Wolszczak, X. Yan, D. L. Carrol, *ACS Nano* 14 (2020) 5161-5169, <https://doi.org/10.1021/acsnano.0c02529>
- [23] D. Cortecchia, S. Neutzner, A. R. S. Kandada, E. Mosconi, D. Meggiolaro, F. De Angelis, C. Soci, A. Petrozza, *Journal of the american chemical society* 139 (2017) 39-42, <https://doi.org/10.1021/jacs.6b10390>
- [24] D. Cortecchia J. yin, A. Bruno, S.-Z. A. Lo, G. G. Gurzadyan, S. Mhaisalkar, J.-L. Brédas, C. Soci, *Journal of Materials Chemistry C* 5 (2017) 2771-2780, <https://doi.org/10.1039/C7TC00366H>
- [25] D. Cortecchia, J. Yin, A. Petrozza, C. Soci, *Journal of Materials Chemistry C* 7 (2019) 4956-4969, <https://doi.org/10.1039/C9TC01036J>
- [26] N. Kawano, M. Koshimizu, Y. Sun, N. Yahaba, Y. Fujimoto, T. Yanagida, K. Asai, *Japanese Journal of Applied Physics*, 53 (2014) 02BC20, <http://doi.org/10.7567/JJAP.53.02BC20>
- [27] F. Maddalena, A. Xie, Arramel, M. E. Witkowski, M. Makowski, B. Mahler, W. Drozdowski, T. Mariyappan, S. V. Springham, P. Coquet, C. Dujardin, M. D. Birowosuto, C. Dang, *Journal of Materials Chemistry C* 9 (2021) 2504, <https://doi.org/10.1039/D0TC05647B>
- [28] N. Kawano, M. Koshimizu, A. Horiai, F. Nishikido, R. Haruki, S. Kishimoto, K. Shibuya, Y. Fujimoto, T. Yanagida, K. Asai, *Japanese Journal of Applied Physics* 55 (2016) 110390, <http://doi.org/10.7567/JJAP.55.110309>
- [29] C. W. E. van Eijk, J. T. M. de Haas, P. A. Rodnyi, I. V. Khodyuk, K. Shibuya, F. Nishikido, M. Koshimizu, *IEEE Nuclear Science Symposium Conference Record* N69-3 (2008) 3525, <https://doi.org/10.1109/NSSMIC.2008.4775096>
- [30] S. Kishimoto, K. Shibuya, F. Nishikido, M. Koshimizu, R. Haruki, Y. Yoda, *Applied Physics Letters* 93 (2008) 261901, <https://doi.org/10.1063/1.3059562>
- [31] D. R. schaat, S. Ziegler, H. Zaidi, *Medical Physics* 47 (2020) 7, <https://doi.org/10.1002/mp.14122>

- [32] E. Auffray, B. Frisch, F. Geraci, A. Ghezzi, S. Gundacker, H. Hillemanns, P. Jarron, T. Meyer, M. Paganoni, K. Pauwels, M. Pizzichemi, P. Lecoq, *IEEE Transactions on Nuclear Science* 60 (2013) 5, <https://doi.org/10.1109/TNS.2013.2270089>
- [33] A. Xie, C. Hettiarachchi, F. Maddalena, M. E. Witkowski, M. Makowski, W. Drozdowski, A. Arramel, A. T. S. Wee, S. V. Springham, P. Q. Vuong, H. J. Kim, C. Dujardin, P. Coquet, M. D. Birowosuto, C. Dang, *Communications Materials* 1 (2020) 37, <https://doi.org/10.1038/s43246-020-0038-x>
- [34] B. Guo, C. Luo, C. Yan, B. Sun, W. Li, W. Yang, *The Journal of Physical Chemistry C* 124 (2020) 26076-26082, <https://doi.org/10.1021/acs.jpcc.0c09334>
- [35] M. D. Smith, A. Jaffe, E. R. Dohner, A. M. Lindenberg, H. I. Karunadasa, *Chemical Science* 8 (2017) 4497, <https://doi.org/10.1039/C7SC01590A>
- [36] H. Shibata, *Japanese Journal of Applied Physics* 37 (1998) 550, <https://doi.org/10.1143/JJAP.37.550>
- [37] S. Kahmann, H. Duim, H.-H. Fang, M. Dyksik, S. Adjokatse, M. R. Medina, M. Pitaro, P. Plochocka, M. A. Loi, *Advanced Functional Materials* 31 (2021) 2103778, <https://doi.org/10.1002/adfm.202103778>
- [38] N. Kitazawa, M. Aono, Y. Watanabe, *Materials Chemistry and Physics* 134 (2012) 2-3, <https://doi.org/10.1016/j.matchemphys.2012.03.083>
- [39] T. Inagaki, *The Journal of Chemical Physics* 57 (1972) 6, <https://doi.org/10.1063/1.1678619>
- [40] J. T. M. De Haas, P. Dorenbos, *IEEE Transactions on Nuclear Science* 53 (2008) 3, <https://doi.org/10.1109/TNS.2008.922819>

Supplementary Information

4

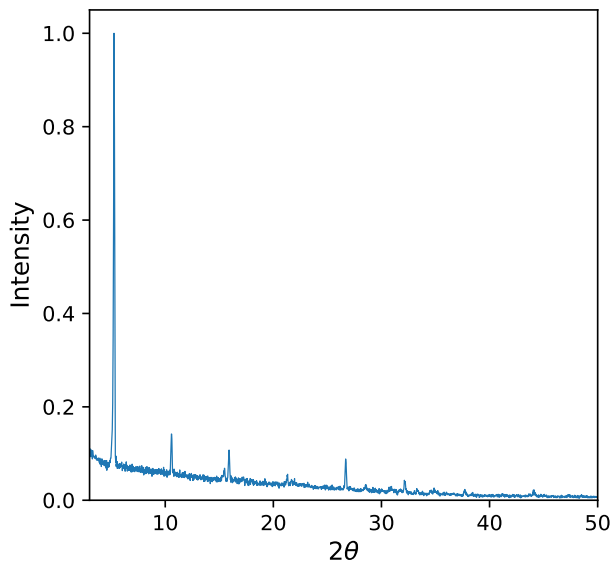


Figure S1: Powder XRD pattern (PEA)₂PbBr₄.

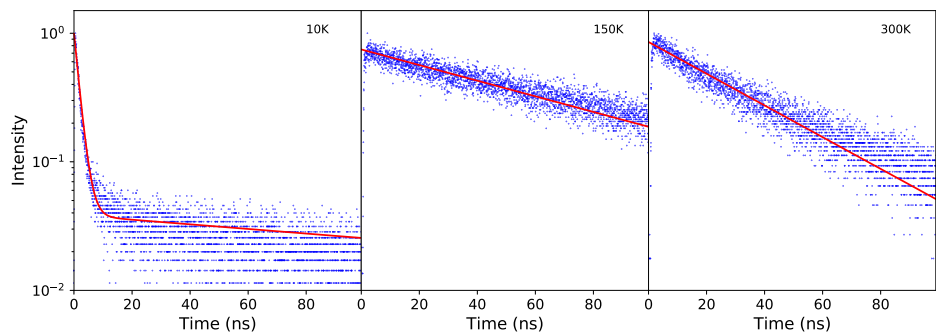


Figure S2: Fitted decay curves, from left to right, at 10, 150, and 300 K.

Table S I: Parameters obtained from fitting the decay spectra shown in Figure S2

	$\tau_{440nm}(ns)$	I_{440nm}	$\tau_{550nm}(ns)$	I_{550nm}	$\tau_{410nm}(ns)$	I_{410nm}
300 K	35.2	0.855				
150 K	90.2	0.748				
10 K			154	0.0385	1.53	1.21

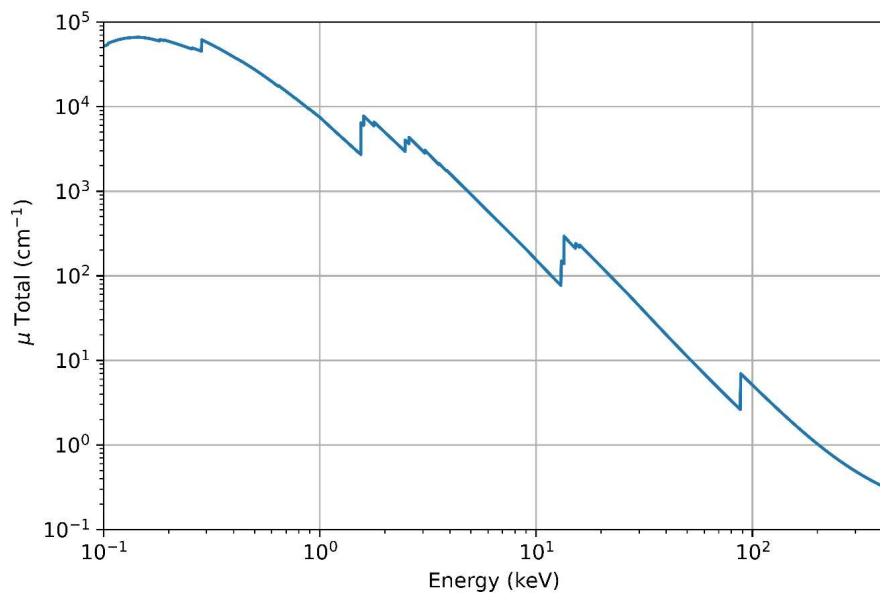


Figure S3: Linear attenuation coefficient $(\text{PEA})_2\text{PbBr}_4$.

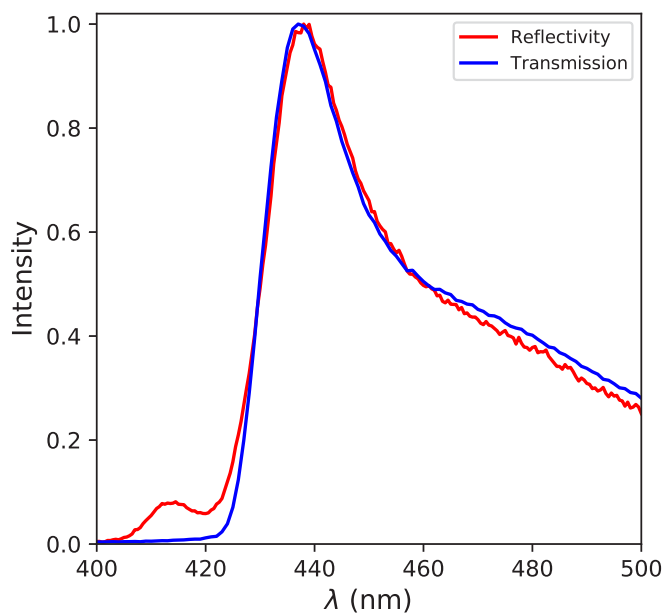


Figure S4: Comparison of the photoluminescence spectra measured in reflectivity mode and transmission mode.

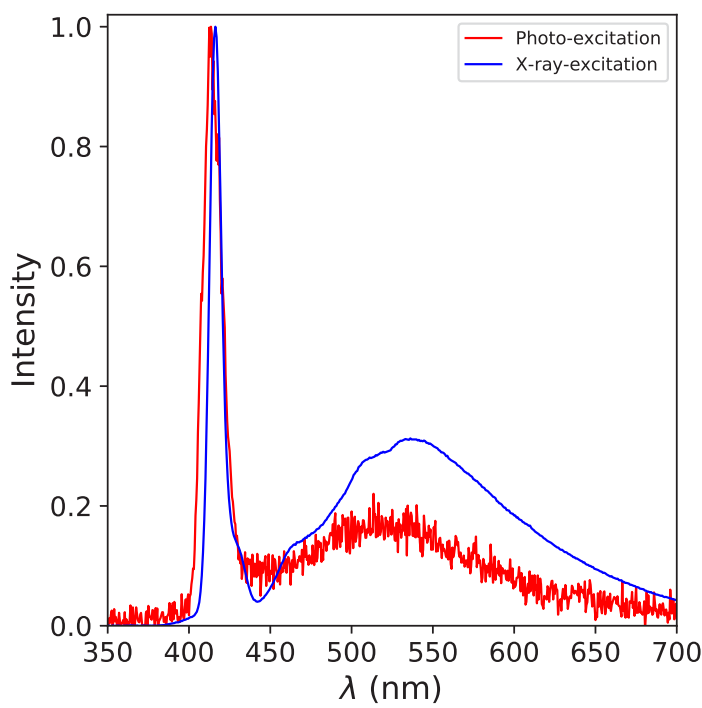


Figure S5: Comparison of the photoluminescence emission and x-ray excited emission spectra recorded at 10 K.

5

(BZA)₂PbBr₄: A Potential Scintillator for Photon-Counting Computed Tomography Detectors

Abstract

Due to recent development in detector technology, photon-counting computed tomography (PCCT) has become a rapidly emerging medical imaging technology. Current PCCT systems rely on the direct conversion of X-ray photons into charge pulses, using CdTe, CZT, or Si semiconductor detectors. Indirect detection using ultrafast scintillators coupled to silicon photomultipliers (SiPM) offers a potentially more straightforward and cost-effective alternative. In this work a new 2D perovskite scintillator, benzylammonium lead bromide (BZA)₂PbBr₄, is experimentally characterised as function of temperature. The material exhibits a 4.2 ns decay time under X-ray excitation at room temperature and a light yield of 3700 photons/MeV. The simulation tool developed by Van der Sar *et al.* was used to model the pulse trains produced by a SiPM-based (BZA)₂PbBr₄ detector. The fast decay time of (BZA)₂PbBr₄ results in outstanding count-rate performance as well as very low statistical fluctuations in the simulated pulses. These features of (BZA)₂PbBr₄, combined with its cost-effective synthesis make (BZA)₂PbBr₄ very promising for PCCT.

The content of this chapter is based on: J. Jasper van Blaaderen, Stefan van der Sar, Djulia Onggo, Md Abdul K. Sheikh, Dennis R. Schaart, Muhammad D. Birowosuto, Pieter Dorenbos, *Journal of Luminescence* 263 (2023) 120012

1. Introduction

One of the most commonly used medical imaging techniques is X-ray computed tomography (CT). CT is nevertheless still limited by its spatial resolution, contrast-to-noise ratio for a given radiation dose, and artefacts [1, 2]. New developments in photon-counting detector technology can help solve these problems. Such detectors must be able to handle the high flux used in CT [3, 4]. Current detectors for photon-counting computed tomography (PCCT) are based on direct conversion of an X-ray photon's energy into charge, using either CdTe [5], CdZnTe (CZT) [6], or Si [7] semiconductors. For the first two materials however, availability and synthesis cost involved with producing low defect density materials are a bottleneck [1, 2]. Si based detectors suffer from their low density ($\rho = 2.3 \text{ g/cm}^3$) and atomic number ($Z = 14$) [8]. Alternatively, PCCT detectors could be based on indirect detection, utilising an ultrafast scintillator to absorb the X-rays and convert their energy into scintillation photons. The later are detected and converted into an electrical pulse by for example a silicon photomultiplier (SiPM). Van der Sar *et al.* have explored this approach, both theoretically and experimentally [9, 10]. $\text{LaBr}_3:\text{Ce}^{3+}$ was used as scintillator, due to its short decay time constant of 16 ns and high light yield of 63.000 photons/keV, and SiPMs as ultra fast photodetector. Hybrid Organic-Inorganic Perovskite (HOIP) scintillators, presented in this work, are another potential candidate for SiPM-based PCCT detectors.

HOIP's have become common materials for many optoelectronic applications in the past decade [11–13]. These materials have also gained interest in other fields, such as scintillation [14–17]. HOIP's differ from traditional scintillators, based on lanthanide activated materials [18–21], by being intrinsic scintillators. This allows for the use of small bandgap materials, significantly enhancing the theoretical light yield compared to traditional scintillators [22–24]. Especially two-dimensional perovskites are promising scintillator materials due to their stable room-temperature exciton luminescence [25, 26].

Currently the best studied 2 dimensional perovskite scintillators are butylammonium lead bromide $(\text{BA})_2\text{PbBr}_4$ and phenethylammonium lead bromide $(\text{PEA})_2\text{PbBr}_4$ [14–6]. These two compounds are especially interesting due to their short decay times of 8.0 and 35 ns, respectively [14, 16]. Combined with the possibility of cost-effective low temperature solution based synthesis, 2 dimensional perovskites are potential candidates to become the next generation scintillators [15, 27]. The short decay times of $(\text{BA})_2\text{PbBr}_4$ and $(\text{PEA})_2\text{PbBr}_4$ make them very interesting for high count rate applications such as PCCT [1]. Unfortunately, as demonstrated by Van der Sar *et al.*, using $\text{LaBr}_3:\text{Ce}^{3+}$, these decay times are still too slow for clinical PCCT applications.

In this work a new scintillator, benzylammonium lead bromide $(\text{BZA})_2\text{PbBr}_4$, is experimentally characterised as function of temperature. Currently, this material has only been studied at room temperature under UV-Vis excitation, showing a short decay time of approximately 3 ns, in addition to studies focusing on the crys-

tal structure [28–31]. $(\text{BZA})_2\text{PbBr}_4$ is a 2D perovskite very similar to $(\text{PEA})_2\text{PbBr}_4$; the later contains two CH_2 groups in the spacer chain between the phenyl group and the NH_3 group while $(\text{BZA})_2\text{PbBr}_4$ only contains one [31]. The goal of this work is to study $(\text{BZA})_2\text{PbBr}_4$ under X-ray and γ -photon excitation and access its scintillation properties. The experimental results are used to simulate the performance of a $(\text{BZA})_2\text{PbBr}_4$ and SiPM-based PCCT detector using the model developed by Van der Sar *et al.* [9, 10]. The output of this simulation is compared with $(\text{PEA})_2\text{PbBr}_4$, $\text{LYSO}:\text{Ce}^{3+}$, $\text{LaBr}_3:\text{Ce}^{3+}$ and CZT in order to develop an understanding of the suitability of $(\text{BZA})_2\text{PbBr}_4$ for use in SiPM-based PCCT detectors.

2. Results

Figure 1a shows the pulse height spectrum of a $(\text{BZA})_2\text{PbBr}_4$ crystal (6 mm x 4 mm x 0.5 mm) measured on a photomultiplier tube (PMT), using 662 keV gamma photons from ^{137}Cs . The rightmost peak is assigned to the total absorption of 662 keV photons, and is used to calibrate the spectrum. Due to the small thickness of the sample (0.5 mm) the probability of a characteristic Pb K_α X-ray to escape from the sample appears larger than 50%. This results in the more intense escape peak at 75 keV lower energy. From the total absorption peak the light yield is determined to be 3700 photons / MeV, based on the method described by

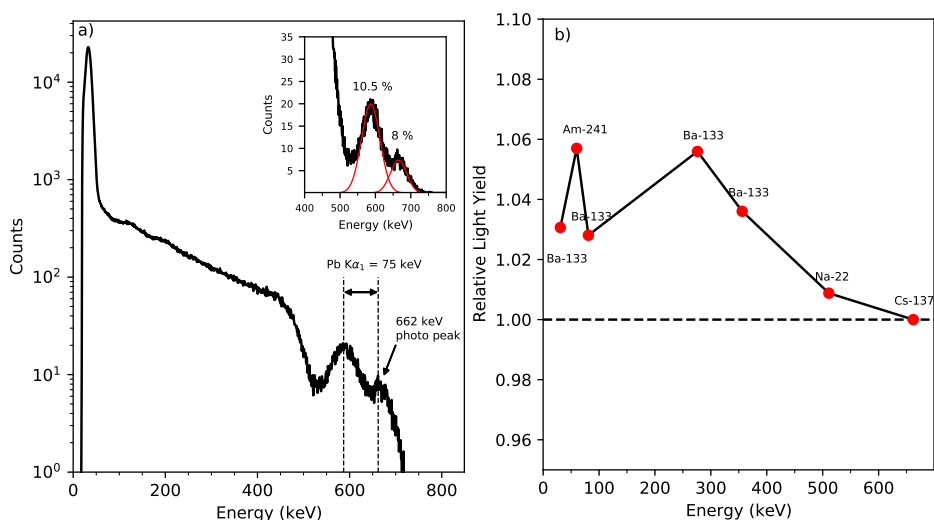


Figure 1: (a) Pulse height spectrum of a $(\text{BZA})_2\text{PbBr}_4$ crystal (6 mm x 4 mm x 0.5 mm) measured on a PMT, using a ^{137}Cs γ -source. In the plot both the total absorption and escape peak are indicated, based on their energy spacing. The insert shows both peaks fitted using a Gaussian function and their respective energy resolutions. (b) Non-proportional response of $(\text{BZA})_2\text{PbBr}_4$, recorded using 662 keV from ^{137}Cs , 511 keV from ^{22}Na , 356, 276, 81, and 30.8 keV from ^{133}Ba , and 60 keV from ^{241}Am . The ideal response is indicated by the dashed horizontal black line.

De Haas and Dorenbos [32]. Both the total absorption and escape peak are fitted using a Gaussian function, see the insert of Figure 1a. From the full width at half maximum of the fit the energy resolution was determined to be 8% at 662 keV.

The same sample was used to study the light output as function of the deposited energy using different gamma photon sources. The resulting non-proportionality curve is shown in Figure 1b. Ideally, this curve is a horizontal line, represented by the dashed line in Figure 1b. For $(\text{BZA})_2\text{PbBr}_4$ the light yield increases at deposited energies below 662 keV. The maximum deviation is 6% with respect to the light yield at 662 keV. The lead K-shell absorption edge is located at 88 keV, corresponding to the same energy where a dip in the light yield is observed. Similar behaviour is observed in traditional scintillators [33, 34].

The 300 and 10 K photoluminescence excitation and emission spectra are shown in Figure 2a. The 300 K excitation spectrum shows 3 distinct bands centred around 285, 370, and 424 nm. A similar excitation spectrum has been measured for $(\text{PEA})_2\text{PbBr}_4$ assigning the three bands to absorption of the phenyl group, the transition to the conduction band, and the exciton absorption peak respectively [16]. At 10 K the band around 424 nm has shifted to 415 nm and decreased both in relative intensity and in peak width. The band around 370 nm shows a shoulder near 395 nm.

The 300 K emission spectrum contains two main emission bands centred around 415 and 440 nm. Additionally, a tail extending from 450 to 600 nm with a weak band around 490 nm is observed. At 10 K one emission peak is observed centred around 416 nm. Additionally, a broad emission extending from 450 to 650 nm with very low intensity is observed. Figure 2b, shows the emission spectra from 300 down to 10 K. The 415 nm emission shows almost no shift, whereas the 440 nm emission starts to blue shift upon cooling, merging with the 415 nm emission around 150 K. This behaviour is very similar to the temperature dependent photoluminescence of $(\text{PEA})_2\text{PbBr}_4$ [16].

The temperature dependent X-ray excited emission spectra of $(\text{BZA})_2\text{PbBr}_4$ are shown in Figure 2c. Compared to the room temperature UV-Vis excited emission spectrum, in Figure 2a, only one emission peak is present in the room temperature X-ray excited emission spectrum. The peak is located at 432 nm and has a tail extending to 600 nm, which is a very suitable wavelength range for SiPMs [35–37]. The insert in Figure 2 shows that upon cooling the emission peak starts to blue shift. This stops at 150 K, corresponding to the same temperature at which the two emissions observed in the UV-Vis excited emission spectrum have merged. The presence of only one emission peak under X-ray excitation versus two emission peaks under UV-Vis excitation was also observed in $(\text{PEA})_2\text{PbBr}_4$. Based on the experiments presented in our previous work on $(\text{PEA})_2\text{PbBr}_4$ this is ascribed to self absorption [16]. X-rays penetrate deeper into the crystal compared to UV-Vis photons resulting in a larger degree of self absorption of the scintillation light.

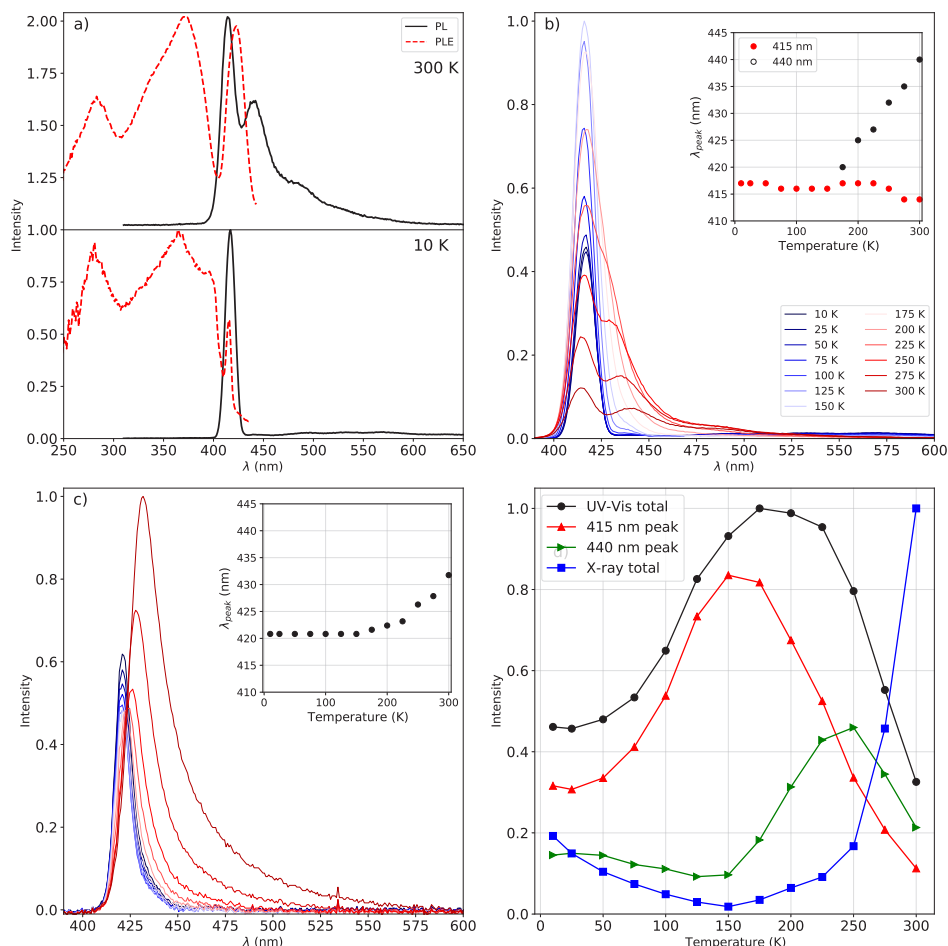


Figure 2: (a) 300 and 10 K photoluminescence emission (PL) ($\lambda_{ex} = 280$ nm) and excitation (PLE) ($\lambda_{em} = 465$ nm) spectra (b) Temperature dependent photoluminescence spectra ($\lambda_{ex} = 280$ nm) from 300 down to 10 K. The legend applies for both (b) and (c). Insert: peak position shift from 300 down to 10 K of the 415 and 440 nm peaks. (c) X-ray excited emission spectra from 300 down to 10 K. Insert: peak position shift from 300 down to 10 K. (d) Spectral intensity under UV-Vis, both the total and separate contributions of the 415 and 440 nm peaks, and X-ray excitation as function of temperature, from 300 down to 10 K.

The spectral intensity under UV-Vis excitation, both the total and contributions of the 415 and 440 nm peaks, are shown in Figure 2d. The later also shows the total spectral intensity under X-ray excitation. Upon cooling down from room temperature the total intensity under UV-Vis excitation increases. Reaching its maximum at 175 K, before decreasing to 45% of the maximum intensity. The initial increase coincides with the observed merging of the 440 nm emission peak with the 415 nm emission peak, see Figure 2b. The integrated intensity of the 415 and 440 nm

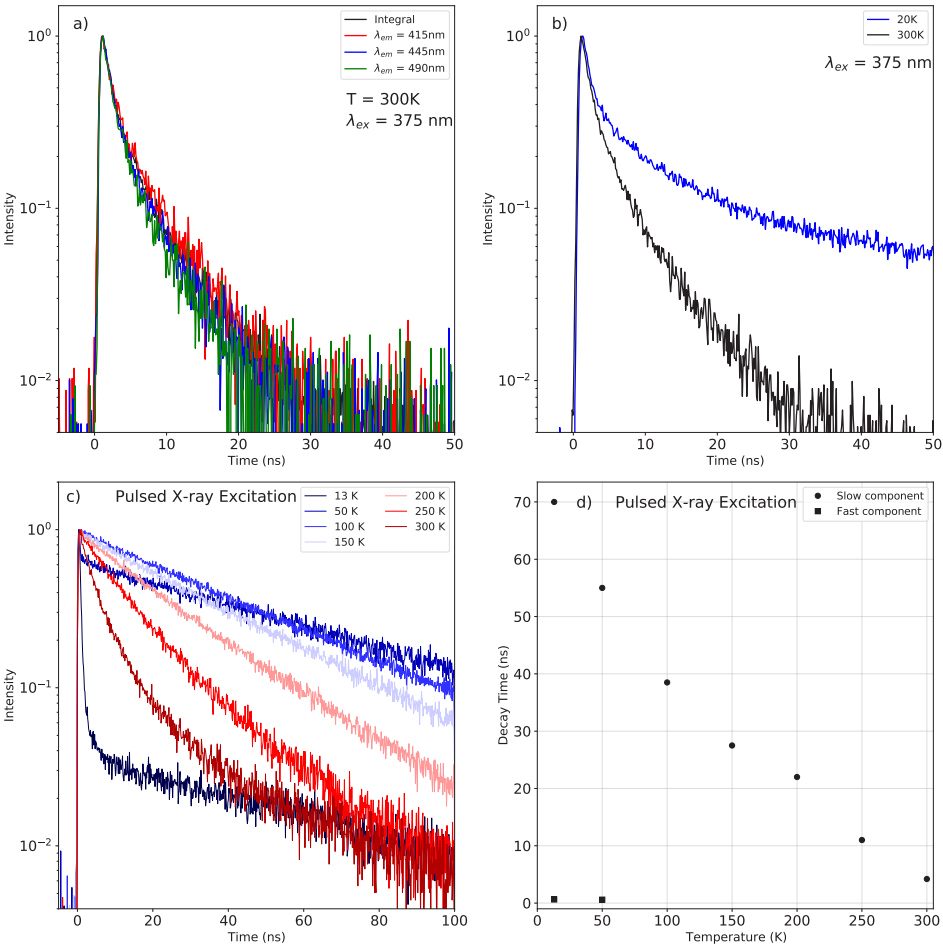


Figure 3: (a) Room temperature time resolved photoluminescence curves measured in integral mode, monitoring all wavelengths at the same time, and at wavelengths of 415, 445, and 490 nm. (b) 20 K and room temperature time resolved photoluminescence curves, measured in integral mode. (c) Temperature dependent pulsed X-ray excited decay curves from 300 down to 13 K. (d) Temperature dependent change of the decay time constants obtained from the pulsed X-ray excited decay curves.

emission peaks show opposite behaviour around this temperature. The intensity of the 440 nm peak reaches its minimum at 150 K, while the integrated intensity of the 415 nm peak reaches its maximum at this temperature. In contrast, the total spectral intensity under X-ray excitation first decreases, almost reaching zero at 150 K. At this temperature the 432 nm emission stops blue shifting, reaching a wavelength of 420 nm, as can be observed in Figure 2c. This behaviour of the total spectral intensity, both under UV-Vis and X-ray excitation, is similar to the behaviour observed for (PEA)₂PbBr₄ and (BA)₂PbBr₄ [14, 16].

Figure 3a shows the 300 K photoluminescence decay curves of $(\text{BZA})_2\text{PbBr}_4$ excited at 375 nm. The curves are recorded in integral mode, monitoring all wavelengths, and at the peaks observed in Figure 2a. The $1/e$ decay time, based on a single exponential model, for each decay spectrum is 3.3 ns which compares well with the average decay time constant of 3 ns reported by Dhanabalan *et al.* [28]. Figure 3b shows a comparison between the photoluminescence decay curves at 300 and 20 K. At 20 K the decay time has increased significantly.

Figure 3c shows the pulsed X-ray excited decay curves measured from 300 down to 13 K. The 300 K decay curve is slightly non-exponential, which disappears at 250 K. Below 100 K a fast decay component appears, with a decay time of 0.60 ns at 13 K. The decay times extracted from the decay curves, using either a single or bi-exponential model, are shown in Figure 3d. The slow component observed at 13 K shows a linear decrease of its decay constant upon heating, reaching 4.2 ns at 300 K.

The combination of the 4.2 ns decay of $(\text{BZA})_2\text{PbBr}_4$ under X-ray excitation and a reasonable light yield of 3700 photons/MeV makes this material very interesting for high count rate applications such as PCCT. To access the potential of $(\text{BZA})_2\text{PbBr}_4$ for PCCT we used the simulation tool developed by Van der Sar *et al.* [9, 10], which is based on a comprehensive model of the pulse trains produced by SiPM-based X-ray photon-counting scintillation detectors. Two metrics were defined to access the detector performance: A pulse duration metric t_{95} and a count rate capability metric r_{50} [9, 10]. These metrics were calculated for $(\text{BZA})_2\text{PbBr}_4$ using the properties reported in this work. For comparison, the properties of $(\text{PEA})_2\text{PbBr}_4$ reported in our previous work [16], and literature values for $\text{LYSO}:\text{Ce}^{3+}$, $\text{LaBr}_3:\text{Ce}^{3+}$ and CZT were used to calculate the same metrics. For the SiPM the following properties were used: photodetection efficiency = 0.28, recharge time constant = 7.0 ns, and optical cross talk parameter = 0.1235 [9]. This combined with a light collection efficiency of 0.75 is used as input for the model [9].

The results of the simulation are summarised in Table I. For $(\text{BZA})_2\text{PbBr}_4$ we found $t_{95} = 26$ ns and $r_{50} = 26.7$ Mcps/pixel. Comparison with the other values in Table I shows that $(\text{BZA})_2\text{PbBr}_4$ performs not only better than $\text{LYSO}:\text{Ce}^{3+}$ and $\text{LaBr}_3:\text{Ce}^{3+}$ but also better than CdTe/CZT.

Furthermore, the level of statistical fluctuations on the raw pulses of a $(\text{BZA})_2\text{PbBr}_4$ based detector, simulated examples are shown in Figure 4, are very low compared to the fluctuations on pulses of $\text{LYSO}:\text{Ce}^{3+}$ and $\text{LaBr}_3:\text{Ce}^{3+}$ based detectors [9]. This is caused by the fast decay of $(\text{BZA})_2\text{PbBr}_4$ (4.2ns), which is in fact faster than the SiPM response (7 ns). Hence, the pulse shapes are dominated by the deterministic SiPM response rather than the statistical response of the scintillator. As such, the negative effect of the moderate light yield (3.7 photons/keV) on the scintillators response doesn't manifest, and hardly any low-pass filtering, which would result in unfavourable pulse elongation, is needed to obtain useful pulses.

Table I: Summary and comparison of physical, scintillation, and detection properties. Both emission wavelengths and decay times are based on X-ray excited measurements. * 60keV is just below the K-edge of Lu.

	(BZA) ₂ PbBr ₄	(PEA) ₂ PbBr ₄	LYSO:Ce	LaBr ₃ :Ce	CZT
Detection Method	Indirect	Indirect	Indirect	Indirect	Direct
Hygroscopic	No	No	No	Yes	No
Production Methode	Solution	Solution	Czochralski	Bridgman	Bridgman
Max Emission Wavelength (nm)	432	440 [16]	420 [38]	380 [38]	
Decay Time (ns)	4.2	35.2 [16]	36 [38]	16 [38]	
Density (g/cm ³)	2.23 [31]	2.26 [31]	7.1 [38]	5.08 [38]	5.78
Light Yield					
@ 662 keV (photons/keV)	3.7	11 [14]	33 [38]	63 [38]	
Energy Resolution @ 662 keV	8%	10 % [14]	8 % [38]	2.6 % [38]	0.6 % [39]
Linear attenuation length					
@ 60 keV (cm ⁻¹)	5.8	5.8	19*	25.8	36
Pulse Duration t ₉₅ (ns) [9]	26	109	112 [9]	57 [9]	34 [9]
Count Rate Capability r ₅₀					
(Mcps/pixel) [9]	26.7	6.4	6.2 [9]	12.2 [9]	20.4 [9]

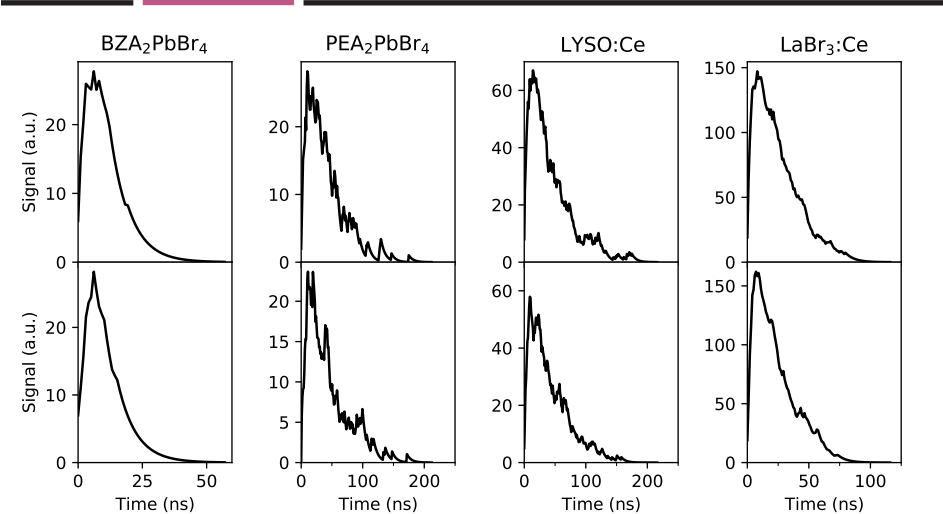


Figure 4: Examples of simulated pulses for (BZA)₂PbBr₄, (PEA)₂PbBr₄, LYSO:Ce³⁺, and LaBr₃:Ce³⁺.

3. Conclusion

The potential use of $(\text{BZA})_2\text{PbBr}_4$ in a PCCT detector has been accessed based on the presented characterisation. An energy resolution of 8% and light yield of 3.7 photons/keV, both at 662 keV, have been measured. Additionally, the non-proportionality of the response of $(\text{BZA})_2\text{PbBr}_4$ has been studied showing a maximum deviation of 6% at 60 keV. At room temperature a single emission peak at 432 nm is observed under X-ray excitation, while under UV-Vis excitation two emission peaks, 415 and 440 nm, are observed. This difference is ascribed to self absorption. The total spectral intensity decreases significantly at lower temperatures. At room temperature an X-ray excited decay time of 4.2 ns has been measured.

Due to this fast decay time the potential X-ray count-rate performance of $(\text{BZA})_2\text{PbBr}_4$ is outstanding, with predicted values of t_{95} and r_{50} of 26 ns and 26.7 Mcps/pixel respectively, outperforming state-of-the-art CdTe/CZT detectors. The simulated pulses showed little statistical fluctuations due to the fact that the 4.2 ns decay of $(\text{BZA})_2\text{PbBr}_4$ is faster than the SiPM response of 7 ns. These features of $(\text{BZA})_2\text{PbBr}_4$, combined with its cost-effective synthesis, which is still a major concern for detector-grade CdTe/CZT, make $(\text{BZA})_2\text{PbBr}_4$ very promising for PCCT. The further development of the growth process of $(\text{BZA})_2\text{PbBr}_4$ could improve its light yield and energy resolution, making this material even more interesting.

4. Experimental

$(\text{BZA})_2\text{PbBr}_4$ crystals were synthesised by dissolving PbBr_2 (0.73g, $\geq 98\%$ Merck) in HBr (5ml, 48% aqueous Merck) until a clear solution was formed. To this solution $\text{C}_6\text{H}_5\text{CH}_2\text{NH}_2$ (0.7ml, $\geq 98\%$ Merck) was added, immediately forming a white suspension. To this suspension 35 ml deionised water was added. The mixture was stirred vigorously and warmed at 100 °C for 1 hour to achieve a homogeneous clear solution. Crystals started to form when the mixture was left overnight at room temperature. The crystals were separated from the solution after two days and dried in aeration. This resulted in a product yield of 45% (0.48g). The crystal structure was determined using XRD and matches the structures presented in literature well [31].

The presented photoluminescence emission and excitation spectra were measured using a 450 W Xenon lamp. The light first passes through a Horiba Gemini 180 monochromator before hitting the sample. Afterwards the emitted light passes through a Princeton Instruments SpectraPro-SP2358 monochromator on which a Hamamatsu R7600U-20 PMT is attached. All spectra are corrected for the lamp intensity. The samples were mounted on a closed cycle helium cryostat operating below 10^{-4} mbar.

The presented X-ray excited emission spectra were recorded by exciting the sample using X-rays from a tungsten anode X-ray tube operating at 79 kV, with an average energy of 40 keV. The low energy side of the produced X-ray spectrum is filtered out of the X-ray beam to prevent radiation damage. The samples were mounted on a closed cycle helium cryostat operating below 10^{-4} mbar. The emitted light is detected by an Ocean Insights QE Pro Spectrometer.

The presented time resolved photoluminescence curves are measured via the time correlated single photon counting method. A PicoQuant LDH-P-C-375M pulsed diode laser excites the sample. The laser is triggered by a PicoQuant laser driver, whose reference output functions as the start signal and is connected to an Ortec 567 time-to-amplitude converter (TAC). An Ortec 462 time calibrator is used to calibrate the bin width. The emitted light passes through a Princeton Instruments VM-504 monochromator and is detected by an ID Quantique id100-50 single-photon counter. The signal is digitised by an Ortec AD144 amplitude to digital converter. The samples were mounted on a closed cycle helium cryostat operating below 10^{-4} mbar.

The presented X-ray excited decay curves are measured via the time-correlated single photon counting method using a Start:Stop ratio of approximately 5000:1 respectively. A PicoQuant LDH-P-C-440M pulsed diode laser is used to generate X-ray pulses from a Hamamatsu N5084 light excited X-ray tube, with an average energy of 18.2 keV. The laser is triggered by a PicoQuant laser driver, whose reference output functions as the start signal and is connected to an Ortec 567 time-to-amplitude converter (TAC). An Ortec 462 time calibrator is used to calibrate the bin width. An ID Quantique id100-50 single-photon counter was used to detect the emitted photons and functions as the stop signal. The signal first goes through a LeCroy 623B Octal Discriminator and analogue delay. The time differences are digitised using an Ortec AD114 amplitude to digital converter. The samples were mounted on a closed cycle helium cryostat operating below 10^{-4} mbar.

Pulse height spectra are recorded by placing the samples on a Hamamatsu R1791 PMT and covering them with PTFE tape. The PMT operates at -700 V. The signal first passes through an integrated pre-amplifier after which it is further processed by an Ortec 672 spectroscopic amplifier and digitized by an Ortec AD144 26 K ADC. All measurements were performed without optical coupling using a shaping time of 0.5 μ s.

5. Author contributions

The manuscript was written through contributions of all authors. All authors have given approval to the final version of the manuscript.

6. Conflicts of interest

There are no conflicts to declare.

7. Acknowledgements

The authors acknowledge financial supports from the TTW/OTP grant no. 18040 of the Dutch Research Council. The authors would like to thank Arramel for his assistance in the crystal growth process.

References

- [1] T. Flohr, M. Petersilka, A. Henning, S. Ulzheimer, J. Freda, B. Schmidt, *Physica Medica* 79 (2020) 126-136, <https://doi.org/10.1016/j.ejmp.2020.10.030>
- [2] U. N. Roy, G. S. Camarda, Y. Cui, R. Gul, A. Hossain, G. Yang, J. Zazvorka, V. Dedic, J. Franc, R. B. James, *Scientific Reports* 9 (2019) 1620, <https://doi.org/10.1038/s41598-01838188-w>
- [3] S. S. Hsieh, S. Leng, K. Rajendran, S. Tao, C. H. McCollough, *IEEE Transactions on Radiation and Plasma Medical Sciences* 5 (2021) 441-452, <https://doi.org/10.1109/TRPMS.2020.3020212>
- [4] M. Persson, R. Buijla, P. Nowik, H. Andersson, L. Kull, J. Andersson, H. Bornefalk, M. Danielsson, *Medical Physics* 43 (2016) 4398-4411, <https://doi.org/10.1118/1.4954008>
- [5] S. Kappler, A. Henning, B. Kreisler, F. Schoeck, K. Stierstorfer, T. Flohr, *Proceedings Volume 9033, Medical Imaging 2014: Physics of Medical Imaging*, 90331C, <https://doi.org/10.1117/12.2043511>
- [6] R. Steadman, C. Herrmann, A. Livne, *Nuclear Instrumenta and Methods in Physics Research Section A: Accelerators, Spectrometers, Detectors and Associated Equipment* 862 (2017) 18-24, <https://doi.org/10.1016/j.nima.2017.05.010>
- [7] J. Da Silva, F. Gronberg, B. Cederstrom, M. Persson, M. Sjolín, Z. Alagic, R. Buijla, M. Danielsson, *Journal of Medical Imaging*, 6 (2019) 043502, <https://doi.org/10.1117/1.JMI.6.4.043502>
- [8] M. Danielsson, M. Persson, M. Sjolín, *Physics in Medicine & Biology* 66 (2021) 03TR01, <https://doi.org/10.1088/1361-6560/abc5a5>
- [9] S. J. van der Sar, S. E. Brunner, D. R. Schaart, *Medical Physics* 48 (2021) 6324-6338, <https://doi.org/10.1002/mp.14886>
- [10] S. J. van der Sar, D. Leibold, S. E. Brunner, D. R. Schaart, *Proceedings Volume 12304, 7th International conference on Image Formation in X-ray Computed Tomography*, 12304A (2022), <https://doi.org/10.1117/12.2646519>

- [11] M. A. Green, A. Ho-Naillie, H. J. Snaith, *Nature Photonics* 8 (2014) 506, <https://doi.org/10.1038/nphoton.2014.134>
- [12] X. Y. Chin, D. Cortecchia, J. Yin, A. Bruno, C. Soci, *Nature Communications* 6 (2015) 7383, <https://doi.org/10.1038/ncomms8383>
- [13] L. Dou, Y. M. Yang, J. You, Z. Hong, W.-H. Chang, G. Li, Y. Yang, *Nature Communications* 5 (2014) 5404, <https://doi.org/10.1038/ncomms6404>
- [14] F. Maddalena, A. Xie, Arramel, M. E. Witkowski, M. Makowski, B. Mahler, W. Drozdowski, T. Mariyappan, S. V. Springham, P. Coquet, C. Dujardin, M. D. Birowosuto, C. Dang, *Journal of Materials Chemistry C* 9 (2021) 2504, <https://doi.org/10.1039/D0TC05647B>
- [15] A. Xie, F. Maddalena, M. E. Witkowski, M. Makowski, B. Mahler, W. Drozdowski, S. V. Springham, P. Coquet, C. Dujardin, M. D. Birowosuto, C. Dong, *Chemistry of Materials* 32 (2020) 8530- 8539, <https://doi.org/10.1021/acs.chemmater.0c02789>
- [16] J. J. van Blaaderen, F. Maddalena, C. Dong, M. D. Birowosuto, P. Dorenbos, *Journal of Materials Chemistry C* 10 (2022) 11598-11606, <https://doi.org/10.1039/D2TC01483A>
- [17] L. J. Diguna, L. Jonathan, M. H. Mahyuddin, Arramel, F. Maddalena, I. Mulyani, D. Onggo, A. Bachiri, M. E. Witkowski, M. Makowski, D. Kowal, W. Drozdowski, M. D. Birowosuto, *Materials Advances* 3 (2022) 5087-5095, <https://doi.org/10.1039/D2MA00258B>
- [18] E. V. D. van Loef, P. Dorenbos, C. W. E. van Eijk, *Applied Physics Letters*, 79 (2001) 1573, <https://doi.org/10.1063/1.1385342>
- [19] P. Dorenbos, *Optical Materials: X* 1 (2019) 100021, <https://doi.org/10.1016/j.omx.2019.100021>
- [20] C. van Aarle, K. W. Krämer, P. Dorenbos, *Journal of luminescence* 238 (2021) 11857, <https://doi.org/10.1016/j.jlumin.2021.118257>
- [21] C. van Aarle, K. W. Krämer, P. Dorenbos, *Journal of luminescence* 251 (2022) 119209, <https://doi.org/10.1016/j.jlumin.2022.119209>
- [22] P. Dorenbos, *IEEE transactions on nuclear science* 57 (2010) 3, <https://doi.org/10.1109/TNS.2009.2031140>
- [23] M. D. Birowosuto, D. Cortecchia, W. Drozdowski, K. Brylew, W. Lachmanski, A. Bruno, C. Soci, *Scientific Reports* 6 (2016) 37254, <https://doi.org/10.1038/srep37254>
- [24] V. B. Mykhaylyk, H. Kraus, V. Kapustianyk, H. J. Kim, P. Mercere, M. Rudko, P. Da Silva, O. Antonyak, M. Dendebera, *Scientific Reports* 10 (2020) 8601, <https://doi.org/10.1038/s41598-020-65672-z>

- [25] W. W. Wolszczak, D. L. Carroll, R. T. Williams, *Advanced X-ray Detector Technologies*, Chapter 1 (2022), https://doi.org/10.1007/978-3-030-64279-2_1
- [26] R. T. Williams, W. W. Wolszczak, X. Yan, D. L. Carrol, *ACS Nano* 14 (2020) 5161-5169, <https://doi.org/10.1021/acsnano.0c02529>
- [27] F. Maddalena, L. Tjahjana, A. Xie, Arramel, S. Zeng, H. Wang, P. Coquet, W. Drozdowski, C. Dujardin, C. Dang, M. D. Birowosuto, *Crystals* 9 (2019) 88, <https://doi.org/10.3390/cryst9020088>
- [28] B. Dhanabalan, A. Castelli, M. Palei, D. Spirito, L. Manna, R. Krahne, M. Arciniegas, *Nanoscale* 11 (2019) 8334-8342, <https://doi.org/10.1039/C9NR00638A>
- [29] B. Dhanabalan, A. Castelli, L. Ceseracciu, D. Spirito, F. Di Stasio, L. Manna, R. Krahne, M. P. Arciniegas, *Nanoscale* 13 (2021) 3948, 3956, <https://doi.org/10.1039/D0NR08043H>
- [30] Z. Yuan, Y. Shy, Y. Tian, Y. Xin, B. Ma, *Chemical Communications* 51 (2015) 16385-16388, <https://doi.org/10.1039/C5CC06750B>
- [31] N. Kawano, M. Koshimizu, Y. Sun, N. Yahaba, Y. Fujimoto, T. Yanagida, K. Asai, *Journal of Physical Chemistry C* 118 (2014) 9101-9106, <https://doi.org/10.1021/jp4114305>
- [32] J. T. M. De Haas, P. Dorenbos, *IEEE Transactions on Nuclear Science* 53 (2008) 3, <https://doi.org/10.1109/TNS.2008.922819>
- [33] P. Dorenbos, J. T. M. de Haas, C. W. E. van Eijk, *IEEE Transactions on Nuclear Science* 42 (1995) 2190-2202, <https://doi.org/10.1109/23.489415>
- [34] I. V. Khodyuk, P. Dorenbos, *IEEE Transactions on Nuclear Science* 59 (2012) 3320-3331, <https://doi.org/10.1109/TNS.2012.2221094>
- [35] W. Wolszczak, K. W. Krämer, P. Dorenbos, *Phys, Status Solidi RRL* 13 (2019) 1900158, <https://doi.org/10.1002/pssr.201900158>
- [36] C. Piemonte, A. Gola, *Nuclear Instruments and Methods in Physics Research Section A: Accelerators, Spectrometers, Detectors and Associated Equipment* 926 (2019) 2-15, <https://doi.org/10.1016/j.nima.2018.11.119>
- [37] Y. Haemisch, T. Frach, C. Degenhardt, A. Thon, *Physics Procedia* 37 (2012) 1546-1560, <https://doi.org/10.1016/j.phpro.2012.03.749>
- [38] Datas Sheet Luxium Solutions, obtained January 2023, <https://www.crystals.saintgobain.com/radiation-detection-scintillators/crystal-scintillators>
- [39] F. Zhang, C. Herman, Z. He, G. De Geronimo, E. Vernon, J. Fried, *IEEE Transactions On Nuclear Science* 59 (2012) 236- 242, <https://doi.org/10.1109/TNS.2011.2175948>

6

Scintillation and Optical Characterisation of CsCu_2I_3 Single Crystals from 10 to 400 K

Abstract

Currently only Eu^{2+} based scintillators have approached the light yield needed to improve the 2% energy resolution at 662 keV of $\text{LaBr}_3:\text{Ce}^{3+},\text{Sr}^{2+}$. Their major limitation however is the significant self-absorption due to Eu^{2+} . CsCu_2I_3 is an interesting new small bandgap scintillator. It is non-hygroscopic, non-toxic, melts congruently, has an extremely low afterglow, a density of 5.01 g/cm^3 , and effective atomic number of 50.6. It shows self-trapped exciton emission at room temperature. The large Stokes shift of this emission ensures that this material is not sensitive to self-absorption, tackling one of the major problems of Eu^{2+} based scintillators. An avalanche photodiode, whose optimal detection efficiency matches the 570 nm mean emission wavelength of CsCu_2I_3 , was used to measure pulse height spectra. From the latter a light yield of 36 000 photons/MeV and energy resolution of 4.82% were obtained. The scintillation proportionality of CsCu_2I_3 was found to be on par with that of $\text{SrI}_2:\text{Eu}^{2+}$. Based on temperature dependent emission and decay measurements it was demonstrated that CsCu_2I_3 emission is already about 50% quenched at room temperature. Using temperature dependent pulse height measurements it is shown that the light yield can be increased up to 60 000 photons/MeV by cooling down to 200 K, experimentally demonstrating the scintillation potential of CsCu_2I_3 . Below this temperature the light yield starts to decrease, which can be linked to the unusually large increase in the bandgap energy of CsCu_2I_3 .

The content of this chapter is based on: J. Jasper van Blaaderen, Liselotte A. van den Brekel, Karl W. Krämer, Pieter Dorenbos, *Chemistry of Materials* 35 (2023) 22

1. Introduction

Scintillation research in the past 30 years has mainly focused on the development of Ce^{3+} - and Eu^{2+} -doped materials [1]. The energy resolution record of 2% at 662 keV γ -energy, achieved by Alekhin *et al.* in 2013 using $\text{LaBr}_3:\text{Ce}^{3+},\text{Sr}^{2+}$ [2], still stands to day. This resolution approaches the fundamental energy resolution limit determined by photon statistics. It could be surpassed by either increasing the number of photons detected in a scintillation event or by increasing the light yield beyond the 70 000 photons/MeV reported for $\text{LaBr}_3:\text{Ce}^{3+},\text{Sr}^{2+}$ [2].

There are several Eu^{2+} -doped halide scintillators which have surpassed the light yield of $\text{LaBr}_3:\text{Ce}^{3+},\text{Sr}^{2+}$. Examples are $\text{CsBa}_2\text{I}_5:\text{Eu}^{2+}$ [3–6] and $\text{SrI}_2:\text{Eu}^{2+}$ [7–11] with reported light yields of 100 000 photons/MeV and 115 000 photons/MeV, and energy resolutions of 2.6% and 2.3%, respectively. Despite these very promising numbers, Eu^{2+} based scintillators suffer from two major drawbacks: self-absorption and concentration quenching [4, 12–16].

These problems can be mitigated by using a co-doping strategy based on Sm^{2+} [17–19], transferring almost all excitation's from Eu^{2+} to Sm^{2+} . This produces only Sm^{2+} emission and limits self-absorption losses. Additionally, this shifts the mean emission wavelength to longer wavelengths, around 700 to 850 nm, allowing the use of modern Si-based photo-detectors [17]. The latter have higher detection efficiencies compared to more traditional photo-multiplier tubes, enabling them to detect more photons from a scintillation event. This wavelength shifting effect has also been demonstrated for Yb^{2+} to Sm^{2+} [20, 21].

More recently intrinsic small bandgap materials have gained significant traction in scintillation research. Hybrid Organic-Inorganic Perovskites (HOIP) are a good example of such a group of materials [22–26]. The small band gap of these materials significantly increases their theoretical scintillation light yield compared to more traditional scintillators [1, 27, 28]. Especially intrinsic small bandgap materials showing self-trapped exciton (STE) emission are very promising candidates. The strong electron-phonon coupling in these materials creates a large Stokes shift resulting in self-absorption free emission, solving the problem of Eu^{2+} based scintillators. Examples of such compounds are Rb_2CuCl_3 [29], Rb_2CuBr_3 [30], and $\text{Cs}_3\text{Cu}_2\text{I}_5$ [31–33]. Especially the latter has shown promising scintillation properties with an energy resolution of 3.4% and light yield of 29.000 photons/MeV [31].

In this work the emerging intrinsic small bandgap scintillator CsCu_2I_3 is characterised as function of temperature. Currently this material has mainly been studied under UV-Vis excitation at room temperature for optoelectronic applications, with some scintillation related studies appearing in recent years [34–39]. Cheng *et al.* have performed a room temperature scintillation characterisation of this material, showing an energy resolution of 7.8% and light yield of 16 000 photons/MeV, measured on a photo-multiplier tube (PMT), and low afterglow level of 0.008% at 10 ms [40]. Liu *et al.* and Shu *et al.* have explored the influence of doping CsCu_2I_3 with Li^+ and Na^+ , respectively, only finding minor improvements of the

quantum yield at room temperature [41, 42]. Zhang *et al.* have explored the use of CsCu_2I_3 for imaging applications [43].

CsCu_2I_3 has many advantageous scintillator properties, it has a density of 5.01 g/cm^3 and Z_{eff} of 50.6. It melts congruently at 656 K [44], and is non-hygroscopic and non-toxic [36, 40]. Although the quantum yield of $\text{Cs}_3\text{Cu}_2\text{I}_5$ is higher at room temperature, CsCu_2I_3 is chosen due to the better match of its mean emission wavelength with modern Si-based photo-detectors [17]. Additionally, $\text{Cs}_3\text{Cu}_2\text{I}_5$ melts incongruently complicating the growth of single crystals [44]. The goal of this work is to study the scintillation and optical properties of CsCu_2I_3 from 400 down to 10 K in order to develop a better understanding of the scintillation and photo-physical properties of CsCu_2I_3 .

2. Results

Figure 1a shows the pulse height spectrum of a CsCu_2I_3 single crystal (10 mm x 3 mm x 3 mm) measured on an avalanche photo diode (APD), using the 662 keV γ -photons of ^{137}Cs . An APD was used to match the detection efficiency to the mean emission wavelength of CsCu_2I_3 , using the same approach as described by Wolszczak *et al.* [17]. Based on the full width at half maximum (FWHM) of the total absorption peak the energy resolution is determined to be 4.8%. The total absorption peak corresponds to the detection of 24 300 electron-hole pairs.

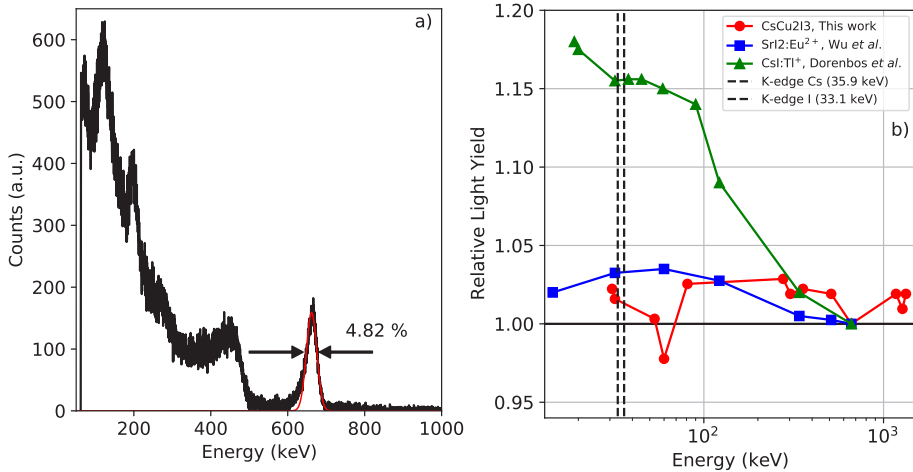


Figure 1: (a) Pulse height spectrum of a CsCu_2I_3 single crystal (10 mm x 3 mm x 3 mm) measured on an avalanche photo diode (APD) using a ^{137}Cs γ -source. The red line in the plot shows a fitted Gaussian function used to obtain the energy resolution and light yield. (b) Non-proportional response of CsCu_2I_3 in comparison to that of $\text{SrI}_2:\text{Eu}^{2+}$ [10] and $\text{CsI}:\text{TI}^+$ [46]. The pulse height spectra were recorded using ^{137}Cs , ^{22}Na , ^{133}Ba , ^{60}Co , and ^{241}Am . The ideal response is indicated by the horizontal line, at a relative light yield of 1. The K-edge of Cs and I at 35.9 and 33.1 keV, respectively, are indicated by the vertical dashed lines.

Based on which the light yield was determined to be 36 000 photons/MeV, using the method described by De Haas and Dorenbos [45]. This is a significant improvement compared to the values reported by Cheng *et al.* performing their measurements on a PMT [40].

The same CsCu_2I_3 sample was used to study the light yield as function of deposition energy, using γ -photons from ^{137}Cs , ^{22}Na , ^{133}Ba , ^{60}Co , and ^{241}Am . The resulting proportionality curve is shown in Figure 1b. The proportionality curves of $\text{SrI}_2:\text{Eu}^{2+}$ [10] and $\text{CsI}:\text{TI}^+$ [46] are plotted as reference. An ideal response would be a straight horizontal line at a relative light yield of 1, indicated by the black horizontal line in Figure 1b. The proportionality of CsCu_2I_3 is on par with that of $\text{SrI}_2:\text{Eu}^{2+}$, showing a deviation of max 4%. Moreover, both are significantly closer to the ideal response than that of $\text{CsI}:\text{TI}^+$.

The 300 and 10 K X-ray excited emission spectra are shown in Figure 2a. At 300 K one broad emission peak is observed located at 570 nm. This agrees with the 300 K X-ray excited emission spectrum presented by Cheng *et al.* [40]. The emission peak shifts to 575 nm at 10 K. The 570 nm emission falls within the wavelength range where the detection efficiency of the APD is at its maximum. Thus, as described by Wolszczak *et al.*, the number of detected photons from a scintillation event is increased compared to the detection with a PMT [17].

Figure 2b shows the 300 and 10 K decay curves under pulsed X-ray excitation. At both temperatures the decay curves show single exponential behaviour. At 300 K the lifetime is 110 ns, increasing to 1.8 μs at 10 K. The 300 K lifetime, under pulsed X-ray excitation, is approximately 50 ns slower compared to reported lifetimes under UV-vis excitation [34, 35, 37, 38]. A comparison between the 300 K decay curve measured under pulsed X-ray excitation and excitation by a 380 nm pulsed laser, detecting all photons with a wavelength longer than 425 nm, is shown in Figure 2c. The optically excited decay curve shows a similar non-exponential shape compared to the reported decay curves for CsCu_2I_3 single crystals [40, 43, 47].

The 300 and 10 K photoluminescence emission (PL) and photoluminescence excitation (PLE) spectra are shown in Figure 3a. At 300 K one broad emission peak is observed at 560 nm, shifting to 570 nm at 10 K. The 300 K excitation spectrum shows four peaks located at 265, 300, 330, and 350 nm. The 330 and 350 nm peaks merge and shift to 310 nm at 10 K while the other peaks show no shift. From Figure 3a it can be observed that CsCu_2I_3 has a large Stokes shift of 1.49 eV at 300 K; therefore preventing self-absorption related losses. At 10 K the Stokes shift increases to 1.82 eV. These features, the large Stokes shift and broad emission bands, are often attributed to self trapped exciton (STE) emission [48]. The 300 K excitation and emission spectra are in good agreement with previously reported spectra [34–36, 40, 41].

The temperature dependent change of the Stokes shift is mainly caused by the shift of the fundamental absorption edge. This is clearly visible in Figure 3b and c, showing temperature dependent PLE spectra of CsCu_2I_3 from 300 down to 10

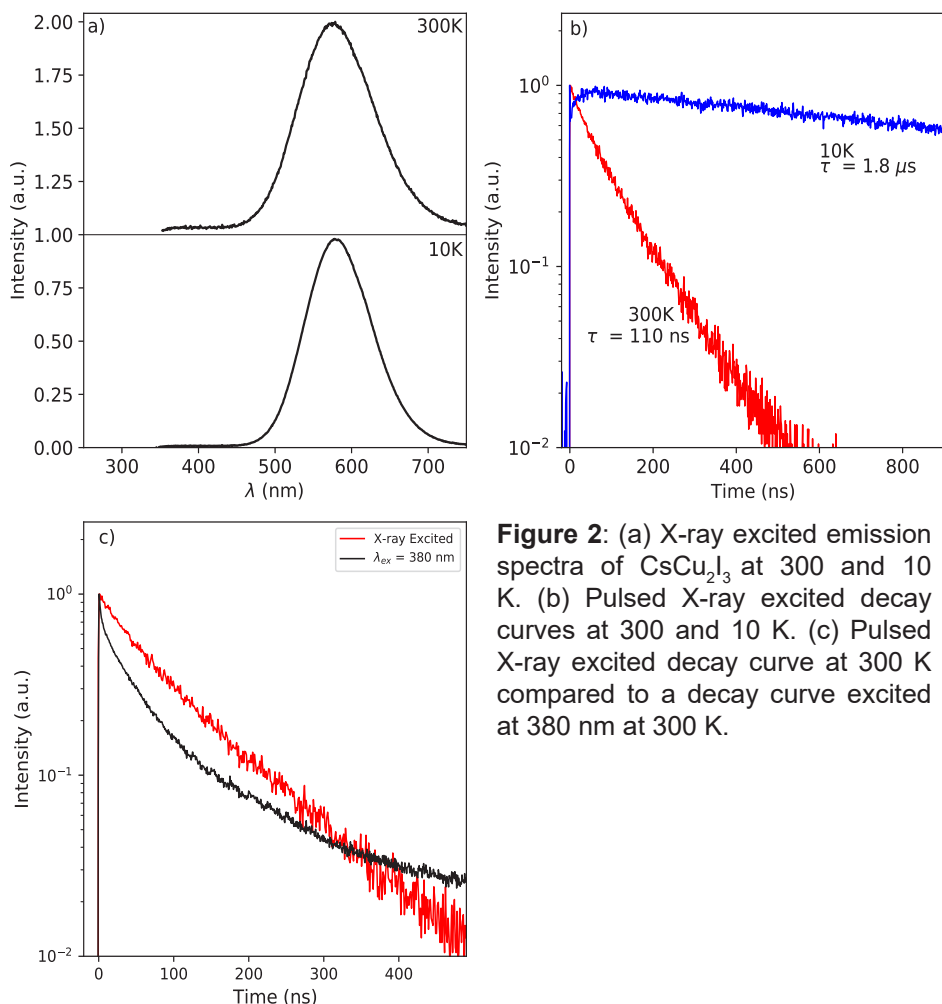
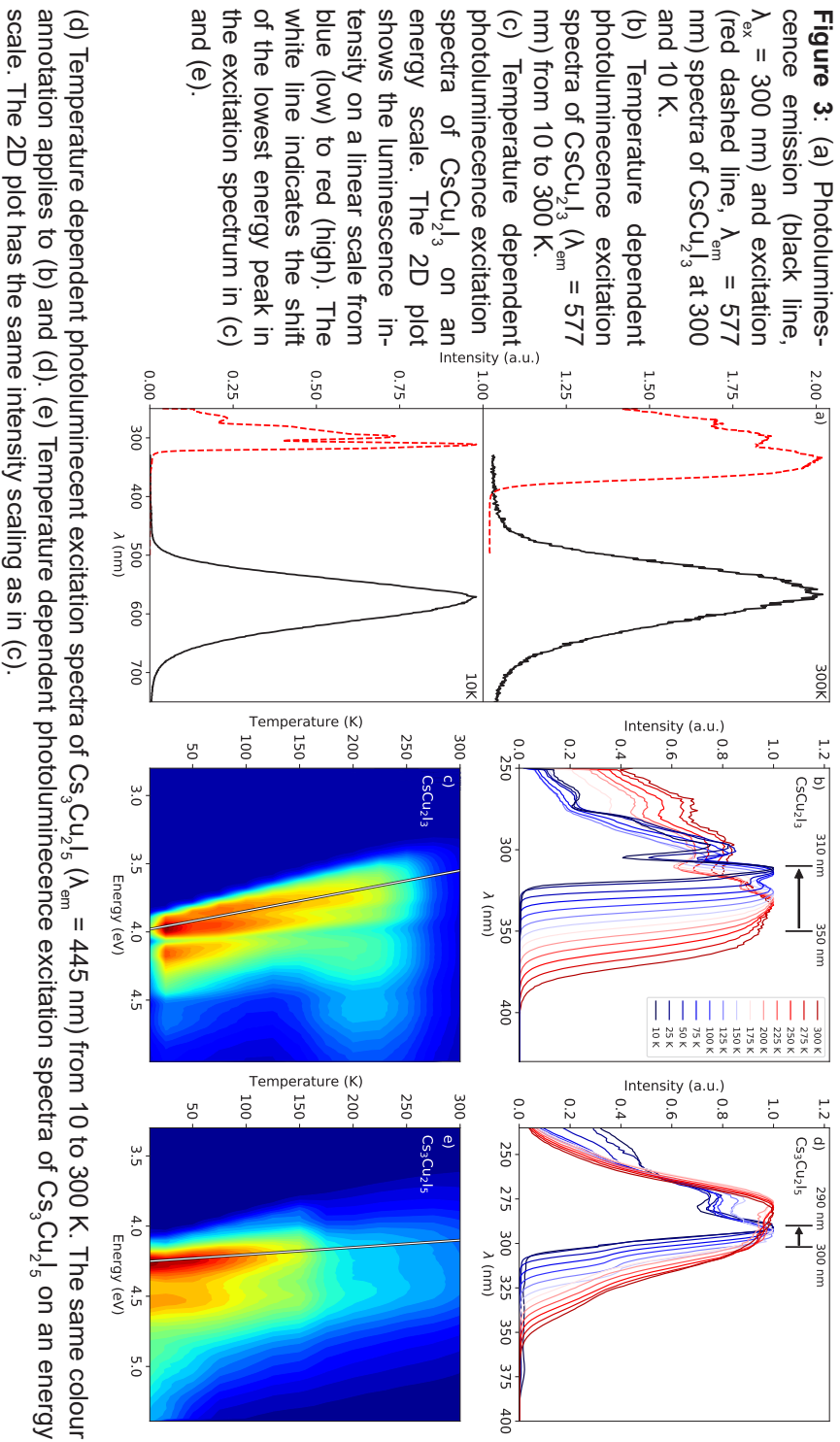


Figure 2: (a) X-ray excited emission spectra of CsCu₂I₃ at 300 and 10 K. (b) Pulsed X-ray excited decay curves at 300 and 10 K. (c) Pulsed X-ray excited decay curve at 300 K compared to a decay curve excited at 380 nm at 300 K.

K. Upon cooling, the fundamental absorption edge starts to shift towards shorter wavelengths. The way in which this happens however, is significantly different compared to the shift of the fundamental absorption edge observed in the temperature dependent PLE spectra measured for Cs₃Cu₂I₅. The latter are shown in Figure 3d and e.

Figure 4a-c show the temperature dependent photoluminescence emission, X-ray excited emission, and pulsed X-ray excited decay curves of CsCu₂I₃, respectively. The trends in the temperature behaviour are summarised in Figure 4d, showing the quenching curves of the integrated spectral intensity and decay time. All measurements show strong thermal quenching above 200 K. The increase and decrease of the photoluminescence intensity below 200 K result from the strong shift of the PLE spectra upon cooling as demonstrated in Figure 3b. The latter is not observed under X-ray excitation. The pulsed X-ray excited de-



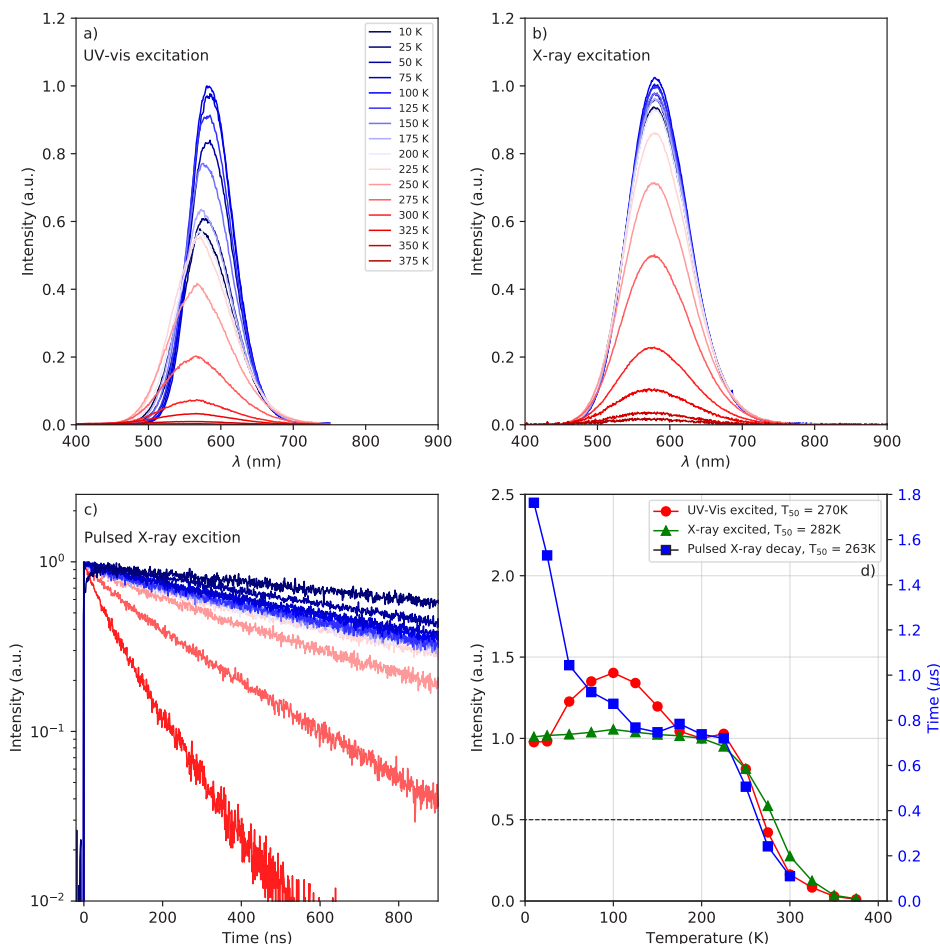


Figure 4: (a) Temperature dependent photoluminescence emission spectra ($\lambda_{\text{ex}} = 300 \text{ nm}$) from 10 to 375 K. (b) Temperature dependent X-ray excited emission spectra from 10 to 375 K. The temperature legend in (a) also applies to (b) and (c). (c) Temperature dependent pulsed X-ray excited decay curves from 10 to 300 K. (d) Integrated emission intensity from the temperature dependent photoluminescence emission (red circles, left axis) and X-ray excited emission (green triangles, left axis) measurements, normalised at 200 K. Life times obtained from the temperature dependent pulsed X-ray excited decay measurements (blue squares, right axis).

decay curves show an increase of the decay time from 110 to 740 ns upon cooling from 300 down to 200 K, respectively. Between 200 and 125 K the decay time is constant, but increases again to more than a micro second at 100 K and below.

The quenching curves, presented in Figure 4d provide the temperatures (T_{50}) at which the intensity and decay time have dropped to 50% of their low temperature value. T_{50} values of 270, 282, and 263 were determined for the photolumi-

nescence emission, X-ray excited emission, and pulsed X-ray excited decay, respectively. The APD used for the pulse height spectrum, shown in Figure 1a, is cooled to 260 K in order to reduce noise and prevent gain drift. The temperature of the sample is estimated to be close to 260 K. Hence, the pulse height spectra shown in Figure 1a was measured around the T_{50} point of the quenching curves. This suggests that the light yield could increase by a factor of 2 by cooling down the sample.

The effect of temperature on the light yield is studied experimentally via a series of pulse height measurements from 325 down to 80 K using 662 keV γ -photons of ^{137}Cs . The measurements are performed using a PMT. Figure 5a shows the pulse height spectra from 325 down to 200 K. From the latter it can be observed that the number of detected photo-electrons increases upon cooling, corresponding with an increase of the light yield. The change in light yield and energy resolution between 80 and 325 K is shown in Figure 5b. Between 325 and 200 K the light yield shows quenching behaviour similar to the curves presented in Figure 4d, yielding a T_{50} of 262 K which is very close to the values obtained from Figure 4d. The temperature dependent light yield reaches its maximum of 60 000 photons/MeV at 200 K, corresponding to the detection of 2 760 photo-electrons. If we manage to engineer the emission such that T_{50} increases to 350 K, one might increase the light yield towards 60 000 photons/MeV. The light yield obtained from the pulse height spectrum measured on an APD, shown in Figure 1a, falls in line with the curve shown Figure in 5b and is indicated by the red circular marker. From 200 down to 80 K the light yield starts to decrease, going down from 60 000 photons/MeV to 52 800 photons/MeV.

Coinciding with the increase of the light yield between 325 and 200 K the energy resolution improves from 30% down to 6.8%, respectively. The measured energy resolutions in this experiment are higher compared to the one shown in Figure 1a. This is the direct result of the geometric restrictions imposed by the cryostat. The sample could not be mounted directly on the entrance window of the PMT, combined with the less suitable match of the PMT detector efficiency with the mean emission wavelength of CsCu_2I_3 .

The pulse height measurements with 662 keV γ -photons, as shown in Figure 5a and b, were extended by measurements with 31, 80, and 365 keV X-ray and γ -photons of ^{133}Ba to study the effect of the deposition energy. The resulting curves are shown in Figure 5c and d. Above 200 K all curves show the same quenching behaviour as observed in Figure 4b and 5b. Below 200 K the light yield decreases, but the reduction is less for smaller deposition energies, see Figure 5d.

3. Discussion

The shape of the room temperature X-ray and photo-excited decay curves is different, as shown in Figure 2c. Under pulsed X-ray excitation of CsCu_2I_3 a single exponential decay curve is observed. However, upon excitation with a 380 nm

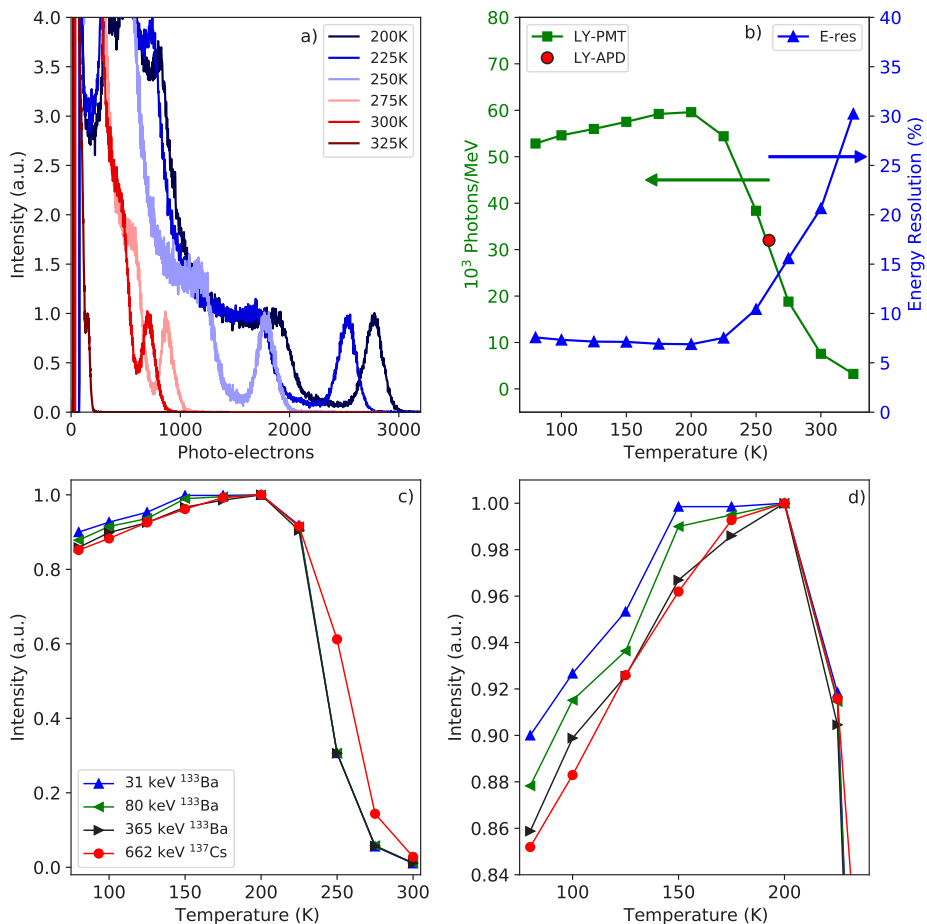


Figure 5: (a) Temperature dependent pulse height spectra, from 325 down to 200 K. (b) Light yield obtained from the temperature dependent pulse height measurements from 325 to 80 K (green squares, left axis). The red circle indicates the light yield obtained from the pulse height spectrum measured on an APD. Energy resolution obtained from the temperature dependent pulse height measurements (blue triangles, right axis). (c) Temperature dependent pulse height spectra, from 300 down to 80 K, using 662 keV γ -photons from ^{137}Cs , and 31, 80, and 365 keV γ -photons from ^{133}Ba . All curves are normalised on the light yield at 200 K. (d) Zoom in of the temperature dependent pulse height spectra in (c) from 80 to 200 K. The legend in (c) also applies to (d).

pulsed laser the decay curve shows non-exponential behaviour. This non-exponential behaviour is observed for both single crystals and films of CsCu_2I_3 [34–38, 43, 47]. Zhang *et al.* and Mo *et al.* suggested that the non-exponential shape stems from excitation of surface trap states and bulk STE emission [36, 43]. Based on the aforementioned and the significantly larger penetration depth of X-rays versus optical photons, it is suggested that the single exponential decay

curve observed under pulsed X-ray excitation results solely from bulk STE emission.

Based on the temperature dependent photoluminescence excitation spectra shown in Figure 3 it was observed that the fundamental absorption edge of CsCu_2I_3 blue shifts in a different way compared to $\text{Cs}_3\text{Cu}_2\text{I}_5$. This difference is further investigated by determining the change in the bandgap as function of temperature based on the shift of the lowest energy peak in the excitation spectra. The position of these peaks at 300 and 10 K, combined with the direction of the shift, are indicated in Figure 3b and d for CsCu_2I_3 and $\text{Cs}_3\text{Cu}_2\text{I}_5$, respectively. It was determined that the bandgap of CsCu_2I_3 shifts from 4 eV at 10 K to 3.55 eV at 300 K, corresponding to a change of 155 meV/ 100 K. The bandgap of $\text{Cs}_3\text{Cu}_2\text{I}_5$ shifts from 4.25 eV at 10 K to 4.1 eV at 300 K, corresponding to a change of 52 meV/ 100 K. The temperature dependent bandgap change is visualised by a white line plotted in Figure 3c and e. The bandgap change of $\text{Cs}_3\text{Cu}_2\text{I}_5$ is very similar to values reported for more traditional semiconductors (50– 100 meV/100 K) [49–51] like silicon or more modern semiconductors (50 meV/100 K) like lead halide perovskites [52, 53]. The bandgap change observed for CsCu_2I_3 , however, is approximately 2 to 3 times larger compared to these values.

The shifts determined from temperature dependent excitation spectra of $\text{Cs}_3\text{Cu}_2\text{I}_5$ show classical behaviour, see Figure 3d; the peaks in the spectrum become broader at higher temperature. The behaviour of CsCu_2I_3 is significantly different. From Figure 3a, b and c it can be observed that the 330 and 350 nm peak observed at 300 K starts to blue shift upon cooling and merge with the 310 nm peak, appearing below 200 K, resulting in the large band-gap shift. The valence band maximum is formed by the Cu 3d and I 5p orbitals, the conduction band minimum by the Cu 4s and I 5p orbitals for both CsCu_2I_3 and $\text{Cs}_3\text{Cu}_2\text{I}_5$ [36, 37, 39]. The main difference between these compounds lays in their crystallographic and the related electronic structure: $\text{Cs}_3\text{Cu}_2\text{I}_5$ as a 0D structure with isolated $[\text{Cu}_2\text{I}_5]^{3-}$ units built from two face-sharing tetrahedra, whereas CsCu_2I_3 has a 1D structure with double chains $[\text{Cu}_2\text{I}_3]^-$ of edge-sharing tetrahedra [39]. The fundamental origin for the large band gap change of CsCu_2I_3 remains unclear.

The temperature dependent light yield measurements presented in Figure 5 b shows an increase of the light yield from 325 down to 200 K, reaching 60 000 photons/MeV. From 200 down to 80 K the light yield decreases by 12% to 52 000 photons/MeV. Coinciding with this decrease, the energy resolution deteriorates from 6.8% at 200 K to 7.6% at 80 K. Between 200 and 80 K the band gap changes by 0.19 eV, from 3.7 eV at 200 K to 3.89 eV at 80 K.

The theoretical light yield of a material, as shown in Equation 1, depends on its band gap energy [1, 54]. Here N_{eh} is the number of created electron hole pairs in the scintillator per MeV deposited ionisation energy, β is usually taken to be ≈ 2.5 , E_g corresponds to the band gap energy. Based on Equation 1 and the observed increase of the bandgap, it is estimated that the theoretical light yield decreases by 5% from 200 down to 80 K. This only partially explains the observed 12% decrease of the light yield in Figure 5b.

$$N_{eh} = \frac{1,000,000}{\beta E_g} \quad (\text{e}^- \text{ - h pairs / MeV}) \quad (1)$$

The decrease of the light yield below 200 K is not observed in the X-ray excited emission spectra shown in Figure 4d. These spectra are recorded using continuous X-ray excitation with an average energy of 40 keV. This difference could be explained either due to the different excitation energies, the different integration times used, or the different experimental setups.

The influence of the deposition energy is studied by recording temperature dependent pulse height spectra using 662 keV γ -photons from ^{137}Cs and 31, 80, and 365 keV γ -photons from ^{133}Ba keeping the sample in the same position for all measurements. The resulting light yields as function of temperature and deposition energy are shown in Figure 5c and d. Above 200 K all curves show the same quenching behaviour as observed in Figure 4b. Below 200 K all curves show a decrease of the light yield. However, the magnitude of this decrease depends on the deposition energy, as shown in Figure 5d. The light yield decreases by approximately 15% between 200 and 80 K upon excitation with 662 keV γ -photons but only by 10% upon excitation with 31 keV γ -photons. Nonetheless, this change is not the same as the one observed in Figure 4d under continuous X-ray excitation.

4. Conclusion

In this work the emerging scintillator CsCu_2I_3 has been characterised as function of temperature. Using an APD, to match the detection efficiency to the mean emission wavelength of CsCu_2I_3 , an energy resolution of 4.8% and light yield of 36 000 photons/MeV have been measured for 662 keV excitation. Using different deposition energies it is demonstrated that the non-proportionality of CsCu_2I_3 is on par with that of $\text{SrI}_2:\text{Eu}^{2+}$. At 300 K CsCu_2I_3 has a Stokes shift of 1.49 eV and shows only one emission peak centred around 560 nm. This mean emission wavelength fits well with the spectral sensitivity of modern Si-based photodetectors with higher detection efficiencies compared to more traditional PMTs. At 300 K a lifetime of 110 ns has been measured under pulsed X-ray excitation.

From temperature dependent photoluminescence emission, X-ray excited emission, and pulsed X-ray excited decay measurements T_{50} values of 270, 282, and 263 K have been determined, respectively. Accordingly, the CsCu_2I_3 emission is already significantly quenched at 300 K. Using temperature dependent pulse height measurements it was proved experimentally that the light yield of CsCu_2I_3 increases to 60 000 photons/MeV at 200 K. Below 200 K the light yield decreases again by 10% to 15% down to 80 K, depending on the deposition energy. The decrease of the light yield below 200 K is attributed to the change of the bandgap energy by 155 meV/100 K. The exact nature of this large change could not be explained. Engineering CsCu_2I_3 by chemical variation and optimisation of the

crystal growth process might shift the T_{50} above 300 K, and improve the room temperature scintillation properties of CsCu_2I_3 .

5. Experimental

Crystals of CsCu_2I_3 and $\text{Cs}_3\text{Cu}_2\text{I}_5$ were grown from stoichiometric mixtures of CsI and CuI using the vertical Bridgman technique with a static ampoule and a moving furnace. CsI (Merck 99.5%) and CuI (ABCR, 99.999%) were dried in vacuum at 200 °C. Stoichiometric amounts of the iodides, about 5 g per sample, were sealed in silica ampoules under vacuum. The ampoules were heated to 10 K above the melting point of the ternary compound and the temperature was kept for one day. The crystal growth was started by slowly moving the furnace up by about 15 mm/day. The ampoule cooled to room temperature within 10 days. CsCu_2I_3 melts congruently at 383 °C [44]. The melting point of $\text{Cs}_3\text{Cu}_2\text{I}_5$ is at about 390 °C [44]. All handling of starting materials and products was done in glove boxes with H_2O and O_2 below 0.1 ppm. For spectroscopic measurements, crystals were sealed in silica ampoules under He or in sample containers under inert gas or vacuum. The crystal structure and the phase purity of the samples was confirmed by powder XRD.

Pulse height spectrum and non-proportionality curves were recorded using an Advanced Photonix APD (type 630-70-72-510) operating at a bias voltage of 1560 V. The APD was stabilised at 260 K to prevent gain drift. The signal was fed to a Cremat CR-112 pre-amplifier, before being processed by an Ortec 672 spectroscopic amplifier, with a shaping time of 3 μs , and digitised by an Ortec AD144 26K ADC. The light yield was calculated based on the channel position of the photopeak maximum and that of the peak from direct detection of 17.8 keV X-rays of ^{241}Am , as described by de Haas and Dorenbos [45].

X-ray emission spectra were recorded using a tungsten anode X-ray tube operating at 79 kV, producing X-rays with an average energy of 40 keV. The low energy side of the X-ray spectrum was filtered out by a 3 mm aluminium filter to prevent radiation damage in the sample. The samples were mounted on the cold finger of a closed cycle helium cryostat.

Pulsed X-ray excited decay curves were measured via the time-correlated single photon counting method. The start signal was generated by a PicoQuant LDH-P-C440M pulsed laser, directly hitting a Hamamatsu N5084 light excited X-ray tube to create X-ray pulses with an average energy of 18.2 keV. The stop signal was generated upon detection of a single photon using an ID Quantique id100-50 single-photon counter. The start and stop signals were processed by an Ortec 567 time-to-amplitude converter, whose output was digitised by an Ortec AD 144 16K ADC. The samples were mounted on the cold finger of a closed cycle helium cryostat.

Time resolved photoluminescence curves were measured via the time-correlated single photon counting method. A PicoQuant LDH-P-C-375M pulsed diode laser was used to excite the sample. The reference output of the PicoQuant laser driver was used as the start signal and was fed to an Ortec 567 time-to-amplitude converter. The emitted light was detected by an ID Quantique id100-50 single-photon counter. The final signal was digitised by an Ortec AD144 amplitude to digital converter.

Photoluminescence emission and excitation spectra were recorded using a 450 W Xenon lamp and Horiba Gemini 180 monochromator to excite the sample. The emitted light was collected at a 90 degree angle with respect to the excitation source. Reflected excitation light was removed by an optical filter. The emission light passed through a Princeton Instruments SpectraPro-SP2358 monochromator connected to a Hamamatsu R7600U-20 PMT. All spectra were corrected for the lamp intensity. The samples were mounted on the cold finger of a closed cycle helium cryostat.

Temperature dependent pulse height spectra were recorded by mounting the sample on a parabolic stainless steel reflector covered with aluminium foil to increase the reflectivity. The reflector was mounted on a Janis VPF-700 cryostat. The sample chamber was kept at a vacuum below 10^{-5} mbar. A Hamamatsu Super Bialkali R6231-100 (SN ZE4500) PMT was used to detect the scintillation photons. It was placed close to the window on the outside of the sample chamber. The distance between the sample and PMT was approximately 5 cm. The light yield was determined based on a comparison with a $(\text{Lu,Y})_2\text{SiO}_5:\text{Ce}^{3+}$ reference sample measured inside the cryostat under identical experimental conditions. The light yield of $(\text{Lu,Y})_2\text{SiO}_5:\text{Ce}^{3+}$ was determined by PMT read out based on the method described by de Haas and Dorenbos [45]. The light yield is corrected for the differences in emission wavelength between $(\text{Lu,Y})_2\text{SiO}_5:\text{Ce}^{3+}$ and CsCu_2I_3 and PMT detection efficiency.

6. Author Contributions

The manuscript was written through contributions of all authors. All author have given approval to the final version of the manuscript.

7. Conflicts of Interest

There are no conflicts to declare.

8. Acknowledgements

The authors acknowledge financial support from the TTW/OTP grant no. 18040 of the Dutch Research Council.

References

- [1] P. Dorenbos, Optical Materials: X 1 (2019) 100021, <https://doi.org/10.1016/j.omx.2019.100021>
- [2] M. S. Alekhin, J. T. M. de Haas, I. V. Khodyuk, K. W. Krämer, P. R. Menge, V. Ouspenski, P. Dorenbos, Applied physics letters 102 (2013) 161915, <https://doi.org/10.1063/1.4803440>
- [3] G. Bizarri, E. D. Bourret-Courchesne, Z. Yan, S. E. Derenzo, IEEE Transactions on nuclear science 58 (2011) 6, <https://doi.org/10.1109/TNS.2011.2166999>
- [4] M. S. Alekhin, D. A. Biner, K. W. Krämer, P. Dorenbos, Journal of Luminescence 145 (2014) 723-728, <http://dx.doi.org/10.1016/j.jlumin.2013.08.058>
- [5] E. D. Bourret-Courchesne, G. Bizarri, R. Borade, Z. Yan, S. M. Hanrahan, G. Gundiah, A. Choudhry, A. Canning, S. E. Derenzo, Nuclear Instruments and Methods in Physics Reserach A 612 (2009) 138-142, <https://doi.org/10.1016/j.nima.2009.10.146>
- [6] U. Shirwadkar, R. Hawrami, J. Glodo, E. V. D. van Loef, K. S. Shah, IEEE Transactions on nuclear science 60 (2013) 02, <https://doi.org/10.1109/TNS.2013.2240696>
- [7] R. Hawrami, J. Glodo, K. S. Shah, N. Cherepy, S. Payne, A. Burger, L. Boatner, Journal of Crystal Growth 379 (2013) 69-72, <https://doi.org/10.1016/j.jcrys-gro.2013.04.035>
- [8] N. J. Cherepy, G. Hull, A. D. Drobshoff, S. A. Payne, E. van Loef, C. M. Wilson, K. S. Shah, U. N. Roy, A. Burger, L. A. Boatner, W.-S Choong, W. W. Moses, Applied physics letters 92 (2008) 083508, <https://doi.org/10.1063/1.2885728>
- [9] L. A. Boatner, J. O. Ramey, J. A. Kolopus, R. Hawrami, W. H. Higgins, E. van Loef, J. Glodo, K. S. Shah, E. Rowe, P. Bhattacharya, E. Tupitsyn, M. Groza, A. Burger, N. J. Cherepy, S. A. Payne, Journal of Crystal Growth 379 (2013) 63/68, <https://doi.org/10.1016/j.jcrys-gro.2013.01.035>
- [10] Y. Wu, Q. Li, D. J. Rutstrom, I. Greeley, L. Stand, M. Loyd, M. Koschan, C. L. Melcher, Nuclear Inst. and Methods in Physics Research, A, 954 (2020) 161242, <https://doi.org/10.1016/j.nima.2018.09.077>
- [11] G. Bizarri, Journal of Crystal Growth 312 (2010) 1213-1215, <https://doi.org/10.1016/j.jcrys-gro.2009.12.063>
- [12] Y. Wu, M. Zhyravleva, A. C. Lindsey, M. Koschan, C. L. Melcher, Nuclear Instruments and Methods in Physics Research Section A: Accelerators, Spectrometers, Detectors and Associated Equipment 820 (2016) 132-140, <https://doi.org/10.1016/j.nima.2016.03.027>
- [13] J. Glodo, E. V. van Loef, N. J. Cherepy, S. A. Payne, K. S. Shah, IEEE Transactions on nuclear science 57 (2010) 3, <https://doi.org/10.1109/TNS.2009.2036352>

- [14] K. Yang, M. Zhuravleva, C. L. Melcher, *Phys. Status Solidi RRL* 5 (2001) 43-45, <https://doi.org/10.1002/pssr.201004434>
- [15] G. Guandiah, M. Gascon, G. Bizarri, S. E. Derenzo, E. D. Bourret-Courchesne, *Journal of Luminescence* 159 (2015) 274-279, <https://doi.org/10.1016/j.jlumin.2014.11.031>
- [16] M. S. Alekhin, K. W. Krämer, P. Dorenbos, *Nuclear Instruments and Methods in Physics Reserach Section A: Accelerators, Spectrometers, Detectors and Associated Equipment* 714 (2013) 13-16, <https://doi.org/10.1016/j.nima.2013.02.025>
- [17] W. Wolszczak, K. W. Krämer, P. Dorenbos, *Phys. Status Solidi RRL* 13 (2019) 1900158, <https://doi.org/10.1002/pssr.201900158>
- [18] R. H. P. Awater, M. S. Alekhin, D. A. Biner, K. W. Krämer, P. Dorenbos, *Journal of Luminescence* 212 (2019) 1-4, <https://doi.org/10.1016/j.jlumin.2019.04.002>
- [19] C. van Aarle, K. W. Krämer, P. Dorenbos, *Journal of Materials Chemistry C* 11 (2023) 2336-2344, <https://doi.org/10.1039/D2TC05311J>
- [20] C. van Aarle, K. W. Krämer, P. Dorenbos, *Journal of Luminescence* 251 (2022) 119209, <https://doi.org/10.1016/j.jlumin.2022.119209>
- [21] C. van Aarle, K. W. Krämer, P. Dorenbos, *Journal of Luminescence* 238 (2021) 118257, <https://doi.org/10.1016/j.jlumin.2021.118257>
- [22] F. Maddalena, A. Xie, Arramel, M. E. Witkowski, M. Makowski, B. Mahler, W. Drozdowski, T. Mariyappan, S. V. Springham, P. Coquet, C. Dujardin, M. D. Birowosuto, C. Dang, *Journal of Materials Chemistry C* 9 (2021) 2504, <https://doi.org/10.1039/D0TC05647B>
- [23] A. Xie, F. Maddalena, M. E. Witkowski, M. Makowski, B. Mahler, W. Drozdowski, S. V. Springham, P. Coquet, C. Dujardin, M. D. Birowosuto, C. Dong, *Chemistry of Materials* 32 (2020) 8530-8539, <https://doi.org/10.1021/acs.chemmater.0c02789>
- [24] J. J. van Blaaderen, F. Maddalena, C. Dong, M. D. Birowosuto, P. Dorenbos, *Journal of Materials Chemistry C* 10 (2022) 11598-11606, <https://doi.org/10.1039/D2TC01483A>
- [25] J. J. van Blaaderen, S. van der Sar, D. Onggo, Md Abdul K. Sheikh, D. R. Schaart, M. D. Birowosuto, P. Dorenbos, *Journal of Luminescence* 263 (2023) 120012, <https://doi.org/10.1016/j.jlumin.2023.120012>
- [26] L. J. Diguna, L. Jonathan, M. H. Mahyuddin, Arramel, F. Maddalena, I. Mulyani, D. Onggo, A. Bachiri, M. E. Witkowski, M. Makowski, D. Kowal, W. Drozdowski, M. D. Birowosuto, *Materials Advances* 3 (2022) 5087-5095, <https://doi.org/10.1039/D2MA00258B>
- [27] P. Dorenbos, *IEEE transactions on nuclear science* 57 (2010) 3, <https://doi.org/10.1109/TNS.2009.2031140>

- [28] M. D. Birowosuto, D. Cortecchia, W. Drozdowski, K. Brylew, W. Lachmanski, A. Bruno, C. Soci, *Scientific Reports* 6 (2016) 37254, <https://doi.org/10.1038/srep37254>
- [29] X. Zhao, G. Niu, J. Zhu, B. Yang, J.-H. Yuan, S. Li, W. Gao, Q. Hu, L. Yin, K.-H. Xue, E. Lifshitz, X. Miao, J. Tang, *The Journal Of Physical Chemistry Letters* 11 (2020) 1873-1880, <https://doi.org/10.1021/acs.jpcllett.0c00161>
- [30] B. Yang, L. Yin, G. Niu, J.-H. Yuan, K.-H. Xue, Z. Tan, X.-S. Miao, M. Niu, X. Du, H. Song, E. Lifshitz, J. Tang, *Advanced Materials* 31 (2019) 1904711, <https://doi.org/10.1002/adma.201904711>
- [31] S. Cheng, A. Beitlerova, R. Kucerkova, M. Nikl, G. Ren, Y. Wu, *Physica Status Solidi (RRL)* 14 (2020) 2000374, <https://doi.org/10.1002/pssr.202000374>
- [32] L. Stand, D. Rutstrom, M. Koschan, M.-H. Du, C. Melcher, U. Shirwadkar, J. Glodo, E. van Loef, K. Shah, M. Zhuravleva, *Nuclear Instruments and Methods in Physics Research Section A: Accelerators, Spectrometers, Detectors and Associated Equipment* 991 (2021) 164963, <https://doi.org/10.1016/j.nima.2020.164963>
- [33] D. Yuan, *ACS Applied Materials and Interfaces* 12 (2020) 38333-38340, <https://doi.org/10.1021/acsami.0c09047>
- [34] R. Lin, Q. Guo, Q. Zhu, Y. Zhu, W. Zheng, F. Huang, *Advanced Materials* 15 (2019) 1905079, <https://doi.org/10.1002/adma.201905079>
- [35] R. Roccanova, A. Yangui, G. Seo, T. D. Creason, Y. Wu, D. Y. Kim, M.-H. Du, B. Saparov, *ACS Materials Letter* 1 (2019) 459-465, <https://doi.org/10.1021/acsmaterialslett.9b00274>
- [36] X. Mo, T. Li, F. Huang, Z. Li, Y. Zhou, T. Lin, Y. Ouyang, X. Tao, C. Pan, *Nano Energy* 81 (2021) 105570, <https://doi.org/10.1016/j.nanoen.2020.105570>
- [37] Y. Hui, S. Chen, R. Lin, W. Zheng, F. Huang, *Materials Chemistry Frontiers* 5 (2021) 7088-7107, <https://doi.org/10.1039/D1QM00552A>
- [38] Y. Li, Z. Zhou, N. Tewari, M. Ng, P. Geng, D. Chen, P. K. Ko, M. Qammar, L. Guo, J. E. Halpert, *Materials Chemistry Frontiers* 5 (2021) 4796-4820, <https://doi.org/10.1039/D1QM00288K>
- [39] Z. Xing, Z. Zhou, G. Zhong, C. C. S. Chan, Y. Li, X. Zou, J. E. Halpert, H. Su, K. S. Wong, *Advanced Functional materials* 32 (2022) 2207638, <https://doi.org/10.1002/adfm.202207638>
- [40] S. Cheng, A. Beitlerova, R. Kucerkova, E. Mihokova, M. Nikl, Z. Zhou, G. Ren, Y. Wu, *Non-Hygroscopic, ACS Applied Materials and interfaces* 13 (2021) 12198-12202, <https://doi.org/10.1021/acsami.0c22505>
- [41] D. Liu, Q. Wei, Y. Tong, P. Xiang, P. Cai, G. Tang, H. Shi, L. Qin, *CrystEngComm* 25 (2023) 58-63, <https://doi.org/10.1039/D2CE01263D>
- [42] C. Shu, Q. Wei, D. Liu, W. Li, H. Yin, H. Li, G. Tang, L. Qin, *Crystals* 13 (2023) 1157, <https://doi.org/10.3390/cryst13081157>

- [43] M. Zhang, J. Zhu, B. Yang, G. Niu, H. Wu, X. Zhao, L. Yin, T. Jin, X. Liang, J. Tang, *Nano Letters* 21 (2021) 1392-1399, <https://doi.org/10.1021/acs.nanolett.0c04197>
- [44] A. Wojakowska, A. Gorniak, A. Y. Kuznetsov, A. Wojakowski, J. Josiak, *Journal of Chemical and Engineering Data* 48 (2003) 468-471, <https://doi.org/10.1021/je020188x>
- [45] J. T. M. De Haas, P. Dorenbos, *IEEE Transactions on Nuclear Science* 53 (2008) 3, <https://doi.org/10.1109/TNS.2008.922819>
- [46] P. Dorenbos, J. T. M. de Haas, C. W. E. van Eijk, *IEEE Transactions on Nuclear Science* 42 (1995) 6, <https://doi.org/10.1109/23.489415>
- [47] M. Hunyadi, G. F. Samu, L. Csige, A. Csik, C. Buga, C. Janaky, *Advanced Functional Materials*, 32 (2022) 2206645, <https://doi.org/10.1002/adfm.202206645>
- [48] S. Li, J. Luo, J. Liu, J. Tang, *Journal of Physical Chemistry Letters* 10 (2019) 1999-2007, <https://doi.org/10.1021/acs.jpclett.8b03604>
- [49] K. P. O'Donnell, X. Chen, *Applied Physics Letters* 58 (1991) 2924-2926, <https://doi.org/10.1063/1.104723>
- [50] G. W. Rubloff, *Physical review B* 5 (1972) 2, <https://doi.org/10.1103/PhysRevB.5.662>
- [51] R. Passler, *Journal of Applied Physics* 88 (2000) 5, <https://doi.org/10.1063/1.1287601>
- [52] G. Mannino, I. Deretzis, E. Smecca, A. La Magna, A. Alberti, D. Ceratti, D. Cahen, *Journal of Physical Chemistry Letters* 11 (2020) 2490-2496, <https://doi.org/10.1021/acs.jpclett.0c00295>
- [53] R. Saxena, J. Kangsabanik, A. Kumar, A. Shahee, S. Singh, N. Jain, S. Ghorui, V. Komar, A. V. Mahajan, A. Alam, D. Kabra, *Physical Review B* 102 (2020) 081201, <https://doi.org/10.1103/PhysRevB.102.081201>
- [54] P. A. Rodnyi, P. Dorenbos, C. W. W. van Wijk, *Physica Status Solidi b*, 187 (1995) 15-29, <https://doi.org/10.1002/pssb.2221870102>



— 7 —

The Search for and Selection of Scintillators for Photon Counting Detectors

Abstract

Photon-counting detectors (PCDs) are a rapidly developing technology. Current PCDs used in medical imaging are based on CdTe, CZT, or Si semiconductor detectors which directly convert X-ray photons into electrical pulses. An alternative approach is to combine ultrafast scintillators with silicon photomultipliers (SiPMs). In this work an overview is presented of different classes of scintillators. The potential application of these materials in scintillator-SiPM based indirect PCDs is assessed using three figures of merit. It is shown that the most promising material classes are Ce³⁺- or Pr³⁺-doped materials, near band-gap exciton emitters, plastics, and corevalence materials. The shortcomings of each of these groups, *i.e.*, emission wavelength and nonproportionality, are discussed. Additionally, the approach of material engineering is explored. For both selecting and/or engineering a material it is important to not only consider material properties but also take the SiPM properties into account, *e.g.*, recharge time and photodetection efficiency.

7

The content of this chapter is based on: J. Jasper van Blaaderen, Casper van Aarle, David Leibold, Pieter Dorenbos, Dennis R. Schaart, Submitted to ACS Chemistry of Materials

1. Introduction

X-ray computed tomography (CT) is a widely used medical imaging technique. Most CT scanners today use a pixelated energy-integrating detector, which yields a signal proportional to the total energy deposited in each pixel during the exposure time. As a result, no discrimination is made between the energy of incident X-rays, with high energy X-rays contributing more to the signal. Moreover, electronic noise is integrated during the exposure time. Energy-integrating detectors are thus limited in signal-to-noise and contrast-to-noise ratio for a given radiation dose [1, 2]. Photon-counting detectors (PCDs) can help mitigate these problems. A PCD counts the number of incident X-ray photons hitting the detector during the exposure time, only registering a count when the electrical output pulse of the PCD passes a predefined threshold. As a result, most of the electronic noise is rejected. In the case of a purely counting detector, all X-ray photons contribute equally to the detector signal. The use of multiple thresholds yields an energy-resolving PCD, which enables the use of PCDs in dual- or multi-energy (spectral) X-ray imaging. Despite their advantages PCDs are thus far not widely implemented in medical X-ray imaging systems. One of the challenges to their implementation are the high X-ray fluence rates that occur in medical imaging. Due to the detector's finite response time, multiple X-ray photons hitting a pixel within a short time can result in a superposition of their respective electrical output pulses. This is referred to as pulse pile-up. It has been estimated by Persson *et al.* that the maximum fluence rate reached in a standard clinical CT protocol is approximately $3.4 \cdot 10^8$ photons/s/mm², however, the fluence rate in most regions of a patient's shadow on the detector are much lower than the maximum [3]. In order to be able to handle this fluence rate and to reduce pulse pile-up, the detector pulse duration should not exceed more than tens of nanoseconds. Additionally, miniaturisation of the pixels, to a size smaller than 0.5×0.5 mm², helps to distribute the incident photons over multiple pixels, reducing the rate requirement per pixel. This does, however, increase the probability of a characteristic or Compton scattered X-ray photon to be absorbed in a neighbouring pixel. This is referred to as inter-pixel X-ray crosstalk and increases pulse pile-up and reduces spatial resolution [4]. Further requirements for PCDs are a sufficient full width at half maximum (FWHM) energy resolution of the detector system in the diagnostic energy range (25 to 150 keV), sufficient density to achieve high X-ray stopping power, and room temperature operation.

The potential of PCDs for CT has been explored extensively in the last 10 years [1, 5–8]. Current PCD detectors are based on direct detection, converting the energy deposited by X-ray photons into a charge pulse using semiconductors such as CdTe [9], Cd_{1-x}Zn_xTe (CZT) [10], or Si [11]. Several prototype photon-counting CT systems have been constructed, based on CdTe or CZT, and used to evaluate their benefits in clinical practice [1, 12]. These systems can reach FWHM energy resolutions in the range of 10 to 20% at 60 keV [10, 13]. However, for CdTe and CZT the production of low defect density semiconductors [1, 2], X-ray crosstalk, charge sharing of the pixels [10], and the low hole mobility pose a challenge.

Additionally, the effects of long-term exposure to the high X-ray fluence rates on detector performance of CdTe and CZT-based detectors is yet to be investigated [5]. For Si-based detectors, the low atomic number ($Z = 14$) and density ($\rho = 2.3 \text{ g/cm}^3$) makes Compton scattering the dominant interaction mechanism of X-ray photons [4], reducing energy and spatial resolution [14].

An alternative to the above mentioned direct PCDs are indirect detectors, utilising ultrafast scintillators to absorb the incident X-rays and convert them into scintillation photons. The scintillation photons are detected and converted into an electrical pulse by silicon photomultipliers (SiPMs). SiPMs consist of a two-dimensional array of single-photon avalanche diodes (SPADs) with a size in the order of $10 \text{ }\mu\text{m}$. SPADs are photodiodes operated above their breakdown voltage. Hence, an avalanche of charge carriers is created upon absorption of a single optical photon and subsequent creation of a single electron-hole pair. In a scintillator-SiPM based indirect PCD the scintillator should have a sufficient density to prevent X-ray crosstalk and a short decay time, in order to handle the high X-ray fluence rates. The SiPM should have a short recharge time and a photodetection efficiency curve matching the emission spectrum of the scintillator. Another important property is the light collection efficiency of the detection system. This is influenced by a combination of the scintillator crystal, the SiPM, the optical properties of their respective surfaces, the optical coupling between the crystal and SiPM, and the detector geometry.

Initial feasibility studies on SiPM based scintillator PCDs have been performed by Van der Sar *et al.* by coupling $(\text{Lu}_{1-x}\text{Y}_x)_2\text{SiO}_5:\text{Ce}^{3+}$ (LYSO: Ce^{3+}), $\text{YAlO}_3:\text{Ce}^{3+}$ (YAP: Ce^{3+}), $\text{LuAlO}_3:\text{Ce}^{3+}$ (LAP: Ce^{3+}), and $\text{LaBr}_3:\text{Ce}^{3+}$ to a single-pixel SiPM with a recharge time of 7 ns [15–18]. The pulse duration, the full width at half maximum of the detector output pulse, of the $\text{LaBr}_3:\text{Ce}^{3+}$ based detector was experimentally determined to be less than 30 ns [16]. With this definition the pulse duration of a CdTe-based detector is 14 ns [13, 16]. Experimentally, the $\text{LaBr}_3:\text{Ce}^{3+}$ -based detector showed a FWHM energy resolution of 20% at 60 keV [15, 17, 18]. The energy resolution of the $\text{LaBr}_3:\text{Ce}^{3+}$ -based detector however, was limited by the low ($< 25\%$) photodetection efficiency of the used SiPM. For CdTe-based PCDs, a FWHM energy resolution of 8% at 60 keV has been demonstrated. [10]. Another study by Arimoto *et al.* used a 1×64 array of $1 \times 1 \text{ mm}^2$ pixels coupled to a cerium doped yttrium-gadolinium-aluminium-gallium garnet (YGAGG) scintillator [19]. Arimoto *et al.* demonstrated that, with a FWHM energy resolution of 32% at 60 keV of the detector system, it was possible to acquire energy-resolved X-ray images, restricted to low fluence rate conditions due to the 70 ns decay time of the YGAGG scintillator [20, 21]. These energy-resolved X-ray images can then be used to perform material decomposition, *i.e.*, creating material maps which represent the presence of two or more different types of tissue or material in the image.

In this work an overview of different types of scintillators is presented. The goal is to identify suitable materials to be used in a scintillator-SiPM based indirect PCD. In order to do so three different figures of merit are formulated to describe the scintillator performance in an indirect PCD. Additionally, potential problems for different classes of scintillators are identified. The presented framework is also used to explore the possibility of engineering a scintillator suitable to be used in an indirect PCD.

2. Indirect PCD Signal Chain and Figures of Merit

In order to theoretically assess the performance of different scintillators in an indirect PCD, a simple model has been formulated. The model describes the essential parts of the detection chain, taking into account properties of both the scintillator crystal and the SiPM. The model can be divided into four different stages, from the generation of X-ray photons to the size of the electrical output pulse of the indirect PCD.

Stage I

In the first stage an X-ray photon is created and passes through the object, e.g., a patient. When an X-ray photon with energy E_x hits a scintillator-pixel of the detector it will deposit an amount of energy E_{dep} in the scintillator-pixel. The amount of energy depends on the probability of secondary photons, i.e., Compton scattered photons or characteristic X-rays, leaving the scintillator pixel. This, next to material properties like density and composition, also depends on the location of the interaction of the incident X-ray with the scintillator pixel. All these effects are summarised in

$$\int_0^\infty p(E_{\text{dep}}|E_x) dE_{\text{dep}} = 1 . \quad (1)$$

where $p(E_{\text{dep}}|E_x)$ represents the probability density function of the amount of deposited energy (E_{dep}), given that the interacting X-ray photon has an energy E_x .

Stage II

In the second stage, the energy deposited by the incident X-ray is converted into a pulse of scintillation photons. The expected number of emitted scintillation photons is represented by \bar{N}_{em} and is defined as

$$\bar{N}_{\text{em}} = \int_0^\infty \bar{N}_p(E_{\text{dep}}) \cdot p(E_{\text{dep}}|E_x) dE_{\text{dep}} . \quad (2)$$

Here, $\bar{N}_p(E_{\text{dep}})$ represents the expected number of scintillation photons produced as a function of the deposited energy. This number depends on the light yield and non-proportionality of the scintillator.

Stage III

In the third stage the scintillation photons are transported through the crystal towards the detector surface of the SiPM where each photon can trigger a SPAD. The expected number of detected scintillation photons (\bar{N}_{det}) is given by

$$\bar{N}_{\text{det}} = \bar{N}_{\text{em}} \cdot \bar{\eta}_{\text{det}}. \quad (3)$$

Here, $\bar{\eta}_{\text{det}}$ represents the photon detection efficiency of the detection system. The photon detection efficiency is defined according to

$$\bar{\eta}_{\text{det}} = \int_0^\infty \lambda_{\text{em}}(\lambda) \cdot \eta_{\text{ot}}(\lambda) \cdot \eta_{\text{pd}}(\lambda) d\lambda. \quad (4)$$

Here, $\lambda_{\text{em}}(\lambda)$ represents the emission spectrum of the scintillator, normalised according to Equation 5, $\eta_{\text{ot}}(\lambda)$ the optical transfer efficiency of the total detection system and $\eta_{\text{pd}}(\lambda)$ the photon detection efficiency of the SiPM.

$$\int_0^\infty \lambda_{\text{em}}(\lambda) d\lambda = 1 \quad (5)$$

The photon detection efficiency of the detection system thus depends on properties of the scintillator, the photodetector, and the total detection system.

Stage IV

In the fourth and final stage, the SiPM generates an electronic pulse. The charge contained in this electrical detector output pulse $Q(E_X)$ does not only depend on the number of detected scintillation photons but also on the nonproportional response of the SiPM due to saturation effects, afterpulsing, and crosstalk. The role of these effects on the nonproportional response of the SiPM has been discussed elaborately by Van Dam *et al.* [22].

The incident X-ray spectrum

The electrical detector output pulse $Q(E_X)$ described in stage IV applies to a given energy of the interacting X-ray photon (E_X). However, the incident X-rays originate from a polychromatic X-ray beam. The X-ray spectrum of this beam behind the object is represented by $S_X(E_X)$ and normalised according to

$$\int_0^\infty S_X(E_X) dE_X = 1. \quad (6)$$

This spectrum can be used to calculate the average charge in an electronic detector output pulse for the incident X-ray spectrum according to

$$\bar{Q} = \int_0^\infty Q(E_X) \cdot S_X(E_X) dE_X. \quad (7)$$

Figures of Merit

Using the model described above, three different figures of merit can be formulated to describe the performance of an indirect PCD. The figures of merit are: the total pulse intensity, the pulse duration, and the pulse amplitude. The pulse intensity is defined as the expected number of SPADs triggered by scintillation photons in the SiPM. It depends on both \bar{N}_{em} and \bar{n}_{det} making it a scintillator, SiPM, and detection system related property. It can be seen as the maximum number of scintillation photons which can be detected. This number is closely related to the energy resolution of the detection system (R). The energy resolution, as demonstrated in Equation 8, is comprised of three different contributions [23–26].

$$R^2 = R_{stat}^2 + R_{np}^2 + R_{in}^2 \quad (8)$$

Here, R_{stat} represents the standard deviation in the number of photons detected by the photon detector and R_{np} the contribution of the nonproportionality of the scintillator. All other factors influencing the energy resolution, for example a non-uniform distribution of dopant ions in the scintillator crystal, are summarised by R_{in} . The influence of the latter however, will be very small due to the sub mm size of the scintillator crystals in a indirect PCD. The term R_{stat} is a fundamental property of the whole detection system. It scales according to Poisson statistics, as demonstrated in

$$R_{stat} \propto 2.35 \cdot \sqrt{\frac{1}{N_{dp}}} \quad (9)$$

Here, N_{dp} represents the number of detected scintillation photons. The theoretical energy resolution of the detector system is reached when N_{dp} is equal to N_{det} , and $\bar{n}_{det} = 1$, resulting in $\bar{N}_{det} = \bar{N}_{em}$. This means that each of the created scintillation photons reaches the SiPM and triggers a SPAD. The theoretical energy resolution of the detection system thus scales directly with the pulse intensity (\bar{N}_{det}).

Non-proportionality ($nP(E_{dep})$) on the other hand, is a material property describing the nonproportional change of the light yield as function of the deposited energy [26, 27]. It has been studied extensively, both experimentally [28–31] and theoretically [32–35] in the last two decades. Traditionally, scintillator energy resolutions are determined using the 662 keV γ -photons of ^{137}Cs [23]. At this energy, the statistical limit of the energy resolution can only be reached when $nP(E_{dep})$ is close to an ideal response, which corresponds to $nP(E_{dep}) = 100\%$ for all values of E_{dep} . This is less important in the diagnostic energy range (25 to 150 keV) where the dominant factor influencing the energy resolution is the statistical contribution. This means that the energy resolution improves when the non-proportionality is larger than 100% in the diagnostic energy range. On the other hand, when the non-proportionality is smaller than 100% the energy resolution will deteriorate. Experimentally, this means that characterising a scintillator using the 59.5 keV gamma photons of ^{241}Am instead of the 662 keV gamma photons of ^{137}Cs will provide more relevant information for their application in indirect PCDs.

The detector pulse duration (t_{FWHM}) is defined as the full width at half maximum of the detector output pulse. The output pulse can be described by a convolution of the single SPAD response and the decay profile of the scintillation photons. The response time of a single SPAD can be approximated by a single exponential decay characterised by the recharge time of the SiPM, τ_{rech} . The time distribution of the emitted scintillation photons, $n_{em}(t)$, can be described according to

$$n_{em}(t) = \frac{\overline{N}_{em}}{\tau_{dec}\tau_{rise}} \cdot (e^{-t/\tau_{dec}} - e^{-t/\tau_{rise}}). \quad (10)$$

Here, τ_{dec} and τ_{rise} are the decay time and the rise time of the scintillator, respectively. Due to the sub mm size of the scintillator crystal it can be assumed that the optical transfer time of the scintillation photons towards the detection surface of the SiPM is significantly shorter compared to the decay time. The triggering of the SPADs can thus directly be described by Equation 10. When the rise time is significantly shorter than the decay time, Equation 10 can be simplified to

$$n_{em}(t) = \frac{\overline{N}_{em}}{\tau_{dec}} \cdot (e^{-t/\tau_{dec}}) \quad (11)$$

which expresses that the scintillator decay can be described as a single exponent. In reality, however, this is not always the case. When the scintillator decay consists of multiple components, the decay can be simplified by describing it with a single exponential decay and a weighted average decay time. The decay of scintillators that show non-exponential behaviour can also be estimated by assuming a single exponent.

The detector output pulse can be estimated using

$$I(t) = I_0 \cdot k \cdot (e^{-\alpha t} - e^{-\beta t}) \quad (12)$$

where α and β are the decay constants of the recharge and decay time, defined as $1/\tau_{rech}$ and $1/\tau_{dec}$, respectively [36]. The pre-factor k , defined as

$$k = \left[e^{-\alpha \frac{\ln(\alpha/\beta)}{\alpha-\beta}} - e^{-\beta \frac{\ln(\alpha/\beta)}{\alpha-\beta}} \right]^{-1} \quad (13)$$

allows for the creation of different pulse shapes, by changing the recharge and decay time, while keeping the amplitude of the pulse constant [37].

Figure 1 shows the calculated pulse duration (t_{FWHM}) as function of the scintillator decay time for different recharge times ranging from 50 to 4 ns. As a reference, the pulse duration of CdTe based detector, 14 ns, is indicated by the red dashed line [16]. Since several prototype PCDs, based on CdTe, have been used to evaluate their use in clinical practice it can be assumed that a pulse duration of at most 14 ns is sufficient to handle the high X-ray fluence rate of medical imaging systems [1, 12]. As a second reference, red circular markers are added at 16 ns that representing the decay time of $\text{LaBr}_3:\text{Ce}^{3+}$. For a SiPM with a recharge time

of 7 ns, as was used experimentally by Van der Sar *et al.* [15–18], the calculated pulse duration of $\text{LaBr}_3:\text{Ce}^{3+}$ is equal to 26.6 ns. Decreasing the recharge time to 4 ns reduces the pulse duration to 21.2 ns. This shows that further decreasing the recharge time of the SiPM only results in marginal improvements of the pulse duration for the case of $\text{LaBr}_3:\text{Ce}^{3+}$.

The pulse amplitude (A_{pulse}) is defined as the pre-exponential factor in Equation 11. Similar as for the pulse duration, it can be assumed that the rise time is significantly shorter compared to the decay time. This means that when the scintillator decay can be described with a single exponent, as shown in Equation 11, the amplitude of the scintillation pulse (A_{puls}) is given by

$$A_{\text{pulse}} = \frac{\overline{N}_{em}}{\tau_{dec}}. \quad (14)$$

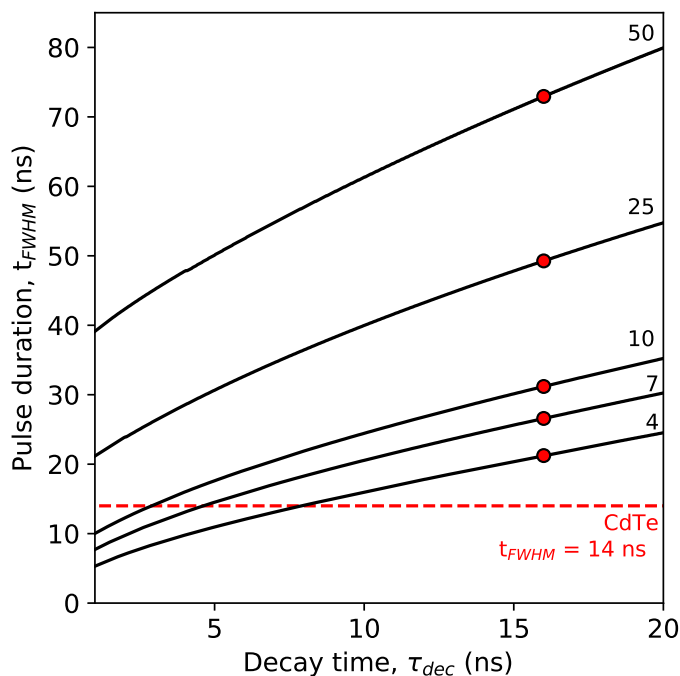


Figure 1: The calculated pulse duration (t_{FWHM}) as function of the scintillator decay time (τ_{dec}) for different recharge times (τ_{rech}). The red dashed line represents the state of the art pulse duration of 14 ns of CdTe. The red markers indicate the calculated pulse duration of $\text{LaBr}_3:\text{Ce}^{3+}$ for different recharge times.

The larger the value of the pulse amplitude, the smaller the statistical fluctuations on the output pulse of the detector systems will be. If these fluctuations are too strong, a single pulse can pass the detection threshold multiple times and be counted multiple times. This can be suppressed by filtering the pulses which leads to pulse elongation [15, 17, 18].

The three figures of merit defined above can thus be used to assess the suitability of a scintillator in an indirect PCD. There are a number of additional material properties, e.g., density, effective atomic number, radiation hardness, and afterglow, which are not taken into account in this assessment.

3. Scintillator Overview

An initial assessment of scintillators for their application in PCDs can be made by a scatter plot of their pulse duration and pulse amplitude. The shorter the pulse duration and the higher the pulse amplitude the more suitable the scintillator for application in a PCD. However, not all scintillator and detector properties are readily available in literature. For a first general material selection, the following assumptions are made: the expected photon detection efficiency is taken to be 100 %. Scintillator light yields are commonly determined and reported using the 662 keV γ -photons of ^{137}Cs . Hence, this is directly used as an estimate for the intensity of the scintillation pulse because data on nonproportionality or the light yield at low deposition energies is not always available. Based on these assumptions, data was collected from literature to assess the performance of different scintillators. Not all scintillators show a single exponential decay. For scintillators which show multiple decay components the average lifetime is calculated according to

$$\langle \tau_{av} \rangle = \frac{\sum_{i=1}^n A_i \tau_{dec,i}^2}{\sum_{i=1}^n A_i \tau_{dec,i}}. \quad (15)$$

Here, A_i represents the amplitude and $\tau_{dec,i}$ the decay time of the different decay components. The separate decay components can be found in the supplementary information.

Solid state scintillators can be divided into two general groups: extrinsically activated scintillators, intrinsic scintillators. Extrinsically activated scintillators can be divided in sub groups based on the used activator ion, typical activator ions are Ce^{3+} , Eu^{2+} , and Tl^+ . In the past three decades scintillation research has mainly focused on the development of Ce^{3+} and Eu^{2+} -doped compounds. An example is the development of $\text{LaBr}_3:\text{Ce}^{3+}$, which has a light yield of 76,000 ph/MeV and decay time of 16 ns [38]. Alekhin *et al.* showed that codoping $\text{LaBr}_3:\text{Ce}^{3+}$ with Sr^{2+} improves the proportionality without affecting the light yield. This resulted in the current record energy resolution of 2% at 662 keV. Co-doping with Sr^{2+} however, introduces several slow decay processes, resulting in an average decay time of 1,209 μs [38, 39]. Other well known Ce^{3+} based scintillators are $\text{Lu}_2\text{SiO}_5:\text{Ce}^{3+}$

[40, 41] and $(\text{Lu}, \text{Y})_2\text{SiO}_5:\text{Ce}^{3+}$ [42–44] which are used in positron emission tomography scanners due to their high density and decay time of around 40 ns [45]. Not all Ce^{3+} -doped scintillators however, emit exclusively through the $\text{Ce}^{3+} 5d \rightarrow 4f$ transition. It can for example be observed in $\text{Cs}_2\text{LiYCl}_6:\text{Ce}^{3+}$, commonly used for the detection of neutrons [46–48], in the form of slow decay components originating from the host matrix. The collected data on Ce^{3+} -doped scintillators are summarised in Table I.

Examples of Eu^{2+} -doped scintillators are $\text{SrI}_2:\text{Eu}^{2+}$ [109, 128, 129] and $\text{CsBa}_2\text{I}_5:\text{Eu}^{2+}$ [130, 131] with light yields of 90,000 and 97,000 photons/MeV, respectively. The $\text{Eu}^{2+} 4f^6 5d \rightarrow 4f^7$ transition however, has a typical decay time between 500 and 1000 ns, making these scintillators 10–50 times slower compared to Ce^{3+} doped scintillators. Additionally, Eu^{2+} doped scintillators often suffer from self-absorption [131–136]. This is mainly a problem in applications where crystals of several millimeters are required. The collected data on Eu^{2+} doped scintillators are summarised in Table II.

Two other divalent lanthanides that have been used as activator are Yb^{2+} and Sm^{2+} . Yb^{2+} is very similar to Eu^{2+} in spin allowed decay time and emission wavelength. However, its decay always includes a slow millisecond component due to the spin forbidden $4f^{13}5d \rightarrow 4f^{14}$ transition [171]. Sm^{2+} on the other hand emits in the near-infrared and has a decay time of approximately 2 μs [172]. It can be used as co-dopant next to Eu^{2+} or Yb^{2+} as their energy can efficiently be transferred to Sm^{2+} [173–177]. The collected data on Yb^{2+} , Eu^{2+} - Sm^{2+} , and Yb^{2+} - Sm^{2+} are summarised in Table III.

The Ti^{3+} -doped scintillators $\text{CsI}:\text{Ti}^{3+}$ [178] and $\text{NaI}:\text{Ti}^{3+}$ [179, 180] have been studied extensively the last decades and are commercially available. The later, discovered by Hofstadter in 1948 [181–183], is one of the first and most used scintillators up to this day. The collected data on Ti^{3+} -doped scintillators are summarised in Table III.

Another less commonly used activator ion is Pr^{3+} . It can show $4f^1 5d \rightarrow 4f^2$ emission in compounds where the energy of its $4f^1 5d$ state lies between that of the $4f^2[{}^1\text{S}_0]$ and $4f^2[{}^3\text{P}_2]$ states [184]. One of the main challenges of utilising the fast $4f^1 5d \rightarrow 4f^2$ transition of Pr^{3+} is that it is located in the UV [185]. However, its shorter emission wavelength compared to the $\text{Ce}^{3+} 5d \rightarrow 4f$ emission also results in shorter lifetimes of typically 10 to 20 ns [185]. This is for example observed in $\text{Lu}_3\text{Al}_5\text{O}_{12}:\text{Pr}^{3+}$ [186, 187]. The collected data on Pr^{3+} -doped scintillator are summarised in Table III.

Intrinsic scintillators can be divided into sub groups based on their emission, either broad band, near band-gap excitonic or plastics. Two well known intrinsic broad band scintillators are $\text{Bi}_4\text{Ge}_3\text{O}_{12}$ (BGO) and PbWO_4 . BGO, due to its 300 ns decay time and density of 7.13 g/cm³, is often used in positron emission tomography detectors (PET) [197–199]. PbWO_4 on the other hand, due to its decay time of 30 ns and density of 8.28 g/cm³ among other properties, has been used in the large hadron collider of CERN [200, 201]. Other intrinsic broad band scintillators

which have been explored more recently are the caesium hafnium based halides [202–205], caesium copper based iodides [206–208], and thallium based halides [209–212]. These compounds typically show decay times in the order of 1 to 2 μs . The collected data on intrinsic broad band emitting scintillators are summarised in Table IV.

A specific group of intrinsic scintillators that gained attention in the last decade are hybrid organic-inorganic perovskites [213–215]. Specifically, two dimensional perovskites have shown to be promising scintillators due to their stable room temperature near bandgap excitonic emission [216, 217]. The nano second decay time of these materials makes them very interesting to use in a PCD. This possibility has been explored with benzylammonium lead bromide ((BZA)₂PbBr₄) [218]. Xia *et al.* have demonstrated that the decay time of these materials can be reduced even further by engineering the dielectric constant of the organic molecule [219, 220]. A downside to these materials, however, is their low density of approximately 2.5 g/cm³. The collected data on the near band-gap exciton scintillators are summarised in Table IV.

Some scintillators can show an additional form of intrinsic emission originating from the recombination of an electron in the valence band with a hole in the highest core band. This is referred to as core-valence luminescence (CVL), cross luminescence, or Auger-free luminescence [235]. CVL can only take place when the condition formulated in Equation 16 is satisfied [236].

$$E_{CV} + \Delta E_V < E_g \quad (16)$$

Here, E_{CV} represents the energy gap between the top of the highest core band and the bottom of the valence band, ΔE_V the width of the valence band, and E_g the band gap. This condition is satisfied in some fluorides, chlorides, and bromides containing Ba²⁺, Cs⁺, Rb⁺, and K⁺ [237]. One of the first compounds in which CVL was discovered is BaF₂ [238]. The emission spectrum of BaF₂ contains three CVL bands, at 183, 196 and 220 nm, in addition to the self-trapped exciton band at 310 nm [239]. The CVL bands have a decay time of 0.8 ns while the self-trapped exciton band has a decay time of 600 ns. The short decay time of the CVL emission makes these materials a good potential candidate to be used in a PCD. One of the main problems however is the presence of STE or other emissions with longer decay times. The self-trapped exciton emission of BaF₂ can be suppressed by doping BaF₂ with for example La³⁺ [240, 241], Cd³⁺ [240, 241], Y³⁺ [242, 243], and Sc³⁺ [244]. The CVL bands of fluoride based compounds lay approximately between 140 and 230 nm. The emission wavelength shifts to longer wavelengths in chloride or bromide based compounds. Examples of chloride based compounds which show CVL emission are the families of Cs-Mg-Cl and Cs-Zn-Cl compounds [245–247]. One of the additional benefits of these compounds is the absence of slow decay components at room temperature. The collected data on fluoride and chloride based compounds that show CVL emission are summarised

in Table V. Bromide based compounds like CsBr, CsCaBr₃, and CsSrBr₃ are not considered due to their low CVL intensity [235, 237, 248, 249].

The last group of intrinsic scintillators is plastic scintillators. These materials are often used for the detection of neutrons and pulse shape discrimination to distinguish between neutrons and γ -photons [258, 259]. Plastic scintillators typically have a density of 1 g/cm³ and contain low Z atoms, like carbon and hydrogen, which makes these materials less suitable for the detection of high energy γ -photons. High Z dopants can be added to the plastic scintillator to increase its absorption [261–263]. The collected data on plastic scintillators are summarised in Table VI.

4. Scintillator Assessment

Using the figures of merit and collected data, discussed above, an assessment of the suitability of different scintillators for their use in a scintillator-SiPM based indirect PCD is made. In order to do so the pulse duration is plotted versus the pulse amplitude of the collected data points, as shown in Figure 2. As a reference, the pulse duration of CdTe (14 ns) is indicated by the red vertical line, providing a bench mark for the pulse duration requirements of an indirect PCD.

Based on the estimated maximum incident X-ray fluence rate of $3.4 \cdot 10^8$ photons/s/mm² in routine clinical scans given by Persson *et al.*, the corresponding event rate in a commercial CdTe based PCD CT system was estimated to be $5.2 \cdot 10^7$ events/s/pixel. This is slightly higher than the 50% pile up probability rate of $2.9 \cdot 10^7$ events/s/pixel, which nevertheless has proven to be sufficient in commercially available PCD CT systems [280]. The event rate was estimated based on simulations using RQA9 spectrum, corresponding to a source voltage of 120 kVp [279]. A pixel size of $333 \times 333 \mu\text{m}^2$ of 2 mm CdTe was assumed. The number of events created in a pixel array, based on the incident RQA9 spectrum, was simulated using the Monte-Carlo simulation software Gate (version 9.2) [281]. The influence of charge sharing was estimated based on geometrical consideration using a simple charge cloud model [282].

From Figure 2 it can be observed that most data points from Eu^{2+} , Yb^{2+} , Sm^{2+} , Tl^+ and broad band emission based scintillators have a pulse duration longer than 500 ns. This results in pulse amplitudes typically below 200 photons/ns, even though light yields of up to 90.000 photons/MeV have been reported for compounds like $\text{SrI}_2:\text{Eu}^{2+}$ [128, 129]. The pulse duration of Ce^{3+} - doped scintillators ranges from tens of nano seconds to tens of micro seconds; the average decay time of Ce^{3+} - doped scintillators strongly depends on the host matrix. This can be explained by inefficient or slow transfer of charge carriers towards Ce^{3+} and the presence of host related emissions next to the intrinsic $5d \rightarrow 4f$ emission of Ce^{3+} . There are several Ce^{3+} - based scintillators which approach the pulse duration of CdTe, *i.e.*, LaBr_3 and PrBr_3 . The situation of Pr^{3+} - doped scintillators is very similar to that of Ce^{3+} - doped scintillators. The average decay time of Pr^{3+} depends on the host matrix, *i.e.*, the occurrence of efficient $5d \rightarrow 4f$ emission. The shorter

emission wavelength of Pr^{3+} decreases its intrinsic $5d \rightarrow 4f$ decay time compared to that of Ce^{3+} . The main challenge for Pr^{3+} however, is the efficient detection of its UV emission.

The shortest pulse durations are achieved by scintillators based on CVL emission, near bandgap exciton emission, and plastics, with some materials showing pulse durations shorter than CdTe. However, these different types of scintillators each have their respective challenges. For CVL emission based scintillators this is the presence of slow decay components and/or the low light yield of the CVL emission. For near band-gap emission based scintillators self-absorption is a big challenge. Plastic scintillators have very low densities, typically in the order of 1 g/cm^3 , which will result in a higher probability of cross-talk between scintillator

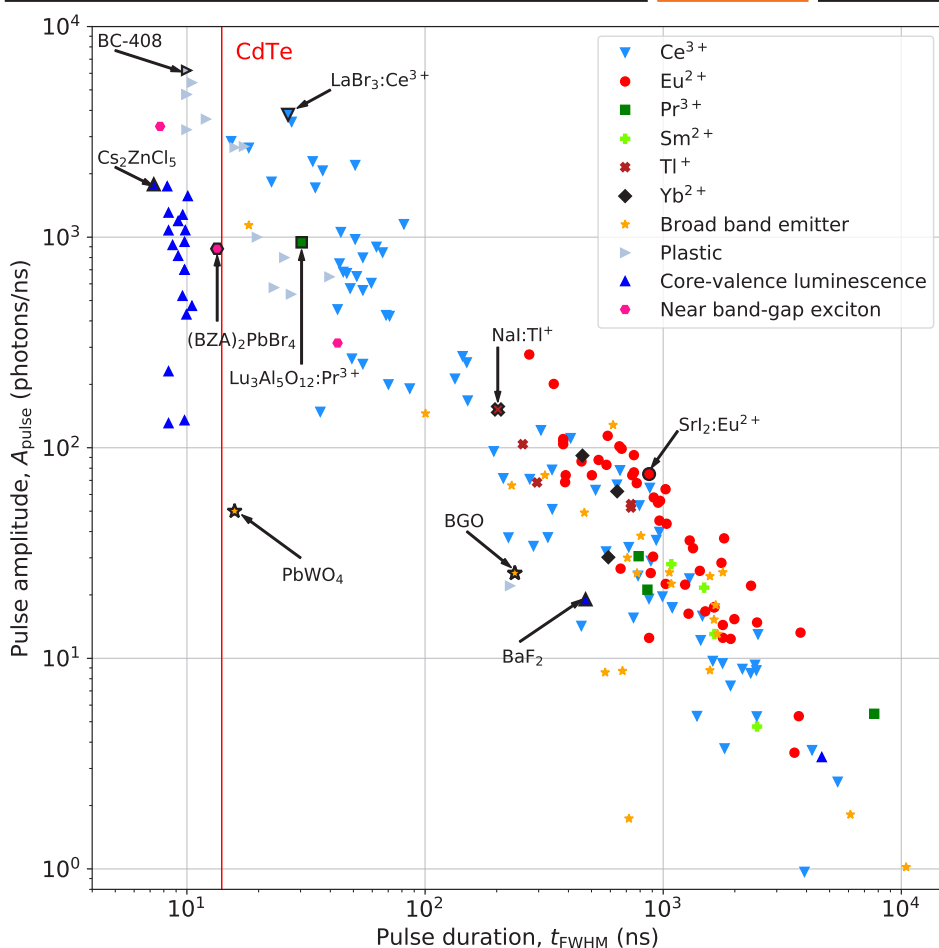


Figure 2: Plot of the pulse duration (t_{FWHM}) versus the pulse amplitude for Ce^{3+} -, Pr^{3+} -, Eu^{2+} -, Yb^{2+} -, Sm^{2+} co-doped, and Tl^{+} - doped scintillators, intrinsic scintillators showing core-valence luminescence, broad band emission, near band-gap exciton emission, and plastic scintillators.

pixels. Most data points of these materials have the same pulse duration, approximately 10 ns, showing only variations in the pulse amplitude.

When the decay time of the scintillator becomes significantly longer than the recharge time of the SiPM, the pulse duration will be mainly determined by the decay time. This behaviour is visualised in Figure 3 by plotting the decay time versus the pulse duration for the collected data points. The red vertical line indicates the 7 ns recharge time of the SiPM used to calculate the pulse duration. In this plot three different regimes can be identified. When the decay time becomes significantly shorter than the recharge time, the pulse duration is mainly determined by the recharge time ($t_{FWHM}(\tau_{rech})$). The recharge time is indicated by the vertical dashed line. There are no data points in this regime. When the decay time becomes significantly longer than the recharge time, the pulse duration is mainly determined by the decay time ($t_{FWHM}(\tau_{dec})$). In these two regimes the pulse duration can thus be estimated based on a single exponential decay. In the last regime the pulse duration depends on both the recharge time and decay time ($t_{FWHM}(\tau_{dec}, \tau_{rech})$). In this regime it is necessary to use Equation 12 to calculate the pulse duration.

5. Scintillator Engineering

Another approach for the development of indirect PCDs is to engineer the quenching of the scintillator decay time. From a theoretical perspective the amplitude of the scintillation pulse, Equation 14, is independent of temperature everywhere along the quenching curve. The influence of the change of the decay time and the pulse amplitude, along the quenching curve, on the pulse duration can be studied by taking a hypothetical scintillator. In order to do so the light yield and decay time are taken to be 140,000 photons/MeV and 140 ns, respectively. The hypothetical light yield and decay time are used to simulate detector output pulses, based on the experimentally validated model of Van der Sar *et al.* [15–18]. The pulse duration is calculated based on the changing decay time and the pulse amplitude is calculated based on the simulated pulses. The change in pulse amplitude upon moving along the quenching curve is shown in Figure 4a. The dimensionless number t_{FWHM}/τ_{rech} on the x-axis makes this curve independent of the recharge time of the SiPM. A selection of the simulated detector output pulses is shown in Figure 4b. The simulated pulses can be grouped into three different regimes based on the recharge and decay time. In the first regime the decay time is larger than the recharge time ($\tau_{dec} \gg \tau_{rech}$). Quenching of the decay time in this regime results in a decrease of the pulse duration with almost no change of the pulse amplitude. In the second regime the decay and recharge times are approximately equal ($\tau_{dec} \approx \tau_{rech}$). Quenching of the decay time in this regime results in a decrease of the pulse duration and a small shift of the pulse amplitude. In the third regime the decay time is smaller than the recharge time ($\tau_{dec} \ll \tau_{rech}$). Quenching the decay time in this regime results in a very minimal decrease of the pulse duration and a significant decrease of the pulse amplitude. In Figure 4a this can be observed by the curve reaching a vertical asymptote along which

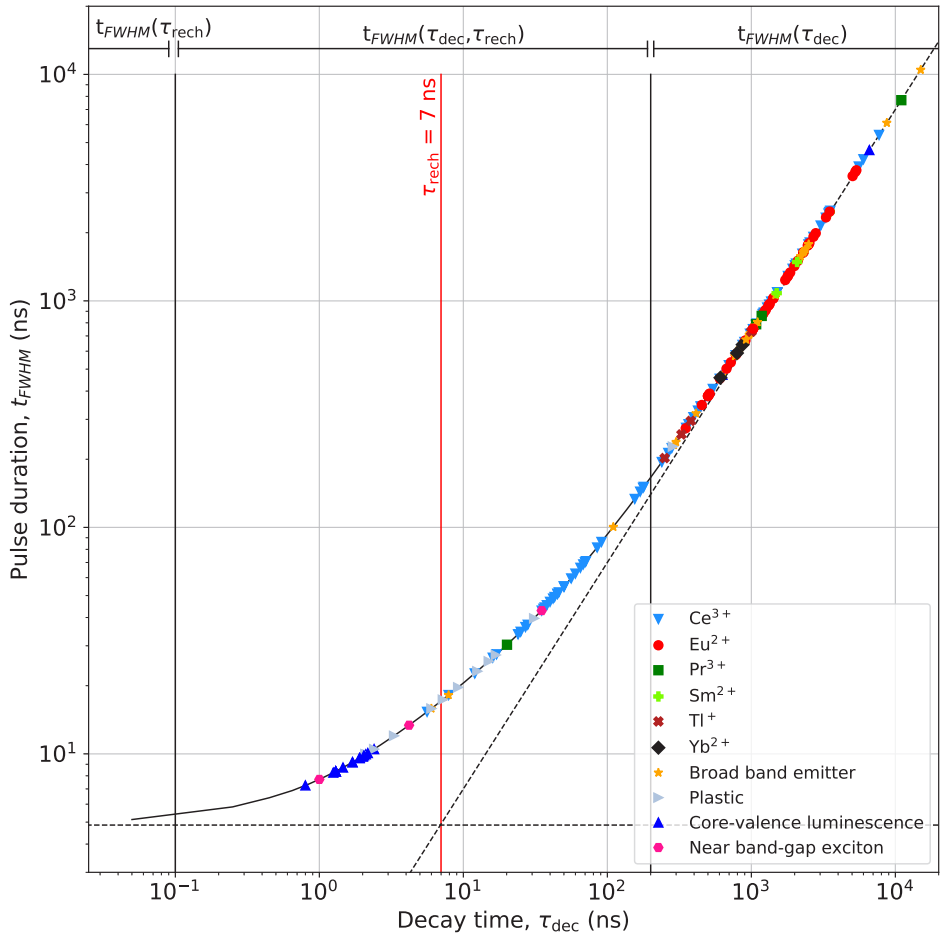


Figure 3: Scintillation decay time (τ_{dec}) versus calculated pulse duration (t_{FWHM}) for Ce^{3+} -, Pr^{3+} -, Eu^{2+} -, Yb^{2+} -, Sm^{2+} co-doped, and Tl^{+} -doped scintillators, intrinsic scintillators showing corevalence luminescence, Broad Band Emission, near band-gap exciton emission, and plastic scintillators. The red vertical line indicates the recharge time of the SiPM. The two black vertical lines indicate the regimes where the pulsduration depends only on the recharge time of the SiPM (τ_{rech}), only the decay time of the scintillator (τ_{dec}), or both.

only the pulse amplitude decreases. This behaviour can also be observed in the simulated detector output pulses in Figure 4b. Ideally, a scintillator should thus be quenched from the first to the second regime, since further quenching of the decay time to the third regime will mostly result in a decrease of the total pulse intensity.

The quenching behaviour of a scintillator can be described using a single barrier Arrhenius equation, as shown in Equation 17 [88, 283].

$$I(T) = \frac{I(0)}{\frac{1}{\tau_D} + \Gamma_0 \cdot e^{\frac{-\Delta E}{k_b T}}} \quad (17)$$

Here, $I(T)$ represents the luminescence intensity at temperature T , $I(0)$ the luminescence intensity at $T = 0$, Γ_0 the attempt rate for thermal quenching, k_b the Boltzmann constant, and ΔE the energy barrier. This shows that there are two options to quench a scintillator, either increase the temperature or decrease the energy barrier. However, due to the requirement of room temperature operation the only viable option is to decrease the energy barrier, *i.e.*, decreasing the quenching temperature or T_{50} . The latter represents the temperature at which the quenching curve reaches 50% of its maximum intensity.

The energy barrier, or T_{50} , can be changed via material engineering; this can also be referred to as T_{50} - engineering. An example of this approach can be found in the family of Ce^{3+} -doped garnets. Depending on the cation composition, thermal quenching can either take place through thermal ionisation to the conduction band or interconfigurational cross-over from the 5d excited state to the 4f ground state [286, 287]. The activation energy of both processes strongly depends on composition and T_{50} values can be gradually tuned down from approximately 650 K in $\text{Y}_3\text{Al}_5\text{O}_{12}$ to well below room temperature [288].

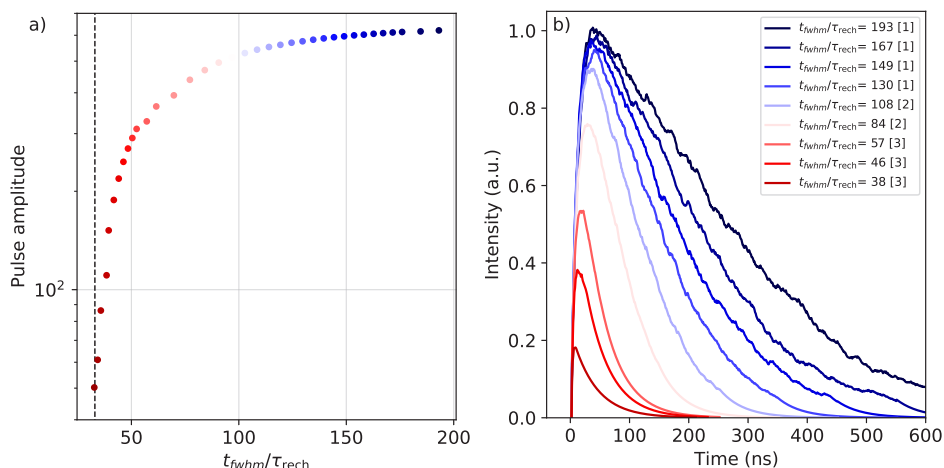


Figure 4: (a): $t_{\text{FWHM}}/\tau_{\text{rech}}$ versus the pulse amplitude, determined from simulated pulses, for different points along the quenching curve of a scintillator. (b): Selection of the simulated detector output pulses along the curve shown in (a). The numbers [1], [2], and [3] indicate whether $\tau_{\text{dec}} \ll \tau_{\text{rech}}$, $\tau_{\text{dec}} \approx \tau_{\text{rech}}$, and $\tau_{\text{dec}} \gg \tau_{\text{rech}}$, respectively.

By replacing Al^{3+} with Ga^{3+} , the room temperature decay time could be shortened from approximately 80 to 18.6 ns [289].

These are only one example of systems for which the quenching temperature can be engineered; this can also be referred to as T_{50} -engineering. As shown in Figure 2 there are a number of Ce^{3+} - doped scintillators that could be improved and tailored via this approach. This can however also be used for intrinsic broad band emitting scintillators. One of the main questions of T_{50} - engineering is how the non-proportionality of the scintillator will be influenced. Changes in composition should lead to minimal changes of the non-proportionality.

5. Conclusions

In this work an overview has been presented of different scintillators. Their suitability for application in indirect PCDs was assessed using the three formulated figures of merit: total pulse intensity, pulse duration, and pulse amplitude. Based on these figures of merit it is concluded that the most interesting groups of scintillators are Ce^{3+} - or Pr^{3+} - doped materials, near band-gap exciton emitters, plastics, and core-valance emitters. Each of these groups has its own challenges, *i.e.* emission wavelength, presence of slow components, density, or non-proportionality. Scintillators can also be engineered for their use in an indirect PCD. However, the decay time of the scintillator should not be quenched to values below the recharge time of the SiPM, which results in the loss of usable scintillation photons. Choosing a suitable material for an indirect PCD does not only depend on the material properties, the properties of the SiPM are just as important.

6. Acknowledgements

The author acknowledge financial supports from the TTW/OTP grant no. 18040 of the Dutch Research Council.

Table I: Light yield (photons/MeV), energy resolution (E%) measured at 662 keV, decay time (τ_{dec} (ns)), mean emission wavelength (λ_{em} (nm)), density (g/cm³), pulse amplitude (pulse Amp. (photons/ns)), and pulse duration (t_{FWHM} (ns)) of Ce³⁺-doped scintillators.

Compound	Light yield E%		τ_{dec} (ns)	λ_{em} (nm)	Density (g/cm ³)	Pulse Amp. t_{FWHM}		Ref
	(Ph/MeV)	@662 keV				(Ph/ns)	(ns)	
CeF ₃	4,000	20%	27	340	6.16	148.1	36.3	[49]
LaCl ₃	46,000	3.1%	169*	337	3.86	272.2	143	[50–52]
LuCl ₃	5,400	11.4%	5,572*	374/400	4	1.0	3,920	[51, 53]
K ₂ LaCl ₅	29,000	5.1%	68	380	2.89	426.4	68.6	[54]
K ₂ CeCl ₅	30,000	5.8%	71	370	2.95	422.5	70.9	[55, 56]
KGd ₂ Cl ₇	30,000	10%	179*	400	3.56	167.6	151	[57]
CsSrCl ₃	8,600	7.2%	603*	360/385	2.96	14.3	453	[58]
Cs ₃ LaCl ₆	16,000	8.6%	1,026*	380/407	3.36	15.6	750	[59]
CsCe ₂ Cl ₇	28,000	5.5%	50	410	3.6	560	54.8	[60]
Cs ₃ CeCl ₆	19,000	8.4%	265*	385	3.4	71.7	213	[61]
Cs ₃ GdCl ₆	24,500	4.5%	2,008*	380/405	3.56	12.2	1,437	[62]
Tl ₂ LaCl ₅	70,000	3.4%	895*	383	5.2	78.2	658	[63, 64]
Tl ₂ GdCl ₅	53,000	5%	1,330*	389	5.1	39.8	963	[65]
Rb ₂ LiCeCl ₆	23,000	7.9%	239*	370	3.1	96.2	194	[66]
Rb ₂ LiGdCl ₆	18,500	6.8%	3,490*	375/420	3.23	5.3	2,471	[67]
Cs ₂ LiYCl ₆	22,000	4.5%	6,000	376/404	3.31	3.7	4,219	[68, 69]
Cs ₂ LiLaCl ₆	35,000	3.4%	445*	340/420	3.3	78.7	341	[70]
Cs ₂ LiCeCl ₆	22,000	5.5%	2,263*	410	3.41	9.7	1,615	[71]
Cs ₂ LiGdCl ₆	20,000	5%	7,706*	380/405	3.67	2.6	5,404	[72]
Cs ₂ NaLaCl ₆	26,400	4.4%	1,513*	373/405	3.26	17.4	1,091	[59]
Cs ₂ NaCeCl ₆	20,000	8.3%	2,696*	410	3.25	7.4	1,917	[73]
Cs ₂ NaGdCl ₆	27,000	4%	3,030*	375/403	3.52	8.9	2,151	[62, 74]
Tl ₂ LiYCl ₆	25,000	4%	777*	435	4.5	32.2	575	[75]
Tl ₂ LiGdCl ₆	58,000	4.6%	868*	376/382	n.r.	66.8	639	[76]
Tl ₂ LiLuCl ₆	27,000	5.6%	1,373*	428	5.06	19.7	993	[77]
BaBr ₂	10,300	9.8%	1,935*	375/410	4.84	5.3	1,386	[78]
LaBr ₃	76,000	2.7%	16	358	5.29	3,812	26.5	[38, 79, 80]
LaBr ₃ :Ce,Sr	78,000	2%	1,209*	356/382	5.29	64.5	878	[38, 39, 81]

Table I: Continued

Compound	Light yield E%		τ_{dec}	λ_{em}	Density	Pulse Amp.	t_{FWHM}	Ref
	(Ph/MeV)	@662 keV	(ns)	(nm)	(g/cm ³)	(Ph/ns)	(ns)	
LaBr _{2.25} I _{0.75}	45,000	4.1%	117*	400/434	5.47	254	149	[82]
LaBr _{1.5} I _{1.5}	58,000	14.6%	28	472/500	5.51	2,071	37.1	[82]
LaBr _{0.75} I _{2.25}	22,000	35.9%	12	460/510	5.6	1,833	22.6	[82]
CeBr ₃	60,000	3.6%	17	370	5.2	3,529	27.5	[83, 84]
CeBr ₃ :Sr	55,000	3%	65*	381	5.2	846.2	66.3	[85–87]
PrBr ₃ :20%Ce	21,000	6.9%	7.9	365/395	5.33	2,658	18.2	[88]
PrBr ₃ :5%Ce	16,000	5.5%	5.6	365/395	5.33	2,857	15.3	[88]
GdBr ₃	44,000	10%	698*	419	4.6	63.0	520	[89]
LuBr ₃	32,000	6%	3,433*	408/448	5.17	9.3	2,430	[51, 53]
K ₂ LaBr ₅	40,000	5%	50	359/391	3.9	800	54.8	[90]
Rb ₂ CeBr ₅	34,000	6.9%	56.1	390	4.26	606.1	59.5	[91]
RbGd ₂ Br ₇	54,000	3.8%	60	425	4.7	900	62.5	[92]
Cs ₃ LaBr ₆	32,500	4.9%	2,042*	395/425	4.55	15.9	1,461	[59, 93]
CsCe ₂ Br ₇	33,500	7%	1,222*	450	4	29.1	888	[94]
Cs ₃ GdBr ₆	47,000	4%	1,289*	396/417	4.14	36.5	935	[62]
Tl ₂ LaBr ₅	43,000	5%	25	375/315	5.9	1,720	34.6	[95]
Rb ₂ LiYBr ₆	23,000	4.7%	1,199*	385/420	3.82	19.2	871	[96]
Rb ₂ LiLaBr ₆	33,000	4.8%	978*	363/387	n.r.	33.7	716	[97]
Rb ₂ LiCeBr ₆	33,000	6.3%	155*	373	4.6	212.9	133	[72]
Cs ₂ LiYBr ₆	23,600	7%	2,492*	389	4.15	9.5	1,775	[69, 98]
Cs ₂ LiLaBr ₆	60,000	2.9%	540*	380/430	4.2	111.1	408	[99–101]
Cs ₂ LiCeBr ₆	28,000	7.4%	3,289*	400/418	4.18	8.5	2,330	[102]
Cs ₂ LiGdBr ₆	30,500	7.1%	3,477*	392/400	4.41	8.8	2,462	[103]
Cs ₂ NaYBr ₆	9,500	6.3%	2,543*	385/420	3.94	3.7	1,810	[104]
Cs ₂ NaYBr ₃ I ₃	43,000	3.3%	1,795*	425/460	n.r.	24.0	1,288	[105]
Cs ₂ NaLaBr ₆	46,000	3.9%	3,535*	382/414	3.93	13.0	2,501	[59, 104]
Cs ₂ NaLaBr ₃ I ₃	58,000	2.9%	1,089*	430	n.r.	53.3	794	[105]
Cs ₂ NaCeBr ₆	25,00	6.7%	352*	377	4.25	71.0	275	[106]
Cs ₂ NaGdBr ₆	48,000	3.3%	396*	393/422	4.18	121.2	306	[62, 107]
Cs ₂ NaLuBr ₆	10,500	5.5%	280*	389/422	4.42	37.5	223	[104]

Table I: Continued

Compound	Light yield E%		τ_{dec}	λ_{em}	Density	Pulse Amp.	Amp. t_{FWHM}	Ref
	(Ph/MeV)	@662 keV				(Ph/ns)	(ns)	
Tl ₂ LiGdBr ₆	17,400	17%	91*	422	5.3	191.2	86.2	[108]
SrI ₂ :Ce,Na	16,000	6.4%	426*	404/434	4.59	37.6	327	[109]
YI ₃	99,000	9.3%	45	532	4.62	2,200	50.8	[110]
GdI ₃	44,000	4.3%	45	532	5.22	977.8	50.8	[110, 111]
LuI ₃	98,000	3.3%	85*	472	5.6	1,153	81.5	[112–114]
K ₂ LaI ₅	55,000	4.5%	24	401/439	4.4	2,291	33.7	[90]
Cs ₃ Lu ₂ I ₉	22,800	9%	446*	429/471	4.78	51.1	342	[93]
Cs ₂ NaLaI ₆	26,400	4.4%	1,513*	420/458	4.17	17.4	1,091	[59]
YAlO ₃	15,900	4.4%	35*	347	5.35	454.3	42.9	[115–117]
Y ₃ Al ₅ O ₁₂	14,000	12%	70	550	4.55	200.0	70.2	[118]
LuAlO ₃	11,400	9.3%	43*	365	8.34	265.1	49.3	[119]
Lu ₃ Al ₅ O ₁₂	12,500	12%	50	500/560	6.7	250.0	54.8	[120]
Y ₂ SiO ₅	24,000	9.4%	42	420	4.45	571.4	48.5	[121, 122]
Gd ₂ SiO ₅	12,500	7%	336*	430	6.71	34.2	285	[121, 123]
Gd ₂ Si ₂ O ₇	30,000	6%	46	372/394	5.5	652.2	51.6	[124]
Lu ₂ SiO ₅	27,000	7.9%	40	420	7.4	675.0	46.9	[40]
Lu ₂ SiO ₅ :Ce,Ca	38,800	7.7%	36.7	420	7.4	1,057	44.3	[41]
Lu ₂ Si ₂ O ₇	26,000	10%	38	378	6.2	684.2	45.3	[125, 126]
(Lu,Y) ₂ SiO ₅	27,000	8%	36	425	7.1	750	43.7	[42–44]
K ₂ Lu(PO ₄) ₂	26,500	17%	1,074*	390	3.90	24.7	784	[127]

* decay time consists of multiple components, tabulated value is an average value for the decay time. The amplitude and decay time of the different components can be found in **Table S I**.

Table II: Light yield (photons/MeV), energy resolution (E%) measured at 662 keV, decay time (τ_{dec} (ns)), mean emission wavelength (λ_{em} (nm)), density (g/cm³), pulse amplitude (pulse Amp. (photons/ns)), and pulse duration (t_{FWHM} (ns)) of Eu²⁺-doped scintillators.

Compound	Light yield E%		τ_{dec}	λ_{em}	Density	Pulse Amp. t_{FWHM}		Ref
	(Ph/MeV)	@662 keV	(ns)	(nm)	(g/cm ³)	(Ph/ns)	(ns)	
CaF ₂	24,000	6.7%	900	440	3.18	26.7	662	[137, 138]
BaFI	55,000	8.5%	500	450	5.45	110	380	[139, 140]
BaCl ₂	52,000	3.5%	604*	402	3.89	86.1	454	[78, 141]
BaClBr	52,000	3.55%	500	425	4.5	104.0	380	[139, 140]
BaClI	54,000	9%	500	425	4.5	108.0	380	[139, 140]
CsCaCl ₃	18,000	8.9%	5,050	450	3	3.6	3,558	[142]
CsSrCl ₃	33,400	11.5%	2,700	448	2.96	12.4	1,920	[143]
CsSrClBr ₂	35,100	3.6%	2,100	462	3.98	16.7	1,502	[144]
CaBr ₂	36,000	8.9%	2,500	448	3.35	14.4	1,780	[145]
BaBr ₂	49,750	6%	672*	408	4.78	74.0	501	[78, 146]
BaBrI	91,000	3.4%	453*	413	5.18	200.9	347	[147, 148]
LiSr ₂ Br ₅	32,000	6.1%	1,418	407/476	3.76	22.6	1,024	[149]
KSr ₂ Br ₅	75,000	3.5%	1,013*	427	3.98	74.0	741	[150]
RbCaBr ₃	43,000	4.0%	2,800	436	3.46	15.4	1,990	[151]
Rb ₄ CaBr ₆	71,000	6.9%	5,360*	457	3.46	13.2	3,774	[151]
RbSr ₂ Br ₅	64,700	4%	780	429	4.18	82.9	577	[152]
CsCaBr ₃	28,000	9.3%	5,270	447	3.68	5.3	3,710	[153]
CsCaBrI ₂	51,800	3.9%	3,500	445	3.59	14.8	2,478	[144]
CsCaBr _{0.8} I _{2.2}	40,000	5.2%	2,290	450	4.06	17.5	1,633	[154]
CsSrBr ₃	40,200	4.9%	2,300	440	3.76	17.5	1,640	[155]
CsSrBrI ₂	65,300	3.4%	1,800	455	4	36.3	1,292	[144]
LiI	15,000	7.5%	1,200	475	4.08	12.5	872	[156, 157]
CaI ₂	90,000	5.2%	790	470	3.96	113.9	584	[158, 159]
SrI ₂	90,000	2.6 %	1,200	453	4.6	75.0	872	[109, 128, 129]
SrI ₂ :Eu,Zr	95,000	2.5%	1,030	436	4.6	92.2	753	[160]
BaI ₂	38,000	5.6%	513	426	5.15	74.1	389	[146]
LiCa ₂ I ₅	90,000	5.6%	1,416	472	4	63.6	1,023	[149]
LiSrI ₃	35,000	5.2%	510	420/460	n.r.	68.6	387	[161]

Table II: Continued

Compound	Light yield E%		τ_{dec}	λ_{em}	Density	Pulse Amp.	t_{FWHM}	Ref
	(Ph/MeV)	@662 keV	(ns)	(nm)	(g/cm ³)	(ph/ns)	(ns)	
LiSr ₂ I ₅	60,000	3.5%	1,331	497	n.r.	45.1	964	[149]
KCaI ₃	72,000	3%	1,060	466	3.81	67.9	774	[162]
KCaI ₃ :Eu,Zr	72,000	2.5%	1,313*	450	3.81	54.8	951	[163]
KCa _{0.8} Sr _{0.2} I ₃	73,000	2.8%	1,258	475	3.81	58.0	913	[132, 164]
KSr ₂ I ₅	94,000	2.4%	2,531*	445	4.39	37.1	1,802	[165]
KBa ₂ I ₅	90,000	2.4%	910	444	4.52	98.9	669	[166]
K ₂ BaI ₄	63,000	2.9%	720	448	4.05	87.5	535	[166]
RbSrI ₃	24,000	2.8%	1,030	462	4.1	76.4	753	[167]
RbSr ₂ I ₅	90,400	3%	890	445	4.55	101.6	654	[152]
CsCaI ₃	38,500	8%	1,720	450	4.06	22.4	1,236	[142]
Cs ₄ CaI ₆	51,800	3.6%	1,990	459	3.99	26.0	1,425	[168, 169]
CsSrI ₃	73,000	3.9%	3,300	452	4.25	22.1	2,338	[134]
Cs ₄ SrI ₆	62,300	3.5%	1,430	462	4.03	43.6	1,033	[168, 169]
CsBa ₂ I ₅	97,000	2.3%	350	430	5	277.1	273	[130, 131]
TlSr ₂ I ₅	70,000	4.2%	2,465*	463	5.3	28.4	1,756	[170]
Cs ₃ KCaI ₆	62,000	3.9%	1,860	472	3.94	33.3	1,334	[168]
Cs ₃ KSrI ₆	29,000	5%	1,780	459	3.85	16.3	1,277	[168]
Cs ₃ RbCaI ₆	38,000	4.5%	1,250	467	3.96	30.4	907	[168]
Cs _{3.5} Rb _{0.5} SrI ₆	75,000	3.3%	1,340	466	4.03	56.0	970	[168]
Cs ₃ RbSrI ₆	31,000	5.1%	1,220	462	3.95	25.4	886	[168]

* decay time consists of multiple components, tabulated value is an average value for the decay time. The amplitude and decay time of the different components can be found in **Table S II**.

Table III: Light yield (photons/MeV), energy resolution (E%) measured at 662 keV, decay time (τ_{dec} (ns)), mean emission wavelength (λ_{em} (nm)), density (g/cm³), pulse amplitude (pulse Amp. (photons/ns)), and pulse duration (t_{FWHM} (ns)) of scintillators with ions other than Ce³⁺ or Eu²⁺.

Compound	Light yield E%		τ_{dec}	λ_{em}	Density	Pulse Amp.	t_{FWHM}	Ref
	(Ph/MeV)	@662 keV	(ns)	(nm)	(g/cm ³)	(Ph/ns)	(ns)	
LaBr ₃ :Pr	60,000	3.2%	11,000	492-682	5.29	5.5	7,695	[188]
Lu ₃ Al ₅ O ₁₂ :Pr	19,000	4.6%	20.1	325	6.7	945.3	30.3	[186, 187]
(Lu,Y) ₃ Al ₅ O ₁₂ :Pr	33,000	4.4%	1,080*	325	6.2	30.6	788	[189–191]
(Lu,Y) ₃ Al ₅ O ₁₂ :Pr, Li	25,000	4.1%	1,180*	325	6.2	21.2	858	[191]
SrI ₂ :Eu, Sm	42,000	10.5%	1,500	740	4.59	28.0	1,082	[173]
CsBa ₂ I ₅ :Eu, Sm	45,000	3.2%	2,077*	755	5	21.7	1,485	[174]
Cs ₄ EuI ₆ :Sm	16,600	7.5%	3,500	850	4.25	4.7	2,478	[175]
CsYbI ₃ :Sm	30,000	7%	2,300	800	4.76	13.0	1,640	[176]
NaI:Tl	38,000	5.4%	250	415	3.67	152.0	202	[178–180]
NaI:Tl, Ca	26,000	5.3%	380*	420	3.67	68.4	295	[192]
NaI:Tl, Sr	34,000	5.4%	327*	420	3.67	104.0	257	[192]
NaI:Tl, Ca, Eu	52,000	4.9%	1,000	450	3.67	52.0	732	[193, 194]
CsI:Tl	54,000	4.8%	1,000	550	4.51	54.0	732	[178, 179, 195]
SrI ₂ :Yb	56,000	4.35%	610	414	4.6	91.8	458	[196]
RbSrI ₃ :Yb	24,000	4.9%	795	457	4.1	30.2	588	[167]
CsBa ₂ I ₅ :Yb	54,000	5.7%	870	414	5	62.1	640	[196]

* decay time consists of multiple components, tabulated value is an average value for the decay time. The amplitude and decay time of the different components can be found in **Table S III**.

Table IV: Light yield (photons/MeV), energy resolution (E%) measured at 662 keV, decay time (τ_{dec} (ns)), mean emission wavelength (λ_{em} (nm)), density (g/cm³), pulse amplitude (pulse Amp. (photons/ns)), and pulse duration (t_{FWHM} (ns)) of undoped scintillators.

Compound	Light yield E%		τ_{dec} (ns)	λ_{em} (nm)	Density (g/cm ³)	Pulse Amp. t_{FWHM}		Ref
	(Ph/MeV)	@662 keV				(Ph/ns)	(ns)	
BaCl ₂	1,700	17.4%	980	300/410	3.89	1.7	718	[221]
(EDBE)PbCl ₄	9,000	30%	7.9	520	2.19	1,139	18.2	[215]
Cs ₂ HfCl ₆	54,000	3.3%	2,200	375/435	3.86	24.5	1,751	[202, 222]
Cs ₂ ZrCl ₆	33,900	4.5%	1,500	440/479	3.36	22.6	1,082	[202, 222]
TlMgCl ₃	30,600	3.7%	413*	409	4.43	74.1	318	[209]
TlCaCl ₃	30,600	5%	622*	425	3.77	49.2	466	[210]
Tl ₂ HfCl ₆	27,000	3.7%	1,063*	460	5.1	25.4	776	[211, 212]
Tl ₂ ZrCl ₆	35,000	3.4%	2,292*	460	4.5	15.3	1,635	[211, 212]
BaBr ₂	19,300	5.4%	2,200	425	4.78	8.8	1,571	[221]
(BM) ₂ PbBr ₄ **	3,190	19.53%	0.95	440	2.05	3,358	7.7	[219]
(BZA) ₂ PbBr ₄ **	3,700	8%	4.2	440	2.3	881.0	13.4	[218]
(PEA) ₂ PbBr ₄ **	11,000	39%	35	440	2.36	314.3	42.9	[214, 223]
TlCaBr ₃	41,700	6.2%	2,328*	470	4.69	17.9	1,660	[224]
TlSr ₂ Br ₅	37,600	4.6%	1,470*	441	5.03	25.6	1,061	[225]
CaI ₂	107,000	3.2%	834	410	3.96	128.3	616	[158, 159, 226]
RbSrI ₃	8,000	7.6%	918*	447	4.1	8.7	674	[167]
CsCu ₂ I ₃	16,000	7.8%	110	560	5.01	145.5	100	[206, 207]
Cs ₃ Cu ₂ I ₅	29,000	3.4%	965*	450	4.51	30.1	707	[208]
Cs ₂ HfI ₆	64,000	4.2%	2,500	700	5.12	25.6	1,780	[204, 205]
Cs ₃ Lu ₂ I ₉	6,600	19.2%	770	390/608	4.82	8.6	570	[93]
TlCaI ₃	42,200	6.2%	1,105*	460/533	4.73	38.2	805	[209]
TlSr ₂ I ₅	31,000	8.5%	2,372*	463	5.3	13.1	1,691	[170]
Sc ₂ O ₃	19,200	16.7%	290*	330	3.83	66.2	231	[227]
CaWO ₄	15,800	6.6%	8,722*	425	6.1	1.8	6,113	[228–230]
CdWO ₄	15,300	9.1%	15,000*	480	7.9	1.02	10,480	[137, 231]
PbWO ₄	300	n.r.	26*	420	8.28	50	15.8	[200, 232, 233]
Bi ₄ Ge ₃ O ₁₂	7,610	9.05%	300	485	7.13	25.4	238	[115, 123, 234]

* decay time consists of multiple components, tabulated value is an average value for the decay time. The amplitude and decay time of the different components can be found in **Table S IV**. ** Compounds show near bandgap exciton emission.

Table V: Light yield (photons/MeV), energy resolution (E%) measured at 662 keV, decay time (τ_{dec} (ns)), mean emission wavelength (λ_{em} (nm)), density (g/cm³), pulse amplitude (pulse Amp. (photons/ns)), and pulse duration (t_{FWHM} (ns)) of scintillators showing core-valance luminescence.

Compound	Light yield E%		τ_{dec}	λ_{em}	Density	Pulse Amp. t_{FWHM}		Ref
	(Ph/MeV)	@662 keV	(ns)	(nm)	(g/cm ³)	(Ph/ns)	(ns)	
RbF	1,700	n.r.	1.3	203/234	3.6	1,307	8.4	[250]
BaF ₂	12,000	11%	630*	220/310	4.88	19.0	472	[251–253]
CsF	1,900	20%	2	390	4.64	950	9.8	[254]
KMgF ₃	1,400	n.r.	1.3	140/170	3.2	1,077	8.4	[235, 250, 255]
KCaF ₃	1,400	n.r.	2	165/200	3	700.0	9.8	[235, 250]
KYF ₄	1,000	n.r.	1.9	170	3.6	526.3	9.6	[235, 250]
K ₂ YF ₅	300	n.r.	1.3	170	3.6	230.8	8.4	[250]
KLuF ₄	170	n.r.	1.3	163/185	5.2	130.8	8.4	[235, 237, 250]
KLuF ₇	270	n.r.	2	165	7.5	135.0	9.8	[250]
CsMgCl ₃	1,113	n.r.	2.36	350	3.23	471.6	10.5	[235]
CsMgCl ₃ :Zn	3,400	16.7	2.17	300	3.23	1,567	10.0	[247]
Cs ₂ MgCl ₄	2,200	22	2.04	300	2.95	1,078	9.8	[246, 247]
Cs ₂ MgCl ₄ :Zn	2,440	19.2	1.91	300	2.95	1,277	9.6	[247]
Cs ₃ MgCl ₅	1,340	33.7	1.46	300	3.15	918	8.7	[246, 247]
Cs ₃ MgCl ₅ :Zn	2,180	22.8	1.25	300	3.15	1,744	8.3	[247]
CsCaCl ₃	1,400	n.r.	2	250/305	2.9	700	9.8	[250, 256]
Cs ₂ ZnCl ₄	1,980	22%	1.66	285/379	3.35	1,193	9.2	[245]
Cs ₂ ZnCl ₅	1,460	25%	0.82	240/289	3.44	1,780	7.3	[245]
CsSrCl ₃	889	n.r.	2.07	248	2.87	429.5	10.0	[235, 257]
Cs ₂ BaCl ₄	1,369	n.r.	1.68	400	3.76	814.9	9.2	[235]
Cs ₂ LiYCl ₆	22,420	11%	6,599*	325	3.31	3.4	4,634	[68, 69]

*decay time consists of multiple components, tabulated value is an average value for the decay time. The amplitude and decay time of the different components can be found in **Table S V**.

Table VI: Light yield (photons/MeV), energy resolution (E%) measured at 662 keV, decay time (τ_{dec} (ns)), mean emission wavelength (λ_{em} (nm)), density (g/cm³), pulse amplitude (pulse Amp. (photons/ns)), and pulse duration (t_{FWHM} (ns)) of plastic scintillators.

Compound	Light yield (Ph/MeV)	E% @662 keV	τ_{dec} (ns)	λ_{em} (nm)	Density (g/cm ³)	Pulse Amp. (Ph/ns)	t_{FWHM} (ns)	Ref
Anthracene	20,100	n.r.	31	460	1.25	648.4	39.7	[264, 265]
Stilbene	16,000	n.r.	6	390	0.97	2,666	15.9	[264, 266]
p-Terphenyl	19,400	n.r.	7.2*	410	1.24	2,694	17.4	[264, 267]
Polyvinylcarbazole:Bi	12,000	9%	15	420	n.r.	800.0	25.6	[268]
BC-400	13,000	n.r.	2.4	423	1.02	5,416	10.5	[269]
BC-408	13,000	n.r.	2.1	425	1.02	6,190	10.0	[270]
BC-412	12,000	n.r.	3.3	434	1.02	3,636	12.0	[271]
BC-428	7,200	n.r.	12.5	480	1.02	576.0	23.2	[272]
BC-430	9,000	n.r.	16.8	580	1.02	536.7	27.3	[273]
BC-452	10,000	n.r.	2.1	424	1.05	4,762	10.0	[274]
EJ-200	10,000	n.r.	2.1	425	1.02	4,761	10.0	[275]
EJ-240	6,300	n.r.	285	430	1.02	22.1	227	[276]
EJ-260	9,200	n.r.	9.2	490	1.02	1,000	19.7	[277]
EJ-256	6,800	n.r.	2.1	425	1.08	3,238	10.0	[278]

* decay time consists of multiple components, tabulated value is an average value for the decay time. The amplitude and decay time of the different components can be found in **Table S VI**.

References

- [1] T. Flohr, M. Petersilka, A. Henning, S. Ulzheimer, J. Freda, B. Schmidt, *Physica Medica* 79 (2020) 126-136, <https://doi.org/10.1016/j.ejmp.2020.10.030>
- [2] U. N. Roy, G. S. Camarda, Y. Cui, R. Gul, A. Hossain, G. Yang, J. Zazvorka, V. Dedic, J. Franc, R. B. James, *Scientific Reports* 9 (2019) 1620, <https://doi.org/10.1038/s41598-01838188-w>
- [3] M. Persson, R. Buijla, P. Norwik, H. Andersson, L. Kull, J. Andersson, H. Bornefalk, M. Danielsson, *Medical Physics* 43 (2016) 7, <https://doi.org/10.1118/1.4954008>
- [4] M. Danielsson, M. Persson, M. Sjölin, *Physics in Medicine and Biology*, 66 (2021) 03TR01, <https://doi.org/10.1088/1361-6560/abc5a5>
- [5] K. Taguchi, J. S. Iwanczyk, *Medical Physics* 40 (2013) 10, <https://doi.org/10.1118/1.4820371>
- [6] M. J. Willemink, M. Persson, A. Pourmorteza, N. J. Pelc, D. Fleischmann, *Radiology* 289 (2018) 2, <https://doi.org/10.1148/radiol.2018172656>
- [7] S. Leng, M. Bruesewitz, S. Tao, K. Rajendran, A. F. Halaweish, N. G. Campeau, J. G. Fletcher, C. H. McCollough, *Radiographics* 39 (2019) 3, <https://doi.org/10.1148/rg.2019180115>
- [8] S. S. Hsieh, S. Leng, K. Rajendran, S. Tao, C. H. McCollough, *IEEE Transactions on Radiation and Plasma Medical Science* 5 (2021) 4, <https://doi.org/10.1109/TRPMS.2020.3020212>
- [9] S. Kappler, A. Henning, B. Kreisler, F. Schoeck, K. Stierstorfer, T. Flohr, *Proceedings Volume 9033, Medical Imaging 2014: Physics of Medical Imaging*, 90331C, <https://doi.org/10.1117/12.2043511>
- [10] R. Steadman, C. Herrmann, A. Livne, *Nuclear Instruments and Methods in Physics Research Section A: Accelerators, Spectrometers, Detectors and Associated Equipment* 862 (2017) 18-24, <https://doi.org/10.1016/j.nima.2017.05.010>
- [11] J. Da Silva, F. Gronberg, B. Cederstrom, M. Persson, M. Sjölin, Z. Alagic, R. Buijla, M. Danielsson, *Journal of Medical Imaging*, 6 (2019) 043502, <https://doi.org/10.1117/1.JMI.6.4.043502>
- [12] A. Esquivel, A. Ferrero, A. Mileto, F. Baffour, K. Horst, P. S. Rajiah, A. Inoue, S. Leng, C. McCollough, J. G. Fletcher, *Korean Journal of Radiology*, 23 (2022) 854-865, <https://doi.org/10.3348/kjr.2022.0377>
- [13] R. Steadman, C. Herrmann, A. Mulhens, D. G. Maeding, *Nuclear Instruments and Methods in Physics Research Section A: Accelerators, Spectrometers, Detectors and Associated Equipment* 648 (2011) s211-s215, <https://doi.org/10.1016/j.nima.2010.11.149>

- [14] M. Persson, B. Huber, S. Karlsson, X. Liu, H. Chen, C. Xu, M. Yveborn, H. Bornefalk, M. Danielsson, *Physics in Medicine and Biology* 59 (2014) 6709, <http://dx.doi.org/10.1088/13616560/59/22/6709>
- [15] S. J. van der Sar, *Exploring X-ray photon-counting scintillation detectors with silicon photomultiplier readout for medical imaging*, ISBN: 978-94-6384-485-7, <https://doi.org/10.4233/uuid:370aa87c-3055-4b2d-9e9e-ca74f2fab2e4>
- [16] S. J. van der Sar, S. E. Brunner, D. R. Schaart, *Medical Physics* 48 (2021) 6324-6338, <https://doi.org/10.1002/mp.14886>
- [17] S. J. van der Sar, D. Leibold, S. E. Brunner, D. R. Schaart, *Proceedings Volume 12304, 7th International conference on Image Formation in X-ray Computed Tomography, 12304A* (2022), <https://doi.org/10.1117/12.2646519>
- [18] S. J. van der Sar, S. Brunner, D. Schaart, *Proceedings Volume 12031, Medical Imaging 2022: Physics of Medical Imaging, 1203101* (2022), <https://doi.org/10.1117/12.2611365>
- [19] M. Arimoto, H. Morita, K. Fujieda, T. Maruhashi, J. Kataoka, H. Nitta, H. Ikeda, *Nuclear Instruments and methods in Physics Research Section A: Accelerators, Spectrometers, Detectors, and Associated Equipment* 912 (2018) 21, <https://doi.org/10.1016/j.nima.2017.11.031>
- [20] H. Kiji, T. Maruhashi, T. Toyoda, J. Kataoka, M. Arimoto, D. Sato, K. Yoshiura, S. Kabayashi, H. Kawashima, S. Terazawa, S. Shiota, H. Ikeda, *Nuclear Instruments and methods in Physics Research Section A: Accelerators, Spectrometers, Detectors, and Associated Equipment* 984 (2020) 21, <https://doi.org/10.1016/j.nima.2020.164610>
- [21] T. Maruhashi, H. Morita, M. Arimoto, J. Kataoka, K. Fujieda, H. Nitta, H. Ikeda, H. Kiji, *Nuclear Instruments and methods in Physics Research Section A: Accelerators, Spectrometers, Detectors, and Associated Equipment* 936 (2019) 21, <https://doi.org/10.1016/j.nima.2018.11.018>
- [22] H. T. van Dam, S. Siefert, R. Vinke, P. Dendooven, H. Lohner, F. J. Beekman, D. R. Schaart, *IEEE Transactions on Nuclear Science* 57 (2010) 4, <https://doi.org/10.1109/TNS.2010.2053048>
- [23] P. Dorenbos, *Optical Materials: X* 1 (2019) 100021, <https://doi.org/10.1016/j.omx.2019.100021>
- [24] P. Dorenbos, *IEEE Transactions on Nuclear Science* 57 (2010) 3, <https://doi.org/10.1109/TNS.2009.2031140>
- [25] P. Dorenbos, J. T. M. de Haas, C. W. E. van Eijk, *IEEE Transactions on Nuclear Science* 42 (1995) 6, <https://doi.org/10.1109/23.489415>
- [26] M. Moszynski, *Nuclear Instruments and Methods in Physics Research Section A: Accelerators, Spectrometers, Detectors, and Associated Equipment*, 505 (2003) 101-110, [https://doi.org/10.1016/S0168-9002\(03\)01030-1](https://doi.org/10.1016/S0168-9002(03)01030-1)

- [27] P. A. Rodnyi, P. Dorenbos, C. W. E. van Eijk, *Physica Status solidi b* 187 (1995) 15, <https://doi.org/10.1002/pssb.2221870102>
- [28] I. V. Khodyuk, P. A. Rodnyi, P. Dorenbos, *Journal of Applied Physics* 107 (2010) 11, <https://doi.org/10.1063/1.3431009>
- [29] I. V. Khodyuk, P. Dorenbos, *Journal of Physics: Condensed Matter* 22 (2010) 48, <https://doi.org/10.1088/0953-8984/22/48/485402>
- [30] I. V. Khodyuk, J. T. M. de Haas, P. Dorenbos, *IEEE Transactions on Nuclear Science* 57 (2010) 3, <https://doi.org/10.1109/TNS.2010.2045511>
- [31] M. Moszynski, *Radiation measurements* 45 (2010) 372-376, <https://doi.org/10.1016/j.radmeas.2009.10.012>
- [32] G. Bizarri, N. J. Cherepy, W. S. Choong, G. Hull, W. W. Moses, S. A. Payne, J. Singh, J. D. Valentine, A. N. Vasilev, R. T. Williams, *IEEE Transactions on Nuclear Science* 59 (2009) 4, <https://doi.org/10.1109/TNS.2009.2022625>
- [33] J. Q. Grim, K. B. Ucer, A. Burger, P. Bhattacharya, E. Tupitsyn, E. Rowe, V. M. Buliga, L. Trefilova, A. Gektin, G. A. Bizarri, W. W. Moses, R. T. Williams, *Physical Review B* 87 (2013) 125117, <https://doi.org/10.1103/PhysRevB.87.125117>
- [34] R. T. Williams, J. Q. Grim, Q. Li, K. B. Ucer, W. W. Moses, *Physica Status Solidi b* 248 (2011) 2, <https://doi.org/10.1002/pssb.201000610>
- [35] J. X. Lu, S. Gridin, R. T. Williams, M. R. Mayhugh, A. Gektin, A. Syntfeld-Kazuch, L. Swiderski, M. Moszynski, *Physical Review Applied* 7 (2017) 014007, <https://doi.org/10.1103/PhysRevApplied.7.014007>
- [36] M. Magdowski, R. Vick, *IEEE Transactions on Electromagnetic Compatibility* 52 (2010) 4, <https://doi.org/10.1109/TEM.2010.2052621>
- [37] M. Camp, H. Garbe, *IEEE Transactions on Electromagnetic Compatibility* 46 (2004) 4, <https://doi.org/10.1109/TEM.2004.838228>
- [38] M. S. Alekhin, D. A. Biner, K. W. Krämer, P. Dorenbos, *Journal of Applied Physics* 113 (2013) 224904, <https://doi.org/10.1063/1.4810848>
- [39] M. S. Alekhin, J. T. M. de Haas, I. V. Khodyuk, K. W. Krämer, P. R. Menge, V. Ouspenski, P. Dorenbos, *Applied Physics Letters* 102 (2013) 161915, <https://doi.org/10.1063/1.4803440>
- [40] C. L. Melcher, J. S. Schweitzer, *IEEE Transactions on Nuclear Science* 39 (1992) 4, <https://doi.org/10.1109/23.159655>
- [41] M. A. Spurrier, P. Szupryczynski, K. Yang, A. A. Carey, C. L. Melcher, *IEEE Transactions on Nuclear Science* 55 (2008) 3, <https://doi.org/10.1109/TNS.2007.913486>
- [42] J. T. M. de Haas, P. Dorenbos, *IEEE Transactions on Nuclear Science* 55 (2008) 3, <https://doi.org/10.1109/TNS.2008.922819>

[43] C. M. Pepin, P. Berard, A.-L. Perrot, C. Pepin, D. Houde, R. Lecomte, C. L. Melcher, H. Dautet, *IEEE Transactions on Nuclear Science* 51 (2004) 3, <https://doi.org/10.1109/TNS.2004.829781>

[44] Data Sheet 1Luxium Solutions LYSO, Obtained February 2024, <https://luxiumsolutions.com/radiation-detection-scintillators/crystal-scintillators/lyso-scintillation-crystals>

[45] D. R. Schaart, *Physics in Medicine and Biology* 66 (2021) 09TR01, <https://doi.org/10.1088/1361-6560/abee56>

[46] M. B. Smith, T. Achtzehn, H. R. Andrews, E. T. H. Clifford, P. Forget, J. Glodo, R. Hawrami, H. Ing, P. O'Dougherty, K. S. Shah, U. Shirwadkar, L. Soundara-Pandian, J. Tower, *Nuclear Instruments and Methods in Physics Research Section A: Accelerators, Spectrometers, Detectors and Associated Equipment* 784 (2015) 162-167, <https://doi.org/10.1016/j.nima.2014.09.021>

[47] N. D'Olympia, P. Chowdhury, C. J. Lister, J. Glodo, R. Hawrami, K. Shah, U. Shirwadkar, *Nuclear Instruments and Methods in Physics Research Section A: Accelerators, Spectrometers, Detectors and Associated Equipment* 714 (2013) 121-127, <https://doi.org/10.1016/j.nima.2013.02.043>

[48] M. M. Bourne, C. Mussi, E. C. Miller, S. D. Clarke, S. A. Pozzim A. gueorguiev, *Nuclear Instruments and Methods in Physics Research Section A: Accelerators, Spectrometers, Detectors and Associated Equipment* 736 (2014) 124-127, <https://doi.org/10.1016/j.nima.2013.10.030>

[49] W. W. Moses, S. E. Derenzo, *IEEE Transactions on Nuclear Science* 36 (1989) 173-176, <https://doi.org/10.1109/23.34428>

[50] E. V. D. van Loef, P. Dorenbos, C. W. E. van Eijk, K. Krämer, H. U. Güdel, *Applied Physics Letters* 77 (2000) 10, <https://doi.org/10.1063/1.1308053>

[51] O. Guillot-Noel, J. T. M. De Haas, P. Dorenbos, C. W. E. van Eijk, K. Krämer, H. U. Gundel, *Journal of Luminescence* 85 (1999) 1-3, [https://doi.org/10.1016/S0022-2313\(99\)00063-0](https://doi.org/10.1016/S0022-2313(99)00063-0)

[52] K. S. Shah, J. Glodo, M. Klugerman, L. Cirignano, W. W. Moses, S. E. Derenzo, M. J. Weber, *Nuclear Instruments and Methods in Physics Research Section A: Accelerators, Spectrometers, Detectors and Associated Equipment* 505 (2003) 1-2, [https://doi.org/10.1016/S01689002\(03\)01024-6](https://doi.org/10.1016/S01689002(03)01024-6)

[53] E. V. D. van Loef, P. Dorenbos, C. W. E. van Eijk, K. W. Krämer, H. U. Güdel, *Nuclear Instruments and Methods in Physics Research Section A: Accelerators, Spectrometers, Detectors and Associated Equipment* 496 (2003) 1, [https://doi.org/10.1016/S0168-9002\(02\)016340](https://doi.org/10.1016/S0168-9002(02)016340)

[54] J. C. Van't Spijker, P. Dorenbos, J. T. M. de Haas, C. W. E. van Eijk, H. U. Güdel, K. Krämer, *Radiation Measurements* 24 (1995) 4, [https://doi.org/10.1016/1350-4487\(95\)00019B](https://doi.org/10.1016/1350-4487(95)00019B)

- [55] U. N. Roy, M. Groza, Y. Cui, A. Burger, N. Cherepy, S. Friedrich, S. A. Payne Nuclear Instruments and Methods in Physics Research Section A: Accelerators, Spectrometers, Detectors and Associated Equipment 579 (2007) 1, <https://doi.org/10.1016/j.nima.2007.04.126>
- [56] G. Rooh, H. Kang, H. J. Kim, H. Park, J. Moon, S. Lee, S. Kim, K. Kim, Journal of the Korean Physical Society 54 (2009) 2093-2097, <https://doi.org/10.3938/jkps.54.2093>
- [57] M. Zhuravleva, K. Yang, A. Green, C. L. Melcher, Journal of Crystal Growth 318 (2011) 1, <https://doi.org/10.1016/j.jcrysgro.2010.10.206>
- [58] Y. Fujimoto, K. Saeki, D. Nakauchi, T. Yanagida, M. Koshimizu, K. Asai, Sensors and Materials 29 (2017) 10, <https://doi.org/10.18494/SAM.2017.1622>
- [59] G. Gundiah, K. Brennan, Z. Yan, E. C. Samulon, G. Wu, G. A. Bizarri, S. E. Derenzo, E. D. Bourret-Courchesne, Journal of Luminescence 149 (2014) 374-384, <https://doi.org/10.1016/j.jlumin.2013.09.057>
- [60] G. Rooh, H. Kang, H. J. Kim, H. Park, S.-H. Doh, S. kim, Journal of Crystal Growth 311 (2008) 1, <https://doi.org/10.1016/j.jcrysgro.2008.10.020>
- [61] M. Zhuravleva, K. yang, C. L. Melcher, Journal of Crystal Growth 318 (2011) 1, <https://doi.org/10.1016/j.jcrysgro.2010.11.090>
- [62] E. C. Samulon, G. Gundiah, M. Gascon, I. V. Khodyuk, S. E. Derenzo, G. A. Bizarri, E. D. Bourret-Courchesne, Journal of Luminescence 153 (2014) 64-72, <https://doi.org/10.1016/j.jlumin.2014.02.021>
- [63] H. J. Kim, G. Rooh, S. Kim, Journal of Luminescence 186 (2017) 219-222, <https://doi.org/10.1016/j.jlumin.2017.02.042>
- [64] R. Hawrami, E. Ariesanti, H. Wei, J. Finkelstein, J. Glodo, K. S. Shah, Nuclear Instruments and Methods in Physics Research Section A: Accelerators, Spectrometers, Detectors and Associated Equipment 869 (2017) 107-109, <https://doi.org/10.1016/j.nima.2017.06.016>
- [65] A. Khan, G. Rooh, H. J. Kim, S. Kim, Journal of Alloys and Compounds 741 (2018) 878-882, <https://doi.org/10.1016/j.jallcom.2018.01.204>
- [66] G. Rooh, H. J. Kim, H. Park, S. Kim, IEEE Transactions on Nuclear Science 59 (2012) 5, <https://doi.org/10.1109/TNS.2012.2200907>
- [67] G. Rooh, H. J. Kim, H. Park, S. Kim, Journal of Crystal Growth 377 (2013) 28-31, <https://doi.org/10.1016/j.jcrysgro.2013.04.036>
- [68] C. M. Combes, P. Dorenbos, C. W. E. van Eijk, K. W. Krämer, H. U. Güdel, Journal of Luminescence 82 (1999) 4, [https://doi.org/10.1016/S0022-2313\(99\)00047-2](https://doi.org/10.1016/S0022-2313(99)00047-2)
- [69] A. Bessiere, P. Dorenbos, C. W. E. van Eijk, K. W. Krämer, H. U. Güdel, IEEE Transactions on Nuclear Science 51 (2004) 5, <https://doi.org/10.1109/TNS.2004.834957>

- [70] J. Glodo, R. Hawrami, E. van Loef, W. Higgins, U. Shirwadkar, K. S. Shah, Proceedings Volume 7449, Hard X-ray, Gamma-ray, and neutron detector physics XI: 74490E (2009), <https://doi.org/10.1117/12.830127>
- [71] G. Rooh, H. J. Kim, S. Kim, IEEE Transactions on Nuclear Science 57 (2010) 3, <https://doi.org/10.1109/TNS.2009.2037903>
- [72] G. Rooh, H. J. kim, S. Kim, Radiation Measurements 45 (2010) 3-6, <https://doi.org/10.1016/j.radmeas.2009.10.018>
- [73] G. Rooh, H. Kang, H. J. Kim, H. Park, S. Kim, Journal of Crystal Growth 311 (2009) 8, <https://doi.org/10.1016/j.jcrysgro.2009.01.091>
- [74] G. Rooh, H. J. Kim, H. Park, S. Kim, H. Jiang, IEEE Transactions on Nuclear Science 61 (2014) 1, <https://doi.org/10.1109/TNS.2013.2283882>
- [75] R. Hawrami, E. Ariesanti, L. Soundara-Pandian, J. Glodo, K. S. Shah, IEEE Transactions on Nuclear Science 63 (2016) 6, <https://doi.org/10.1109/TNS.2016.2627523>
- [76] H. J. Kim, G. Rooh, H. Park, S. Kim, Journal of Luminescence 164 (2015) 86-89, <https://doi.org/10.1016/j.jlumin.2015.03.026>
- [77] G. Rooh, H. J. Kim, J. Jang, S. Kim, Journal of Luminescence 187 (2017) 347-351, <https://doi.org/10.1016/j.jlumin.2017.03.051>
- [78] J. Selling, S. Schweizer, M. D. Birowosuto, P. Dorenbos, IEEE Transactions on Nuclear Science 55 (2008) 3, <https://doi.org/10.1109/TNS.2008.922825>
- [79] E. V. D. van Loef, P. Dorenbos, C. W. E. van Eijk, K. Krämer, H. U. Güdel, Applied Physics Letters 79 (2001) 1573-1575, <https://doi.org/10.1063/1.1385342>
- [80] G. Bizarri, P. Dorenbos, Physical Review B 75 (2007) 184302, <https://doi.org/10.1103/PhysRevB.75.184302>
- [81] K. Yang, P. R. Menge, J. J. Buzniak, V. ouspenski, IEEE Nuclear Science Symposium and Medical Imaging Conference Record (NSS/MIC) 2012 308-311, <https://doi.org/10.1109/NSSMIC.2012.6551113>
- [82] M. D. Birowosuto, P. Dorenbos, K. W. Krämer, H. U. Güdel, Journal of Applied Physics 103 (2008) 103517, <https://doi.org/10.1063/1.2930884>
- [83] K. S. Shah, J. Glodo, W. Higgins, E. V. D. van Loef, W. W. Moses, S. E. Derenzo, M. J. Weber, IEEE Symposium Conference Record Nuclear Science 2004 4278-4281, <https://doi.org/10.1109/NSSMIC.2004.1466835>
- [84] W. Drozdowski, P. Dorenbos, A. J. J. Bos, G. Bizarri, A. Owens, F. G. A. Quarati, IEEE Transactions on Nuclear Science 55 (2008) 3, <https://doi.org/10.1109/TNS.2007.908579>
- [85] P. Guss, M. E. Foster, B. M. Wong, F. P. Doty, K. Shah, M. R. Squillante, U. Shirwadkar, R. Hawrami, J. Tower, D. Yuan, Journal of Applied Physics 115 (2014) 034908, <https://doi.org/10.1063/1.4861647>

- [86] F. G. A. Quarati, M. S. Alekhin, K. W. Krämer, P. Dorenbos, *Nuclear Instruments and Methods in Physics Research Section A: Accelerators, Spectrometers, Detectors and Associated Equipment* 735 (2014) 655-658, <https://doi.org/10.1016/j.nima.2013.10.004>
- [87] R. H. P. Awater, K. W. Krämer, P. Dorenbos, *IEEE Transactions on Nuclear Science* 62 (2015) 5, <https://doi.org/10.1109/TNS.2015.2463736>
- [88] M. D. Birowosuto, P. Dorenbos, C. W. E. van Eijk, K. W. Krämer, H. U. Güdel, *IEEE Transactions on Nuclear Science* 53 (2006) 5, <https://doi.org/10.1109/TNS.2006.880969>
- [89] E. V. D. van Loef, P. Dorenbos, C. W. E. van Eijk, K. W. Krämer, H. U. Güdel, *Optics Communications* 189 (2001) 4-6, [https://doi.org/10.1016/S0030-4018\(01\)01039-2](https://doi.org/10.1016/S0030-4018(01)01039-2)
- [90] E. V. D. van Loef, P. Dorenbos, C. W. E. van Eijk, K. W. Krämer, H. U. Güdel, *Nuclear Instruments and Methods in Physics Research Section A: Accelerators, Spectrometers, Detectors and Associated Equipment* 537 (2005) 1-2, <https://doi.org/10.1016/j.nima.2004.08.016>
- [91] S. Kim, J. Lee, S.-H. Doh, H. J. Kim, H. Park, H. Kang, D. Kim, H. U., *IEEE Transactions on Nuclear Science* 56 (2009) 3, <https://doi.org/10.1109/TNS.2009.2018838>
- [92] P. Dorenbos, J. C. van't Spijker, O. W. V. Frijns, C. W. E. van Eijk, K. Krämer, H. U. Güdel, A. Ellens, *Nuclear Instruments and Methods in Physics Research Section A: Accelerators, Spectrometers, Detectors and Associated Equipment* 132 (1997) 4, [https://doi.org/10.1016/S0168-583X\(97\)00490-4](https://doi.org/10.1016/S0168-583X(97)00490-4)
- [93] M. D. Birowosuto, P. Dorenbos, C. W. E. van Eijk, K. W. Krämer, H. U. Güdel, *Physica Status Solidi A Applications and Materials Science* 204 (2007) 3, <https://doi.org/10.1002/pssa.200622459>
- [94] Y. Wu, H. Shi, B. C. Chakoumakos, M. Zhuravleva, M.-H. Du, C. L. Melcher, *Journal of Materials Chemistry C* 3 (2015) 11366-11376, <https://doi.org/10.1039/C5TC02721G>
- [95] H. J. Kim, G. Rooh, A. Khan, S. Kim, *Nuclear Instruments and Methods in Physics Research Section A: Accelerators, Spectrometers, Detectors and Associated Equipment* 849 (2017) 72-75, <https://doi.org/10.1016/j.nima.2017.01.012>
- [96] M. D. Birowosuto, P. Dorenbos, J. T. M. de Haas, C. W. E. van Eijk, K. W. Krämer, H. U. Güdel, *Journal of Applied Physics* 101 (2007) 6, <https://doi.org/10.1063/1.2713948>
- [97] M. D. Birowosuto, P. Dorenbos, J. T. M. de Haas, C. W. E. van Eijk, K. W. Krämer, H. U. Güdel, *IEEE Transactions on Nuclear Science* 55 (2008) 3, <https://doi.org/10.1109/TNS.2008.922826>

- [98] U. Shirwadkar, J. Glodo, E. van Loef, R. Hawrami, S. Mukhopadhyay, K. S. Shah, IEEE Nuclear Science Symposium and Medical Imaging Conference 2010 1585-1588, <https://doi.org/10.1109/NSSMIC.2010.5874043>
- [99] J. Glodo, E. van Loef, R. Hawrami, W. M. Higgins, A. Churilov, U. Shirwadkar, K. S. Shah, IEEE Transactions on Nuclear Science 58 (2011) 1, <https://doi.org/10.1109/TNS.2010.2098045>
- [100] J. Qin, J. Xiao, T. Zhu, X. Lu, Z. Han, M. Wang, L. Jiang, Y. Mou, J. Sun, Z. Wen, X. Wang, Nuclear Instruments and Methods in Physics Research Section A: Accelerators, Spectrometers, Detectors and Associated Equipment 905 (2018) 112-118, <https://doi.org/10.1016/j.nima.2018.05.006>
- [101] K. Yang, P. R. Menge, J. Lejay, V. Ouspenski, IEEE Nuclear Science Symposium and Medical Imaging Conference (2013) 1-6, <https://doi.org/10.1109/NS-SMIC.2013.6829676>
- [102] J. K. Cheon, S. Kim, G. Rooh, J.H. So, H. J. Kim, H. Park, Nuclear Instruments and Methods in Physics Research Section A: Accelerators, Spectrometers, Detectors and Associated Equipment 652 (2011) 1, <https://doi.org/10.1016/j.nima.2011.02.038>
- [103] G. Rooh, H. J. Kim, H. Park, S. Kim, Journal of Luminescence 146 (2014) 404-407, <https://doi.org/10.1016/j.jlumin.2013.09.047>
- [104] M. D. Birowosuto, P. Dorenbos, C. W. E. van Eijk, K. W. Krämer, H. U. Güdel, Journal of Physics: Condensed Matter 18 (2006) 6133, <https://doi.org/10.1088/0953-8984/18/26/031>
- [105] H. Wei, L. Stand, M. Zhuravleva, F. Meng, V. Martin, C. L. Melcher, Optical Materials 38 (2014) 154-160, <https://doi.org/10.1016/j.optmat.2014.09.038>
- [106] S. Kim, G. Rooh, H. J. Kim, W. Kim, U. hong, IEEE Transactions on Nuclear Science 57 (2010) 3, <https://doi.org/10.1109/TNS.2010.2041789>
- [107] G. Rooh, H. J. Kim, H. Park, S. Kim, Journal of Luminescence 132 (2012) 3, <https://doi.org/10.1016/j.jlumin.2011.10.015>
- [108] H. J. Kim, G. Rooh, H. Park, S. Kim, Radiation Measurements, 90 (2016) 279-281, <https://doi.org/10.1016/j.radmeas.2015.12.021>
- [109] C. M. Wilson, E. V. van Loef, J. Glodo, N. Cherepy, G. Hull, S. Payne, W.-S. Choong, W. Moses, K. S. Shah, Proceedings Volume 7079, Hard X-ray, Gamma-Ray and Neutron Detector PhysicsX, 707917 (2008), <https://doi.org/10.1117/12.806291>
- [110] E. V. van Loef, W. M. Higgins, J. Glodo, A. V. Churilov, K. S. Shah, Journal of Crystal Growth 310 (2008) 7-9, <https://doi.org/10.1016/j.jcrysgro.2007.11.168>
- [111] M. D. Birowosuto, P. Dorenbos, G. Bizarri, C. W. E. van Eijk, K. W. Krämer, H. U. Güdel, IEEE Transactions on Nuclear Science 55 (2008) 3, <https://doi.org/10.1109/TNS.2007.908581>

- [112] Birowosuto, P. Dorenbos, C. W. E. van Eijk, K. W. Krämer, H. U. Güdel, *IEEE Transactions on Nuclear Science* 52 (2005) 4, <https://doi.org/10.1109/TNS.2005.852630>
- [113] M. D. Birowosuto, P. Dorenbos, C. W. E. van Eijk, K. W. Krämer, H. U. Güdel, *Journal of Applied Physics* 99 (2005) 1235200, <https://doi.org/10.1063/1.2207689>
- [114] K. S. Shah, J. Glodo, M. Klugerman, W. Higgins, T. Gupta, P. Wong, W. W. Moses, S. E. Derenzo, M. J. Weber, P. Dorenbos, *IEEE Transactions on Nuclear Science* 51 (2004) 5, <https://doi.org/10.1109/TNS.2004.832321>
- [115] J. T. M. de Haas, P. Dorenbos, C. W. E. van Eijk, *Nuclear Instruments and Methods in Physics Research Section A: Accelerators, Spectrometers, Detectors and Associated Equipment* 537 (2005) 1-2, <https://doi.org/10.1016/j.nima.2004.07.243>
- [116] M. Kapusta, M. Balcerzyk, M. Moszynski, J. Pawelke, *Nuclear Instruments and Methods in Physics Research Section A: Accelerators, Spectrometers, Detectors and Associated Equipment* 421 (1999) 3, [https://doi.org/10.1016/S0168-9002\(98\)01232-7](https://doi.org/10.1016/S0168-9002(98)01232-7)
- [117] S. E. Dorenzo, M. J. Weber, W. W. Moses, C. Dujardin, *IEEE Transactions on Nuclear Science* 47 (2000) 3, <https://doi.org/10.1109/23.856531>
- [118] M. Moszynski, T. Ludziejewski, D. Wolski, W. Klamra, L.O. Norlin, *Nucl. Instrum. Methods Phys. Res., Sect. A* 345 (1994) 461, [https://doi.org/10.1016/0168-9002\(94\)90500-2](https://doi.org/10.1016/0168-9002(94)90500-2)
- [119] M. Moszynski, D. Wolski, T. Ludziejewski, M. Kapusta, A. Lempicki, C. Brecher, D. Wisniewski, A. J. Wojtowicz, *Nuclear Instruments and Methods in Physics Research Section A: Accelerators, Spectrometers, Detectors and Associated Equipment* 385 (1997) 1, [https://doi.org/10.1016/S0168-9002\(96\)00875-3](https://doi.org/10.1016/S0168-9002(96)00875-3)
- [120] J. A. Mares, A. Beitlerova, M. Nikl, N. Solovieva, C. D'Ambrosio, K. Blazek, P. Maly, K. Nejezchleb, F. de Notaristefani, *Radiation Measurements* 38 (2004) 4-6, <https://doi.org/10.1016/j.radmeas.2004.04.004>
- [121] M. Balcerzyk, M. Moszynski, M. Kapusta, D. Wolski, J. Pawelke, C. L. Melcher, *IEEE Transactions on Nuclear Science* 47 (2000) 4, <https://doi.org/10.1109/23.872971>
- [122] P. A. Cutler, C. L. Melcher, M. A. Spurrier, P. Szupryczynski, L. A. Eriksson, *IEEE Transactions on Nuclear Science* 56 (2009) 3, <https://doi.org/10.1109/TNS.2009.2016421>
- [123] E. Sakai, *IEEE Transactions on Nuclear Science* 34 (1987) 1, <https://doi.org/10.1109/TNS.1987.4337375>
- [124] S. Kawamura, J. H. Kaneko, M. Higuchi, T. Yamaguchi, J. Haruna, Y. Yagi, K. Susa, F. Fujita, A. Homma, S. Nishiyama, K. Kurashige, H. Ishibashi, M. Furusaka, *IEEE Transactions on Nuclear Science* 54 (2007) 4, <https://doi.org/10.1109/TNS.2007.902372>

- [125] L. Pidol, A. Kahn-Harari, B. Viana, E. Virey, B. Ferrand, P. Dorenbos, J. T. M. de Haas, C. W. E. van Eijk, *IEEE Transactions on Nuclear Science* 51 (2004) 3, <https://doi.org/10.1109/TNS.2004.829542>
- [126] D. Pauwels, N. Le Masson, B. Viana, A. Kahn-Harari, E.V.D. van Loef, P. Dorenbos, C. W. E. van Eijk, *IEEE Transactions on Nuclear Science* 47 (2000) 6, <https://doi.org/10.1109/23.914446>
- [127] D. Wisniewski, A. J. Wojtowicz, W. Drozdowski, J. M. Farmer, L. A. Boatner, *Journal of Alloys and Compounds* 380 (2004) 1-2, <https://doi.org/10.1016/j.jallcom.2004.03.042>
- [128] N. J. Cherepy, G. Hull, A. D. Drobshoff, S. A. Payne, E. van Loef, C. M. Wilson, K. S. Shah, U. N. Roy, A. Burger, L. A. Boater, W.-S. Choong, W. W. Moses, *Applied Physics Letters* 92 (2008) 8, <https://doi.org/10.1063/1.2885728>
- [129] L. A. Boatner, J. O. Ramey, J. A. Kolopus, R. Hawrami, W. M. Higgins, E. van Loef, J. Glodo, K. S. Shah, E. Rowe, P. Bhattacharya, E. Tupitsyn, M. Groza, A. Burger, N. J. Cherepy, S. A. Payne, *Journal of Crystal Growth* 379 (2013) 63-68, <https://doi.org/10.1016/j.jcrysgr.2013.01.035>
- [130] E. D. Bourret-Courchesne, G. Bizarri, R. Borade, Z. Yan, S. M. Hanrahan, G. Gundiah, A. Chaudhry, A. Canning, S. E. Derenzo, *Nuclear Instruments and Methods in Physics Research Section A: Accelerators, Spectrometers, Detectors and Associated Equipment* 612 (2009) 1, <https://doi.org/10.1016/j.nima.2009.10.146>
- [131] M. S. Alekhin, D. A. Biner, K. W. Krämer, P. Dorenbos, *Journal of Luminescence* 145 (2014) 723-728, <https://doi.org/10.1016/j.jlumin.2013.08.058>
- [132] Y. Wu, M. Zhuravleva, A. C. Lindsey, M. Koschan, C. L. Melcher, *Nuclear Instruments and Methods in Physics Research Section A: Accelerators, Spectrometers, Detectors and Associated Equipment* 820 (2016) 132-140, <https://doi.org/10.1016/j.nima.2016.03.027>
- [133] J. Glodo, E. V. van Loef, N. J. Cherepy, S. A. Payne, K. S. Shah, *IEEE Transactions on Nuclear Science* 57 (2010) 3, <https://doi.org/10.1109/TNS.2009.2036352>
- [134] K. Yang, M. Zhuravleva, C. L. Melcher, *Physica Status Solidi Rapid Research Letters* 5 (2011) 1, <https://doi.org/10.1002/pssr.201004434>
- [135] G. Gundiah, M. Gascon, G. Bizarri, S. E. Derenzo, E. D. Bourret-Courchesne, *Journal of Luminescence* 159 (2015) 274-279, <https://doi.org/10.1016/j.jlumin.2014.11.031>
- [136] M. S. Alekhin, K. W. Krämer, P. Dorenbos, *Nuclear Instruments and Methods in Physics Research Section A: Accelerators, Spectrometers, Detectors and Associated Equipment* 714 (2013) 13-16, <https://doi.org/10.1016/j.nima.2013.02.025>

- [137] I. Holl, E. Lorenz, G. Mageras, IEEE Transactions on Nuclear Science 35 (1998) 1, <https://doi.org/10.1109/23.12684>
- [138] J. Menefee, C. F. Swinehart, E. W. O'Dell, IEEE Transactions on Nuclear Science 13 (1966) 1, <https://doi.org/10.1109/TNS.1966.4324036>
- [139] K. G. Rajan, A. J. Lenus, Pramana Journal of Physics, 65 (2005) 323-338, <https://doi.org/10.1007/BF02898620>
- [140] E.D. Bourret-Courchesne, G. A. Bizarri, R. Borade, G. Gundiah, E. C. Samulon, Z. Yan, S. E. Derenzo, Journal of Crystal Growth 352 (2012) 1, <https://doi.org/10.1016/j.jcrysgro.2012.01.014>
- [141] Z. Yan, G. Bizarri, E. Gourret-Courchesne, Nuclear Instruments and Methods in Physics Research Section A: Accelerators, Spectrometers, Detectors and Associated Equipment 698 (2013) 7-10 <https://doi.org/10.1016/j.nima.2012.09.026>
- [142] M. Zhuravleva, B. Blalock, K. Yang, M. Koschan, C. L. Melcher, Journal of Crystal Growth 352 (2012) 1, <https://doi.org/10.1016/j.jcrysgro.2012.02.025>
- [143] V. L. Cherginets, N. V. Rebrova, A. Y. Grippa, y. N. Datsko, T. V. Ponomarenko, V. Y. Pedash, N. N. Kosinov, V. A. Tarasov, O. V. Zelenskaya, I. M. Zenya, A. V. Lopin. Materials Chemistry and Physics 143 (2014) 3, <https://doi.org/10.1016/j.matchemphys.2013.11.037>
- [144] L. Stand, M. Zhuravleva, B. Chakoumakos, H. Wei, J. Johnson, V. Martin, M. Loyd, D. Rutstrom, W. McAlexander, Y. Wu, M. Koschan, C. L. Melcher, Journal of Luminescence 207 (2019) 70-77, <https://doi.org/10.1016/j.jlumin.2018.10.108>
- [145] A. Y. Grippa, N. V. Rebrova, T. E. Gorbacheva, V. Y. Pedash, N. N. Kosinov, V. L. Cherginets, V. A. Cherginets, V. A. Tarasov, O. A. Tarasenko, Nuclear Instruments and Methods in Physics Research Section A: Accelerators, Spectrometers, Detectors and Associated Equipment 729 (2013) 356-359, <https://doi.org/10.1016/j.nima.2013.07.077>
- [146] Z. Yan, G. Gundiah, G. A. Bizarri, E. C. Samulon, S. E. Derenzo, E. D. Bourret Courchesne, Nuclear Instruments and Methods in Physics Research Section A: Accelerators, Spectrometers, Detectors and Associated Equipment 735 (2014) 83-87, <https://doi.org/10.1016/j.nima.2013.09.021>
- [147] G. Bizarri, E. D. Bourret-Courchesne, Z. Yan, S. E. Derenzo, IEEE Transactions on Nuclear Science 58 (2011) 6, <https://doi.org/10.1109/TNS.2011.2166999>
- [148] E. D. Bourret-Courchesne, G. Bizarri, S. M. Hanrahan, G. Gundiah, Z. Yan, S. E. Derenzo, Nuclear Instruments and Methods in Physics Research Section A: Accelerators, Spectrometers, Detectors and Associated Equipment 613 (2010) 1, <https://doi.org/10.1016/j.nima.2009.11.036>
- [149] L. Soundara-Pandian, R. Hawrami, J. Glodo, E. Ariesanti, E. V. van Loef, K. Shah, IEEE Transactions on Nuclear Science 63 (2016) 2, <https://doi.org/10.1109/TNS.2016.2535355>

- [150] L. Stand, M. Zhuravleva, H. Wei, C. L. Melcher, *Optical Materials* 46 (2015) 59-63, <https://doi.org/10.1016/j.optmat.2015.04.002>
- [151] K. S. Pestovich, L. Stand, E. van Loef, C. L. Melcher, M. Zhuravleva, *IEEE Transactions on Nuclear Science* 70 (2023) 7, <https://doi.org/10.1109/TNS.2023.3280733>
- [152] L. Stand, M. Zhuravleva, J. Johnson, M. Koschan, E. Lukosi, C.L. Melcher, *Optical Materials* 73 (2017) 408-414, <https://doi.org/10.1016/j.optmat.2017.08.013>
- [153] A. Y. Grippa, N. V. Rebrova, T. E. Gorbacheva, V. Y. Pedash, N. N. Kosinov, V. L. Cherginets, V. A. Tarasov, O. A. Tarasenko, A. V. Lopin, *Journal of Crystal Growth* 371 (2013) 112-116, <https://doi.org/10.1016/j.jcrysgr.2013.02.020>
- [154] M. Loyd, A. Lindsey, L. Stand, M. Zhuravleva, C. L. Melcher, M. Koschan, *Optical Materials*, 68 (2017) 47-52, <https://doi.org/10.1016/j.optmat.2016.11.009>
- [155] S. S. Gokhale, L. Stand, A. Lindsey, M. Koschan, M. Zhuravleva, C. L. Melcher, *Journal of Crystal Growth* 445 (2016) 1-8, <https://doi.org/10.1016/j.jcrysgr.2016.04.006>
- [156] A. Synthfeld, M. Moszynski, R. Arlt, M. Balcerzyk, M. Kapusta, M. Majorov, R. Marcinkowski, P. schotanus, M. Swoboda, D. Wolski, *IEEE Transactions on Nuclear Science* 52 (2005) 6, <https://doi.org/10.1109/TNS.2005.860193>
- [157] T. Yasumune, M. Kurihara, K. Maehata, N. Iyomoto, K. Ishibashi, *Journal of Low Temperature Physics* 1678 (2011) 442-446, <https://doi.org/10.1007/s10909-011-0436-z>
- [158] R. Hofstadter, E. W. I'Dell, C. T. Schmidt, *IEEE Transactions on Nuclear Science*, 11 (1964) 3, <https://doi.org/10.1109/TNS.1964.4323397>
- [159] L. A. Boatner, J. O. Ramey, J. A. kolopus, J. S. Neal, *Nuclear Instruments and Methods in Physics Research Section A: Accelerators, Spectrometers, Detectors and Associated Equipment* 786 (2015) 23-31, <https://doi.org/10.1016/j.nima.2015.02.031>
- [160] Y. Wu, Q. Li, D. J. Rutstrom, I. Greeley, L. Stand, M. Loyd, M. Koschan, C. L. Melcher, *Nuclear Instruments and Methods in Physics Research Section A: Accelerators, Spectrometers, Detectors and Associated Equipment* 954 (2020) 21, <https://doi.org/10.1016/j.nima.2018.09.077>
- [161] K. Kamada, H. chiba, M. Yoshino, A. Yamaji, Y. Shoji, S. Kurosawa, Y. Yokota, Y Ohashi, A. Yoshikawa, *Optical Materials* 68 (2017) 70-74, <https://doi.org/10.1016/j.optmat.2017.05.010>
- [162] A. C. Lindsey, M. Zhuravleva, L. Stand, Y. Wu, C. L. Melcher, *Optical Materials* 48 (2015) 1-6, <https://doi.org/10.1016/j.optmat.2015.07.017>

- [163] Y. Wu, Q. Li, D. J. rutstrom, M. Zhuravleva, M. Loyd, I. Stand, M. Koschan, C. L. Melcher, *Physica Status Solidi Rapid Research Letters* 12 (2018) 2, <https://doi.org/10.1002/pssr.201700403>
- [164] Y. Wu, Q. Li, B. C. Chakoumakos, M. Zhuravleva, A. C. Lindsey, J. A. Johnson, L. Stand, M. Koschan, C. L. Melcher, *Advanced Optical Materials* 4 (2013) 10, <https://doi.org/10.1002/adom.201600239>
- [165] L. Stand, M. Zhuravleva, A. Lindsey, C. L. Melcher, *Nuclear Instruments and Methods in Physics Research Section A: Accelerators, Spectrometers, Detectors and Associated Equipment* 780 (2015) 40-44, <https://doi.org/10.1016/j.nima.2015.01.052>
- [166] L. Stand, M. Zhuravleva, B. Chakoumakos, J. Johnson, A. Lindsey, C. L. Melcher, *Journal of Luminescence* 169 (2016) 301-307, <https://doi.org/10.1016/j.jlumin.2015.09.013>
- [167] K. S. Pestovich, L. Stand, C. L. Melcher, E. van Loef, M. Zhuravleva, *Journal of Crystal Growth* 627 (2024) 1, <https://doi.org/10.1016/j.jcrysgr.2023.127540>
- [168] J. A. Johnson, M. Zhuravleva, L. Stand, B. C. Chakoumakos, Y. Wu, I. Greely, D. rutstrom, M. Koschan, C. L. Melcher, *Crystal Growth and Design* 18 (2018) 9, <https://doi.org/10.1021/acs.cgd.8b00661>
- [169] L. Stand, M. Zhuravleva, B. Chakoumakos, J. Johnson, M. Loyd, Y. Wu, M. Koschan, C. L. Melcher, *Journal of Crystal Growth* 486 (2018) 15, <https://doi.org/10.1016/j.jcrysgr.2018.01.017>
- [170] H. J. Kim, G. Rooh, A. Khan, H. Park, S. Kim, *Optical materials* 82 (2018) 7-10, <https://doi.org/10.1016/j.optmat.2018.05.036>
- [171] M. Suta, C. Wickleder, *J. Lumin.* 210 (2019) 210, <https://doi.org/10.1016/j.jlumin.2019.02.031>
- [172] C. van Aarle, K. W. Krämer, P. Dorenbos, *Journal of Luminescence* 266 (2024) 120329, <https://doi.org/10.1016/j.jlumin.2023.120329>
- [173] R. H. P. Awater, M. S. Alekhin, D. A. Biner, K. W. Krämer, P. Dorenbos, *Journal of Luminescence* 212 (2019) 1-4, <https://doi.org/10.1016/j.jlumin.2019.04.002>
- [174] W. Wolszczak, K. W. Krämer, P. Dorenbos, *Physica Status Solidi Rapid Research Letters* 13 (2019) 9, <https://doi.org/10.1002/pssr.201900158>
- [175] C. van Aarle, K. W. Krämer, P. Dorenbos, *Journal of Materials Chemistry C* 11 (2023) 2336-2344, <https://doi.org/10.1039/D2TC05311J>
- [176] C. van Aarle, K. W. Krämer, P. Dorenbos, *Journal of Luminescence* 251 (2022) 119209, <https://doi.org/10.1016/j.jlumin.2022.119209>
- [177] C. van Aarle, K. W. Krämer, P. Dorenbos, *Journal of Luminescence* 238 (2021) 118257, <https://doi.org/10.1016/j.jlumin.2021.118257>

- [178] R. Hawrami, E. Ariesanti, A. Farsoni, D. Szydel, H. Sabet, *Crystals* 12 (2022) 1517, <https://doi.org/10.3390/cryst12111517>
- [179] D. W. Aitken, B. L. Beron, G. Yenicyay, H. R. zulliger, *IEEE Transactions on Nuclear Science*, 14 (1967) 1, <https://doi.org/10.1109/TNS.1967.4324457>
- [180] L. Swiderski, M. Moszynski, A. Syntfeld-Kazuch, M. Szawlowski, T. Szczesniak, *Nuclear Instruments and Methods in Physics Research Section A: Accelerators, Spectrometers, Detectors and Associated Equipment* 749 (2014) 68-73, <https://doi.org/10.1016/j.nima.2014.02.045>
- [181] R. Hofstadter, *Physical Review Journals Archive* 74 (1948) 1 <https://doi.org/10.1103/PhysRev.74.100>
- [182] R. Hofstadter, *Physical Review Journals Archive* 75 (1949) 5 <https://doi.org/10.1103/PhysRev.75.796>
- [183] R. Hofstadter, J. A. McIntyre, *Physical Review Journals Archive* 80 (1950) 4, <https://doi.org/10.1103/PhysRev.80.631>
- [184] A. M. Srivastava, *J. Lumin.* 169 (2016) 445, <http://dx.doi.org/10.1016/j.jlumin.2015.07.001>
- [185] A. Zych, M. de Lange, C. de Mello Donega, A. Meijerink, *Journal of Applied Physics* 112 (2012) 1, <https://doi.org/10.1063/1.4731735>
- [186] H. Ogino, A. Yoshikawa, M. Nikl, A. Krasnikov, K. Kamada, T. Fukuda, *Journal of Crystal Growth* 287 (2006) 2, <https://doi.org/10.1016/j.jcrysgro.2005.11.023>
- [187] W. Drozdowski, P. Dorenbos, J. T. M. de Haas, R. Drozdowska, A. Owens, K. Kamada, K. Tsutsumi, Y. Usuki, T. Yanagida, A. Yoshikawa, *IEEE Transactions on Nuclear Science* 55 (2008) 4, <https://doi.org/10.1109/TNS.2008.2000845>
- [188] J. Glodo, R. Farrell, E. V. D. van Loef, W. M. Higgins, K. S. Shah, *IEEE Nuclear Science Symposium conference Record* (2005) <https://doi.org/10.1109/NSSMIC.2005.1596215>
- [189] J. A. Mares, M. Nikl, A. Beitlerova, P. Horodysky, K. Blazek, K. Bartos, C. D'Ambrosio, *IEEE Transactions on Nuclear Science* 59 (2012) 5, <https://doi.org/10.1109/TNS.2012.2191573>
- [190] W. Drozdowski, K. Brylew, A. J. Wojtowicz, J. Kisielewski, M. Swirkowicz, T. Lukasiewicz, J. T. M. de Haas, P. Dorenbos, *Optical Materials Express* 4 (2014) 6, <https://doi.org/10.1364/OME.4.001207>
- [191] C. Foster, Y. Wu, M. Koschan, C. L. Melcher, *Physica Status Solidi Rapid Research Letters* 12 (2018) 9, <https://doi.org/10.1002/pssr.201800280>
- [192] K. Yang, P. R. Menge, *Journal of Applied Physics* 118 (2015) 21, <https://doi.org/10.1063/1.4937126>
- [193] I. V. Khodyuk, S. A. Messina, T. J. Hayden, E. D. Bourret, G. A. Bizarri, *Journal of Applied Physics* 118 (2015) 8, <https://doi.org/10.1063/1.4928771>

- [194] N. V. Shiran, A. V. Gektin, Y. Boyarintseva, S. Vasyukov, A. Boyarintsev, V. Pedash, S. Tkachenko, O. Zelenskaya, N. Kosinov, O. Kisil, L. Philippovich, *IEEE Transactions on Nuclear Science* 57 (2010) 3, <https://doi.org/10.1109/TNS.2010.2048578>
- [195] A. Synthfeld-Kazuch, L. Swiderski, W. Czarnacki, M. Gierlink, W. Klamara, M. Moszynski, P. Schotanus, *IEEE Transactions on Nuclear Science* 54 (2007) 5, <https://doi.org/10.1109/TNS.2007.906168>
- [196] E. Rowe, P. Bhattacharya, E. Tupitsyn, M. Groza, A. Burger, N. J. Cherepy, S. A. Payne, B. W. Strum, C. Pedrini, *IEEE Transactions on Nuclear Science* 60 (2013) 2, <https://doi.org/10.1109/TNS.2013.2253330>
- [197] S. Weber, D. Christ, M. Kurzeja, R. Engels, G. Kemmerling, H. Halling, *IEEE Transactions on Nuclear Science* 50 (2003) 5, <https://doi.org/10.1109/TNS.2003.817952>
- [198] M. Moszynski, C. Gresset, J. Vacher, R. Odru, *Nuclear Instruments and Methods in Physics Research* 188 (1981) 2, [https://doi.org/10.1016/0029-554X\(81\)90521-8](https://doi.org/10.1016/0029-554X(81)90521-8)
- [199] S. E. Brunner, D. R. Schaart, *Physics in Medicine and Biology* 62 (2017) 4421, <https://doi.org/10.1088/1361-6560/aa6a49>
- [200] P. Lecoq, I. Dafinei, E. Auffray, M. Schneegans, M. V. Korlzhik, O. V. Missevitch, V. B. Pavlenko, A. A. Fedorov, A. N. Annenkov, V. L. Kostylev, V. D. Ligon, *Nuclear Instruments and Methods in Physics Research Section A: Accelerators, Spectrometers, Detectors and Associated Equipment* 365 (1995) 2-3, [https://doi.org/10.1016/0168-9002\(95\)00589-7](https://doi.org/10.1016/0168-9002(95)00589-7)
- [201] W. W. Moses, *Nuclear Instruments and Methods in physics Research Section A: Accelerators, Spectrometers, Detectors and Associated Equipment* 487 (2002) 1-2, [https://doi.org/10.1016/S0168-9002\(02\)00955-5](https://doi.org/10.1016/S0168-9002(02)00955-5)
- [202] K. Saeki, Y. Fujimoto, M. Koshimizu, T. Yanagida, K. Asai, *Applied Physics Express* 9 (2016) 042602, <https://doi.org/10.7567/APEX.9.042602>
- [203] K. Saeki, Y. Fujimoto, M. Koshimizu, D. Nakauchi, H. Tanaka, T. Yanagida, K. Asai, *Japanese Journal of Applied Physics* 57 (2018) 030310, <https://doi.org/10.7567/JJAP.57.030310>
- [204] S. Kodama, S. Kurosawa, M. Ohno, A. Yamaji, M. Yoshino, J. Pejchal, R. Kral, Y. Ohashi, K. Kamada, Y. Yokota, M. Nikl, A. Yoshikawa, *Radiation Measurements* 124 (2019) 54-58, <https://doi.org/10.1016/j.radmeas.2019.03.005>
- [205] S. Kodama, S. Kurosawa, A. Yamaji, J. Pejchal, R. kral, Y. Ohashi, K. Kamada, Y. Yokota, M. Nikl, A. Yoshikawa, *Journal of Crystal Growth* 492 (2018) 1-5, <https://doi.org/10.1016/j.jcrysgro.2018.03.033>
- [206] J. Jasper van Blaaderen, L. A. van den Brekel, K. W. Krämer, P. Dorenbos, *Chemistry of Materials* 35 (2023) 22, <https://doi.org/10.1021/acs.chemmater.3c01810>

- [207] S. Cheng, A. Beitlerova, R. Kucerkova, E. Mihokova, M. Nikl, Z. Shou, G. Ren, Y. Wu, *ACS Applied Materials and Interfaces* 13 (2021) 10, <https://doi.org/10.1021/acsami.0c22505>
- [208] S. Cheng, A. Beitlerova, B. Kucerkova, M. nikl, G. Ren, Y. Wu, *Physica Status Solidi Rapid Research Letters* 14 (2020) 11, <https://doi.org/10.1002/pssr.202000374>
- [209] R. Hawrami, E. Ariesanti, H. Wei, J. Finkelstein, J. Glodo, K. S. Shah, *Journal of Crystal Growth* 475 (2017) 216-219, <https://doi.org/10.1016/j.jcrys-gro.2017.06.012>
- [210] A. Khan, G. Rooh, H. J. Kim, H. Park, S. Kim, *Radiation Measurements* 107 (2017) 115-118, <https://doi.org/10.1016/j.radmeas.2017.09.003>
- [211] R. Hawrami, E. Ariesanti, V. Buliga, A. Burger, S. Lam, S. Motakef, *Journal of Crystal Growth* 531 (2020) 125316, <https://doi.org/10.1016/j.jcrys-gro.2019.125316>
- [212] Y. Fujimoto, K. Saeki, D. Nakauchi, T. Yanagida, M. Koshimizu, K. Asai, *Sensors and Materials* 30 (2018) 7, <https://doi.org/10.18494/SAM.2018.1927>
- [213] A. Xie, F. Maddalena, M. E. Witkowski, M. Makowski, B. Mahler, W. Drozdowski, S. V. Springham, P. Coquet, C. Dujardin, M. D. Birowosuto, C. Dong, *Chemistry of Materials* 32 (2020) 8530- 8539, <https://doi.org/10.1021/acs.chemmater.0c02789>
- [214] A. Xie, C. Hettiarachchi, F. Maddalena, M. E. Witkowski, M. Makowski, W. Drozdowski, A. Arramel, A. T. S. Wee, S. V. Springham, P. Q. Vuong, H. J. Kim, C. Dujardin, P. Coquet, M. D. Birowosuto, C. Dang, *Communications Materials* 37 (2020) 1, <https://doi.org/10.1038/s43246-020-0038-x>
- [215] M. D. Birowosuto, D. Cortecchia, W. Drozdowski, K. Brylew, W. Lachmanski, A. Pruno, C. Soci, *Scientific Reports* 6 (2016) 37254, <https://doi.org/10.1038/srep37254>
- [216] W. W. Wolszczak, D. L. Carroll, R. T. Williams, *Advanced X-ray Detector Technologies*, Chapter 1 (2022), https://doi.org/10.1007/978-3-030-64279-2_1
- [217] R. T. Williams, W. W. Wolszczak, X. Yan, D. L. Carrol, *ACS Nano* 14 (2020) 5161-5169, <https://doi.org/10.1021/acsnano.0c02529>
- [218] J. J. van Blaaderen, S. van der Sar, D. Onggo, M. A. K. Sheikh, D. R. Schaart, M. D. Birowosuto, P. Dorenbos, *Journal of Luminescence* 236 (2023) 120012, <https://doi.org/10.1016/j.jlumin.2023.120012>
- [219] M. Xia, Z. Xie, H. Wang, T. Jin, L. Liu, J. Kang, Z. Sang, X. Yan, B. Wu, H. Hu, J. Tang, G. Niu, *Advanced Materials* 35 (2023) 18, <https://doi.org/10.1002/adma.202211769>
- [220] B. Chen, R. Yu, G. Xing, Y. Wang, W. Wang, Y. Chen, X. Xu, Q. Zhao, *ACS Energy Letters* 9 (2024) 1, <https://doi.org/10.1021/acsenenergylett.3c02069>

- [221] J. Selling, M. D. Birowosuto, P. Dorenbos, S. Schweizer, *Journal of Applied Physics* 101 (2007) 3, <https://doi.org/10.1063/1.2432306>
- [222] A. Burger, E. Rowe, M. Groza, K. M. Figueroa, N. J. Cherepy, P. R. Beck, S. Hunter, S. A. Payne, *Applied Physics Letters* 107 (2015) 14, <https://doi.org/10.1063/1.4932570>
- [223] J. J. van Blaaderen, F. Maddalena, C. Dang, M. D. Birowosuto, P. Dorenbos, *Journal of Materials Chemistry C* 10 (2022) 11598-11606, <https://doi.org/10.1039/D2TC01483A>
- [224] E. van Loef, L. S. Pandian, N. Kaneshige, G. Ciampi, L. Stand, D. Rutstrom, Y. Tratsiak, M. Zhuravleva, C. Melcher, K. S. Shah, *IEEE Transactions on Nuclear Science* 70 (2023) 7, <https://doi.org/10.1109/TNS.2023.3258065>
- [225] G. Rooh, A. Khan, H. J. Kim, H. Park, S. Kim, *Optical Materials* 73 (2017) 523-526, <https://doi.org/10.1016/j.optmat.2017.08.047>
- [226] T. Iida, K. Kamada, M. Yoshino, K. J. kim, K. Ichimura, A. Yoshikawa, *Nuclear Instruments and Methods in Physics Research Section A: Accelerators, Spectrometers, Detectors and Associated Equipment* 958 (2020) 162629, <https://doi.org/10.1016/j.nima.2019.162629>
- [227] A. Fukabori, L. An, A. Ito, V. Chani, K. Kamada, T. Goto, A. Yoshikawa, *IEEE Transactions on Nuclear Science* 59 (2012) 5, <https://doi.org/10.1109/TNS.2012.2206211>
- [228] V. B. Mikhailik, H. Kraus, S. Henry, A. J. B. Tolhurst, *Physical Review B* 75 (2007) 184308, <https://doi.org/10.1103/PhysRevB.75.184308>
- [229] Y. G. Zdesenko, F. T. Avigone III, V. B. Brudanin, F. Danevich, S. S. Nagorny, I. M. Solsky, V. I. Tretyak, *Nuclear Instruments and Methods in Physics Research Section A: Accelerators, Spectrometers, Detectors and Associated Equipment* 538 (2005) 1-3, <https://doi.org/10.1016/j.nima.2004.09.030>
- [230] M. Moszynski, M. Balcerzyk, W. Czarnacki, A. Nassalski, T. Szczesniak, H. Kraus, V. B. Mikhailik, I. M. Solskii, *Nuclear Instruments and Methods in Physics Research Section A: Accelerators, Spectrometers, Detectors and Associated Equipment* 553 (2005) 3, <https://doi.org/10.1016/j.nima.2005.07.052>
- [231] C. L. Melcher, R. A. Manente, J. S. Schweitzer, *IEEE Transactions on Nuclear Science* 36 (1989) 1, <https://doi.org/10.1109/23.34629>
- [232] A. A. Annenkov, M. V. Korzhik, P. Lecoq, *Nuclear Instruments and Methods in Physics Research Section A: Accelerators, Spectrometers, Detectors and Associated Equipment* 490 (2002) 1-2, [https://doi.org/10.1016/S0168-9002\(02\)00916-6](https://doi.org/10.1016/S0168-9002(02)00916-6)
- [233] M. Kobayashi, M. Ishii, Y. Usuki, H. Yahagi, *Nuclear Instruments and Methods in Physics Research Section A: Accelerators, Spectrometers, Detectors and Associated Equipment* 333 (1993) 2-3, [https://doi.org/10.1016/0168-9002\(93\)91187-R](https://doi.org/10.1016/0168-9002(93)91187-R)

- [234] B. C. Grabmaier, IEEE Transactions on Nuclear Science 31 (1984) 1, <https://doi.org/10.1109/TNS.1984.4333280>
- [235] V. Khanin, I. Venevtsev, P. Rodnyi, Optical Materials 136 (2023) 113399, <https://doi.org/10.1016/j.optmat.2022.113399>
- [236] P. A. Rodnyi, J. R. X. Anderson, Soviet Physics Solid State 34 (1992) 7, <http://pascalfrancis.inist.fr/vibad/index.php?action=getRecordDetail&idt=4512194>
- [237] P. A. Rodnyi, MRS Online Proceedings Library, 348 (1994) 77-88, <https://doi.org/10.1557/PROC-348-77>
- [238] M. Loyal, M. Moszynski, R. Allemand, E. Cormoreche, P. Guinet, R. Odru, J. Vacher, Nuclear Instruments and Methods in Physics Research, 206 (1983) 1-2, [https://doi.org/10.1016/0167-5087\(83\)91254-1](https://doi.org/10.1016/0167-5087(83)91254-1)
- [239] P. A. Rodnyi, Radiation measurements 38 (2004) 4-6, <https://doi.org/10.1016/j.radmeas.2003.11.003>
- [240] E. Radzhabov, A. Istomin, A. Nepomnyashikh, A. Egranov, V. Ivashechkin, Nuclear Instruments and Methods in physics Research Section A: Accelerators, Spectrometers, Detectors and Associated Equipment 537 (2005) 1-2, <https://doi.org/10.1016/j.nima.2004.07.237>
- [241] S. Gundacker, R. H. Pots, A. Nepomnyashchikh, E. Radzhabov, E. Shendrik, S. Omelkov, M. Krim, F. Acerbi, M. Capassa, G. Paternoster, Physics in Medicine and Biology 66 (2021) 114002, <https://doi.org/10.1088/1361-6560/abf476>
- [242] C. Hu, C. Xu, L. Zhang, Q. Zhang, R.-Y. Zhy, IEEE Transactions on Nuclear Science 66 (2019) 7, <https://doi.org/10.1109/TNS.2019.2918305>
- [243] J. Chen, F. Yang, L. Zhang, R.-Y. Zhu, Y. Du, S. Wang, S. Sun, X. Li, IEEE Transactions on Nuclear Science 65 (2018) 8, <https://doi.org/10.1109/TNS.2017.2786042>
- [244] D. Rutstrom, L. Stand, C. Delzer, M. Kapusta, J. Glodo, E. van Loef, K. Shah, M. Koschan, C. L. Melcher, M. Zhuravleva, Optical Materials 133 (2022) 112912, <https://doi.org/10.1016/j.optmat.2022.112912>
- [245] D. Rutstrom, L. Stand, D. Windsor, H. Xu, M. Kapusta, C. L. Melcher, M. Zhuravleva, Journal of Materials Chemistry C 12 (2024) 6920-6931, <https://doi.org/10.1039/D4TC00877D>
- [246] D. Rutstrom, L. Stand, M. Kapusta, D. Windsor, H. Xu, C. L. Melcher, M. Zhuravleva, Optical Materials: X 24 (2024) 100349, <https://doi.org/10.1016/j.omx.2024.100349>
- [247] D. M. Seliverstov, A. A. Demidenko, E. A. Garibin, S. D. Gain, Y. I. Gusev, P. P. Fedorov, S. V. Kosyanenko, I. A. Mironov, V. V. Osiko, P. A. Rodnyi, A. N. Smirnov, V. M. Suvorov, Nuclear Instruments and Methods in physics Research Section A: Accelerators, Spectrometers, Detectors and Associated Equipment 695 (2012) 369-372, <https://doi.org/10.1016/j.nima.2011.11.080>

- [248] A. S. Voloshinovskii, V. B. Mikhailik, P. A. Rodnyi, S. N. Pidzyrailo, *Jour Fizika Iverdogo Tela* 34 (1992) 2, <http://mi.mathnet.ru/ft7360>
- [249] S. Kubota M. Itoh, J.-Z. Ruan, S. Sakuragi, S. Hashimoto, *Physical Review Letters* 60 (1988) 2319, <https://doi.org/10.1103/PhysRevLett.60.2319>
- [250] F. De Notaristefani, P. Lecoq, M. Schneegans, *Heavy Scintillators for Scientific and Industrial Applications*, proceedings of the Cristal 2000 international workshop (1992), ISBN: 2-86332128-5
- [251] M. Laval, M. Moszynski, R. Allemand, E. Cormoreche, P. Guinet, R. Odru, J. Vacher, *Nuclear Instruments and Methods in physics Reserach* 206 (1983) 1-2, [https://doi.org/10.1016/0167-5087\(83\)91254-1](https://doi.org/10.1016/0167-5087(83)91254-1)
- [252] M. Biasini, D. B. Cassidy, S. H. M. Dena, H. K. M. Tanaka, A. P. Mills, *Nuclear Instruments and Methods in Physics Research Section A: Accelerators, Spectrometers, Detectors and Associated Equipment* 553 (2005) 3, <https://doi.org/10.1016/j.nima.2005.07.022>
- [253] V. Nanal, B. B. Back, D. J. Horman, *Nuclear Instruments and Methods in Physics Research Section A: Accelerators, Spectrometers, Detectors and Associated Equipment* 389 (1997) 3, [https://doi.org/10.1016/S0168-9002\(97\)00326-4](https://doi.org/10.1016/S0168-9002(97)00326-4)
- [254] M. Moszynski, R. Allemand, M. Laval, R. Odru, J. Vacher, *Nuclear Instruments and Methods in Physics Research* 205 (1983) 1-2, [https://doi.org/10.1016/0167-5087\(83\)90194-1](https://doi.org/10.1016/0167-5087(83)90194-1)
- [255] K. Yamanoi, R. Nishi, K. Takeda, Y. Shinzato, M. Tsuboi, M. V. Luong, T. Nakazato, T. Shimizu, N. Sarukura, M. Cadatal-Raduban, M. H. Pham, H. D. Nguyen, S. Kurosawa, Y. Yokota, A. Yoshikawa, T. Togashi, M. Nagasono, T. Ishikawa, *Optical Materials* 36 (2014) 4, <https://doi.org/10.1016/j.optmat.2013.11.023>
- [256] M. Koshimizu, N. Yahaba, R. Haruki, F. Nishikido, S. Kishimoto, K. Asai, *Optical Materials* 36 (2014) 12, <https://doi.org/10.1016/j.optmat.2014.04.004>
- [257] J. Jansons, Z. Rachko, J. Valbis, J. Andriessen, P. Dorenbos, C. W. E. van Eijk, N. M. Khaidukov, *Journal of Physics Condensed Matter* 5 (1993) 10, <https://doi.org/10.1088/09538984/5/10/015>
- [258] G. H. V. Bertrand, M. Hamel, F. Sguerra, *Chemistry A European Journal* 20 (2014) 48, <https://doi.org/10.1002/chem.201404093>
- [259] N. P. Zaitseva, A. M. Glenn, A. N. Mabe, M. L. Carman, C. R. Hurlbut, J. W. Inman, S. A. Payne, *Nuclear Instruments and Methods in physics Research Section A: Accelerators, Spectrometers, Detectors and Associated Equipment* 889 (2018) 97-104, <https://doi.org/10.1016/j.nima.2018.01.093>
- [260] J. F. Wiliamson, J. F. Dempsey, A. S. Kirov, J. Monroe, W. R. Binns, H. Hedtjarn, *Physics in Medicine and Biology* 44 (1999) 857, <https://doi.org/10.1088/0031-9155/44/4/004>

- [261] T. J. Hajagos, C. Liu, N. J. Cherepy, Q. Pei, *Advanced Materials* 30 (2018) 27, <https://doi.org/10.1002/adma.201706956>
- [262] E. van Loef, G. Markosyan, U. Shirwadkar, M. McClush, K. Shah, *Nuclear Instruments and Methods in physics Research Section A: Accelerators, Spectrometers, Detectors and Associated Equipment* 788 (2015) 71-72, <https://doi.org/10.1016/j.nima.2015.03.077>
- [263] A. Sato, A. Magi, M. Koshimizu, Y. Fujimoto, S. Kishimoto, K. Asai, *RSC Advances* 11 (2021) 15581-15589, <https://doi.org/10.1039/D1RA01878G>
- [264] T. Yanagida, K. Watanabe, Y. Fujimoto, *Nuclear Instruments and Methods in Physics Research Section A: Accelerators, Spectrometers, Detectors and Associated Equipment* 784 (2015) 111-114, <https://doi.org/10.1016/j.nima.2014.12.031>
- [265] J. B. Birks, *Proceedings of the Physical Society* 79 (1962) 494
- [266] R. F. Post, N. S. Shiren *Physical Review Journals Archive* 78 (1950) 80, <https://doi.org/10.1103/PhysRev.78.80>
- [267] M. De Gerone, M. Biasotti, V. Ceriale, D. Corsini, F. Gatti, A. Orlando, G. Pizzigoni, *Nuclear Instruments and Methods in Physics Research Section A: Accelerators, Spectrometers, Detectors and Associated Equipment* 824 (2016) 192-193, <https://doi.org/10.1016/j.nima.2015.11.021>
- [268] B. L. Rupert, N. J. Cherepy, B. W. Sturm, R. D. Sanner, S. A. Payne, *Europhysics Letters* 97 (2012) 2, <https://doi.org/10.1209/0295-5075/97/22002>
- [269] Data Sheet Luxium Solutions BC-400, Obtained March 2024, <https://luxium-solutions.com/radiation-detection-scintillators/plastic-scintillators/bc400bc404-bc408-bc412-bc416>
- [270] Data Sheet Luxium Solutions BC-408, Obtained March 2024, <https://luxium-solutions.com/radiation-detection-scintillators/plastic-scintillators/bc400bc404-bc408-bc412-bc416>
- [271] Data Sheet Luxium Solutions BC-412, Obtained March 2024, <https://luxiumsolutions.com/radiation-detection-scintillators/plastic-scintillators/bc400bc404-bc408-bc412-bc416>
- [272] Data Sheet Luxium Solutions BC-428, Obtained March 2024, <https://luxiumsolutions.com/radiation-detection-scintillators/plastic-scintillators/greenemitting-bc-428>
- [273] Data Sheet Luxium Solutions BC-430, Obtained March 2024, <https://luxiumsolutions.com/radiation-detection-scintillators/plastic-scintillators/redemitting-bc-430>
- [274] Data Sheet Luxium Solutions Lead Loaded BC-452, Obtained March 2024, <https://luxiumsolutions.com/radiation-detection-scintillators/plastic-scintillators/leadloaded-bc-452>

- [275] Data Sheet Eljen Technology EJ-200, Obtained March 2024, <https://eljen-technology.com/products/plastic-scintillators/ej-200-ej-204-ej-208-ej-212>
- [276] Data Sheet Eljen Technology EJ-240, Obtained March 2024, <https://eljen-technology.com/products/plastic-scintillators/ej-240>
- [277] Data Sheet Eljen Technology EJ-260, Obtained March 2024, <https://eljen-technology.com/products/plastic-scintillators/ej-260-ej-262>
- [278] Data Sheet Eljen Technology Lead Loaded EJ-256, Obtained March 2024, <https://eljentechnology.com/products/plastic-scintillators/ej-256>
- [279] International Electrotechnical Commission., "IEC 61267:2005 standard, Medical diagnostic X-ray equipment- Radiation conditions used in the determination of characteristics" (2005)
- [280] K. rajendran, M. Petersilka, A. Henning, E. R. Shanblatt, B. Schmidt, T. G. Flohr, A. Ferrero, F. Baffour, F. E. Diehn, L. Yu, P. Rajiah, J. G. Fletcher, S. Leng, C. H. McCollough, *Radiology* 303 (2022) 1, <https://doi.org/10.1148/radiol.212579>
- [281] D. Surrat, M. Bardies, N. Boussion, N. Freud, S. Jan, J-M. Letang, G. Lourdos, L. Maigne, S. Marcatili, T. Mauxion, P. Papadimitroulas, Y. Perrot, U. Pietrzyk, C. Robert, D. R. Schaart, D. Visvikis, I. Buvat, *Medical Physics* 41 (2014) 6, <https://doi.org/10.1118/1.4871617>
- [282] K. Taguchi, C. Polster, O. Lee, K. Stierstorfer, S. Kappler, *Medical Physics* 43 (2016) 12, <https://doi.org/10.1118/1.4966699>
- [283] C. van Aarle, N. Roturier, D. A. Biner, K. W. Krämer, P. Dorenbos, *Optical Materials* 145 (2023) 114375, <https://doi.org/10.1016/j.optmat.2023.114375>
- [284] Y. Yokota, T. Ito, M. Yoshino, A. Yamaji, Y. Ohashi, S. Kurosawa, K. Kamada, A. Yoshikawa, *Jpn. J. Appl. Phys.* 57 (2018) 070312, <https://doi.org/10.7567/JJAP.57.070312>
- [285] J. Glodo, E. V. D. van Loef, C. Kyba, J. S. Karp, K. S. Shah, *IEEE Nuclear Science Symposium Conference Record* (2007) 2178, 10.1109/NSS-MIC.2007.4436583
- [286] J. Ueda, P. Dorenbos, A. J. J. Bos, A. Meijerink, S. Tanabe, *J. Phys. Chem. C* 119 (2015) 25003, <https://doi.org/10.1021/acs.jpcc.5b08828>
- [287] J. Ueda, *J. Ceram. Soc. Jpn.* 123 (2015) 1059, <https://doi.org/10.2109/jcersj2.123.1059>
- [288] Y.-C. Lin, M. Bettinelli, M. Karlsson, *Chem. Mater.* 31 (2019) 3851, <https://doi.org/10.1021/acs.chemmater.8b05300>
- [289] L. Jiang, X. Zhang, S. Zhu, H. Tang, Q. Li, W. Zhang, X. Mi, L. Lu, H. Liu, X. Liu, *J. Mater. Sci.- Mater. Electron.* 29 (2018) 9045, <https://doi.org/10.1007/s10854-018-8930-6>



Supplementary Information

Table S I: Components of the decay time of Ce^{3+} doped scintillators for which average values are tabulated in the main text.

Compound	τ_{dec} (ns)	Ref	Compound	τ_{dec} (ns)	Ref
LaCl ₃	26 (70%)	[1–3]	Cs ₃ LaCl ₆	79 (32%)	[9]
	210 (30%)			291 (33%)	
LuCl ₃	56 (45%)	[2, 4]		Cs ₃ GdCl ₆	
	337 (25%)		39 (7%)		
	5900 (30%)		129 (12%)		
Cs ₂ LiGdCl ₆	129 (51%)	[5]	462 (15%)		
	573 (32%)		2110 (66%)		
	8900 (17%)		Tl ₂ LiGdCl ₆	34 (81%)	[12]
Cs ₂ LiLaCl ₆	2 (9%)	191 (10%)			
	40 (11%)	[6]		1200 (9%)	
	450 (80%)		Tl ₂ LiYCl ₆	57 (3%)	[13]
KGd ₂ Cl ₇	50 (40%)	431 (64%)			
	200 (60%)	[7]		1055 (33%)	
Rb ₂ LiGdCl ₆	107 (21%)		[8]	Tl ₂ LaCl ₅	36 (90%)
	791 (41%)	217 (6%)			
	4100 (38%)	1500 (34%)			
Cs ₂ NaLaCl ₆	40 (33%)	[9]	Tl ₂ LiLuCl ₆	72 (8%)	[16]
	105 (33%)			366 (30%)	
	338 (14%)			1500 (62%)	
	1848 (20%)		Tl ₂ GdCl ₅	32 (76%)	[17]
Cs ₂ NaGdCl ₆	107 (23%)	271 (10%)			
	697 (41%)	[10, 11]		1600 (14%)	
	3600 (36%)				

Table S I: Continued

Compound	τ_{dec} (ns)	Ref	Compound	τ_{dec} (ns)	Ref
Cs ₂ NaCeCl ₆	91 (36%)	[18]	LuBr ₃	19 (33%)	[2, 4]
	601 (33%)			369 (22%)	
	3200 (31%)			3600 (45%)	
Cs ₂ LiCeCl ₆	101 (42%)	[19]	GdBr ₃	20 (26%)	[29]
	557 (35%)			212 (65%)	
	2900 (23%)			1300 (9%)	
Cs ₃ CeCl ₆	50 (50%)	[20]	Cs ₂ LiYBr ₆	65 (11%)	[30, 31]
	300 (50%)			2500 (89%)	
Rb ₂ LiCeCl ₆	71 (85%)	[21]	Cs ₂ NaLaBr ₆	48 (20%)	[9, 32]
	405 (15%)			205 (21%)	
Cs ₂ NaLaCl ₆	66 (26%)	[9]		854 (23%)	
	340 (18%)			4021 (36%)	
	1620 (56%)				
CsSrCl ₃	3.8 (23%)	[22]	Cs ₂ NaLuBr ₆	61 (65%)	[32]
	57 (23%)			350 (35%)	
	626 (54%)				
Cs ₂ LiLaBr ₆	122 (61%)	[23–25]	Cs ₂ NaYBr ₆	61 (26%)	[32]
	661 (39%)			350 (23%)	
LaBr ₃ :Ce,Sr		[26–28]	Cs ₃ LaBr ₆	2700 (51%)	[9, 33]
	16.8 (56%)			44 (17%)	
	56 (16%)			124 (18%)	
	240 (16%)			399 (20%)	
	1530 (12%)			2230 (45%)	

Table S I: Continued

Compound	τ_{dec} (ns)	Ref	Compound	τ_{dec} (ns)	Ref
Rb ₂ LiYBr ₆	42 (35%)	[34]	Cs ₂ LiGdBr ₆	73 (63%)	[39]
	250 (32%)			542 (14%)	
	1400 (33%)			3900 (23%)	
Rb ₂ LiLaBr ₆	26 (5%)	[35]	Tl ₂ LiGdBr ₆	29 (92%)	[40]
	310 (37%)			197 (8%)	
	1100 (58%)		Cs ₂ NaCeBr ₆	140 (94%)	[41]
BaBr ₂	80 (27%)	[36]	Rb ₂ LiCeBr ₆	55 (87%)	[5]
	490 (22%)			284 (13%)	
	2100 (51%)		CsCe ₂ Br ₇	78 (52%)	[42]
Cs ₂ NaGdBr ₆	72 (67%)	[10, 37]	CsCe ₂ Br ₇	316 (32%)	[42]
	266 (22%)			1723 (16%)	
	698 (11%)			CeBr ₃ :Sr	
Cs ₂ NaLaBr ₃ I ₃	78 (25%)	[38]	CeBr ₃ :Sr	211 (3%)	[43–45]
	294 (40%)			86 (76%)	
	1338 (34%)		Cs ₂ LiCeBr ₆	444 (8%)	[46]
Cs ₂ NaYBr ₃ I ₃	56 (47%)	[38]	Cs ₂ LiCeBr ₆	3800 (16%)	[46]
	284 (25%)			31 (70%)	
	2060 (28%)		LaBr _{2.25} I _{0.75}	224 (30%)	[47]
Cs ₃ GdBr ₆	72 (26%)	[10]	LuI ₃	23 (75%)	[48–50]
	270 (25%)			120 (25%)	
	1421 (49%)				

Table S I: Continued

Compound	τ_{dec} (ns)	Ref	Compound	τ_{dec} (ns)	Ref
Cs ₃ Lu ₂ I ₉	18 (2%)	[33]	LuAlO ₃	17 (90%)	[55]
	42 (6%)			88 (10%)	
	120 (40%)		Gd ₂ SiO ₅	56 (89%)	[56, 57]
	510 (52%)			600 (11%)	
SrI ₂ :Ce,Na	32 (46%)	[51]	K ₂ Lu(PO ₄) ₂	34 (81%)	[58]
	450 (54%)			1200 (19%)	
YAlO ₃	26 (90%)	[52–54]			
	67 (10%)				

Table S II: Components of the decay time of Eu²⁺ doped scintillators for which average values are tabulated in the main text.

Compound	τ_{dec} (ns)	Ref	Compound	τ_{dec} (ns)	Ref
BaCl ₂	25 (15%)	[36, 59]	Rb ₄ CaBr ₆	2830 (79%)	[64]
	138 (21%)			8520 (21%)	
	642 (64%)		TlSr ₂ I ₅	525 (73%)	[65]
BaBr ₂	35 (8%)	3300 (27%)			
	415 (47%)	KSr ₂ I ₅	990 (89%)	[66]	
	814 (45%)		5000 (11%)		
BaBrI	297 (23%)	[61, 62]	KCaI ₃ :Eu,Zr	1030 (88%)	[67]
	482 (77%)			2260 (12%)	
KSr ₂ Br ₅	520 (21%)	[63]			
	1076 (79%)				

Table S III: Components of the decay time of Pr³⁺, Sm²⁺, and Tl⁺ doped scintillators for which average values are tabulated in the main text.

Compound	τ_{dec} (ns)	Ref	Compound	τ_{dec} (ns)	Ref
(Lu,Y) ₃ Al ₅ O ₁₂ :Pr	43.9 (55%)	[68–70]	CsBa ₂ I ₅ :Eu,Sm	240 (6%)	[71]
	333 (24%)			2090 (94%)	
	1374 (21%)				
(Lu,Y) ₃ Al ₅ O ₁₂ :Pr,Li	47.8 (47%)	[70]	NaI:Tl,Ca	172 (92%)	[72]
	374 (27%)			860 (8%)	
	1461 (26%)			173 (94%)	

Table S IV: Components of the decay time of intrinsic scintillators for which average values are tabulated in the main text.

Compound	τ_{dec} (ns)	Ref	Compound	τ_{dec} (ns)	Ref
TlMgCl ₃	46 (9%)	[73]	TlCaI ₃	62 (13%)	[73]
	166 (23%)			200 (62%)	
	449 (68%)			1440 (25%)	
TlCaCl ₃	317 (44%)	[74]	TlSr ₂ I ₅	151 (33%)	[65]
	727 (56%)			605 (39%)	
Tl ₂ HfCl ₆	300 (15%)	[75, 76]			
	1100 (85%)		RbSrI ₃	375 (71%)	[79]
Tl ₂ ZrCl ₆	500 (2%)	[75, 76]			
	2300 (98%)		CaWO ₄	1400 (30%)	[80–82]
TlSr ₂ Br ₅	390 (66%)	[77]			
	1900 (34%)				
TlCaBr ₃	56 (76%)	[78]			
	2490 (24%)				

Table S IV:Continued

Compound	τ_{dec} (ns)	Ref
CdWO ₄	5000 (60%)	[83, 84]
	20000 (40%)	
PbWO ₄	2.2 (50%%)	[85–87]
	9.9 (34%)	
	39 (16%)	
Sc ₂ O ₃	64 (8%)	[88]
	295 (92%)	

Table S V: Components of the decay time of intrinsic scintillators which show core-valence emission for which average values are tabulated in the main text.

Compound	τ_{dec} (ns)	Ref
BaF ₂	1 (20%)	[89–91]
	630 (80%)	
Cs ₂ LiYCl ₆	4 (10%)	[30, 92]
	6600 (90%)	

Table S VI: Components of the decay time of plastic scintillators for which average values are tabulated in the main text.

Compound	τ_{dec} (ns)	Ref
p-Terphenyl	2.1 (97%)	[93, 94]
	22.6 (3%)	

References

- [1] E. V. D. van Loef, P. Dorenbos, C. W. E. van Eijk, K. Krämer, H. U. Güdel, *Applied Physics Letters* 77 (2000) 10, <https://doi.org/10.1063/1.1308053>
- [2] O. Guillot-Noel, J. T. M. De Haas, P. Dorenbos, C. W. E. van Eijk, K. Krämer, H. U. Gundel, *Journal of Luminescence* 85 (1999) 1-3, [https://doi.org/10.1016/S0022-2313\(99\)00063-0](https://doi.org/10.1016/S0022-2313(99)00063-0)
- [3] K. S. Shah, J. Glodo, M. Klugerman, L. Cirignano, W. W. Moses, S. E. Derenzo, M. J. Weber, *Nuclear Instruments and Methods in Physics Research Section A: Accelerators, Spectrometers, Detectors and Associated Equipment* 505 (2003) 1-2, [https://doi.org/10.1016/S01689002\(03\)01024-6](https://doi.org/10.1016/S01689002(03)01024-6)
- [4] E. V. D. van Loef, P. Dorenbos, C. W. E. van Eijk, K. W. Krämer, H. U. Güdel, *Nuclear Instruments and Methods in Physics Research Section A: Accelerators, Spectrometers, Detectors and Associated Equipment* 496 (2003) 1, [https://doi.org/10.1016/S0168-9002\(02\)01634-0](https://doi.org/10.1016/S0168-9002(02)01634-0)
- [5] G. Rooh, H. J. kim, S. Kim, *Radiation Measurements* 45 (2010) 3-6, <https://doi.org/10.1016/j.radmeas.2009.10.018>
- [6] J. Glodo, R. Hawrami, E. van Loef, W. Higgins, U. Shirwadkar, K. S. Shah, *Proceedings Volume 7449, Hard X-ray, Gamma-ray, and neutron detector physics XI: 74490E* (2009), <https://doi.org/10.1117/12.830127>
- [7] M. Zhuravleva, K. Yang, A. Green, C. L. Melcher, *Journal of Crystal Growth* 318 (2011) 1, <https://doi.org/10.1016/j.jcrysgro.2010.10.206>
- [8] G. Rooh, H. J. Kim, H. Park, S. Kim, *Journal of Crystal Growth* 377 (2013) 28-31, <https://doi.org/10.1016/j.jcrysgro.2013.04.036>
- [9] G. Gundiah, K. Brennan, Z. Yan, E. C. Samulon, G. Wu, G. A. Bizarri, S. E. Derenzo, E. D. Bourret-Courchesne, *Journal of Luminescence* 149 (2014) 374-384, <https://doi.org/10.1016/j.jlumin.2013.09.057>
- [10] E. C. Samulon, G. Gundiah, M. Gascon, I. V. Khodyuk, S. E. Derenzo, G. A. Bizarri, E. D. Bourret-Courchesne, *Journal of Luminescence* 153 (2014) 64-72, <https://doi.org/10.1016/j.jlumin.2014.02.021>
- [11] G. Rooh, H. J. Kim, H. Park, S. Kim, H. Jiang, *IEEE Transactions on Nuclear Science* 61 (2014) 1, <https://doi.org/10.1109/TNS.2013.2283882>
- [12] H. J. Kim, G. Rooh, H. Park, S. Kim, *Journal of Luminescence* 164 (2015) 86-89, <https://doi.org/10.1016/j.jlumin.2015.03.026>
- [13] R. Hawrami, E. Ariesanti, L. Soundara-Pandian, J. Glodo, K. S. Shah, *IEEE Transactions on Nuclear Science* 63 (2016) 6, <https://doi.org/10.1109/TNS.2016.2627523>
- [14] H. J. Kim, G. Rooh, S. Kim, *Journal of Luminescence* 186 (2017) 219-222, <https://doi.org/10.1016/j.jlumin.2017.02.042>

- [15] R. Hawrami, E. Ariesanti, H. Wei, J. Finkelstein, J. Glodo, K. S. Shah, *Nuclear Instruments and Methods in Physics Research Section A: Accelerators, Spectrometers, Detectors and Associated Equipment* 869 (2017) 107-109, <https://doi.org/10.1016/j.nima.2017.06.016>
- [16] G. Rooh, H. J. Kim, J. Jang, S. Kim, *Journal of Luminescence* 187 (2017) 347-351, <https://doi.org/10.1016/j.jlumin.2017.03.051>
- [17] A. Khan, G. Rooh, H. J. Kim, S. Kim, *Journal of Alloys and Compounds* 741 (2018) 878-882, <https://doi.org/10.1016/j.jallcom.2018.01.204>
- [18] G. Rooh, H. Kang, H. J. Kim, H. Park, S. Kim, *Journal of Crystal Growth* 311 (2009) 8, <https://doi.org/10.1016/j.jcrysgr.2009.01.091>
- [19] G. Rooh, H. J. Kim, S. Kim, *IEEE Transactions on Nuclear Science* 57 (2010) 3, <https://doi.org/10.1109/TNS.2009.2037903>
- [20] M. Zhuravleva, K. yang, C. L. Melcher, *Journal of Crystal Growth* 318 (2011) 1, <https://doi.org/10.1016/j.jcrysgr.2010.11.090>
- [21] G. Rooh, H. J. Kim, H. Park, S. Kim, *IEEE Transactions on Nuclear Science* 59 (2012) 5, <https://doi.org/10.1109/TNS.2012.2200907>
- [22] Y. Fujimoto, K. Saeki, D. Nakauchi, T. Yanagida, M. Koshimizu, K. Asai, *Sensors and Materials* 29 (2017) 10, <https://doi.org/10.18494/SAM.2017.1622>
- [23] J. Glodo, E. van Loef, R. Hawrami, W. M. Higgins, A. Churilov, U. Shirwadkar, K. S. Shah, *IEEE Transactions on Nuclear Science* 58 (2011) 1, <https://doi.org/10.1109/TNS.2010.2098045>
- [24] J. Qin, J. Xiao, T. Zhu, X. Lu, Z. Han, M. Wang, L. Jiang, Y. Mou, J. Sun, Z. Wen, X. Wang, *Nuclear Instruments and Methods in Physics Research Section A: Accelerators, Spectrometers, Detectors and Associated Equipment* 905 (2018) 112-118, <https://doi.org/10.1016/j.nima.2018.05.006>
- [25] K. Yang, P. R. Menge, J. Lejay, V. Ouspenski, *IEEE Nuclear Science Symposium and Medical Imaging Conference* (2013) 1-6, <https://doi.org/10.1109/NS-SMIC.2013.6829676>
- [26] M. S. Alekhin, J. T. M. de Haas, I. V. Khodyuk, K. W. Krämer, P. R. Menge, V. Ouspenski, P. Dorenbos, *Applied Physics Letters* 102 (2013) 161915, <https://doi.org/10.1063/1.4803440>
- [27] K. Yang, P. R. Menge, J. J. Buzniak, V. ouspenski, *IEEE Nuclear Science Symposium and Medical Imaging Conference Record (NSS/MIC)* 2012 308-311, <https://doi.org/10.1109/NSSMIC.2012.6551113>
- [28] M. S. Alekhin, D. A. Biner, K. W. Krämer, P. Dorenbos, *Journal of Applied Physics* 113 (2013) 224904, <https://doi.org/10.1063/1.4810848>
- [29] E. V. D. van Loef, P. Dorenbos, C. W. E. van Eijk, K. W. Krämer, H. U. Güdel, *Optics Communications* 189 (2001) 4-6, [https://doi.org/10.1016/S0030-4018\(01\)01039-2](https://doi.org/10.1016/S0030-4018(01)01039-2)

- [30] A. Bessiere, P. Dorenbos, C. W. E. van Eijk, K. W. Krämer, H. U. Güdel, *IEEE Transactions on Nuclear Science* 51 (2004) 5, <https://doi.org/10.1109/TNS.2004.834957>
- [31] U. Shirwadkar, J. Glodo, E. van Loef, R. hawrami, S. Mukhopadhyay, K. S. Shah, *IEEE Nuclear Science Symposium and Medical Imaging Conference 2010* 1585-1588, <https://doi.org/10.1109/NSSMIC.2010.5874043>
- [32] M. D. Birowosuto, P. Dorenbos, C. W. E. van Eijk, K. W. Krämer, H. U. Güdel, *Journal of Physics: Condensed Matter* 18 (2006) 6133, <https://doi.org/10.1088/0953-8984/18/26/031>
- [33] M. D. Birowosuto, P. Dorenbos, C. W. E. van Eijk, K. W. Krämer, H. U. Güdel, *Physica Status Solidi A Applications and Materials Science* 204 (2007) 3, <https://doi.org/10.1002/pssa.200622459>
- [34] M. D. Birowosuto, P. Dorenbos, J. T. M. de Haas, C. W. E. van Eijk, K. W. Krämer, H. U. Güdel, *Journal of Applied Physics* 101 (2007) 6, <https://doi.org/10.1063/1.2713948>
- [35] M. D. Birowosuto, P. Dorenbos, J. T. M. de Haas, C. W. E. van Eijk, K. W. Krämer, H. U. Güdel, *IEEE Transactions on Nuclear Science* 55 (2008) 3, <https://doi.org/10.1109/TNS.2008.922826>
- [36] J. Selling, S. Schweizer, M. D. Birowosuto, P. Dorenbos, *IEEE Transactions on Nuclear Science* 55 (2008) 3, <https://doi.org/10.1109/TNS.2008.922825>
- [37] G. Rooh, H. J. Kim, H. Park, S. Kim, *Journal of Luminescence* 132 (2012) 3, <https://doi.org/10.1016/j.jlumin.2011.10.015>
- [38] H. Wei, L. Stand, M. Zhuravleva, F. Meng, V. Martin, C. L. Melcher, *Optical Materials* 38 (2014) 154-160, <https://doi.org/10.1016/j.optmat.2014.09.038>
- [39] G. Rooh, H. J. Kim, H. Park, S. Kim, *Journal of Luminescence* 146 (2014) 404-407, <https://doi.org/10.1016/j.jlumin.2013.09.047>
- [40] H. J. Kim, G. Rooh, H. Park, S. Kim, *Radiation Measurements*, 90 (2016) 279-281, <https://doi.org/10.1016/j.radmeas.2015.12.021>
- [41] S. Kim, G. Rooh, H. J. Kim, W. Kim, U. hong, *IEEE Transactions on Nuclear Science* 57 (2010) 3, <https://doi.org/10.1109/TNS.2010.2041789>
- [42] Y. Wu, H. Shi, B. C. Chakoumakos, M. Zhuravleva, M.-H. Du, C. L. Melcher, *Journal of Materials Chemistry C* 3 (2015) 11366-11376, <https://doi.org/10.1039/C5TC02721G>
- [43] P. Guss, M. E. Foster, B. M. Wong, F. P. Doty, K. Shah, M. R. Squillante, U. Shirwadkar, R. Hawrami, J. Tower, D. Yuan, *Journal of Applied Physics* 115 (2014) 034908, <https://doi.org/10.1063/1.4861647>

- [44] F. G. A. Quarati, M. S. Alekhin, K. W. Krämer, P. Dorenbos, *Nuclear Instruments and Methods in Physics Research Section A: Accelerators, Spectrometers, Detectors and Associated Equipment* 735 (2014) 655-658, <https://doi.org/10.1016/j.nima.2013.10.004>
- [45] R. H. P. Awater, K. W. Krämer, P. Dorenbos, *IEEE Transactions on Nuclear Science* 62 (2015) 5, <https://doi.org/10.1109/TNS.2015.2463736>
- [46] J. K. Cheon, S. Kim, G. Rooh, J.H. So, H. J. Kim, H. Park, *Nuclear Instruments and Methods in Physics Research Section A: Accelerators, Spectrometers, Detectors and Associated Equipment* 652 (2011) 1, <https://doi.org/10.1016/j.nima.2011.02.038>
- [47] M. D. Birowosuto, P. Dorenbos, K. W. Krämer, H. U. Güdel, *Journal of Applied Physics* 103 (2008) 103517, <https://doi.org/10.1063/1.2930884>
- [48] Birowosuto, P. Dorenbos, C. W. E. van Eijk, K. W. Krämer, H. U. Güdel, *IEEE Transactions on Nuclear Science* 52 (2005) 4, <https://doi.org/10.1109/TNS.2005.852630>
- [49] M. D. Birowosuto, P. Dorenbos, C. W. E. van Eijk, K. W. Krämer, H. U. Güdel, *Journal of Applied Physics* 99 (2005) 1235200, <https://doi.org/10.1063/1.2207689>
- [50] K. S. Shah, J. Glodo, M. Klugerman, W. Higgins, T. Gupta, P. Wong, W. W. Moses, S. E. Derenzo, M. J. Weber, P. Dorenbos, *IEEE Transactions on Nuclear Science* 51 (2004) 5, <https://doi.org/10.1109/TNS.2004.832321>
- [51] C. M. Wilson, E. V. van Loef, J. Glodo, N. Cherepy, G. Hull, S. Payne, W.-S. Choong, W. Moses, K. S. Shah, *Proceedings Volume 7079, Hard X-ray, Gamma-Ray and Neutron Detector PhysicsX*, 707917 (2008), <https://doi.org/10.1117/12.806291>
- [52] J. T. M. de Haas, P. Dorenbos, C. W. E. van Eijk, *Nuclear Instruments and Methods in Physics Research Section A: Accelerators, Spectrometers, Detectors and Associated Equipment* 537 (2005) 1-2, <https://doi.org/10.1016/j.nima.2004.07.243>
- [53] M. Kapusta, M. Balcerzyk, M. Moszynski, J. Pawelke, *Nuclear Instruments and Methods in Physics Research Section A: Accelerators, Spectrometers, Detectors and Associated Equipment* 421 (1999) 3, [https://doi.org/10.1016/S0168-9002\(98\)01232-7](https://doi.org/10.1016/S0168-9002(98)01232-7)
- [54] S. E. Dorenzo, M. J. Weber, W. W. Moses, C. Dujardin, *IEEE Transactions on Nuclear Science* 47 (2000) 3, <https://doi.org/10.1109/23.856531>
- [55] M. Moszynski, D. Wolski, T. Ludziejewski, M. Kapusta, A. Lempicki, C. Brecher, D. Wisniewski, A. J. Wojtowicz, *Nuclear Instruments and Methods in Physics Research Section A: Accelerators, Spectrometers, Detectors and Associated Equipment* 385 (1997) 1, [https://doi.org/10.1016/S0168-9002\(96\)00875-3](https://doi.org/10.1016/S0168-9002(96)00875-3)
- [56] E. Sakai, *IEEE Transactions on Nuclear Science* 34 (1987) 1, <https://doi.org/10.1109/TNS.1987.4337375>

- [57] M. Balcerzyk, M. Moszynski, M. Kapusta, D. Wolski, J. Pawelke, C. L. Melcher, *IEEE Transactions on Nuclear Science* 47 (2000) 4, <https://doi.org/10.1109/23.872971>
- [58] D. Wisniewski, A. J. Wojtowicz, W. Drozdowski, J. M. Farmer, L. A. Boatner, *Journal of Alloys and Compounds* 380 (2004) 1-2, <https://doi.org/10.1016/j.jallcom.2004.03.042>
- [59] Z. Yan, G. Bizarri, E. Gourret-Courchesne, *Nuclear Instruments and Methods in Physics Research Section A: Accelerators, Spectrometers, Detectors and Associated Equipment* 698 (2013) 7-10 <https://doi.org/10.1016/j.nima.2012.09.026>
- [60] Z. Yan, G. Gundiah, G. A. Bizarri, E. C. Samulon, S. E. Derenzo, E. D. Bourret-Courchesne, *Nuclear Instruments and Methods in Physics Research Section A: Accelerators, Spectrometers, Detectors and Associated Equipment* 735 (2014) 83-87, <https://doi.org/10.1016/j.nima.2013.09.021>
- [61] G. Bizarri, E. D. Bourret-Courchesne, Z. Yan, S. E. Derenzo, *IEEE Transactions on Nuclear Science* 58 (2011) 6, <https://doi.org/10.1109/TNS.2011.2166999>
- [62] E. D. Bourret-Courchesne, G. Bizarri, S. M. Hanrahan, G. Gundiah, Z. Yan, S. E. Derenzo, *Nuclear Instruments and Methods in Physics Research Section A: Accelerators, Spectrometers, Detectors and Associated Equipment* 613 (2010) 1, <https://doi.org/10.1016/j.nima.2009.11.036>
- [63] L. Stand, M. Zhuravleva, H. Wei, C. L. Melcher, *Optical Materials* 46 (2015) 59-63, <https://doi.org/10.1016/j.optmat.2015.04.002>
- [64] K. S. Pestovich, L. Stand, E. van Loef, C. L. Melcher, M. Zhuravleva, *IEEE Transactions on Nuclear Science* 70 (2023) 7, <https://doi.org/10.1109/TNS.2023.3280733>
- [65] H. J. Kim, G. Rooh, A. Khan, H. Park, S. Kim, *Optical materials* 82 (2018) 7-10, <https://doi.org/10.1016/j.optmat.2018.05.036>
- [66] L. Stand, M. Zhuravleva, A. Lindsey, C. L. Melcher, *Nuclear Instruments and Methods in Physics Research Section A: Accelerators, Spectrometers, Detectors and Associated Equipment* 780 (2015) 40-44, <https://doi.org/10.1016/j.nima.2015.01.052>
- [67] Y. Wu, Q. Li, D. J. rutstrom, M. Zhuravleva, M. Loyd, I. Stand, M. Koschan, C. L. Melcher, *Physica Status Solidi Rapid Research Letters* 12 (2018) 2, <https://doi.org/10.1002/pssr.201700403>
- [68] J. A. Mares, M. Nikl, A. Beitlerova, P. Horodysky, K. Blazek, K. Bartos, C. D'Ambrosio, *IEEE Transactions on Nuclear Science* 59 (2012) 5, <https://doi.org/10.1109/TNS.2012.2191573>
- [69] W. Drozdowski, K. Brylew, A. J. Wojtowicz, J. Kisielewski, M. Swirkowicz, T. Lukasiewicz, J. T. M. de Haas, P. Dorenbos, *Optical Materials Express* 4 (2014) 6, <https://doi.org/10.1364/OME.4.001207>

- [70] C. Foster, Y. Wu, M. Koschan, C. L. Melcher, *Physica Status Solidi Rapid Research Letters* 12 (2018) 9, <https://doi.org/10.1002/pssr.201800280>
- [71] W. Wolszczak, K. W. Krämer, P. Dorenbos, *Physica Status Solidi Rapid Research Letters* 13 (2019) 9, <https://doi.org/10.1002/pssr.201900158>
- [72] K. Yang, P. R. Menge, *Journal of Applied Physics* 118 (2015) 21, <https://doi.org/10.1063/1.4937126>
- [73] R. Hawrami, E. Ariesanti, H. Wei, J. Finkelstein, J. Glodo, K. S. Shah, *Journal of Crystal Growth* 475 (2017) 216-219, <https://doi.org/10.1016/j.jcrysgro.2017.06.012>
- [74] A. Khan, G. Rooh, H. J. Kim, H. Park, S. Kim, *Radiation Measurements* 107 (2017) 115-118, <https://doi.org/10.1016/j.radmeas.2017.09.003>
- [75] R. Hawrami, E. Ariesanti, V. Buliga, A. Burger, S. Lam, S. Motakef, *Journal of Crystal Growth* 531 (2020) 125316, <https://doi.org/10.1016/j.jcrysgro.2019.125316>
- [76] Y. Fujimoto, K. Saeki, D. Nakauchi, T. Yanagida, M. Koshimizu, K. Asai, *Sensors and Materials* 30 (2018) 7, <https://doi.org/10.18494/SAM.2018.1927>
- [77] G. Rooh, A. Khan, H. J. Kim, H. Park, S. Kim, *Optical Materials* 73 (2017) 523-526, <https://doi.org/10.1016/j.optmat.2017.08.047>
- [78] E. van Loef, L. S. Pandian, N. Kaneshige, G. Ciampi, L. Stand, D. Rutstrom, Y. Tratsiak, M. Zhuravleva, C. Melcher, K. S. Shah, *IEEE Transactions on Nuclear Science* 70 (2023) 7, <https://doi.org/10.1109/TNS.2023.3258065>
- [79] K. S. Pestovich, L. Stand, C. L. Melcher, E. van Loef, M. Zhuravleva, *Journal of Crystal Growth* 627 (2024) 1, <https://doi.org/10.1016/j.jcrysgro.2023.127540>
- [80] V. B. Mikhailik, H. Kraus, S. Henry, A. J. B. Tolhurst, *Physical Review B* 75 (2007) 184308, <https://doi.org/10.1103/PhysRevB.75.184308>
- [81] Y. G. Zdesenko, F. T. Avigone III, V. B. Brudanin, F. Danevich, S. S. Nagorny, I. M. Solsky, V. I. Tretyak, *Nuclear Instruments and Methods in Physics Research Section A: Accelerators, Spectrometers, Detectors and Associated Equipment* 538 (2005) 1-3, <https://doi.org/10.1016/j.nima.2004.09.030>
- [82] M. Moszynski, M. Balcerzyk, W. Czarnacki, A. Nassalski, T. Szczesniak, H. Kraus, V. B. Mikhailik, I. M. Solskii, *Nuclear Instruments and Methods in Physics Research Section A: Accelerators, Spectrometers, Detectors and Associated Equipment* 553 (2005) 3, <https://doi.org/10.1016/j.nima.2005.07.052>
- [83] C. L. Melcher, R. A. Manente, J. S. Schweitzer, *IEEE Transactions on Nuclear Science* 36 (1989) 1, <https://doi.org/10.1109/23.34629>
- [84] I. Holl, E. Lorenz, G. Mageras, *IEEE Transactions on Nuclear Science* 35 (1998) 1, <https://doi.org/10.1109/23.12684>

- [85] A. A. Annenkov, M. V. Korzhik, P. Lecoq, Nuclear Instruments and Methods in Physics Research Section A: Accelerators, Spectrometers, Detectors and Associated Equipment 490 (2002) 1-2, [https://doi.org/10.1016/S0168-9002\(02\)00916-6](https://doi.org/10.1016/S0168-9002(02)00916-6)
- [86] M. Kobayashi, M. Ishii, Y. Usuki, H. Yahagi, Nuclear Instruments and Methods in Physics Research Section A: Accelerators, Spectrometers, Detectors and Associated Equipment 333 (1993) 2-3, [https://doi.org/10.1016/0168-9002\(93\)91187-R](https://doi.org/10.1016/0168-9002(93)91187-R)
- [87] P. Lecoq, I. Dafinei, E. Auffray, M. Schneegans, M. V. Korzhik, O. V. Missevitch, V. B. Pavlenko, A. A. Fedorov, A. N. Annenkov, V. L. Kostylev, V. D. Ligon, Nuclear Instruments and Methods in Physics Research Section A: Accelerators, Spectrometers, Detectors and Associated Equipment 365 (1995) 2-3, [https://doi.org/10.1016/0168-9002\(95\)00589-7](https://doi.org/10.1016/0168-9002(95)00589-7)
- [88] A. Fukabori, L. An, A. Ito, V. Chani, K. Kamada, T. Goto, A. Yoshikawa, IEEE Transactions on Nuclear Science 59 (2012) 5, <https://doi.org/10.1109/TNS.2012.2206211>
- [89] M. Laval, M. Moszynski, R. Allemand, E. Cormoreche, P. Guinet, R. Odru, J. Vacher, Nuclear Instruments and Methods in physics Reserach 206 (1983) 1-2, [https://doi.org/10.1016/01675087\(83\)91254-1](https://doi.org/10.1016/01675087(83)91254-1)
- [90] M. Biasini, D. B. Cassidy, S. H. M. Dena, H. K. M. Tanaka, A. P. Mills, Nuclear Instruments and Methods in Physics Research Section A: Accelerators, Spectrometers, Detectors and Associated Equipment 553 (2005) 3, <https://doi.org/10.1016/j.nima.2005.07.022>
- [91] V. Nanal, B. B. Back, D. J. Horman, Nuclear Instruments and Methods in Physics Research Section A: Accelerators, Spectrometers, Detectors and Associated Equipment 389 (1997) 3, [https://doi.org/10.1016/S0168-9002\(97\)00326-4](https://doi.org/10.1016/S0168-9002(97)00326-4)
- [92] C. M. Combes, P. Dorenbos, C. W. E. van Eijk, K. W. Krämer, H. U. Güdel, Journal of Luminescence 82 (1999) 4, [https://doi.org/10.1016/S0022-2313\(99\)00047-2](https://doi.org/10.1016/S0022-2313(99)00047-2)
- [93] T. Yanagida, K. Watanabe, Y. Fujimoto, Nuclear Instruments and Methods in Physics Research Section A: Accelerators, Spectrometers, Detectors and Associated Equipment 784 (2015) 111-114, <https://doi.org/10.1016/j.nima.2014.12.031>
- [94] M. De Gerone, M. Biasotti, V. Ceriale, D. Corsini, F. Gatti, A. Orlando, G. Pizzigoni, Nuclear Instruments and Methods in Physics Research Section A: Accelerators, Spectrometers, Detectors and Associated Equipment 824 (2016) 192-193, <https://doi.org/10.1016/j.nima.2015.11.021>



Summary

The record energy resolution of 2%, measured using $\text{LaBr}_3:\text{Ce}^{3+},\text{Sr}^{2+}$, is currently limited by the number of detected scintillation photons, *i.e.*, Poisson statistics [1]. Increasing the number of detected scintillation photons can be realised in two different ways. The first one is by replacing photomultiplier tubes (PMT) by modern silicon based detectors, *e.g.* avalanche photodiodes (APD) and silicon photomultipliers (SiPM). Silicon based photodetectors typically have a much higher detection efficiency compared to photomultiplier tubes. In order to attain the best results, the emission wavelength of the scintillator should be matched to the wavelength of the maximum detection efficiency of the photodetector. This approach has for example been explored elaborately by Van Aarle *et al.* for silicon based detectors using Sm^{2+} based scintillators [2].

The second way to increase the number of detected scintillation photons is to increase the light yield of the scintillator, of which the theoretical limit scales inversely with the size of the bandgap. Scintillators are commonly based on the 5d-4f emission of Ce^{3+} or Eu^{2+} . The degree to which the bandgap can be decreased is thus limited by this emission; if the bandgap becomes too small, 5d-4f emission will no longer be observed [3]. An elaborate discussion on the bandgap and the occurrence of 5d-4f emission is presented in **Chapter 1**. This limitation can be avoided by shifting to intrinsic, or self activated, scintillators, which no longer rely on 5d-4f emission. The goal of this dissertation is to study small bandgap materials for their use as intrinsic scintillators. The development of small bandgap intrinsic scintillators is a largely unexplored field [4]. Initial studies have focused on the family of lead halide perovskites and related compounds [5,6], which have a bandgap of less than 3 eV and mainly gained popularity for their use in optoelectronic applications [7,8]. Due to their crystal structure, ABX_3 , consisting of a three dimensional network of corner sharing BX_6 octahedra perovskites are often referred to as three dimensional perovskites.

The main problem of perovskites, however, is their small Stokes shift which increases the probability of a scintillation photon being reabsorbed after emission. This increases the chance of scintillation photons reaching a quenching site. **Chapter 2** starts off with the scintillation characterisation of the caesium lead halide perovskites CsPbCl_3 and CsPbBr_3 . Both compounds show a sub nanosecond decay component at 10 K originating from near band edge excitons, which have a very small Stokes shift. Only under X-ray excitation a new broad emission band, with a very large Stokes shift, was observed at wavelengths longer than 700 nm. In the case of CsPbBr_3 this new broad emission band contained most of the scintillation photons and falls outside the effective detection range of a PMT. The combination of scintillation photons not leaving the crystal due to self-absorption or being emitted at wavelengths longer than 700 nm made it impossible to measure a pulse height spectrum for CsPbCl_3 and CsPbBr_3 .

Both Williams *et al.* [9] and Wolszczak *et al.* [10] have proposed potential solutions to deal with the self absorption problem of perovskites. One of the solutions is to shift to compounds with a lower dimensional crystal structure. In **Chapter 3**, the zero dimensional compound Cs_4PbBr_6 is studied. The crystal structure of Cs_4PbBr_6 , A_4BX_6 , consist of isolated BX_6 octahedra resulting in the formation of localised states on the BX_6 octahedra. This means that the emission of Cs_4PbBr_6 resembles the emission of isolated Pb^{2+} ions which has a large stokes shift. Depending on the synthesis method, Cs_4PbBr_6 can, next to a 380 nm emission band, also show a green emission band at 540 nm. This band can be linked to the presence of CsPbBr_3 inclusions. Additionally, a new emission band was discovered at 610 nm which can be linked too defects. Under X-ray excitation, most of the scintillation photons are present in the 610 nm emission band.

Another class of lower dimensional compounds which have been studied are the hybrid organic-inorganic perovskites, or two dimensional perovskites. In these compounds, the small A site cation in the perovskite structure is replaced by a larger organic molecule. This creates a structure of alternating layers of organic molecules and corner sharing sheets of BX_6 octahedra. In **Chapter 4** the scintillation properties of the two dimensional perovskite phenethylammonium lead bromide $((\text{PEA})_2\text{PbBr}_4)$ are explored. This compound crystallises in the Ruddlesden-Popper phase with a flat layer of PbBr_6 octahedra. Due to the exciton confinement, created by the organic layers, $(\text{PEA})_2\text{PbBr}_4$ shows room temperature near band edge exciton emission. Unfortunately it was found that part of the emission still suffers from self absorption. In **Chapter 5** the scintillation properties of the two dimensional perovskite benzylammonium lead bromide $((\text{BZA})_2\text{PbBr}_4)$ are explored. At room temperature $(\text{BZA})_2\text{PbBr}_4$ showed a decay time of 4 ns. This short decay time makes this material very interesting to be used in a scintillator-SiPM indirect photon counting detector (PCD). However, it shows similar self absorption related problems as $(\text{PEA})_2\text{PbBr}_4$. One of the effects of self absorption is that the decay time will increase when the crystal size increases. This means that the measured 4 ns decay time for $(\text{BZA})_2\text{PbBr}_4$ could be a direct result of the small samples used.

In **Chapter 6** the scintillation properties of CsCu_2I_3 are explored. CsCu_2I_3 is an interesting small bandgap material with many good scintillation properties, *i.e.*, it is nonhygroscopic, nontoxic, melts congruently, has a low afterglow, and a density and effective atomic number of 5.01 g/cm³ and 50.6, respectively. It has a one dimensional crystal structure formed by double chains of Cu_2I_3^- edge sharing tetrahedra, separated by Cs^+ ions. At room temperature, one emission band at 560 nm, related to self trapped exciton emission, is observed. The latter has a Stokes shift of 1.49 eV, preventing any self absorption related problems. Additionally, the 560 nm emission wavelength matches well with the detection efficiency of modern silicon based photodetectors. Previously, pulse height spectra for this material were only measured on a PMT. From a pulse height spectrum, measured on an APD, an energy resolution and light yield of 4.8% and 36.000 photons/MeV were determined, respectively. It should be noted that the used APD needs to be cooled to 260 K. The T_{50} temperature of CsCu_2I_3 is approximately 270 K,

which means that most of the emission will be quenched at room temperature. It is shown that upon cooling down to 200 K CsCu_2I_3 can reach a light yield of 60.000 photons/MeV by measuring a set of temperature dependent pulse height spectra.

The final Chapter of this dissertation, Chapter 7, focuses on the emerging development of scintillator-SiPM based indirect PCDs. These are detectors, contrary to the energy integrating detectors often used in traditional CT scanners, which detect individual photons. These detectors are based on a fast scintillator coupled to a SiPM with a very short recharge time. Both the scintillator and SiPM need to be fast in order to handle the high X-ray fluence rates used in CT-scanners. Current PCDs applied in CT scanners are based on the semiconductor CdTe. In **Chapter 7** a prospect view is presented on potential scintillators and their selection to be used in a scintillator SiPM based indirect PCD. Firstly a framework is presented based on which three figures of merit (FOM) are formulated. The first FOM is the total pulse intensity which represent the mean number of scintillation photons produced upon absorbing an X-ray photon in the medically relevant energy range (25 to 150 keV). This is related to the energy resolution of the PCD. The second FOM is the pulse duration which represents the length of the detector output pulse, consisting of a convolution of the scintillator decay and SiPM recharge time. The third FOM is the pulse amplitude which represents the amplitude of the detector output pulse. This provides an indication for the statistical fluctuations on the detector output pulse. These three FOMs are used to analyse a database of more than 200 scintillators for their use in indirect PCDs. The pulse duration of a CdTe based direct PCD (14 ns), also used in commercially available CT scanners, was used as a bench mark.

The pulse duration of Eu^{2+} , Yb^{2+} , Sm^{2+} , Ti^+ based scintillators, and broad band emitters are generally longer than 500 ns. Hence, these scintillators will not be able handle the X-ray fluence rates used in CT scanners and will suffer from significant pulse pile-up related problems. Two very promising potential candidates are Ce^{3+} and Pr^{3+} based scintillators. The pulse duration of Ce^{3+} based scintillators strongly depends on the host matrix. Next to the intrinsic decay of Ce^{3+} , slow components due to inefficient transfer to Ce^{3+} and host related emissions can be observed. The pulse duration of Pr^{3+} based scintillators also show a strong dependence on the host matrix, *i.e.*, whether efficient 5d-4f emission can occur or not. The shortest pulse durations are achieved by scintillators based on CVL emission, near bandgap excitonic emission, and plastic scintillators. Each of these categories however, has its own set of problems. For scintillators based on CVL emission it is the presence of slow components. For near bandgap exciton emission based scintillators it is self-absorption and for plastic scintillators it is their low density. It is also possible to quench the decay time of a scintillator in order to decrease the pulse duration. This approach is explored by simulating the detector output pulses along the quenching curve of a hypothetical scintillator. This demonstrates that the decay time of the scintillator should not become smaller than the recharge time of the SiPM, which otherwise will lead to the loss of scintillation photons. For all materials discussed in this Chapter it is important

to realise that not only the scintillator properties are important but also the properties of the photodetector used for readout, *i.e.*, the scintillator and photodetector can be tailored to each other. Hence, one should think in terms of a detection system consisting of both a scintillator crystal and a photodetector.

References

- [1] M. S. Alekhin, J. T. M. de Haas, I. V. Khodyuk, K. W. Krämer, P. R. Menge, V. Ouspenski, P. Dorenbos, *Applied physics letters* 102 (2013) 161915, <https://doi.org/10.1063/1.4803440>
- [2] C. van Aarle, *Black scintillators*, thesis Delft University of Technology (2024), ISBN: 978-94-6366-873-6, <http://resolver.tudelft.nl/uuid:37091b0a-1a34-4213-a2f1-4a883d4da721>
- [3] C. van Aarle, Chapter 7, *Black scintillators*, thesis Delft University of Technology (2024), ISBN: 978-94-6366-873-6, <http://resolver.tudelft.nl/uuid:37091b0a-1a34-4213-a2f1-4a883d4da721>
- [4] P. Dorenbos, *Optical Materials: X 1* (2019) 100021, <https://doi.org/10.1016/j.omx.2019.100021>
- [5] V. B. Mykhaylyk, H. Kraus, V. Kapustianyk, H. J. Kim, P. Mercere, M. Rudko, P. Da Silva, O. Antonyak, M. Dendebera, *Scientific Reports* 10 (2020) 8601, <https://doi.org/10.1038/s41598020-65672-z>
- [6] M. D. Bitowosuto, D. Cortecchia, W. Drozdowski, K. Brylew, W. Lachmanski, A. Bruno, C. Soci, *Scientific Reports* 6 (2016) 37254, <https://doi.org/10.1038/srep37254>
- [7] M. A. Green, A. Ho-Naillie, H. J. Snaith, *Nature Photonics* 8 (2014) 506, <https://doi.org/10.1038/nphoton.2014.134>
- [8] X. Y. Chin, D. Cortecchia, J. Yin, A. Bruno, C. Soci, *Nature Communications* 6 (2015) 7383, <https://doi.org/10.1038/ncomms8383>
- [9] R. T. Williams, W. W. Wolszczak, X. Yan, D. L. Carrol, *ACS Nano* 14 (2020) 5161-5169, <https://doi.org/10.1021/acsnano.0c02529>
- [10] W. W. Wolszczak, D. L. Carroll, R. T. Williams, *Advanced X-ray Detector Technologies*, Chapter 1 (2022), https://doi.org/10.1007/978-3-030-64279-2_1



Samenvatting

De record energieresolutie van 2%, gemeten met $\text{LaBr}_3:\text{Ce}^{3+},\text{Sr}^{2+}$, wordt momenteel beperkt door het aantal gedetecteerde scintillatiefotonen, *i.e.*, de Poisson statistiek [1]. Het aantal gedetecteerde scintillatiefotonen kan op twee manieren vergroot worden. De eerste manier is het vervangen van de fotonmultiplicatorbuizen {Engels: photomultiplier tubes} (PMT) door moderne op silicium gebaseerde detectoren, *e.g.*, lawinefotodiodes {Engels: avalanche photodiodes} (APD) en siliciumfotomultiplicatoren {Engels: silicon photomultipliers} (SiPM). Op silicium gebaseerde fotonendetectoren hebben doorgaans een veel hogere detectie-efficiëntie in vergelijking tot fotonmultiplicatorbuizen. Om de beste resultaten te behalen, moeten de emissiegolflengte van de scintillator en de golflengte van de maximale detectie-efficiëntie van de fotonendetector op elkaar afgestemd worden. Deze aanpak is bijvoorbeeld door Van Aarle *et al.* uitgebreid onderzocht voor silicium gebaseerde detectoren in combinatie met op Sm^{2+} gebaseerde scintillatoren [2].

De tweede manier om het aantal gedetecteerde scintillatiefotonen te vergroten, is door de lichtopbrengst van de scintillator te vergroten, waarvan het theoretisch limiet omgekeerd evenredig is met de grootte van de bandkloof. Scintillatoren zijn doorgaans gebaseerd op de 5d – 4f emissie van Ce^{3+} of Eu^{2+} . De mate waarin de bandkloof verkleind kan worden, wordt dus beperkt door deze emissie; als de bandkloof te klein wordt, kan de 5d – 4f emissie niet langer worden waargenomen [3]. Een uitgebreide bespreking van de invloed van de grootte van de bandkloof en het voorkomen van de 5d – 4f emissie wordt gepresenteerd in **Hoofdstuk 1**. Deze beperking kan worden omzeild door over te schakelen naar intrinsieke scintillatoren, ook wel zelf geactiveerde scintillatoren genoemd. Deze zijn niet langer afhankelijk van de aanwezigheid van 5d – 4f emissie. Het doel van dit proefschrift is om materialen met een kleine bandkloof te bestuderen voor hun toepassing als intrinsieke scintillatoren. De ontwikkeling van kleine bandkloof scintillatoren is een grotendeels onontgonnen gebied [4]. Initiële studies hebben zich gericht op de familie van lood halide perovskieten en verwante verbindingen [5,6]. Deze verbindingen hebben een bandkloof van 3 eV of minder en zijn voornamelijk populair geworden wegens hun gebruik in opto-elektronische toepassingen [7,8]. Vanwege hun kristalstructuur, ABX_3 , bestaande uit een driedimensionaal netwerk van hoekdelende BX_6 octaëders, worden perovskieten ook wel driedimensionale perovskieten genoemd.

Het grootste probleem van perovskieten is echter hun kleine Stokes-verschuiving. Hierdoor wordt de kans op reabsorptie van een scintillatiefoton verhoogt en kan deze eerder een doofplaats in het kristal rooster bereiken. **Hoofdstuk 2** begint met de scintillatiekarakterisatie van de cesium lood halide perovskieten CsPbCl_3 en CsPbBr_3 . Beide verbindingen vertonen een excitonische emissie band afkomstig van de randen van de bandkloof met een vervaltijd van minder dan een nanoseconde bij 10 K. Deze excitonische emissie banden hebben een zeer kleine Stokes-verschuiving. Alleen onder Röntgenexcitatie werd een nieu-

we brede emissieband, met een zeer grote Stokes-verschuiving, waargenomen bij golflengtes langer dan 700 nm. In het geval van CsPbBr_3 bevat deze brede emissieband de meeste scintillatiefotonen maar valt buiten het effectieve detectiebereik van een PMT. De combinatie van scintillatiefotonen die het kristal niet verlaten vanwege zelf-absorptie of die worden uitgezonden bij een golflengte langer dan 700 nm, maakt het onmogelijk om een puls hoogte spectrum te meten voor CsPbCl_3 en CsPbBr_3 .

Zowel Williams *et al.* [9] als Wolszczak *et al.* [10] hebben verscheidene oplossingen voorgedragen om het zelf-absorptie probleem van perovskieten aan te pakken. Een van de geformuleerde oplossingen is het overgaan op verbindingen met een lagere dimensionale kristalstructuur. In **Hoofdstuk 3** wordt de nuldimensionale verbinding Cs_4PbBr_6 bestudeerd. De kristalstructuur van Cs_4PbBr_6 , A_4BX_6 , bestaat uit geïsoleerde BX_6 octaëders, wat resulteert in de vorming van gelocaliseerde toestanden op de BX_6 octaëders. Dit betekent dat de emissie van Cs_4PbBr_6 lijkt op de emissie van geïsoleerde Pb^{2+} ionen, die een grote Stokes-verschuiving hebben. Afhankelijk van de synthesesmethode kan Cs_4PbBr_6 , naast zijn 380 nm emissieband, ook een groene emissieband vertonen bij 540 nm. Deze band kan gekoppeld worden aan de aanwezigheid van CsPbBr_3 microdomeinen. Daarnaast werd een nieuwe emissieband ontdekt bij 610 nm die gekoppeld kan worden aan de aanwezigheid van defecten. Onder röntgenexcitatie zijn de meeste scintillatiefotonen aanwezig in de 610 nm emissieband.

Een ander klasse van lager dimensionale verbindingen zijn de hybride organisch-anorganische perovskieten, ook wel tweedimensionale perovskieten genoemd. In deze verbindingen wordt het kleine A-site kation in de perovskiet structuur vervangen door een groter organisch molecuul. Dit creëert een structuur van afwisselende lagen aan organische moleculen en hoekdelende lagen van BX_6 octaëders. In **Hoofdstuk 4** worden de scintillatie-eigenschappen van het tweedimensionale perovskiet fenethylammonium lood bromide $((\text{PEA})_2\text{PbBr}_4)$ onderzocht. Deze verbinding kristalliseert in de Ruddlesden-Popper fase met een vlakke laag van PbBr_6 octaëders. De excitonische insluiting in de PbBr_6 laag, gecreëerd door de organische lagen, zorgt er voor dat $(\text{PEA})_2\text{PbBr}_4$ bij kamertemperatuur excitonische emissie afkomstig van de randen van de bandkloof vertoont. Helaas werd ontdekt dat een deel van de emissie nog steeds lijdt aan zelf-absorptie. In **Hoofdstuk 5** worden de scintillatie-eigenschappen van het twee dimensionale perovskiet benzylammonium lood bromide $((\text{BZA})_2\text{PbBr}_4)$ onderzocht. Bij kamertemperatuur vertoont $(\text{BZA})_2\text{PbBr}_4$ een vervaltijd van 4 ns. Deze korte vervaltijd maakt dit materiaal zeer interessant voor applicatie in een scintillator-SiPM indirecte fotonenteldetector {Engels: photon-counting detector} (PCD). Vergelijkbaar met $(\text{PEA})_2\text{PbBr}_4$ wordt de emissie van $(\text{BZA})_2\text{PbBr}_4$ ook beïnvloed door zelf-absorptie. Een onfortuinlijk neveneffect hiervan is dat de vervaltijd van $(\text{BZA})_2\text{PbBr}_4$ zal toenemen wanneer de kristalgrootte toeneemt. Dit betekent dat de gemeten vervaltijd van 4 ns een direct resultaat kan zijn van de kleine kristallen die gebruikt zijn voor de meting.

In **Hoofdstuk 6** worden de scintillatie-eigenschappen van CsCu_2I_3 onderzocht. CsCu_2I_3 is een interessant materiaal met een kleine bandkloof en veel goede scintillatie-eigenschappen, *i.e.*, het is niet-hygroscopisch, niet-toxisch, smelt congruent, heeft een laag nagloei niveau, en een dichtheid en effectief atoomnummer van respectievelijk 5.01 g/cm^3 en 50.6. Het heeft een eendimensionale kristalstructuur gevormd door dubbele ketens van Cs_2I_3^- randdelende tetraëders, gescheiden door Cs^+ ionen. Bij kamertemperatuur wordt één emissieband waargenomen bij 560 nm, deze kan worden gerelateerd aan zelf ingevangen excitonische emissie. De emissie heeft een Stokes-verschuiving van 1.49 eV waardoor zelf-absorptie gerelateerde problemen worden voorkomen. Bovendien komt de 560 nm emissiegolflengte goed overeen met de detectie-efficiëntie van moderne silicium gebaseerde fotonendetectors. Eerder gemeten pulshoogte spectra van CsCu_2I_3 zijn voornamelijk gemeten door gebruik te maken van fotonmultiplicatorbuizen. Uit een pulshoogte spectrum, gemeten op een APD, zijn een energieresolutie en licht opbrengst van respectievelijk 4.8% en 36.000 fotonen/MeV bepaald. Hierbij dient opgemerkt te worden dat de APD gekoeld moet worden tot een temperatuur van 260 K. De T_{50} temperatuur van CsCu_2I_3 is ongeveer 270 K. Dit betekent dat het grootste gedeelte van de emissie bij kamertemperatuur gedooft is. Er is ook aangetoond dat, als CsCu_2I_3 wordt afgekoeld tot 200 K, dat de lichtopbrengst kan toenemen tot 60.000 fotonen/MeV. Dit is bepaald aan de hand van een reeks temperatuurafhankelijke puls hoogte spectra.

Het slot hoofdstuk van dit proefschrift, Hoofdstuk 7, richt zich op de opkomende ontwikkeling van scintillator-SiPM gebaseerde indirecte PCD's. Dit zijn detectoren, in tegenstelling tot de energie-integrerende detectoren, die vaak worden gebruikt in traditionele CT-scanners die individuele fotonen detecteren. Deze detectoren zijn gebaseerd op een snelle scintillator gekoppeld aan een SiPM met een zeer korte oplaadtijd. Zowel de scintillator als de SiPM moeten snel zijn om de hoge Röntgenstralingsintensiteiten te verwerken die worden gebruikt in CT-scanners. De huidige PCD's die toegepast worden in CT-scanners zijn gebaseerd op de halfgeleider CdTe. In **Hoofdstuk 7** wordt een prospectieve visie gepresenteerd van potentiële scintillatoren en hun selectie voor gebruik in een scintillator-SiPM gebaseerde indirecte PCD. Als eerste stap wordt een beschrijving gepresenteerd van de processen die plaatsvinden in de PCD. Gebaseerd op deze beschrijving worden drie prestatie-indicatoren geformuleerd. De eerste indicator is de totale pulsintensiteit, dit weerspiegelt het gemiddeld aantal scintillatiefotonen dat geproduceerd wordt na de absorptie van een Röntgenfoton in het medisch relevante energiebereik (25 to 150 keV). Dit is gerelateerd aan de energieresolutie van de PCD. De tweede prestatie-indicator is de pulsduur, dit weerspiegelt de lengte van de detectoruitgangspuls en bestaat uit een convolutie van het scintillatorverval en de SiPM-oplaadtijd. De laatste prestatie-indicator is de pulsamplitude, dit weerspiegelt de amplitude van de detectoruitgangspuls en geeft een indicatie voor de graad van statistische fluctuaties op de puls. De drie prestatie indicatoren zijn gebruikt om een database van meer dan 200 scintillatoren te analyseren voor hun gebruik in indirecte PCD's.

De pulsduur van een op CdTe gebaseerde directe PCD (14 ns), tevens gebruikt in commercieel verkrijgbare CT-scanners, wordt gebruikt als benchmark.

De pulsduur van Eu^{2+} , Yb^{2+} , Sm^{2+} , Tl^+ gebaseerde scintillatoren en breedband emitters zijn over het algemeen langer dan 500 ns. Deze scintillatoren zullen daarom om ook niet in staat zijn om de hoge Röntgenstralingsintensiteit van een CT-scanner aan te kunnen en zullen leiden aan problemen door het overlappen van detectoruitgangspulsen. Twee zeer veel belovende potentiële kandidaten zijn op Ce^{3+} en Pr^{3+} gebaseerde scintillatoren. De pulsduur van op Ce^{3+} gebaseerde scintillatoren hangt sterk af van het gastrooster. Naast het intrinsieke verval van Ce^{3+} , zijn er ook langzame verval componenten aanwezig vanwege inefficiënte overdracht naar Ce^{3+} en gastrooster gerelateerde emissies. De pulsduur van Pr^{3+} gebaseerde scintillatoren vertonen ook een sterke afhankelijkheid van het gastrooster, *i.e.*, of efficiënte 5d – 4f emissie kan optreden of niet. De kortste pulsduren worden bereikt door scintillatoren gebaseerd op emissie afkomstig uit de overgang tussen de valentie band en de eerste daar onder gelegen gevulde band, op excitonische emissie afkomstig van de randen van de bandkloof, en op plastic gebaseerde scintillatoren. Jammer genoeg vertoont elk van deze categorieën zijn eigen scala aan problemen. Voor scintillatoren gebaseerd op emissie tussen de valentie en de eerst volgende gevulde band is de aanwezigheid van langzamere componenten door overgangen tussen de valentie en geleidingsbanden een probleem. Voor scintillatoren gebaseerd op excitonische emissie afkomstig van de randen van de bandkloof is zelf-absorptie een probleem. Voor op plastic gebaseerde scintillatoren is hun lage dichtheid het probleem. Het is ook mogelijk om de vervaltijd van een scintillator gericht te doven om de pulsduur te verkorten. Deze aanpak is onderzocht door de detectoruitgangspulsen te simuleren gebaseerd op punten van een hypothetische uitdovingscurve van een scintillator. Hiermee is aangetoond dat de vervaltijd van de scintillator niet kleiner gemaakt moet worden dan de oplaadtijd van de SiPM, dit leidt anders tot het verlies van scintillatiefotonen. Voor alle materialen die in dit hoofdstuk besproken worden is het belangrijk om te beseffen dat niet alleen de scintillatoreigenschappen van belang zijn maar ook de eigenschappen van de fotonendetector, *i.e.*, de scintillatoren en de fotonendetector kunnen elkaar worden afgestemd. Het is dan ook beter om na te denken in termen van een detectiesysteem wat bestaat uit zowel een scintillatiekristal als een fotonendetector.

Referenties

- [1] M. S. Alekhin, J. T. M. de Haas, I. V. Khodyuk, K. W. Krämer, P. R. Menge, V. Ouspenski, P. Dorenbos, *Applied physics letters* 102 (2013) 161915, <https://doi.org/10.1063/1.4803440>
- [2] C. van Aarle, *Black scintillators*, thesis Delft University of Technology (2024), ISBN: 978-94-6366-873-6, <http://resolver.tudelft.nl/uuid:37091b0a-1a34-4213-a2f1-4a883d4da721>
- [3] C. van Aarle, Chapter 7, *Black scintillators*, thesis Delft University of Technology (2024), ISBN: 978-94-6366-873-6, <http://resolver.tudelft.nl/uuid:37091b0a-1a34-4213-a2f1-4a883d4da721>
- [4] P. Dorenbos, *Optical Materials: X 1* (2019) 100021, <https://doi.org/10.1016/j.omx.2019.100021>
- [5] V. B. Mykhaylyk, H. Kraus, V. Kapustianyk, H. J. Kim, P. Mercere, M. Rudko, P. Da Silva, O. Antonyak, M. Dendebera, *Scientific Reports* 10 (2020) 8601, <https://doi.org/10.1038/s41598020-65672-z>
- [6] M. D. Bitowosuto, D. Cortecchia, W. Drozdowski, K. Brylew, W. Lachmanski, A. Bruno, C. Soci, *Scientific Reports* 6 (2016) 37254, <https://doi.org/10.1038/srep37254>
- [7] M. A. Green, A. Ho-Naillie, H. J. Snaith, *Nature Photonics* 8 (2014) 506, <https://doi.org/10.1038/nphoton.2014.134>
- [8] X. Y. Chin, D. Cortecchia, J. Yin, A. Bruno, C. Soci, *Nature Communications* 6 (2015) 7383, <https://doi.org/10.1038/ncomms8383>
- [9] R. T. Williams, W. W. Wolszczak, X. Yan, D. L. Carrol, *ACS Nano* 14 (2020) 5161-5169, <https://doi.org/10.1021/acsnano.0c02529>
- [10] W. W. Wolszczak, D. L. Carrroll, R. T. Williams, *Advanced X-ray Detector Technologies*, Chapter 1 (2022), https://doi.org/10.1007/978-3-030-64279-2_1



Acknowledgements

"Life can only be understood backwards; but it must be lived forwards"
Søren Kierkegaard

Dear reader, you have now reached, or more probably looked for and found, the section in which I would like to thank a "small" number of people for their indispensable contributions to the work you are currently holding or have put your gaze upon. In true fashion large parts of this section are written in hastily typed email around 3 am. I am very sorry if you excitedly arrived here, of course expecting your name to be in a very lengthy and elaborate paragraph, to discover that I missed it. Let me reassure you, every contribution, big and small has been important to my journey.

In the first year of my bachelor, I had the fortunate opportunity to do one of my practicals in the nuclear reactor institute of the TU Delft. At the time, as an "unknown" bachelor student I found this a very special experience. I would not have thought that 5 year later it would be very normal for me to "just stroll into" a nuclear reactor or that I would spend nine years at the TU Delft. This is something I realise every know and then upon entering the reactor. This acknowledgement section opens with one of my favourite quotes, something that for me strongly correlates with doing a PhD and science in general. It is only with the end in sight that I start to realise what the impact many different people around me has been on my professional and personal growth, my PhD journey, this book, and live in general. I would not have finished this journey with out you.

In the first place, I would like to thank **Pieter**. I have often wondered why you chose me for this position, but I am very happy you did. Your wisdom and guidance have been essential for the completion of this dissertation. Your door was always open for questions and discussions, even when I arrived faster than my emails, containing the topic of discussion. You gave me the space to explore and develop my own interests and helped me to focus on the important parts. Moreover, you took the time and had the patience to read my manuscripts and deal with my dyslexia. Together with Casper we agreed that your most valuable lessons came on the many trips we made: its easiest to travel light and the concept of "economical drinking". There are many more things I have learned from you. Upon writing this section it really starts to sink in what your impact has been on my qualities as researcher and on my life.

Every one that has ever done anything in our labs will quickly realise that **Johan** is the most essential member of our group, deserving more credits than he would ever admit. My interaction with Johan can be categorised in two groups. The first: "Johan, one of the set ups is broken", which would always be answered by a grumpy sound and the statement that the particular set up is not broken. The second: "Coffee?". Interestingly, this would also always be answered by a grumpy sound, a look at the clock, and a yes. I admire your extensive practical knowledge on scintillators and measurements. Thank you for all your help and patience

during the last four years.

A similar, or maybe even bigger contribution, to my project came from our collaborators in Bern. **Karl**, I think Casper has been very accurate by calling the Bern team Legendary Crystal growers. This made our trip to your laboratory only more special. For the non scientist reading this, it feels like entering the sagrada familia on the perfect day, epic and humbling. You did not only gave us more crystals than we could have wished for but also took a lot of time to look at our manuscripts, in detail. With comments like: "the word heatmap is slang, it is a image plot", it is this level of detail that I really appreciate. Casper and I did have a good laugh of appreciation about this specific comment. Thank you very much for all your input, help, and effort the last years, I have learned a lot from you.

Of course I should not forget the second halve of the Bern team, **Daniel**. Thank you for all your time and effort for the production of the crystal. Some of the most special moments of the project were when we got to open a new package from Bern. Casper and I both described this as a Christmas like experience, but with significantly cooler gifts than you would probably ever get on Christmas. It was very nice to meet you in Bern and see your passion and enthusiasm for growing these crystals.

Vladimir, John, Peter, our collaborators from Luxium/Saint Gobain, thank you for all the comments and scientific discussion you provided during our bi-yearly meetings. It was very nice to continue most of these discussions during the informal dinners that would typically follow such a meeting.

Then there are a number of colleagues I would like to thank. First of all, **Casper**, with whom I shared this project. We have been on many adventures together like running up a mountain in new mexico, or the Eiffel tower. It was quite refreshing to travel with someone who also does not mind walking an hour, especially, when you have been sitting at a conference the whole day. The weather app says that is only light blue, right? In the early stages of the project we also discovered that we have a very similar taste in music, which resulted in many hours of scrolling trough rate your music and many album recommendations. Dear reader, don't ask me to describe our taste in music, this will turn out to be a rather length and complex monologue. At the end of the project we also have spend a lot of rather lengthy lunches going through LPs at Sounds to find what we were looking for. It is still very funny to me that we separately had the experience of going into the store with an idea of what to buy and go back to the RID with completely different records. It was nice to have someone to share all my tea with. Thank you for the many scientific discussions and fun we have had the last four years. Casper and I had the luck to share our office with Max. **Max** you introduced us too meme stocks and influencers. It was a bit daunting to approach our office when you were playing the kazoo. Thank you for sharing many pictures of Apollo with us, who became the main character of a number of scientific cat memes placed in our office. I really appreciated that you made our office feel more alive, and sometimes even a bit to much like a living room. Sometimes, we were also accompanied by **Francesco**. If you would like to know anything about pulseheight

spectra you should talk to Francesco. I really admire your extensive knowledge on pulseheight spectroscopy and scintillators in general. You were always open for scientific discussions, which would typically derail towards many other subjects. I learned quite a lot from you. Thanks for the cans of black eyed beans, sometimes randomly appearing on my desk, they have truly become my favourite. **Justin**, you elaborately introduced us to the many good things from Taiwan. This includes both snacks and tea, I still really enjoy the red tea you brought back from the sun moon lake. It was very nice to have our small tea ceremonies in the pantry, accompanied by many conversations. The latest addition to our group was **Jeffery**. I think I have never seen anybody with such a passion and enthusiasm for luminescence, which often led to many deep and elaborate discussions. Then there are the other members of our group. Firstly my second promotor **Erik**, your office was always open for a talk or discussion. I really appreciate your hands on, just try it mentality. It was always nice to hear you talk about your side projects, like your tiny house or bathroom renovations. **Bert**, it was always very interesting to talk to you. I admire your fast knowledge on luminescence and the occasional follow up emails after our discussions. There are not many people to which you can talk and learn something new every time. **Trudy** thank you for all your help with booking plane and train tickets and navigating the 'lovely and intuitive' electronic systems and bureaucracy that we needed to navigate. Without you I would probably still be lost with some form spitting out errors, thank you for all the help. Then there are the people in the downstairs medical physics and technology office. **Stefan**, even though you were in the final steps of your PhD you still took the time to help and introduce me to indirect photon-counting detectors. Your contributions were essential for the paper which forms the basis for chapter 5. **David**, you are one of the most kind scientists I have ever met, feeding everybody your famous mocha beans. I really appreciate the time you took to answer all my questions regarding medical imaging and I will keep repeating, your contributions have been essential for the work presented in chapter 7. Thanks to you I even managed to put an em dash in my introduction. Together with **Jack** you missed Stefan so much that the two of you made several attempts to mirror his behaviourism's in the office. Jack, I really enjoyed working on the LYSO samples with you and the many accompanying conversations and discussions. **Marc** it was always very nice to enter your office with some science related discussion point that would spiral towards discussions about mechanical keyboards or coffee. I still laugh about the fact that you decided to go to the conference dinner in Milano in a full three piece suite in 35 degrees. A similar thing can be sad regarding **Lukas**, it was nice to have someone to complain about the struggles of finishing your dissertation and to see your promotion. In general to the four of you I would like to say thanks for all the nice talks and getting not to annoyed with me visiting your office. It was nice to be part of the experimental part of your projects. A special thanks is also in place for **Dennis**. Even though I was not one of your PhD students you always made time to answer questions and help with the development of the content of chapter 7. Of course our discussions would often dwindle to other subjects like jazz.

Lastly I would like to thank a number of people which have also been part of the luminescence materials group during my PhD. **Vasya, Giacomo, and Maarten** thank you for all the nice conversations, lunch breaks, and scientific discussions we have had.

Then there are a number of people that probably do not realise how big their actual impact has been on my PhD. Without you it would have been significantly harder to finish this dissertation.

First of all I would like to start with my old master thesis supervisor **Jence**. Both of us know that the end of my project might not have been the easiest. But I have learned a lot from you, both scientifically and as a person. You thought me one of the most important lessons: A good researcher also needs to take time to care for him self. It was really nice to also during my PhD do some measurements with you, and the accompanying "discussions". Thank you for teaching me so many different things.

Another big thank you goes to the people frequently participating in the coffee breaks at the RPNM group: **John, Dick, Andries, Sebastian, Dennis, and Trudy**, sorry if I forget anyone here. It was nice to have an escape upstairs sometimes. Our many discussions on a large variety of subjects were always very nice. It even resulted in a collaboration with Andries. Thank you all.

To my fellow PhDs which were also part of the PhD council: **Dennis, Marc, Andries, Svenja, David, Mark, and Rogier** and of course the most important member from the staff **Pedro**. Thank you all for the nice lunch meetings we have had, it was always nice to just sit down and have a casual conversation once in a while. It was always a pleasure to organise the pizza talks, colloquia, and the PhD day.

One of the things I have really appreciated during my PhD was helping with the course chemical thermodynamics. **Tom and Bijoy** thank you for the opportunity to do this for five years I have always really enjoyed it. It was nice to be able to both design exam questions as well as to correct them.

I have also been lucky enough to get the opportunity to supervise a number of students. **Douwe, Oscar, Lucas, Lisselotte, Elias, Baris, Quadim, and Giles** it was a pleasure to work with you. I am very happy that, up to some degree, have been able to provide you with some hands on experience and enthusiasm which I have also once received by my supervisor. Thanks you all for the great work.

Then there are a number of people that most definitely do not realise how big their impact has been. Even though most of you do not understand what I have done in the last four years your contributions have been crucial.

Starting with **Bob and Lisa**. Bob and I have been roommates for the largest part of my PhD, I still am not sure why Lisa decided to join. I will repeat it once more for you Bob, no my work does not explode and I would not describe it as "glow in the dark stuff". Our movie nights, with the occasional beer, and "huis uitjes" have always been a very nice escape.

To my friends, **Bob, Felix, Hidde, Mark, Michael, Nancy** and **Rhiannon**, it has been a pleasure to go on our many adventures. I have always really enjoyed our holidays, the counter is currently on 10 trips it should increase soon. Thanks for all the evenings of just grabbing dinner and drinks. We have been friends since high school and have started to do many different things. Most of you will not understand the content of the book you are currently holding upon reading this words, but you should realise you have significantly contributed to it.

One of the most important things for my sanity these last years has been our weekly climbing sessions. **Remco, Klaudia, Michael, Rhiannon** and **Felix**. Thank you for the many attempts to conquer the wall and accompanying drinks. A special thanks goes to Remco, I really admire your attitude during climbing, just look at what you can do. It has been very nice to have a climbing buddy that is just as stubborn and wanted to climb three times a week. Even though climbing has resulted in many scrapes and painful fingers I has been worth every bit. The downside was that it has made building some experimental setups a bit painful.

Marijn and **Timon**, I think that there are very few people that understand and have mastered the art of consuming a slightly to expensive bottle of wine, with appropriate snacks on the side. I still miss the times of our 5 minute anger coffee breaks. But I think that they have found a worthy replacement. From struggling in our bachelor and master to struggling in finding a job or just the job it self, it has always been very nice to have someone to discuss these things with.

Julien, Laurens, Lucas, Marijn, Nienke, Robert and **Twan**. Thanks for all the nice afternoons of boards games and as Twan would described it "kaarjtes leggen". These moments have always been perfect to just wind down and relax a bit. Thanks for all the good company and fun in the last four years.

Lastly I would like to thanks the most important people: my **Parents** and **Brother**. Thank you for all the support in the last nine years. Even though it has not been easy to explain to you what I was doing exactly you were always interested. Thanks for the many long phone calls, walks, dinners and city trips.

J. Jasper van Blaaderen
October 2024, Amsterdam



Supervised Thesis Projects

Dear reader, below you can find a list of bachelor and master students I have supervised during my PhD. It was a pleasure to see each one of you grow, develop and graduate. I feel honoured that I have been part of your work.

Douwe C. Mulder - Bachelor thesis: Optical Characteristics of Lead(II)Iodide - A study of its potential use in modern applications

Oscar van Baar - Bachelor thesis: In search of scintillators for X-ray radiography - An optical characterisation of cesium bismuth iodide

Lucas Foucher - Master thesis: Characterising perovskite materials and their structures' influence on luminescence: towards a new generation of scintillators

Lisselotte van de Brekel - Bachelor thesis: Temperature dependent optical and scintillation characterisation of CsCu_2I_3

Elias Verschoor - Bachelor thesis: On the luminescent properties and applications of 0D metal halide single crystals - An optical and scintillation characterisation of $\text{Cs}_3\text{Cu}_2\text{I}_5$

Baris Savci - Bachelor thesis: The characterisation of cesium lead halide perovskites - Understanding their limitations for scintillation

Qadim Sarucco - Luminescence properties of Bi^{3+} doped PbI_2 - The influence of the Bi^{3+} dopant on the fast scintillator PbI_2

Giles Bangoyina - Characterisation of core - valence luminescence materials for photon - counting computed tomography - A comprehensive study on the scintillation properties of Cs - M - Cl compounds ($\text{M} = \text{Zn}, \text{Mg}$)

List of Publications

J. Jasper van Blaaderen, Casper van Aarle, David Leibold, Pieter Dorenbos, Dennis R. Schaart, The Search for and Selection of Scintillators for Photon - Counting Detectors, 2024, Submitted to ACS Chemistry of Materials

J. Jasper van Blaaderen, Daniel Rutstrom, Giles Bangoyina, Charles L. Melcher, Dennis R. Schaart, Mariya Zhuravleva, P. Dorenbos, The potential application of Cs - M - Cs (M = Mg, Zn) Core - Valence Scintillators and the role nonproportionality, (2024), in preparation

Marc Snoeyink, **J. Jasper van Blaaderen**, Martijn M. A. Dietze, Hugo W. A. M. de Jong, Dennis R. Schaart, A Study on Novel Scintillators for Interventional Multimodal X - ray and Scintigraphy Imaging, 2024, in preparation

Jack Wehr, **J. Jasper van Blaaderen**, Coen R. N. Rasch, Dennis R. Schaart, Comparative Analysis of Three Generations of LYSO:Ce Crystals for Medical Imaging Applications, 2024, In preparation

J. Jasper van Blaaderen, Andries van Hattem, Jence T. Mulder, Daniel Biner, Karl W. Krämer, Pieter Dorenbos, Photoluminescence and Scintillation Mechanism of Cs_4PbBr_6 , 2024, The Journal of Physical Chemistry C 128 (2024) 46

J. Jasper van Blaaderen, Daniel Biner, Karl W. Krämer, P. Dorenbos, The Temperature Dependent Optical and Scintillation Characterisation of Bridgman Grown CsPbX_3 (X = Br, Cl) Single Crystals, Nuclear Instruments and Methods in Physics Research Section A: Accelerators, Spectrometers, Detectors and Associated Equipment 1064 (2024) 169322

J. Jasper van Blaaderen, Lisselotte van den Brekel, Karl W. Krämer, P. Dorenbos, Scintillation and Optical Characterisation of CsCu_2I_3 Single Crystals from 10 to 400 K, Chemistry of Materials 35 (2023) 22

J. Jasper van Blaaderen, Stefan van der Sar, Djulia Onggo, Abdul K. Sheikh, Dennis R. Schaart, Muhammad D. Birowosuto, Pieter Dorenbos, $(\text{BZA})_2\text{PbBr}_4$: A Potential Scintillator for Photon - Counting Computed Tomography Detectors, Journal of Luminescence 263 (2023) 120012

Jence T. Mulder, Michael S. Meijer, **J. Jasper van Blaaderen**, Indy Du Fosse, Kellie Jenkinson, Sara Bals, Liberato Manna, Arjan J. Houtepen, Understanding and Preventing Photoluminescence Quenching to Achieve Unity Photoluminescence Quantum Yield in Yb:YLF Nanocrystals, ACS Applied Materials and Interfaces 15 (2023) 2

J. Jasper van Blaaderen, Francesco Maddalena, Cuong Dang, Muhammad D. Birowosuto, Pieter Dorenbos, Temperature Dependent Scintillation Properties and Mechanisms of $(\text{PEA})_2\text{PbBr}_4$ Single Crystals, Journal of Materials Chemistry C 10 (2022) 32

Curriculum Vitae

Jacob Jasper van Blaaderen was born on the 24th of May 1997 in Amsterdam, the Netherlands. He received his primary education at Het Bovenland from 2001 to 2009. He received his secondary education at Het Calandlyceum from 2009 to 2015, where he was among the first to finish the Technasium program. In 2015 he joined the Delft University of Technology, where he studied Molecular Science and Technology, a joint degree with the Leiden University. In 2018 he obtained his bachelor degree after successfully defending his thesis titled: "The Influence of Different Precursors on Methyl-ammonium Lead Bromide Films and Solar Cells", under the supervision of Dr. T. J. Savenije in the opto-electronic materials group. Subsequently, he started the masters program Chemical Engineering at the Delft University of Technology. In 2020 He obtained his masters degree in chemical engineering after successfully defending his thesis titled: "Synthesis and Optical Analysis of Ytterbium Doped Yttrium Lithium Tetrafluoride Nanocrystals, Towards Laser Cooling in Nanocrystals", under the supervision of Dr. J. T. Mulder and Prof. Dr. A. J. Houtepen in the opto-electronic materials group. On the 1st of January 2021 Jasper started his PhD in the luminescence materials group at Delft University of Technology, under the guidance of Prof. Dr. P. Dorenbos. The main focus of his PhD was the exploration and characterisation of small bandgap intrinsic scintillators.

Apart from his scientific endeavours Jasper likes to listen to music and collect vinyl records, to climb (both top rope and lead climbing, indoors), collect books on varying topics, maintaining his healthy collection of house-plants and to curate his tea collection. If he can find the time he also likes to draw and paint which has resulted in a number of sold paintings and the task to design an album cover.

